Yvon, Carine. (2014) *Bringing polyoxometalates to peptide chemistry: a modular approach.* PhD thesis.

http://theses.gla.ac.uk/5248/

Bringing Polyoxometalates to Peptide Chemistry –

A Modular Approach

Carine Yvon

A thesis submitted to the University of Glasgow for the degree of

Doctor of Philosophy

School of Chemistry

April 2014

A ma mamounette qui n'en n'aurait pas compris un mot, mais qui aurait été très fière.

Tu me manques.

Acknowledgments

TABLE OF CONTENTS

PUBLICATIONS

The following articles were published as a result of the work undertaken over the course of this Ph.D. programme.

Mapping the Synthesis of Low Nuclearity Polyoxometalates from Octamolybdates to Mn-Anderson Clusters, M. H. Rosnes, <u>C. Yvon</u>, D.-L. Long, L. Cronin, *Dalton Trans.*, **2012**, 41, 10071-10079

Programming the Assembly of Carboxylic Acid-Functionalised Hybrid Polyoxometalates, M. Hutin, <u>C. Yvon</u>, J. Yan, A. Macdonell, D.-L. Long and L. Cronin, *CrystEngComm*, **2013**, 22, 4422-4430

A Collection of Robust Methodologies for the Preparation of Asymmetric Hybrid Mn-Anderson Polyoxometalates for Multifunctional Materials, <u>C. Yvon</u>, A. Macdonell, S. Buchwald, A. J. Surman, N. Follet, J. Alex, D.-L Long and L. Cronin, *Chem. Sci.*, **2013**, 4, 3810-3817

Polyoxometalate Clusters Integrated into Peptide Chains and as Inorganic Amino Acids: Solution and Solid Phase Approaches, <u>C. Yvon</u>, A. J. Surman, M. Hutin, J. Alex, B. O. Smith, D.-L Long and L. Cronin, *Angew. Chem. Int. Ed.,* **2014**, 53, 3336-3341

ABBREVIATIONS

In addition to standard notation, the following abbreviations were used in this thesis:

Ala, A	Alanine
Arg, R	Arginine
Asn, N	Asparagine
Asp, D	Aspartic Acid
ATRP	Atom Transfer Radical Polymerisation
CD	Circular Dichroism
COSY	Correlation Spectroscopy
CPP	Cell-Penetrating Peptide
Cys, C	Cysteine
DCC	*N, N'*-Dicyclohexylcarbodiimide
DCM	Dichloromethane
DCU	*N, N'*-Dicyclohexylurea
DEPTQ	Distortionless Enhancement by Polarisation Transfer with retention of Quaternaries
DIC	*N, N'*-diisopropylcarbodiimide
DIPEA	*N, N*-diisopropylethylamine
DMF	*N, N*-Dimethylformamide
DMSO	Dimethyl Sulfoxide
EEDQ	2-Ethoxy-ethoxycarbonyl-1,2-dihydroquinoline
ELSD	Evaporative Light Scattering Detector
equiv.	Equivalent
ESI-MS	Electrospray Ionisation Mass Spectrometry
Et_2O	Diethyl Ether
Fmoc	9-Fluorenylmethyloxycarbonyl
Gln, Q	Glutamine
Glu, E	Glutamic Acid
Gly, G	Glycine
HBTU	*N,N,N',N'*-Tetramethyl-*O*-(1*H*-benzotriazol-1-yl)uronium hexafluorophosphate
HFIP	1,1,1,3,3,3-hexafluoro-2-propanol
His, H	Histidine
HPLC	High-Performance Liquid Chromatography

Hyb	Hybrid Mn-Anderson Amino Acid Residue
Ile, I	Isoleucine
IR	Infrared
LC	Liquid Chromatography
Leu, L	Leucine
Lys, K	Lysine
MeCN	Acetonitrile
Met, M	Methionine
NHS	*N*-Hydroxysuccinimide
NMR	Nuclear Magnetic Resonance Spectroscopy
NOESY	Nuclear Overhauser Effect Spectroscopy
PEG	Polyethylene Glycol
Phe, F	Phenylalanine
POM	Polyoxometalate
PS	Polystyrene
RAFT	Reversible Addition-Fragmentation Chain-Transfer
ROMP	Ring Opening Metathesis Polymerisation
RP	Reverse Phase
Ser, S	Serine
SPPS	Solid-Phase Peptide Synthesis
TBA	Tetra-*n*-butylammonium
TEA	Tetraethylammonium
TEM	Transmission Electron Microscopy
TGA	Thermogravimetric Analysis
Thr, T	Threonine
TMA	Tetramethylammonium
TOCSY	Total Correlation Spectroscopy
TPA	Tetra-*n*-propylammonium
TRIS	Tris-(hydroxylmethyl)-aminomethane
Trp, W	Tryptophan
Trt, Trityl	Triphenylmethyl
Tyr, Y	Tyrosine
UV	Ultra-Violet
Val, V	Valine

ABSTRACT

This thesis focuses on the development of modular approaches that permit the integration of hybrid polyoxometalates (POMs) into peptide chains. This goal is of considerable interest in the field of POM chemistry, as it could provide a new approach to explore, develop and tune the properties of POM clusters (*e.g.* toxicity, self-assembly and recognition properties). The organic-inorganic Mn-Anderson cluster, a bi-substituted cluster incorporating two TRIS-based moieties, was used as a model compound to develop these methodologies.

A "modification tool box" was created to facilitate the reaction of hybrid metal-oxide building blocks with peptides. Solvent compatibility was first explored and four DMF- and water-soluble TRIS Mn-Anderson compounds were synthesised by adapting the original synthesis protocol to different octamolybdate salts. Peptide bond formation investigations on an amine functionalised hybrid POM were then carried out, and anhydride intermediates were found to be suitable reagents for amide bond formation. Furthermore, cyclic anhydrides proved an efficient means of incorporating carboxylic acid functions onto TRIS-based Mn-Anderson POM clusters, a functionality which had never been introduced on this hybrid type. Activation of the carboxylic acid function by formation of an *N*-hydroxysuccinimide (NHS)-ester hybrid POM building block permitted the formation of amide bonds by reaction with amines.

With this synthetic "tool box" established, the activated NHS-ester hybrid POM building block approach was further explored and proved a simple and efficient means to graft pre-synthesised peptides onto the metal-oxide framework in solution. Using this technique, a POM hybrid of unprecedented scale, 30 amino acid residues, was synthesised. This introduction of the POM cluster as a linking component between two peptides demonstrated an impact on the spatial arrangement of the chains, with the observation of an unexpected α-helix conformation.

The aforementioned work solely focused on symmetric TRIS-based Mn-Anderson clusters, which was due to a dearth of methods permitting the isolation of asymmetric clusters from symmetric by-products. To fully exploit the potential of the di-substituted hybrid Mn-Anderson unit, the problem of its isolation as an asymmetric cluster had to be dealt with. A chromatographic methodology to isolate asymmetric hybrids was developed relying on the difference in affinity of the compounds' organic moieties for reverse phase (RP) media.

For cases where this method could not be applied, a "universal" asymmetric Mn-Anderson precursor was designed and isolated, and its use as a precursor to synthesise practically any asymmetric Mn-Anderson system was demonstrated.

This new set of methods permitting the routine isolation of asymmetric Mn-Anderson clusters allowed the first hybrid POM combining one amine and one carboxylic acid functional group to be designed and synthesised. This new building block, which could be produced in large batches, is the first unnatural hybrid POM amino acid ever isolated. An in-depth study was carried out to establish the reaction conditions that permit its use in solid phase peptide synthesis (SPPS). From this study, a customised SPPS protocol was created which allows the 'hybrid POM amino acid' unit to be introduced into growing peptide chains as easily as any natural amino acid. Following this SPPS protocol, the first POM-peptide hybrid, embedding an amino acid Mn-Anderson residue in its sequence, was synthesised and isolated.

1   Introduction

Engineers and physicists are developing sophisticated techniques (*e.g.* lithography, patterning) to manipulate always smaller pieces of matter and produce nanosized materials. This process of miniaturisation, called the "*top-down*" approach, permits the construction of devices "as small as" 100 nm. This size, very small by common standards (one thousandth of the width of a human hair) can also be viewed as very large if compared to atoms and molecules. As highlighted by the Nobel physicist Richard Feynman fifty years ago: "there is plenty of room at the bottom".[1]

Chemists have learnt to tailor molecules and create "programmable" building blocks that can self-assemble into super-structures to form new smart materials. This enlargement strategy, the "*bottom-up*" approach, finds its founding principles in the field of supramolecular chemistry and in particular in the pioneering work of Pedersen, Cram and Lehn.[2] Molecular components can now be designed to self-assemble into larger functional materials under specific recognition processes and may be able to fill the current gap in the engineering of small-scale devices.

Moreover, biology has now evolved from a purely descriptive and phenomenological discipline to a molecular science. Nature's building blocks can rationally be used to design and produce bio-mimicking assemblies and an important field of science is now based on the fusion of biotechnology and material science.[3,4]

As described by the Nobel laureate Jean Marie Lehn "The essence of chemical science finds its full expression in the words of that epitome of the artist – scientist Leonardo da Vinci *'Where Nature finishes producing its own species, man begins, using natural things and with the help of this nature, to create an infinity of species'*".[5]

1.1 Polyoxometalates

Polyoxometalates (POMs) or polyoxoanions are defined metal-oxygen clusters of early transition metal in their highest oxidation states.[6,7] This class of materials is often divided into two groups: iso- and hetero-polyoxometalates. Clusters of the former group are made of numerous oxygen atoms, sometimes hydrogens and only one type of transition metal (M, addenda atoms) giving the general Formula 1. On the other hand, POMs in the latter group also incorporate one or more *p- d-* or *f*-block element in positive oxidation state (Formula 2). These additional atoms are known as *heteroatoms*.

$$[H_nM_mO_x]^{q-}$$

Formula 1: General formula of iso-polyoxometalate clusters, with M the early transition metal (addenda atom) in its highest oxidation state and q the overall charge.

$$[X_yH_nM_mO_x]^{q-}$$

Formula 2: General formula of hetero-polyoxometalate clusters, with X the heteroatom, M the early transition metal (addenda atom) in its highest oxidation state and q the overall charge.

POMs are formed through a polymerisation process which occurs in acidified solution. Tetrahedral metal-oxide building blocks $\{MO_4\}$, rearrange upon acidification as octahedral units which polymerise *via* corner, edge or face sharing to form discrete polyoxoanion complexes (*e.g.* in Equations 1 and 2). Elements that can act as addenda atoms should therefore: i) be able to change their coordination to oxygen from 4 to 6, ii) bear a high positive charge and iii) have a small ionic radius for favourable octahedral packing with oxygen.[7] The ability to form double bonds with unshared oxygen atoms (*pπ-dπ* metal oxygen bonds) is also an important feature of addenda atoms. $W^{(VI)}$, $Mo^{(VI)}$ and $V^{(V)}$ are the most common addenda atoms encountered in POM chemistry.[6-9]

$$8\ H^+ + 7\ [WO_4]^{2-} \longrightarrow [W_7O_{24}]^{6-} + 4\ H_2O \qquad (1)$$

$$23\ H^+ + [HPO_4]^{2-} + 12\ [MoO_4]^{2-} \longrightarrow [PMo_{12}O_{40}]^{3-} + 12\ H_2O \qquad (2)$$
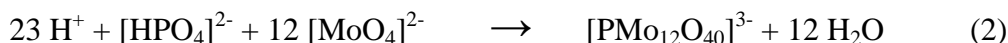
Equation: (1) formation of isopolyoxotungstate in acidic conditions;[10] (2) formation of heteropolyoxomolybdate in acidic conditions.[11]

In POMs, the addenda atom is located off-centre of its polyhedra toward the unshared oxygen atoms (exterior of the framework; see Figure 1). This distortion of the addenda polyhedra can be explained by the formation of double bonds between the unshared oxygens and the metal centre (by definition shorter than single bonds) and the greater polarisability of these oxygen atoms creating strong ion-induced dipole attractions between the unshared oxo groups and the addenda atoms.[7] Polyoxoanion clusters are thus "wrapped" by a layer of unshared oxygen atoms strongly polarised toward the interior of the framework which prevents further polymerisation. These distortion and polarisation phenomenon are responsible for the existence of POMs as discrete species and not as infinite solid matrixes.
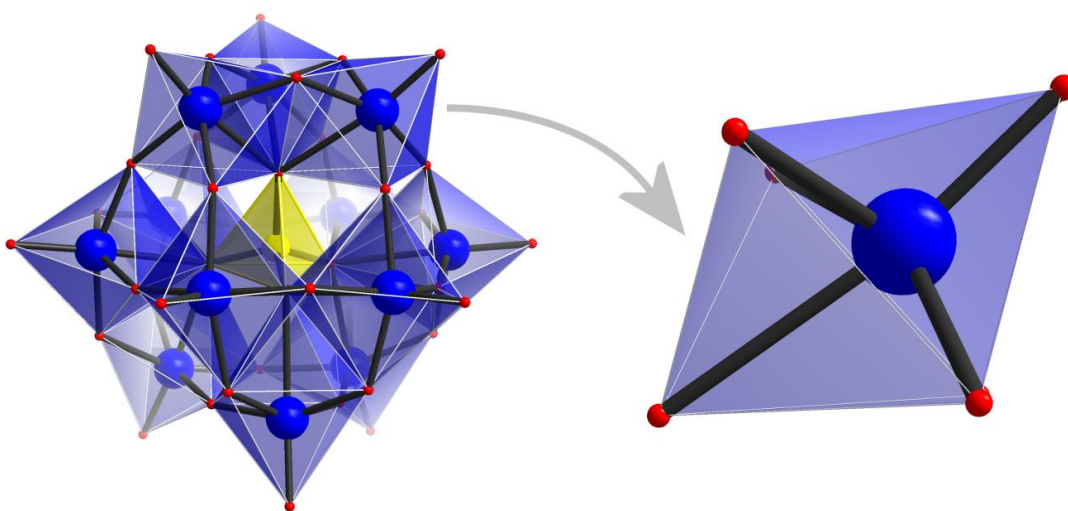
Figure 1: Distortion of the addenda octahedra illustrated through the Keggin structure with zoomed in representation of a single octahedral unit. Colour scheme: addenda atom (M), blue (polyhedra); heteroatom (X), yellow (polyhedra); O, red.

POMs are an interesting class of molecules, since nearly all the properties that influence their reactivity can be modified during their synthesis. This includes size, shape, electron and proton transfer/storage abilities, redox potential, surface charge distribution and high Brönsted acidity.[12] They are therefore promising candidates for numerous applications[13] including medicine,[14] catalysis,[15,16] hydrogen and oxygen evolution,[17] data storage devices[18] and dopants of polymer matrices.[19-21] However, the full exploration of the potential of POMs is still hampered by the lack of a reliable processing step to incorporate them into materials and devices. Recent developments are focusing on the alteration of POMs to increase their functionality and possible applications.[8,9,22-29] One approach is the design and synthesis of organic-inorganic hybrid POM complexes, which will be discussed further in Section 1.2.

1.1.1 Polyoxometalates history and discoveries

POM chemistry is an important field in contemporary research, but its journey started two centuries ago, when, in 1826, J. J. Berzelius observed the formation of "the yellow precipitate" produced by the addition of excess ammonium molybdate to phosphoric acid.[11] This compound, now known as ammonium 12-molybdophosphate ($(NH_4)_3[PMo_{12}O_{40}]$), was an enigma which took almost a century, as well as the contribution of numerous scientists, to elucidate its composition and structure. Analytical chemistry studies were first undertaken by Svanberg and Struve in 1848,[30] but the final composition of the complex was revealed only in 1864 by Marignac's publication.[31] Scientists, including A. Werner (1893),[32] A. Miolati and R. Pizzighelli (1908)[33] and A. Rosenheim (1917),[34] tried to understand the chemistry behind this phenomenon, proposing diverse theories on the coordination of complexes. These theories, although later proven proved to be incorrect, were essential steps toward the comprehension of the formation of metal-oxygen clusters. Two breakthroughs allowed for definitive structural determination of POMs; first Laue[35] and Bragg's[36] publications on the development of X-ray crystallography in 1913, followed by L. Pauling's proposition in 1929 that the "rules for the structures of complex ionic crystals" (theory established by Pauling in 1927[37]) should also apply to the internal structure of POMs.[38] The combination of these two major developments permitted the structural characterisation of POM clusters. In 1933, J. F. Keggin exploiting 17 powder X-ray lines established the first POM structure – the cubic $H_3[PW_{12}O_{40}] \cdot 5H_2O$, of which the exact formula is nowadays known as: $(H_5O_2)_3[PW_{12}O_{40}]$.[39,40] The structure elucidation was an incredible challenge and only the positions of tungsten atoms were established directly with this technique; the location of the oxygen atoms had to then be deduced from the interatomic distances between the tungstens. Since then, many 12-heteropolyoxoanions have demonstrated the same atomic arrangement and are now classified as the Keggin structure, of general formula $[XM_{12}O_{40}]^{q-}$. Four years after Keggin's discovery, J. S. Anderson published a paper suggesting a structure for the 6-molybdoperiodate ion $[I^{VII}Mo_6O_{24}]^{5-}$ based exclusively on Pauling's theory (no experimental work was involved).[41] In 1948, the structure elaborated by Anderson was confirmed by a single crystal X-ray experiment carried out by H. T. Evans on $[Te^{VI}Mo_6O_{24}]^{6-}$.[42] This crystal structure type often encountered in POM chemistry is now referred to as the Anderson – Evans structure, of general formula $[XM_6O_{24}]^{q-}$. In 1945, A. F. Wells suggested a theoretical structure based on Pauling's principles for the dimeric 9-tungstophosphate anion.[43] The structural arrangement was confirmed eight years later by a single crystal X-ray study conducted by B. Dawson.[44]

Wells's prediction of the tungsten atom positions in the $[P_2W_{18}O_{62}]^{6-}$ were correct and a new POM structure type was established named the Wells – Dawson structure of general formula $[X_2M_{18}O_{62}]^{q-}$. In 1950, Lindqvist published the structure of an isopolyoxoanion; structure now known as the Lindqvist structure type of general formula $[M_6O_{19}]^{q-}$.[45]

In the second half of the 20th century, many structures with ever increasing structural accuracy were discovered thanks to vast improvements in diffraction instruments coupled with the advent of cheap and powerful computing power for structure solution and refinement. Technology advances allowed scientists to focus on matters beyond simply the structure of POMs, allowing scientists to study their mechanisms of formation,[6,8,9,29] and to investigate potential applications.[13,23,25-27]

1.1.2 Specific polyoxometalate structures

Although the traditional one-pot reaction which leads to the formation of POMs can appear somewhat simple, the number of reaction parameters to accurately adjust to form the desired product complicates this task significantly. The most important parameters to consider when controlling the formation of a specific POM cluster are: the reaction medium, the temperature, the pH, the transition metal precursor, the addition of heteroatoms, the salt addition of alkali or alkaline earth metals to adjust the ionic strength and the crystallisation process.[6,8,9,29,46] Automatic systems have recently been implemented to explore the variation of these parameters.[47,48]

The work presented in this thesis focuses on the organic-inorganic TRIS-based Mn-Anderson hybrid complexes (TRIS-based ligands having the general formula: $(HOCH_2)_3CR$). Their formation is well-established and is presented along with the reaction conditions in Figure 2.[49,50] The POM structures discussed in this thesis are essentially the ones of the octamolybdate isopolyoxoanion and the Anderson heteropolyoxoanion; these structures are presented in details in this section.
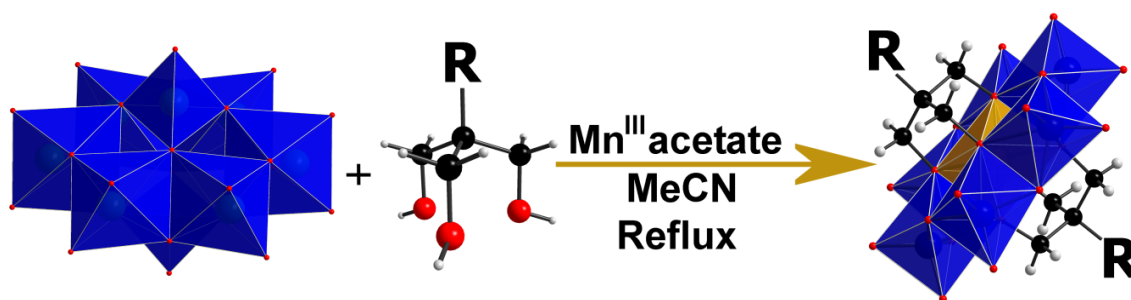
Figure 2: Reaction scheme of the synthesis yielding TRIS-based Mn-Anderson complexes. Colour scheme: Mn, orange (polyhedra); Mo, blue (polyhedra); C, black; O, red; H, grey.

1.1.2.1 The octamolybdate isomers

The α-octamolybdate isomer isolated as a tetra-n-butylammonium (TBA) salt, $((TBA)_4[\alpha\text{-}Mo_8O_{26}]$, is the starting material employed in the formation of the hybrid TRIS-based Mn-Anderson complexes.[49] Its structure was first reported by Fuchs and Hartl in 1976[51] and consists of a planar ring arrangement of six $\{MoO_6\}$ units, similar to the one observed for the Anderson structure (see Section 1.1.2.2.),[42] with two tetrahedral $\{MoO_4\}$ units capping the central cavity. This gives rise to an approximate D_{3d} symmetry (Figure 3).
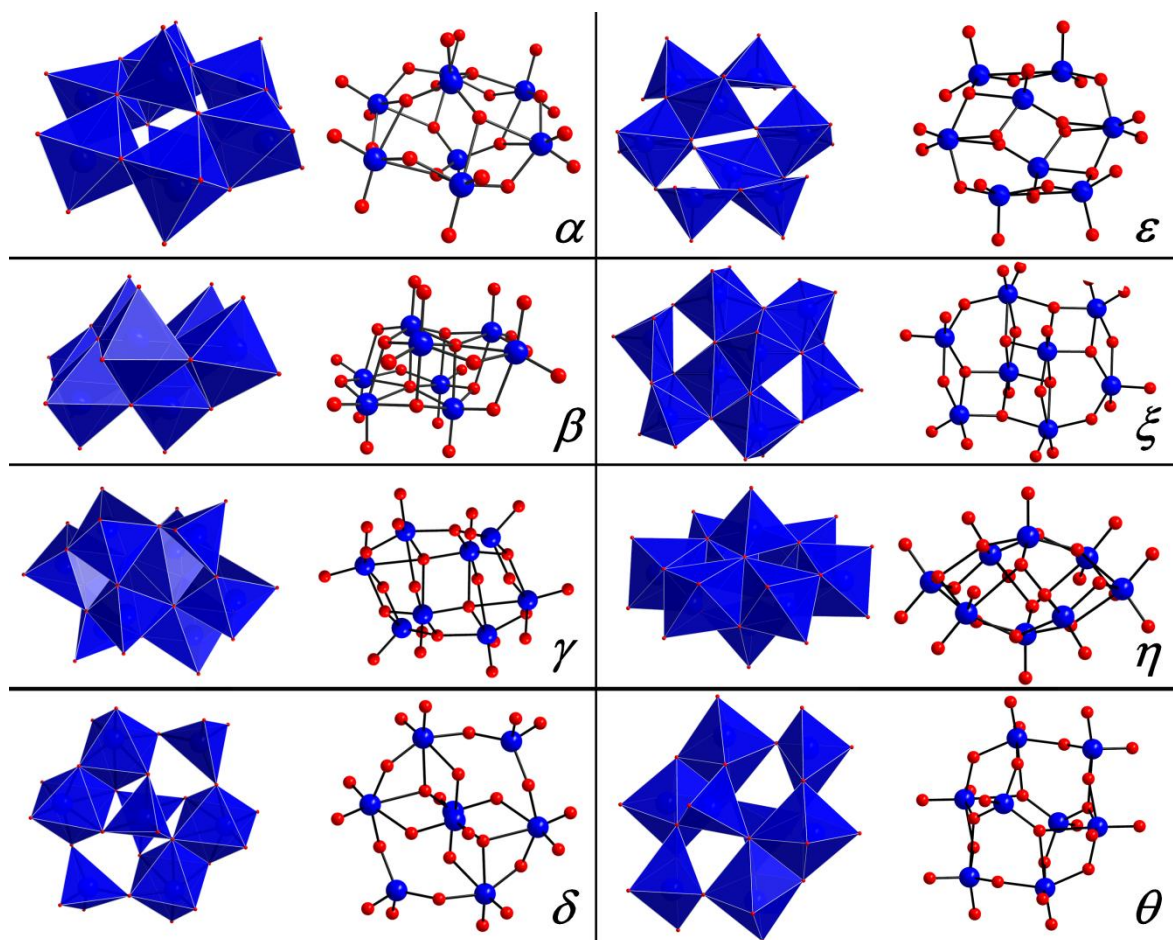
Figure 3: Polyhedral and ball-and-stick representations of the eight isomers of the octamolybdate $[Mo_8O_{26}]^{4-}$. α, β, γ and δ isomers are isolated by conventional methods while ε, ζ, η, and θ isomers are only observed under hydrothermal conditions. Colour scheme: Mo, blue (polyhedra); O, red.

However, this isomer is only one of the eight isomers that have been discovered from this isopolyoxoanion (Figure 3). Three other isomers, β-[52,53], γ-[54] *and* δ-[55], were also isolated by conventional methods − crystallisation from acidified aqueous solution in the presence of the appropriate cation − while the ε-,[56] ζ-,[57] η-[58] and θ-[59] isomers were observed under hydrothermal conditions with the use of organic or metal based cations to direct the polyoxometalate assemblies. The structural compositions of each isomeric form are given in Table 1.

Table 1: List of the isomers observed for the isopolyoxoanion $[Mo_8O_{26}]^{4-}$ with description of the polyhedral components and the oxo-group types of each structure.

Isomer	Polyhedra	Oxo-group types
α	6 octahedra, 2 tetrahedra	14t, $6\mu^2$, $6\mu^3$
β	8 octahedra	14t, $6\mu^2$, $4\mu^3$, $2\mu^5$
γ	6 octahedra, 2 square pyramids	14t, $10\mu^2$, $2\mu^3$
δ	4 octahedra, 4 tetrahedra	14t, $10\mu^2$, $2\mu^3$
ε	6 square pyramids, 2 octahedra	16t, $4\mu^2$, $6\mu^3$
ξ	4 octahedra, 4 square pyramids	14t, $6\mu^2$, $6\mu^3$
η	6 octahedra, 2 square pyramids	14t, $4\mu^2$, $8\mu^3$
θ	6 octahedra, 2 square pyramids, 2 tetrahedra	14t, $8\mu^2$, $4\mu^3$

The most common isomers, α and β, are both isolated from aqueous solution of molybdate at pH 2-5;[60] the main parameter used for the discrimination of one isomer over the other is the nature of the organic cation. Large cations, such as TBA or $PPrPh_3^+$, lead to the crystallisation of the α type, while smaller organic molecules (*e.g.* NH_4^+, Me_4N^+, Et_4N^+) lead to the isolation of the β form.[61,62] Both isomers were proven to give an $\alpha - \beta$ mixture once dissolved in acetonitrile (MeCN), this equilibrium can then be shifted toward one structural arrangement by addition of the appropriate cation.[62] Two isomerisation mechanisms were proposed to explain this phenomenon;[61,63] the isolation of the γ-isomer by Niven *et al.* in 1991,[54] an intermediate species suggested by Kemperer and Shum in their mechanism in 1976,[61] would tend to favour their theory.

1.1.2.2 The Anderson – Evans structure

Two isomers, α and β, are known for the POM clusters of general formula $[H_y(XO_6)M_6O_{18}]^{q-}$ (y = 0; 6, q = 2 − 6, M= Mo or W; X: metallic or non-metallic heteroatom).[6] The β-isomer is a non-planar bent arrangement of edge-sharing octahedra (Figure 4a) and was observed for the isopolyoxoanions $[Mo_7O_{24}]^{6-}$ [64] and $[W_7O_{24}]^{6-}$.[10,65] The α-isomer, also called the Anderson – Evans structure, is a planar arrangement of six edge-sharing octahedra around a central heteroatom (Figure 4b).[42]
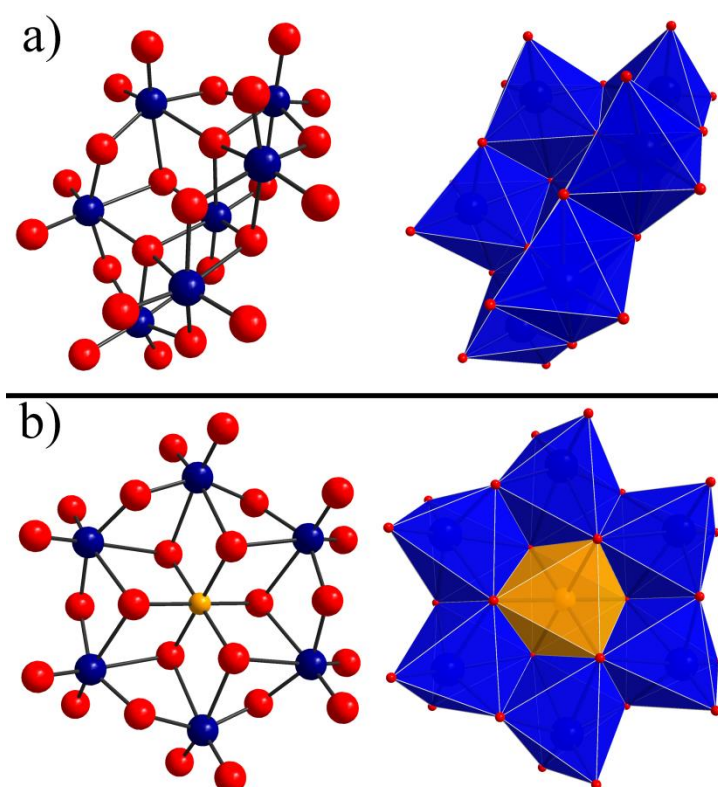
Figure 4: (a) Crystal structure of the isopolyoxoanion $[Mo_7O_{24}]^{6-}$ characteristic of the β-isomer;[64] (b) Crystal structure of the heteropolyoxoanion $[H_6Mn^{III}Mo_6O_{24}]^{3-}$ characteristic of the α-isomer also called Anderson (-Evans) structure.[66] Cations and hydrogen atoms are omitted for clarity. Colour scheme: Mn, orange (polyhedra); Mo, blue (polyhedra); O, red.

In 1937, through a letter to Nature, J. S. Anderson suggested the following structure:[41] "It may readily be seen that six {MoO_6} octahedra may be so arranged, by sharing corners with each of two neighbouring octahedra, that a hexagonal {Mo_6O_{24}} annulus is built up. The central cavity of this structure is then the same size and shape as one of the {MoO_6} octahedra, and can therefore accommodate another cation in the same 6-fold co-ordination.". This suggestion was later confirmed by H. T. Evans with the crystallographic determination of the hexamolybdotellurate structure, $K_6[TeMo_6O_{24}]$.[42] From these discoveries, polyoxometalates composed of the same metal arrangements are now referred to as Anderson – Evans structures. Evans is frequently omitted when referring to this structure; herein the structure will be referred to only as the Anderson structure.

Two types of Anderson structure are present in the literature, A-type and B-type. In both cases this structural arrangement is only obtained for heteropolyoxometalates with molybdenum or tungstate as the addenda atoms.[6,67] The A-type, the non-protonated form, is observed in clusters where the heteroatoms are in high oxidation states, while the

protonated form, B-type, is observed for systems containing heteroatoms of low oxidation states. A list of compounds that display the classic Anderson structure is given in Table 2.

Table 2: Heteropolyoxo molybdates and tungstates displaying the Anderson structure with the corresponding heteroatom and its oxidation states.

	Formula	Heteroatom (X)
A-Type	$[XO_6Mo_6O_{18}]^{q-}$	Te^{VI}, I^{VII}
	$[XO_6W_6O_{18}]^{q-}$	Mn^{IV}, Ni^{IV}, Te^{VI}, I^{VII}
B-Type	$[X(OH)_6Mo_6O_{18}]^{q-}$	Fe^{II}, Co^{II}, Ni^{II}, Cu^{II}, Zn^{II},
		Al^{III}, Ga^{III}, Cr^{III}, Fe^{III}, Co^{III}, Rh^{III}, Mn^{III},
	$[X(OH)_6W_6O_{18}]^{q-}$	Ni^{II}

The six non-acidic protons found in the B-type structure can be located at two different positions; the positioning of the hydrogen atoms on the six oxygen atoms bound to the central heteroatom is the most common protonation mode (Figure 5a),[66] but protonation of the oxygen atoms surrounding cavities can also be observed (Figure 5b).[68]
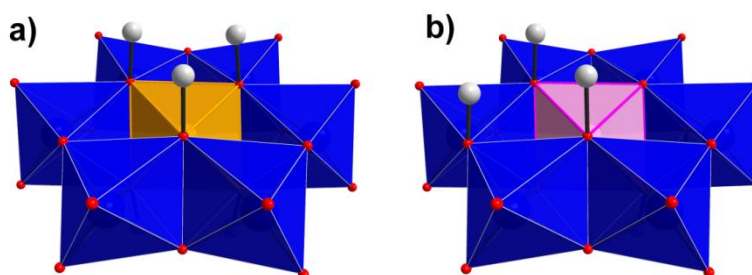
Figure 5: Representation of the protonation modes observed for the B-Type Anderson compounds. (a) most common protonation mode depicted for Mn^{III} as the heteroatom;[66] (b) less common protonation mode depicted with Pt^{IV} as the heteroatom.[68] Colour scheme: Mn, orange (polyhedra); Pt, pink (polyhedra); Mo, blue (polyhedra); O, red; H, light grey.

1.2   Organic-inorganic hybrid polyoxometalate clusters

The idea of mixing organic and inorganic components to tune the properties of materials is not new;[69] one of the most famous examples of this concept comes from the paint industry, with the suspension of inorganic pigments (*e.g.* TiO_2) in organic media (*e.g.* solvent or surfactant…). Nowadays the field of organic-inorganic hybrid materials is extremely diverse but is always pursuing the same goal: forming innovative advanced materials, not only from the combination of the properties of the organic and inorganic components, but also by exploring the synergy that could result from interactions between the two entities.

POMs promise new applications in many fields, but the poor processability of POM materials, which are often isolated as crystalline insoluble inorganic salts, hampers their use in materials and devices. The incorporation of organic functions could improve solubility, enhance bioavailability, increase selectivity and facilitate integration of POMs into devices, which explains the rising interest in organic-inorganic hybrid POM clusters. POMs can be "mixed" with organic compounds in many different ways.[22,27,46,70-72] Organic-inorganic hybrid POM materials are often divided into two types (class I and class II) depending on the nature of the interactions between the POM and the organic components.[22] The system is of class I when only weak interactions (electrostatic interactions, hydrogen bonds or van der Waals interactions) govern the assembly of the inorganic parts with the organic components.[22,23,46,72] Class II involves systems in which the metal-oxygen cluster is linked *via* covalent or iono-covalent bonds to organic moieties (commonly called ligands).[22,70,71] Due to the anionic character of POMs, class I systems can readily formed by association with organic counter cations during the synthesis of POMs. Class II compounds require an anchorage point for the organic ligand to be grafted on. So far, this feature has been established only for an extremely narrow set of clusters compared to the large number of POM structures discovered. Two main categories are found in the investigation of class II POMs;[22] the first is where ligands are incorporated in the metal-oxygen framework directly through *p*-block elements; and the second is where ligands are linked to *f*- and *d*-block elements which are embedded in POM structures or linked to the surface of the POM assembly.

The work in this thesis focuses on class II compounds, the covalent bond offering a better control at the molecular level and a greater chance of conserving the hybrid material properties from the solid state to the solution phase. Within the class II POMs, this work

explores the direct grafting of the ligand *via p*-block elements. Comprehensive reviews on other types of organic-inorganic hybrid POMs are given in references [22] and [70].[22,70]

1.2.1   Class II – *via p*-block elements

Conventionally, the functionalisation of POM clusters *via p*-block elements arises from bond formation with oxygen atoms located at the periphery of the POM structure (M-O-X coordination mode, with X a *p*-block element). Many *p*-block elements can be linked to oxygen atoms bound to the metal centre,[22,71] the main coordination modes being *via* i) alkoxide groups (Figure 6a),[73] ii) carboxylate groups (Figure 6b),[74] iii) organosilyl groups (Figure 6c),[75-77] and iv) organotin groups (Figure 6d).[78] The organosilyl and organotin coordination modes occur predominantly for lacunary POM species, as the nucleophilic properties of the oxygen atoms localised at the surface of the lacuna are increased, enhancing their reactivity towards electrophilic groups such as organotins, organosilyls, *etc*. Other elements such as organogermanyl[79,80] derivatives have also been reported but are less common in this field.
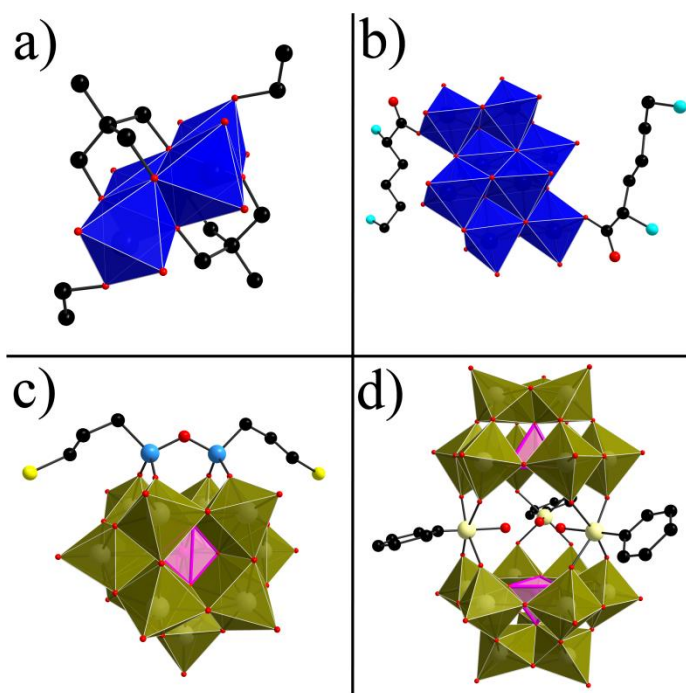
Figure 6: Examples of the main coordination modes *via p*-block elements found in class II hybrid POMs: (a) *via* alkoxide groups,[73] (b) carboxylate groups ,[74] (c) organosilyl groups[77] (d) organotin groups[78] Colour scheme: P, pink (polyhedra); W, green (polyhedra); Mo, blue (polyhedra); O, red; C, black; N, cyan; S, yellow; Si, light blue; Sn, light yellow.

Systems with a nitrogen linkage were found to have an unconventional coordination mode compared to other *p*-block elements; the nitrogen atom is directly linked to metal centres of POMs *via* multiple metal-nitrogen bonds. This organoimido derivation was extensively studied for the hexamolybdate Lindqvist type POM[81] and with only few examples for other POM systems.[82-84] Several synthetic paths were established to selectively synthesise mono- or di-substituted hexamolybdate hybrid species;[81,85] over the course of these studies multi-substituted clusters were found ranging from di- up to hexa-substituted (Figure 7).[86,87]
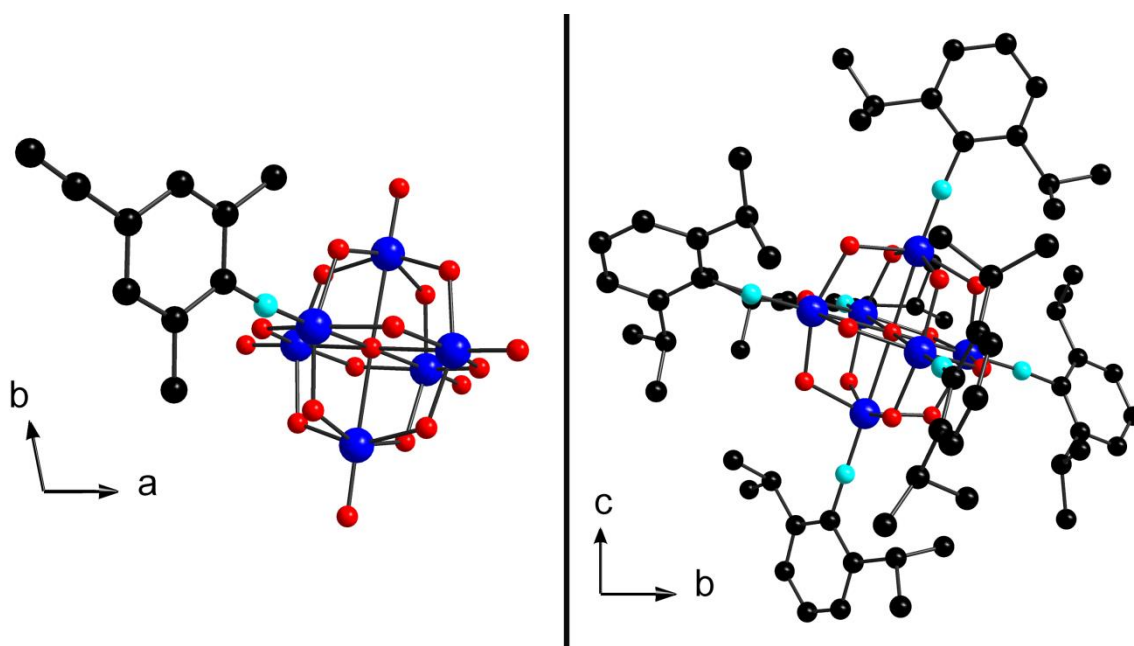
Figure 7: ball-and-stick crystal structure of hexamolybdate organoimido derivatives. (left) Example of a mono-substituted mode obtained with the 4-ethynyl-2,6-dimethylphenylimido ligand;[85] (right) example of a hexa-substituted cluster containing six 2,6-diisopropylphenylimido ligands.[86] Cations and H are omitted for clarity. Colour scheme: Mo, blue; O, red; C, black; N, cyan.

1.2.1.1 Hybrid formation with alkoxide ligands

The present work will focus on organic-inorganic hybrid POM of class II formed by incorporation of alkoxide ligands in their metal oxygen-framework and, more precisely, on the hybrid obtained for the Anderson structure. The formation of such hybrid POMs is presented here in further detail.

The TRIS compound (tris-(hydroxymethyl)-aminomethane; represented in Figure 8a) is commonly used either as a tris-alkoxide ligand directly incorporated into the POM structure or as a precursor for the synthesis of TRIS-based ligands (general formula $(HOCH_2)_3CR$; Figure 8b). Hereafter "TRIS" hybrid POMs refers to compounds

incorporating the TRIS molecule as a ligand, while "TRIS-based" hybrid POMs is used as a generic term for any tris-alkoxide ligand.
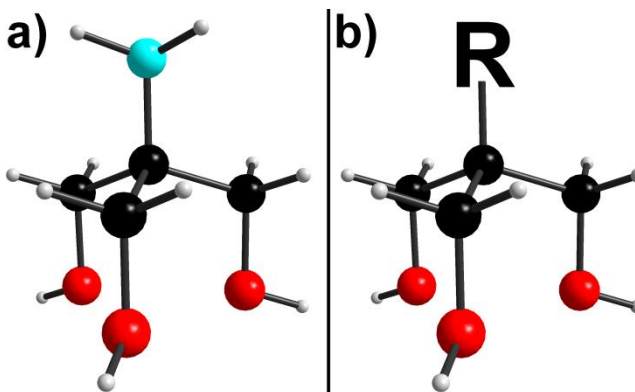
Figure 8: Tris-alkoxide ligands commonly used for organic-inorganic hybrid POM systems. (a) tris-(hydroxymethyl)-aminomethane (TRIS); (b) TRIS-based ligand. Colour scheme: O, red; C, black; N, cyan; H, light grey.

It has been known for more than two decades, mostly through the investigations carried out by J. Zubieta, that alkoxide ligands (*e.g.* methanol) and TRIS-based ligands can be incorporated in the metal-oxygen framework of POMs,[88-90] but it is only recently that these ligands are viewed as remote sites to control the POM properties and form novel hybrid POM-based materials. The covalent link formed between the metal-oxygen framework and the tris-alkoxide ligands allows a direct interaction of the two moieties and has been found to stabilise the POM structures.

This stabilising effect of TRIS-based ligands is best illustrated through the polyoxovanadate species. Polyoxovanadates containing "naked" trinuclear units ($[V_3O_{13}]^{q-}$ with q = 14 for V^{IV} and q = 11 for V^V) are rare due to their high negative charge density, explaining why the "naked" hexavanadate Lindqvist structure has never been obtained.[91] In order to access these low nuclearity systems, the overall charge of the polyoxovanadate clusters should be decreased, which is realised by the incorporation of tris-alkoxide ligands whose geometry correlates the one of the trinuclear units. Many TRIS-based hybrid polyoxovanadates not accessible without the stabilising effect of the ligand have since been reported,[88,89,91-95] examples of which are given in Figure 9. Interestingly, mixed valence clusters were also isolated, demonstrating the diverse aggregation patterns that polyoxovanadate chemistry offers.[91] Organic-inorganic hybrid chemistry of the hexavanadate POM has been further developed and more intricate ligands were incorporated into the cluster, yielding the formation of coordination complexes[94] and polymers.[92] The hybrid hexavanadate system is interesting because of its stability towards

hydrolysis and its capacity to be extensively and reversibly reduced. It also offers the possibility of forming "asymmetric" clusters, bearing two different ligands at each coordination site, as established by C. Hill et al.;[95] nevertheless, the pure asymmetric cluster was never isolated.
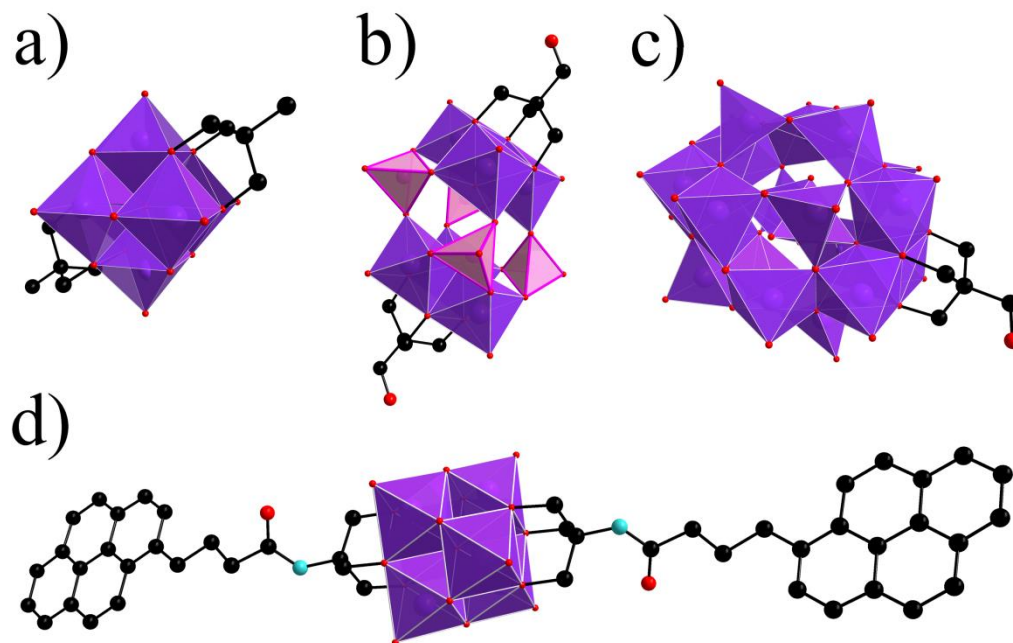
Figure 9: Examples TRIS-based hybrid polyoxovanadate clusters. (a) Hexavanadate cluster $[V_6^VO_{11}(OH)_2((OCH_2)_3CCH_3)_2]$;[89] (b) $[H_4V_6^{IV}P_4O_{30}((OCH_2)_3CCH_2OH)_2]^{6-}$;[91] (c) mixed valence clusters $[H_7V_{12}^{IV}V_7^VO_{50}((OCH_2)_3CCH_2OH)]^{7-}$;[91] (d) Pyrene moieties di-substituted hexavanadate structure $[V_6^VO_{13}((OCH_2)_3CNHCOCH_2CH_2CH_2(C_{16}H_9))_2]^{2-}$.[95] Cations and H are omitted for clarity. Colour scheme: V, purple (polyhedra); O, red; C, black; N, cyan.

Similarly it was demonstrated that methanol and tris-alkoxide ligands can, through an esterification process, substitute the hydroxyl groups bridging the vanadium atoms in the $\{V_3\}$ capping unit of the Dawson type cluster $[H_4P_2V_3W_{15}O_{62}]^{5-}$.[96] Depending on the organic ligand designed, this process was shown to lead to the formation of monomers,[97] "dumb-bells"[98-100] as well as dendrimers[96,100] (Figure 10).
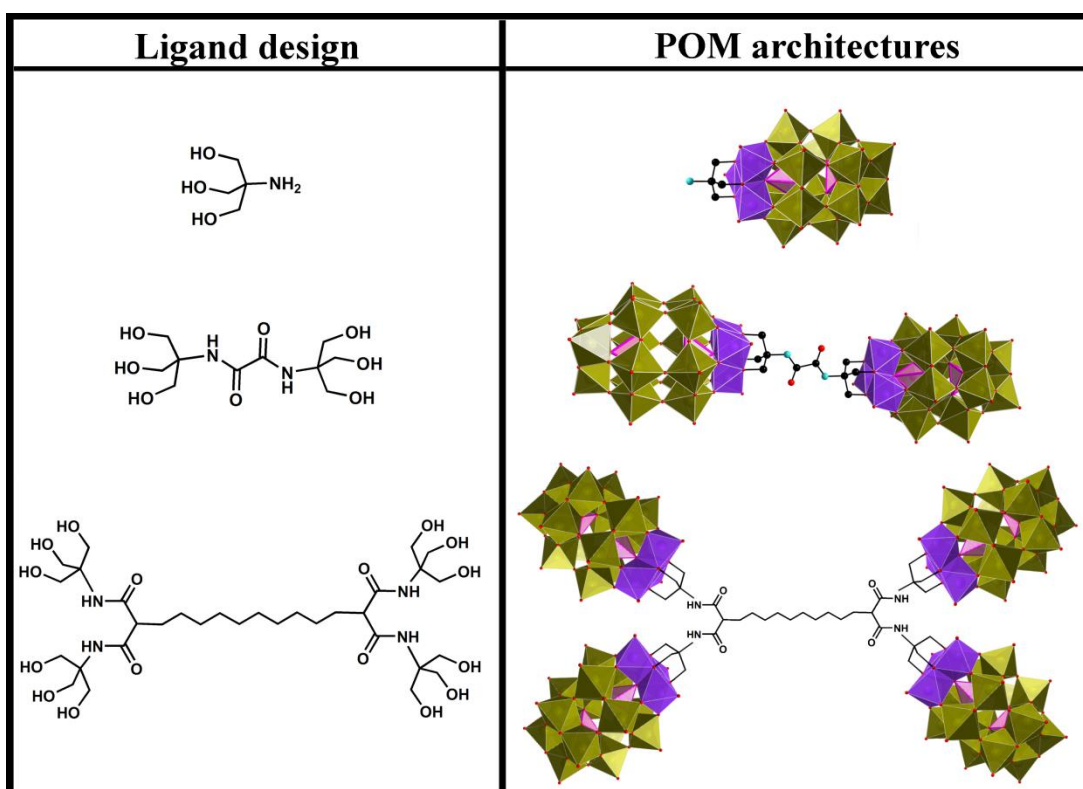
Figure 10: Examples of POM architectures accessible by esterification of $[H_4P_2V_3W_{15}O_{62}]^{5-}$ depending on the ligand design: (top) mono-(tridentate) ligand leads to monomeric architectures;[97] (center) bi-(tridentate) ligand forms dumbbell like structures;[98] (bottom) poly-(tridentate) ligand yields dendrimeric clusters.[96] Colour scheme: P, pink (polyhedra); V, purple (polyhedra); W, green (polyhedra); O, red; C, black; N, cyan.

Another substitution mode involving 2-acetamido-2-ethyl-1,3-propanediol as a ligand has recently been demonstrated (Figure 11).[101] This ligand was linked to the POM cluster *via* substitution of three hydroxy groups located in the {V_3} cap of the POM but, unlike tris-alkoxide ligands, one of these oxo group was replaced by the carbonyl oxygen atom, leading to the formation of a double bond type linkage between the organic moieties and the POM cluster. This new substitution mode demonstrated better electronic exchange properties among the two components of the hybrid POM cluster, attributed to the presence of a double bond.
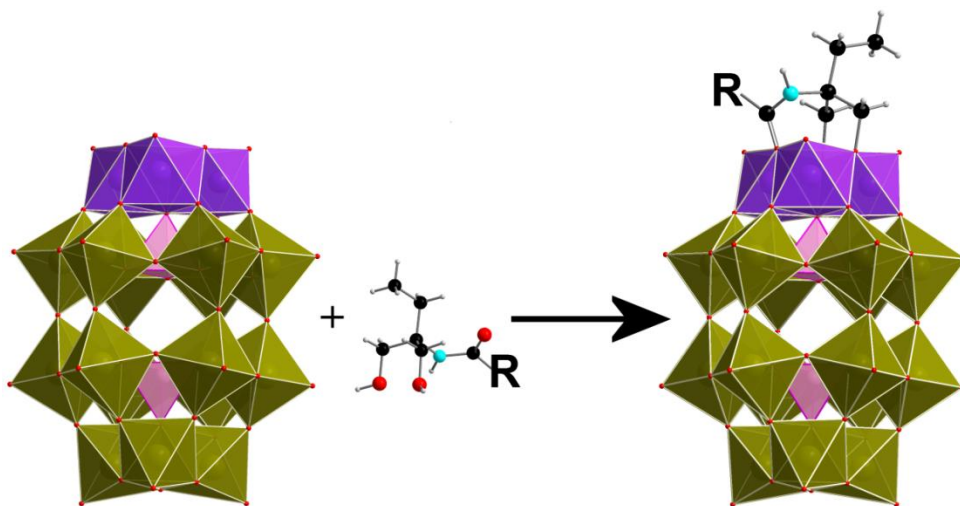
Figure 11: Scheme of the reaction of $\{P_2W_{15}V_3O_{62}\}$ with the 2-acetamido-2-ethyl-1,3-propanediol ligand, resulting in the substitution of one of the bridging oxo group by a carbonyl group (while the two other bridging oxo groups are substituted by alkoxo groups).[101] Colour scheme: P, pink (polyhedra); V, purple (polyhedra); W, green (polyhedra); O, red; C, black; N, cyan; H, grey.

1.2.1.2 TRIS-based Mn-Anderson clusters

The substitution of the six non acidic protons found in the B-type Anderson structure by alkoxo groups was first demonstrated by P. Gouzerh *et al.* with the formation of a TRIS-based hybrid Anderson series: $[XMo_6O_{18}((OCH_2)_3CR)_2]^{3-}$ for $X = Mn^{III}$, Fe^{III} and $[H_2XMo_6O_{18}((OCH_2)_3CR)_2]^{2-}$ for $X = Ni^{II}$, Zn^{II} with $R = CH_3$, NO_2 and CH_2OH.[49] In this now standard protocol, TRIS-based ligands are incorporated during the formation of the metal-oxygen cluster by treatment of the octamolybdate precursor $(TBA)[\alpha\text{-}Mo_8O_{26}]$ with acetylacetonate or acetate complexes of the suitable heteroatom (Mn^{III}, Fe^{III}, Ni^{II} or Zn^{II}) in refluxed MeCN. This yields TBA salts of the corresponding heteroatom di-substituted Anderson hybrid cluster.

As for the B-type Anderson structure, the TRIS-based Anderson hybrids present two different isomers depending on the location of the two grafted ligands (Figure 12). The two tris-alkoxide ligands can be capping the two faces of the central octahedron on either side of the planar arrangement of the Anderson structure (δ isomer), or capping one tetrahedral cavity on each side (χ isomer). The δ isomer is a highly symmetric cluster (D_{3d} symmetry) in which the organic moieties are equivalent, as shown by the presence of a unique signal for all six CH_2O groups by NMR.[49] The χ structure is of lower symmetry (close to C_{2h}) where the CH_2O hydrogen atoms are no longer equivalent, but can be divided into three groups (giving rise to three signals in ^1H NMR), the carbon atoms into two (giving two signals in ^{13}C NMR) while seven types of oxygen atoms are present in the cluster.[49] The δ

isomer is systematically observed for the tri-valent heteroatoms (Mn^{III} and Fe^{III}) while formation of either of the δ- or χ-isomers, or even mixtures of both, are observed for divalent heteroatoms (Ni^{II} and Zn^{II}).[49]
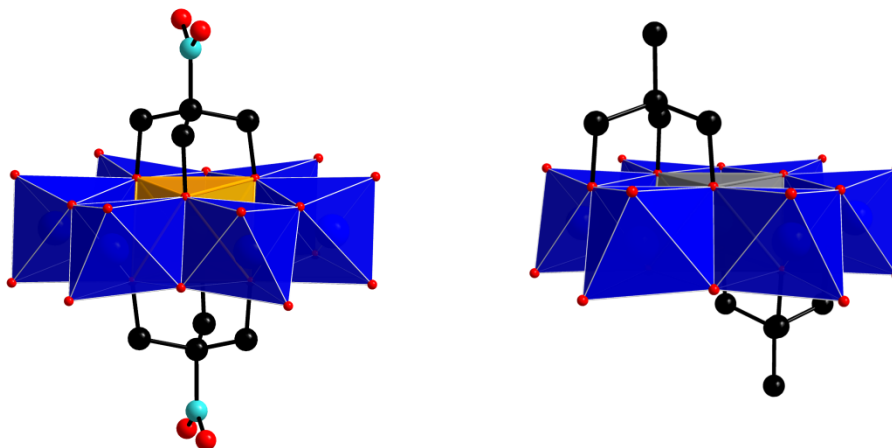
Figure 12: polyhedral and ball-and-stick representation of the δ-isomer (left) and the χ-isomer (right) observed for TRIS-based Anderson compounds.[49] Colour scheme: Mn, orange (polyhedra); Zn, grey (polyhedra); Mo, blue (polyhedra); O, red; C, black; N, cyan.

The mechanism leading to the formation of TRIS-based hybrid Anderson systems was explored through real-time electrospray ionisation mass spectrometry (ESI-MS) studies of the synthesis of the TRIS Mn-Anderson compound $(TBA)_3[MnMo_6O_{18}((OCH_2)_3CNH_2)_2]$.[102] ESI-MS analysis is based on a "soft" ionisation technique, which allows the transfer from solution to the gas phase of large inorganic POM clusters with minimal or no fragmentation. The technique thus permits the investigation of the building blocks present in solution during the synthesis of the POM clusters and allows elucidation of the formation mechanisms. The formation of the TRIS Mn-Anderson cluster was studied following the original protocol consisting of the reaction of $(TBA)_4[\alpha-Mo_8O_{26}]$ with the TRIS ligand and Mn^{III} acetate in refluxed MeCN.[50]
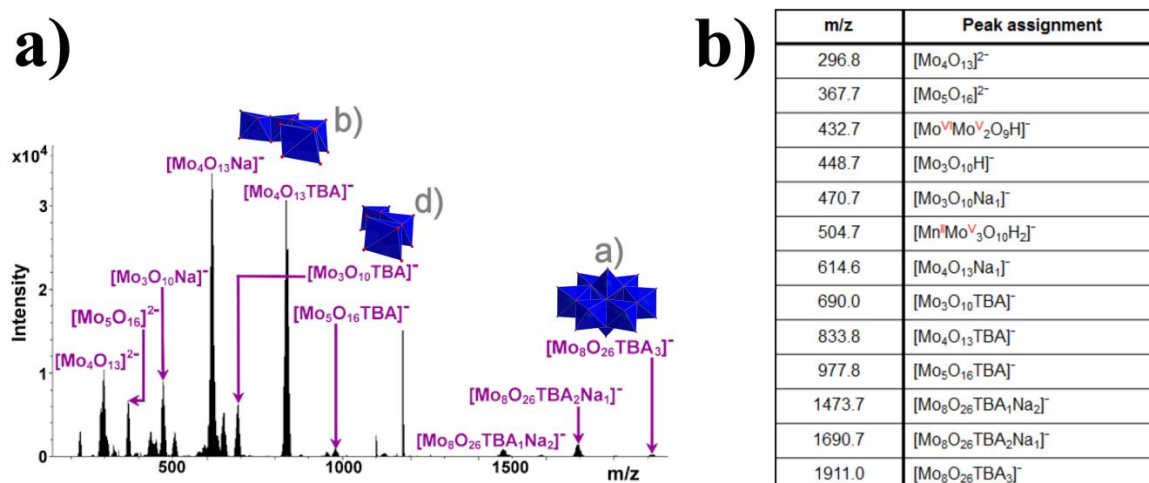
Figure 13: ESI-MS spectra taken at the start (13 minutes) of the reaction of $(TBA)_4[\alpha\text{-}Mo_8O_{26}]$ with Mn^{III} acetate and TRIS and assignment table of the most intense peak envelopes.[102] Colour scheme: Mn, orange (polyhedra); Mo, blue (polyhedra); O, red.

ESI-MS analysis of the reaction mixture 13 minutes after mixing all the reagents in MeCN at room temperature indicates a rearrangement of the $(TBA)_4[\alpha\text{-}Mo_8O_{26}]$ cluster into smaller isopolyoxomolybdate fragments (Figure 13). Reaction intermediates such as $[Mo_2O_5((OCH_2)_3CNH_2)]^-$, $[Mo_3O_{10}TBA]^-$ and $[Mn^{III}Mo_3O_8((OCH_2)_3CNH_2)_2]^-$ were identified as the prominent species after 1 h 20 min of reaction, hence the general mechanism proposed for the formation of the TRIS Mn-Anderson cluster presented in Figure 14.
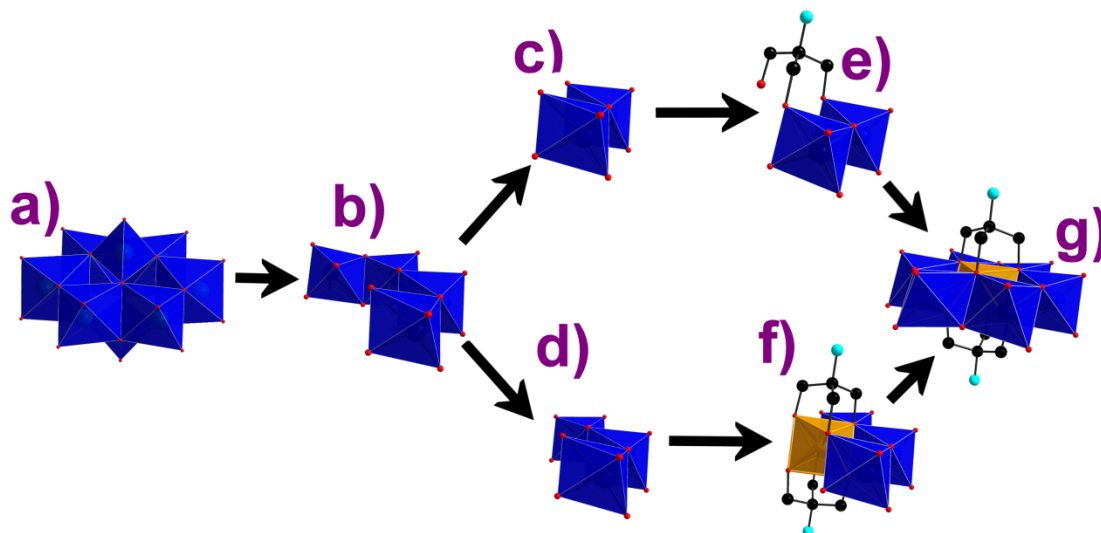
Figure 14: General mechanism proposed for the formation of the TRIS Mn-Anderson cluster $[MnMo_6O_{18}((OCH_2)_3CNH_2)_2]^{3-}$ (labelled g) through rearrangement of the starting material, $[\alpha\text{-}Mo_8O_{26}]^{4-}$ anion (a).[102] Structures (b-f) (based on crystallographic data[50]) represent the following fragment ions identified during the ESI-MS investigations: (b) $[(TBA)_1Mo_4O_{13}]^-$, (c) $[(H)_1Mo_2O_7]^-$, (d) $[(TBA)_1Mo_3O_{10}]^-$, (e) $[Mo_2O_5((OCH_2)_3CNH_2)]^-$, (f) $[MnMo_3O_8((OCH_2)_3CNH_2)_2]^-$. Colour scheme: Mn, orange (polyhedra); Mo, blue (polyhedra); O, red; C, black; N, cyan.

Syntheses of more intricate TRIS-based hybrid Anderson systems were also explored with the development of pre-functionalisation[103-106] and post-functionalisation techniques. [50,107-109] Pre-functionalisation methods are based on the synthesis by standard organic reactions of complex tris-alkoxide ligands (TRIS-based ligands) which are then introduced in the standard protocol to form the new hybrid complexes, while post-functionalisation techniques exploit readily available hybrid clusters (typically the TRIS Anderson compound (TBA)$_3$[XMo$_6$O$_{18}$((OCH$_2$)$_3$CNH$_2$)$_2$] with M = Mn or Fe; TRIS ligand being commercially available) to then modify the hybrid compound by post-synthetic reactions. The post-functionalisation introduces the concept of exploiting POM clusters as modular building blocks which can be modified and incorporated into more intricate chemistries (this approach is detailed in Section 1.2.2).

Synthetically, TRIS-based Mn-Anderson compounds are solely formed from (TBA)$_4$[α-Mo$_8$O$_{26}$] following the procedure established in 2002 by P. Gouzerh *et al.*[49] and therefore isolated as TBA salt compounds soluble in organic solvents such as DMF, MeCN and hot MeOH. However, the properties of the synthesised hybrid POMs can be further tuned by post-synthetic cation exchange treatments giving the cluster new solubility and self-assembly properties.[110-112]

The Anderson structure being able to accommodate two TRIS-based ligands, "asymmetric" clusters, bearing two different ligands at each binding site, should intrinsically be accessible. Nevertheless, to date no synthetic methodology exists that allow the sole formation of the asymmetric cluster, symmetric compounds being systematically present as by-products of the reaction. The isolation of the first asymmetric hybrid POM by separation based on fractionalised crystallisation was demonstrated on the Mn-Anderson type by Cronin *et al.* (Figure 15).[113] Since then, a few reports have described the synthesis of Mn-Anderson asymmetric clusters and have demonstrated that the ligands are another parameter that can be used to tune the hybrid POM properties.[112,114,115] Still, systematic synthesis of asymmetric clusters is hampered by low isolation yields and the lack of reliable and widely applicable isolation techniques with current published procedures requiring constant alterations depending on the ligand system used.
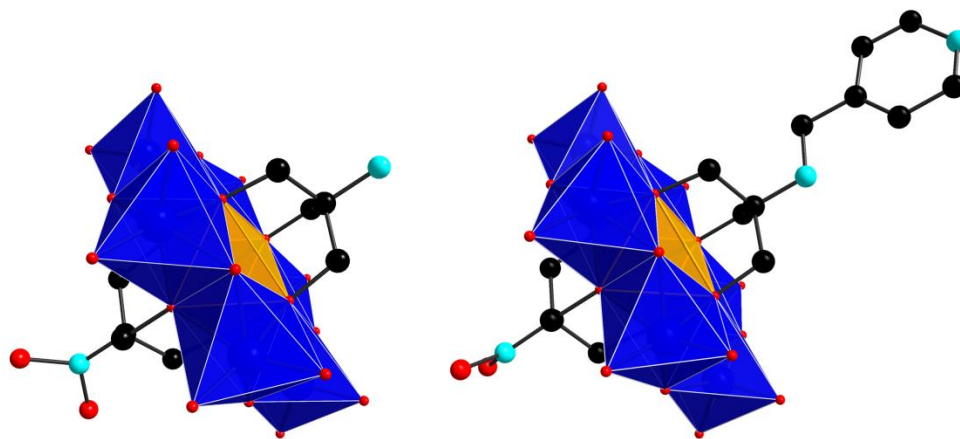
Figure 15: Crystal structure of asymmetric TRIS-based Mn-Anderson compounds [MnMo$_6$O$_{18}$((OCH$_2$)$_3$CR$_1$) ((OCH$_2$)$_3$CR$_2$)]$^{3-}$; (left) R$_1$= −NO$_2$ and R$_2$= −NH$_2$; (right) R$_1$= −NO$_2$ and R$_2$= −NHCH$_2$(C$_5$NH$_5$).[113] Colour scheme: Mn, orange (polyhedra); Mo, blue (polyhedra); O, red; C, black; N, cyan.

Recently, two novel substitution modes were established for a {CrMo$_6$O$_{24}$} Anderson type cluster (Figure 16). A mono-substituted species was formed by the post-functionalisation of the parent compound [CrMo$_6$O$_{18}$(OH)$_6$]$^{3-}$ by treatment in refluxed water with a pentaerylthritol ligand.[116] Following similar reaction conditions, two carboxylic acid containing ligands (3-hydroxy-2-hydroxymethyl-2-methyl-propionic acid) were incorporated symmetrically into the metal-oxide framework, one oxygen of the carboxyl group substituting an oxo group and the two other bridging oxo being replaced by alkoxo groups.[117]
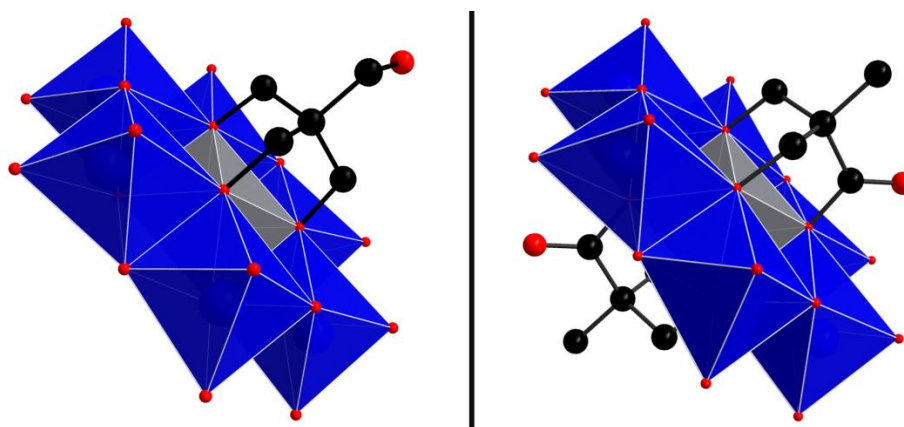
Figure 16: Crystal structure of the mono-substituted TRIS-based Anderson cluster [CrMo$_6$O$_{21}$((OCH$_2$)$_3$C-CH$_2$OH)]$^{3-}$ (left)[116] and the symmetric cluster incorporating two 3-hydroxy-2-hydroxymethyl-2-methyl-propionic acid ligands [CrMo$_6$O$_{21}$((OCH$_2$)$_2$(COO)CCH$_3$)$_2$]$^{3-}$ (right).[117] Colour scheme: Cr, grey (polyhedra); Mo, blue (polyhedra); O, red; C, black.

1.2.2 Hybrid POMs as modular building blocks

Two different approaches exist to covalently functionalise POMs: pre-functionalisation and the post-functionalisation.[24,28] The pre-functionalisation approach requires the incorporation of a pre-synthesised target ligand into the metal-oxide framework, whereas the post-functionalisation approach is based on the synthesis of hybrid POM precursors from generic ligands presenting at least one active site, which are then modified by standard organic reactions to introduce more complex functions (Figure 17). While both approaches present some advantages, the post-functionalisation approach with the prospect of generic building blocks which can be modified in a modular manner seems a more robust strategy for the discovery of viable applications of hybrid POMs. However, modification by organic reactions is not a straight forward process, and protocols established for organic components have to be adapted to the unusual reactivity of the metal-oxide core. The narrow solubility of POMs, their incompatibility with strong bases or acids and their oxidant nature, drastically reduce the reaction conditions available and the number of organic molecules that can be employed.
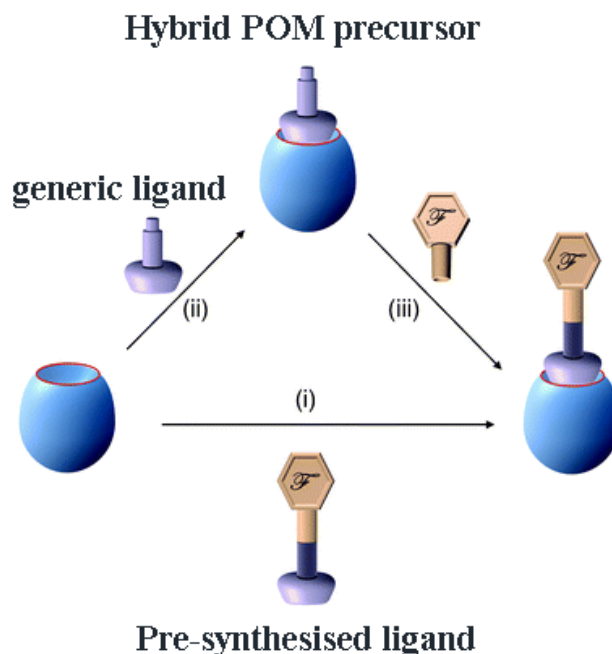
Figure 17: Schematic representation of the two approaches for the synthesis and design of complex organic-inorganic hybrid POMs. Route (i): direct functionalisation by pre-synthesis of a target ligand which is then grafted onto the metal-oxide framework; Route (ii) followed by (iii): synthesis of a hybrid POM precursor *via* incorporation of a generic ligand into the POM cluster, which can then be used as a modular building block and get further functionalised by organic reactions. Colour Scheme: POM, blue; anchoring tether, lilac; added functional moiety, beige. Adapted from Ref. 28 with permission from The Royal Society of Chemistry.

In the present thesis, the concept of organic-inorganic POM precursors for the rational design of functional materials is explored, thus an overview of the existing post-functionalisation techniques is given here (comprehensive reviews can be found in the literature).[22,28] These post-functionalisation techniques require the synthesis of hybrid POM precursors; examples of common precursors encountered in post-functionalisation strategies are given in Figure 18. For the purpose of this thesis a particular emphasis is placed upon the incorporation of amino acids or peptide units into hybrid POMs, since the functionalisation of hybrid POMs with these ligands is the object of this thesis.
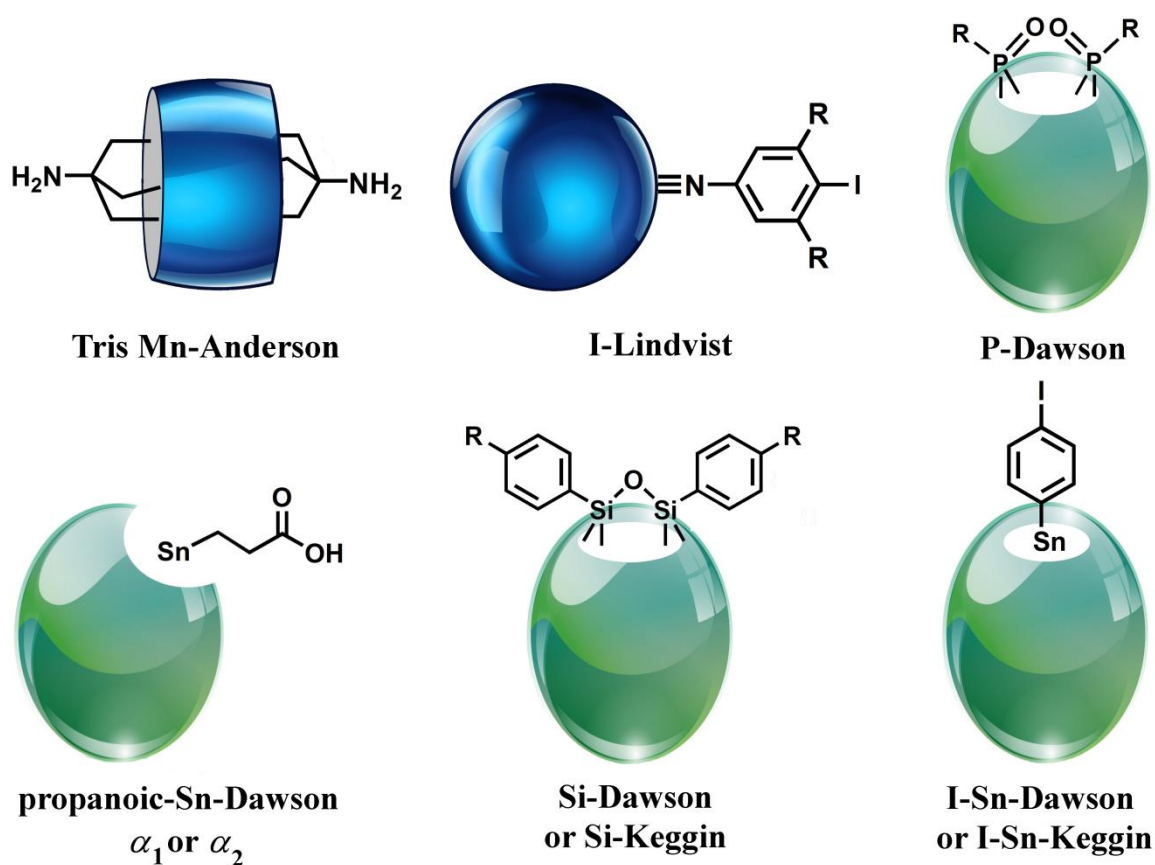
Figure 18: Schematic representation of common precursors encountered in post-functionalisation strategies; the metal-oxide framework is represented by geometric forms to highlight their role as a "spectator" in post-functionalisation processes. POM core: **Tris Mn-Anderson**: $\{MnMo_6O_{24}\}$;[49] **I-Lindvist**: $\{Mo_6O_{18}\}$;[85] **P-Dawson**: $\{P_2W_{17}O_{61}\}$;[118] **propanoic-Sn-Dawson**: $\{P_2W_{17}O_{61}\}$. The α_1-isomer is observed when the lacuna is formed on the "belt", while for the α_2- type the lacuna is located on the "cap";[119] **Si-Dawson** and **Si-Keggin**: $\{P_2W_{17}O_{61}\}$ and $\{PW_{11}O_{39}\}$, respectively;[118,120] **I-Sn-Dawson** and **I-Sn-Keggin:** $\{P_2W_{17}O_{61}\}$ and $\{PW_{11}O_{39}\}$.[121]

1.2.2.1 Peptide bond formation

The first protocol for the functionalisation of POMs by amide bond formation was established by B. Hasenknopf and M. Malacria *et al*. in 2003[119] and consists of the post-functionalisation of the **propanoic-Sn-Dawson** precursor (α_1 and α_2) *via* the reaction of primary amines and 2-ethoxy-N-ethoxycarbonyl-1,2-dihydroquinoline (EEDQ) refluxed in MeCN. As highlighted by its authors "*it should be noted that simple α-aminoacids failed to give any amide (no conversion)*" and only the NH$_2$-Tyr-Boc (*tert*-butyloxycarbonyl (Boc) protected tyrosine) led to a reasonable yield (90%). The reason for the amino acids' poor reactivity is their low solubility in the solvent system (MeCN). Nevertheless, the reaction condition established (EEDQ in MeCN) are often employed for post-functionalisation through amide bonds of this Dawson building block[122-125] and were found to be applicable to other POM units such as the **TRIS Mn-Anderson** type.[109,115]

Further developments of the post-functionalisation methodology of the **propanoic-Sn-Dawson** unit were later reported by the same group.[126-128] Firstly, an in-depth study of the coupling reagents and reaction conditions (reflux, room temperature, 0 °C) was realised.[126] Chloroformate mediated coupling in the presence of base was found to be the most suitable path for amide formation; yet no actual peptide chains were used as reagents in this report, only a series of amines and a few amino acids (Phe, Tyr). Interestingly, the same reaction in absence of a nucleophile was found to lead to the formation of an **acylated-Sn-Dawson** precursor (α_1 and α_2; Figure 19).[127] The α_1- type exhibiting a chiral arrangement, a mixture of the two enantiomers was isolated.
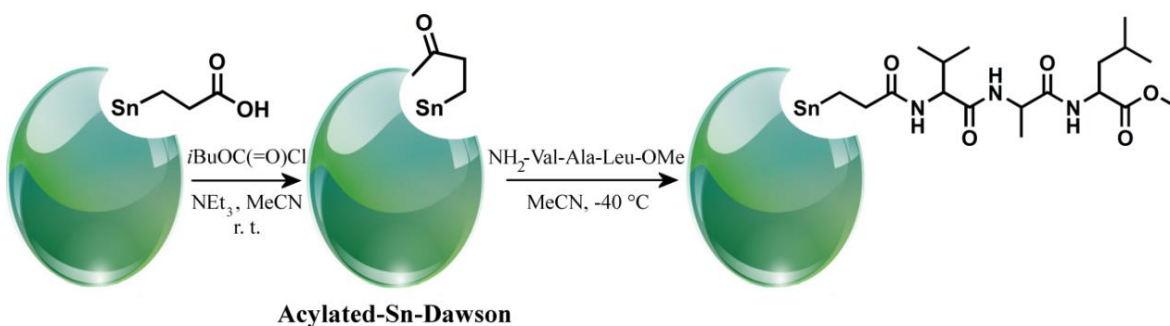
Figure 19: Synthesis of an **acylated-Sn-Dawson** precursor which can react to form peptidic bonds with peptide chains under mild conditions, as shown here with the addition of the tri-peptide NH$_2$-Val-Ala-Leu-OMe.[128]

The ligand of this novel building block is activated by the POM-framework allowing reactions with primary amines to occur under very mild conditions (in MeCN or DMSO and at room temperature) without the addition of coupling agents.[127] Using this approach,

tri-peptides were successfully grafted onto the POM cluster without the requirement of a protecting group (Figure 19).[127,128] It was demonstrated that these tri-peptides could be used for enantiomeric kinetic resolution of the α_1-acylated precursor since the amino acid sequence was able to interact with the metal-oxygen framework and therefore preferentially react with one of the enantiomeric compounds.[128]

Pre-activated organic moieties, by *N*-Hydroxysuccinimide (NHS)-ester or acyl chloride groups, were also proven to successfully form amide bonds on pre-formed hybrid POM precursors.[95,107]

1.2.2.2 "Click chemistry" type reaction

The concept of "click chemistry" was introduced by Sharpless in 2001 to describe reactions that "*must be modular, wide in scope, give very high yields, generate only inoffensive by-products that can be removed by non-chromatographic methods, and be stereospecific (but not necessarily enantioselective). The required process characteristics include simple reaction conditions (ideally, the process should be insensitive to oxygen and water), readily available starting materials and reagents, the use of no solvent or a solvent that is benign (such as water) or easily removed, and simple product isolation.*"[129] While POMs are not necessarily compatible with the "green" click chemistry idea, the reactions that result are still applicable and are particularly interesting for modular modification of preformed hybrids.

Many reactions fall into the large definition of "click chemistry" among which are the nucleophilic opening of spring-loaded rings and cycloaddition reactions.[129,130] Only the latter type was explored for POM post-functionalisation through the copper catalysed Huisgen 1,3-dipolar cycloaddition and the Diels-Alder reaction.

The copper-catalysed 1,3-dipolar cycloaddition reaction between alkynes and azides to form selectively 1,4-disubstituted 1,2,3-triazoles[131,132] is intensively used as a "fusion" process in polymer chemistry,[133,134] nanotechnology[135] and chemical biology.[136] Its ability to link together two complex molecules was also explored in POM chemistry but exclusively for polyoxotungstate species since they are weaker oxidants than polyoxomolybdate clusters.[122] Reaction conditions for the formation of the triazole bond were first established by Malacria *et al.*[122] using the **propanoic**-**Sn-Dawson** precursors and its Keggin equivalent ({$PW_{11}O_{39}$} POM core) modified by amidation to introduce an alkyne or an azide group using the peptide bond formation technique reported in Section 1.2.2.1.[126] Although not drastically different from standard protocol,[131] the reaction

conditions were adapted to the solubility of the POM and its tendency to form ion pairs with Cu^{2+}. A water/MeCN mixture was preferred to the usual water/alcohol conditions and the number of equivalents of sodium ascorbate, the reductant, was increased to ensure the *in situ* formation of the Cu^{I} catalyst. These reaction conditions allowed the grafting of the **propanoic-Sn-Dawson** precursor to carbohydrates, amino acids (such as tyrosine), and a tri-peptide (tri-valine; Figure 20).
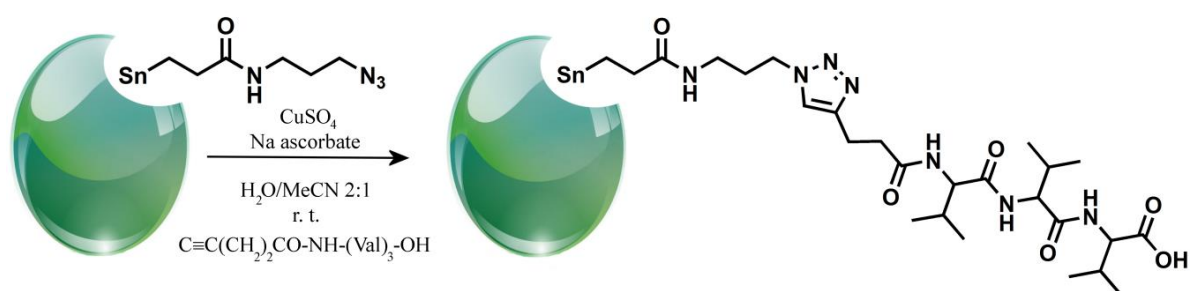
Figure 20: Copper-catalysed 1,3-dipolar cycloaddition reaction performed on the azide functionalised **propanoic-Sn-Dawson** precursor yielding a covalently grafted tri-peptide onto a Sn-Dawson POM.

Similar reaction conditions applied on **Si-** and **P-Dawson** type precursors with an azide or alkyne anchoring tether led to the formation of POM-chromophore dyads, with the introduction of perylene[118] (Figure 21) and porphyrin[137] pendant groups. A fluorescence quenching was observed, attributed to an intramolecular electron transfer from the chromophore to the POM. However, poor electronic conductivity of the triazole bond was observed: one electron reduced POM species were formed but the electron transfer from the organic antenna to the POM was a slow process.
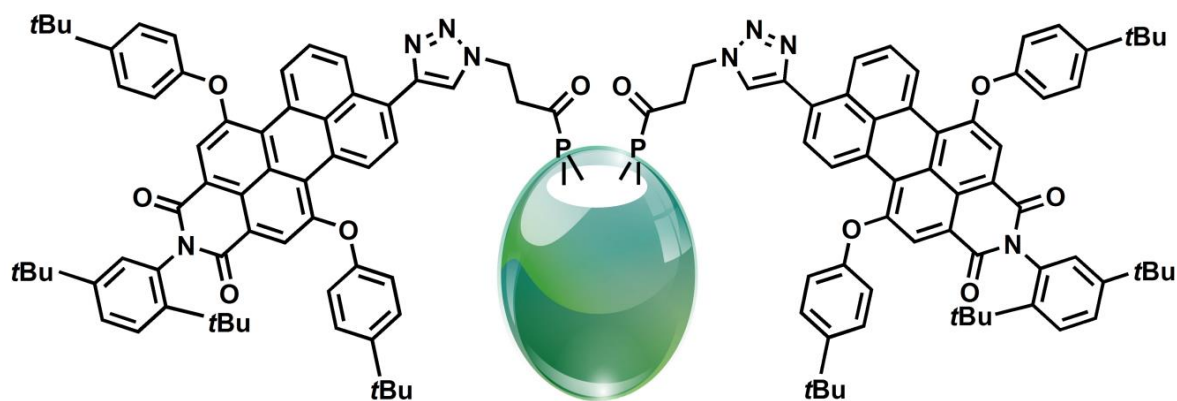
Figure 21: POM-chromophore dyad synthesised by copper-catalysed 1,3-dipolar "click reaction" on the **P-Dawson** precursor.

Through these reactions, the copper-catalysed 1,3-dipolar cycloaddition proved to be an efficient mean of linking covalently intricate organic functional units with polyoxotungstate precursors.

The Diels-Alder reaction of a diene with an alkene to form a six membered ring present numerous advantages for modular additions of two components: no intermediate is generated over the course of the reaction, no catalyst is required, and under specific conditions the process can be reversible.[138,139] This reaction was explored for the **TRIS Mn-Anderson** precursor functionalised with diene and dienophile moieties by peptide bond techniques. A large variety of organic motifs – among which a biotin group, a polyhedral oligomeric silsesquioxane cluster and a second generation poly(urethane amide) were grafted onto the POM precursor by [4+2] cycloaddition in refluxed MeCN or DMF (examples given in Figure 22). Surprisingly, this report[109] is the only recent use of the Diels-Alder click reaction for the post-functionalisation of POMs; Prior to this, in 1986, a publication[140] described the use of this reaction to post-functionalise some Keggin and Dawson type cyclopentadienyltitanium polyoxotungstates, which led to the introduction of a wide range of organic functions.
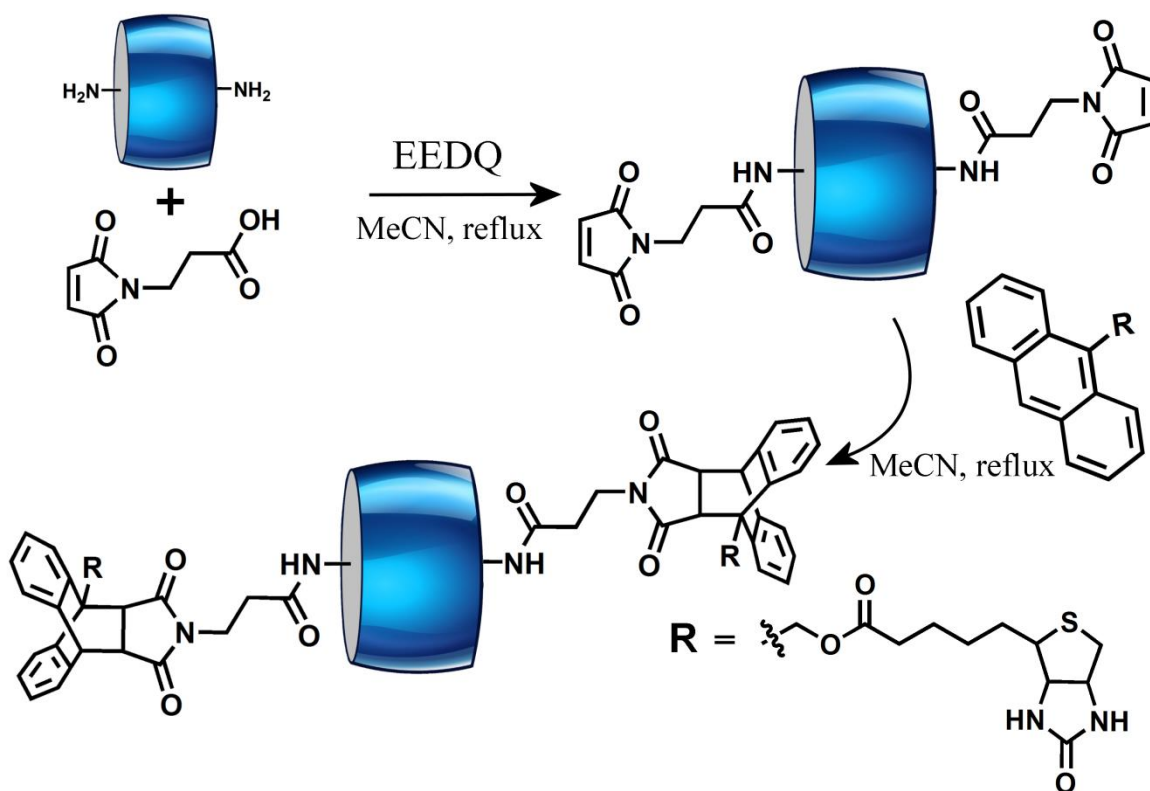
Figure 22: Diels-Alder click reaction on the **TRIS Mn-Anderson** precursor. The POM unit is first functionalised with a dienophile *via* peptide bond formation to then react by [4+2] cycloaddition with an anthracene group bearing functional side chains, here a biotin moiety.[109]

1.2.2.3 Pd-catalysed cross coupling reactions

Pd-catalysed cross coupling reactions are powerful organic chemistry tools which permit the formation of carbon-carbon or carbon-heteroatom bonds under mild conditions and are compatible with a wide range of functional groups.[141-143] Such modification tools are interesting for post-functionalisation of hybrid POM precursors and some reported studies have explored the compatibility of these organic reactions with the metal-oxide core.
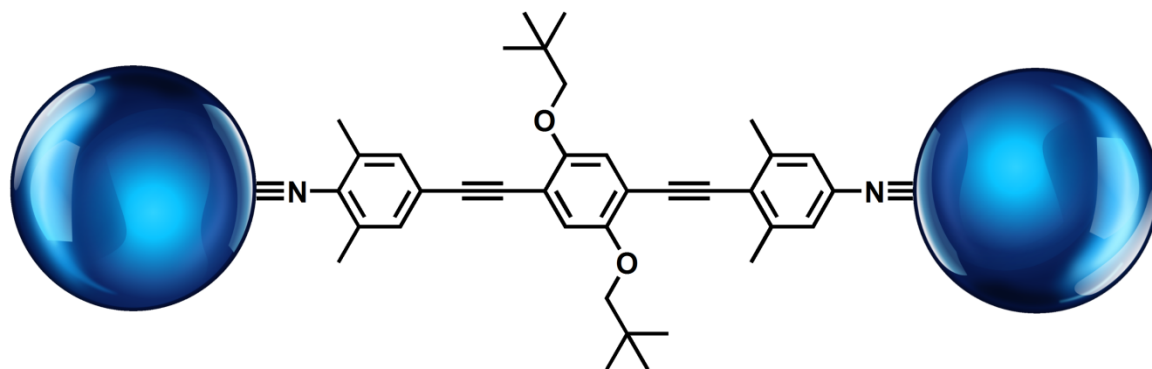
Figure 23: A dumbbell like cluster synthesised by Sonogashira coupling performed on the **I-Lindvist** precursor.[144]

The Sonogashira coupling reaction was widely employed to modify iodoaryl functionalised POM precursors. The penchant for this type of coupling may be explained by the fact that the reaction conditions established for purely organic compounds are compatible as is with most POM precursors.[145] The modification of the **I-Lindqvist** by the Sonogashira coupling reaction was intensively explored by Peng's group;[146] using this technique they introduced the POM unit into dumbbell like clusters[144,147] (Figure 23) or polymers.[148] For these reactions, the POM precursor was treated with the appropriate alkyne in presence of triethyl amine, Copper(I) iodide, potassium carbonate and the palladium catalyst, $[PdCl_2(PPh_3)_2]$ in MeCN at room temperature. They noticed that, not only did the POM cluster survive in these conditions, but the iodo group presented an unusually high reactivity, resulting in the completion of the reaction in only a few minutes.[146] This enhanced reactivity is explained by the electron withdrawing effect of the Mo≡N bond. This coupling type was further used with similar reaction conditions to attach organometallic (a cyclometalated Ru^{II} polypyridine complex) and organic (pyrene) chormophores on **Si-Keggin** and **Si-Dawson** (with R = I in Figure 18) to form photoactive hybrid POM based materials.[120,149] A fluorescence quenching was observed, attributed to an intramolecular electron transfer from the chromophore to the POM: a phenomenon which was faster for the pyrene functionalised materials. Comparison of the covalent bond

with electrostatic interactions demonstrated the importance of the covalent bond for a faster transfer. The results suggest that this type of linkage (the triple C-C bond) is a better candidate for POM-chromophore dyads and electronic conductivity than the previously viewed triazole bond in Section 1.2.2.2.

The reaction conditions for a Pd-catalysed Heck reaction on the **I-Lindqvist** precursor were explored.[150] The protocol established for this type of coupling is somewhat unusual as a bromomagnesium compound was used as a base.

Recently, an in depth study was carried out to establish the reaction conditions of a handful of C-C cross coupling reactions on the **I-Sn-Keggin** and **I-Sn-Dawson** units.[121] The reaction conditions for each reaction were carefully optimised and the resulting procedures are summarised in Figure 24. This work is of high importance since Suzuki, Miyaura and Hiyama couplings had never been attempted before in hybrid POM chemistry.
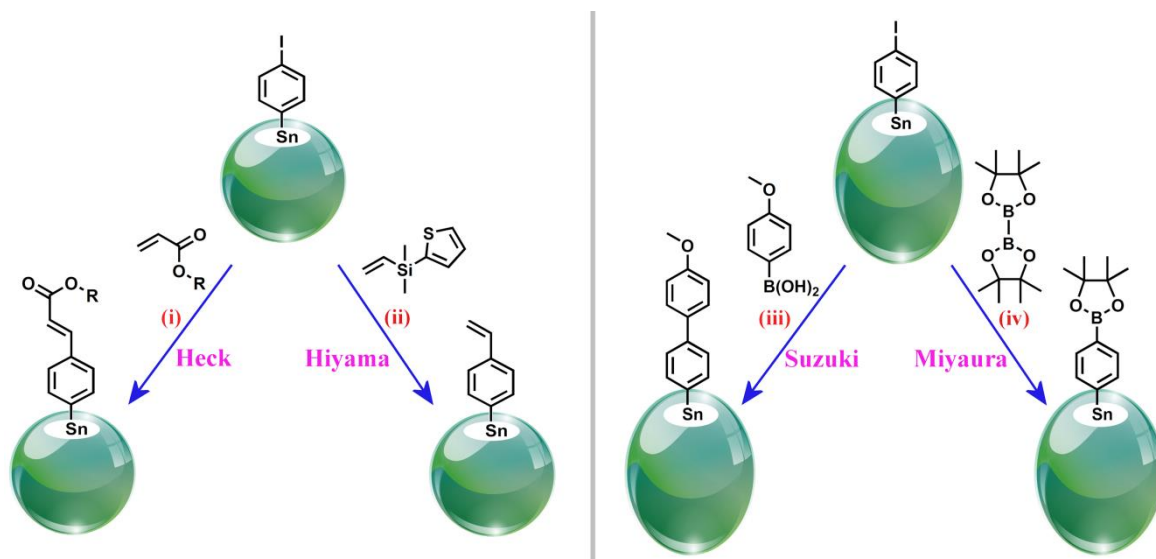
Figure 24: Pd-catalysed cross coupling reactions established for the **I-Sn-Keggin** (left) and **I-Sn-Dawson** (right) building blocks. For optimised reaction conditions see reference.[121]

1.2.2.4 Polymerisation

The incorporation of POMs into ductile polymer host matrices could be a simple and practical means of developing POM-based materials and devices. Early work toward this goal was mainly involving a free radical polymerisation process which led to highly polydisperse materials and difficulties in the characterisation of the resulting polymers.[151-154] The recent development of controlled polymerisation processes,[155,156] such as atom transfer radical polymerisation (ATRP) and reversible addition-fragmentation chain-transfer (RAFT), permits better control of the polydispersities and molecular weights of the obtained polymers, allowing the design of POM-polymer hybrid system.

The formation of a hybrid POM-polymer can be achieved following three different routes: "graft onto", "grown onto" and "grown with". Firstly, the "graft onto" approach, consists of synthesising a polymer chain functionalised in such a way that post-functionalisation can then be used to graft it onto the POM precursors. This was demonstrated for the **α₂-acylated-Sn-Dawson** building block, the **Si-Dawson** precursor (with R = -CH₂N₃) through peptide bond formation[123] and a click chemistry reaction (see Figure 25),[157] respectively.
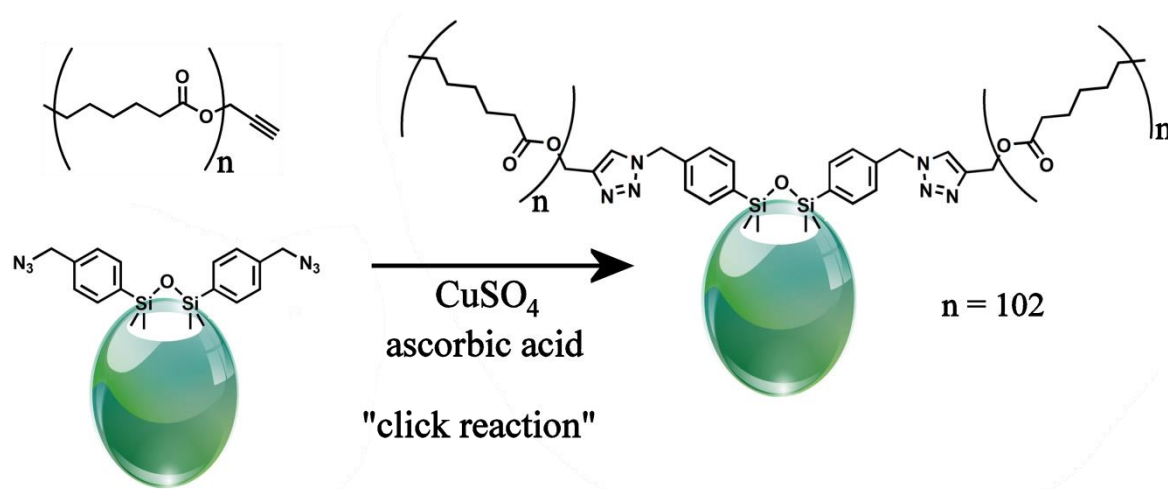
Figure 25: Example of the "graft onto" technique on the **Si Dawson** building block functionalised with an azide group. 1,3- Dipolar cycloaddition reaction is used to attach the polymer moiety to the hybrid POM unit.[157]

In the second approach, a "grown onto" route, the POM precursor is first modified to incorporate a polymerisation initiator and then the polymer is grown onto the POM cluster using controlled polymerisation techniques. In the literature, three examples illustrate this method: an ATRP performed on a TRIS-based $\{P_2W_{15}V_3\}$ type cluster (Figure 26),[158-160] a RAFT performed on a **α1-Sn-Dawson**[125] and a ring opening polymerisation (ROP) on a TRIS Mn-Anderson unit.[108] The "grown onto" approach leads to the localisation of the POM at one end of the polymeric chain. It permits, when hydrophobic monomers are employed, the formation of amphiphilic clusters as demonstrated by Wang *et al.*[158-160] with their synthesis of a polystyrene (PS) tail *via* ATRP onto the TRIS-based $\{P_2W_{15}V_3\}$ type POM precursor (Figure 26). Kinetically favoured vesicular aggregates of an average diameter of 166 ± 32 nm were proved to form when dissolved in DMF. Upon annealing, the self-assembly was modified and nanotubes were formed, showing that over time the POM-polymer molecules rearrange into a more thermodynamically stable assembly.
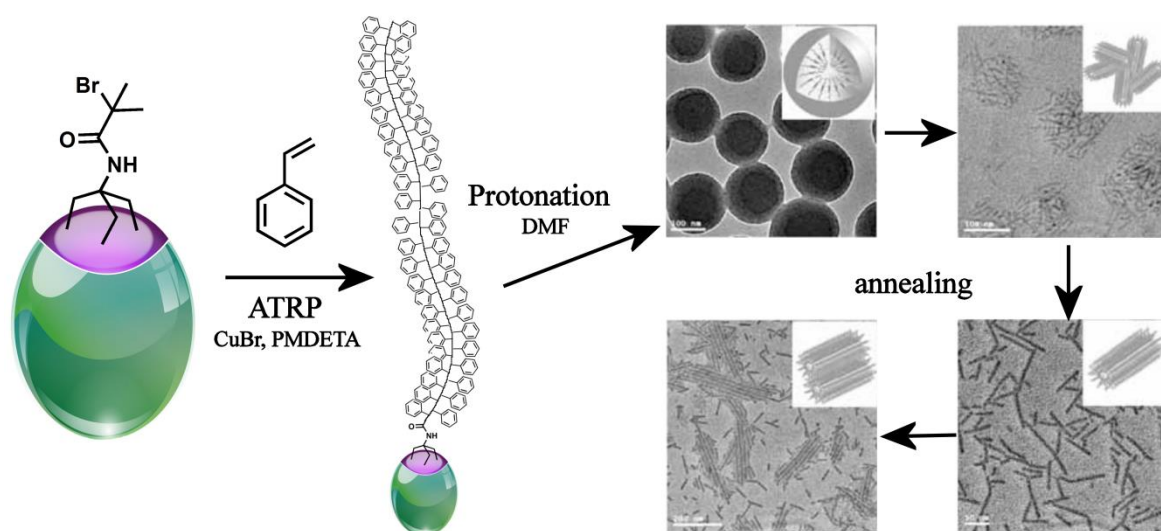
Figure 26: Example of a "grown onto" route with a polystyrene (PS) polymer synthesise on a TRIS-based $\{P_2W_{15}V_3\}$ building block functionalised with an ATRP initiator. [158-160] The resulting POM-polymer hybrid exhibited anamphiphilic behaviour: self-assembly into vesicular structures was observed *via* TEM analysis in DMF upon protonation. Annealing of the polymer makes the vesicules rearrange into fibrils, a more thermodynamically stable structure.

In the third approach, the polymer is "grown with" the POM moiety as part of the monomer employed, resulting in the POM being evenly distributed along the polymer backbone; this approach was recently demonstrated through the synthesis of a norbornene TRIS-based $\{P_2W_{15}V_3\}$ monomer (obtained by pre-functionalisation technique) which was then polymerised by ring-opening metathesis polymerisation (ROMP) catalysed by a Grubbs catalyst (Figure 27).[161,162] Good quality thin films of the hybrid POM-polymer observed by TEM (Figure 27; homogenous and with the POM cluster evenly distributed) were obtained, proving that the incorporation of POMs in polymer matrices is an efficient way to improve their processabilities.
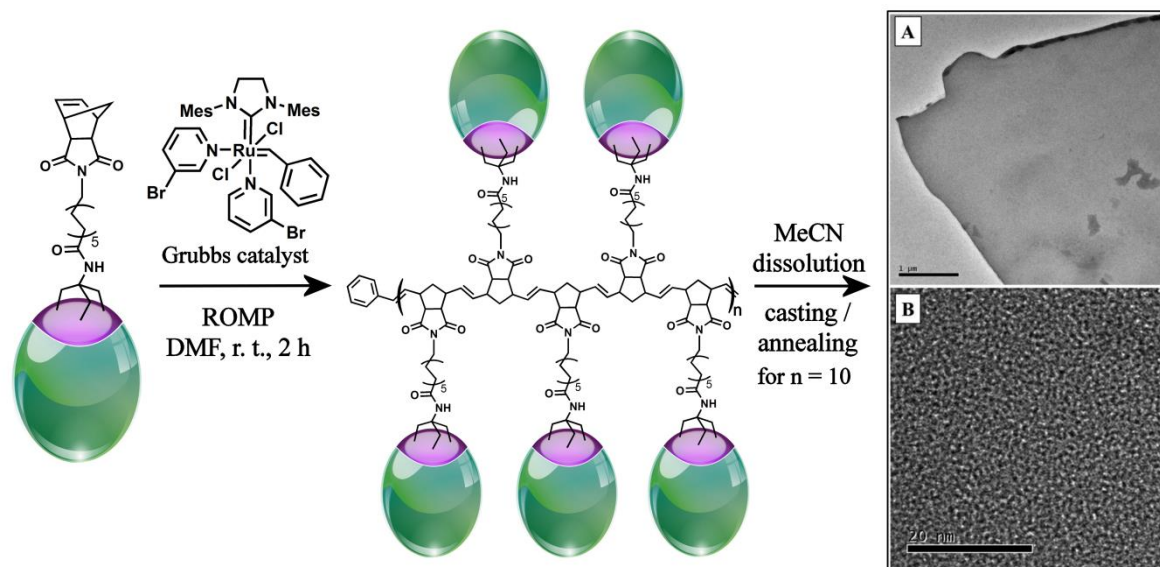
Figure 27: (left) Schematic representation of a "grown with" POM-polymer hybrid by ROMP from a norbornene TRIS-based $[P_2W_{15}V_3]$. (right) Transmission electron microscopy (TEM) images of a thin film prepared by casting/annealing of an MeCN solution of the POM-polymer hybrid. (A) Scale bar represents 1 μm; (B) Scale bar represents 20 nm.

1.3 Amino acids, peptides and proteins

With functions such as transcription, regulation, transport, storage and structural support, peptides and proteins are key components to most biomolecular functional systems, even mechanisms of DNA replication and of gene expression are controlled by proteins. This functional diversity can be bewildering considering that they are all bio-polymers made out of the same fundamental building units, *i.e.* amino acids. Most of this functional diversity comes from their remarkable ability to fold into supramolecular superstructures. Their relative compositional simplicity and their astounding range of properties generated chemist's and material scientist's interests to reliably organise molecules and tailor their properties.

In this section an overview of the structure of peptides is given, followed by the presentation of their chemical synthesis. The use of peptides in nanotechnologies is then shown through a series of recent examples.

1.3.1 Structures of peptides and proteins

Peptides and proteins are formed, under the control of nucleic acids, by the assembly of 20 building blocks (Figure 28): L-α-amino acids (which differ from one another by the composition of their side chain (R)).[163,164] In numerous articles, the term "amino acid" is used as shorthand for L-α-amino acid; although not strictly correct this convenient and common shorthand is used hereafter. Proteins can consist of thousands of amino acids, thus for convenience amino acids are often referred to using their abbreviated name or one-letter code (given in Figure 28).[165]

Amino acids are linked to each other in a head-to-tail fashion by amide or "peptide" bonds, which result in the formation of linear polypeptide backboned macromolecules with a free amino group at one end (termed N-terminus) and a free carboxylic acid group (termed C-terminus) at the other end of the chain. Some exceptions to this simple presentation exist, like the potassium carrier, valinomycin, made of a macrocycle "biting its own tail". The amino acids in the chain are commonly referred to as residues; a polypeptide chain can be as short as two residues (di-peptide) up to thousands of residues long. The frontier between "peptides" and "proteins" is unclear since the differentiation of the terms does not rely on a scientific reality. Conventionally the word peptide is used for short amino acid chains (up to 50 amino acids), while the term protein is usually favoured for longer chains.
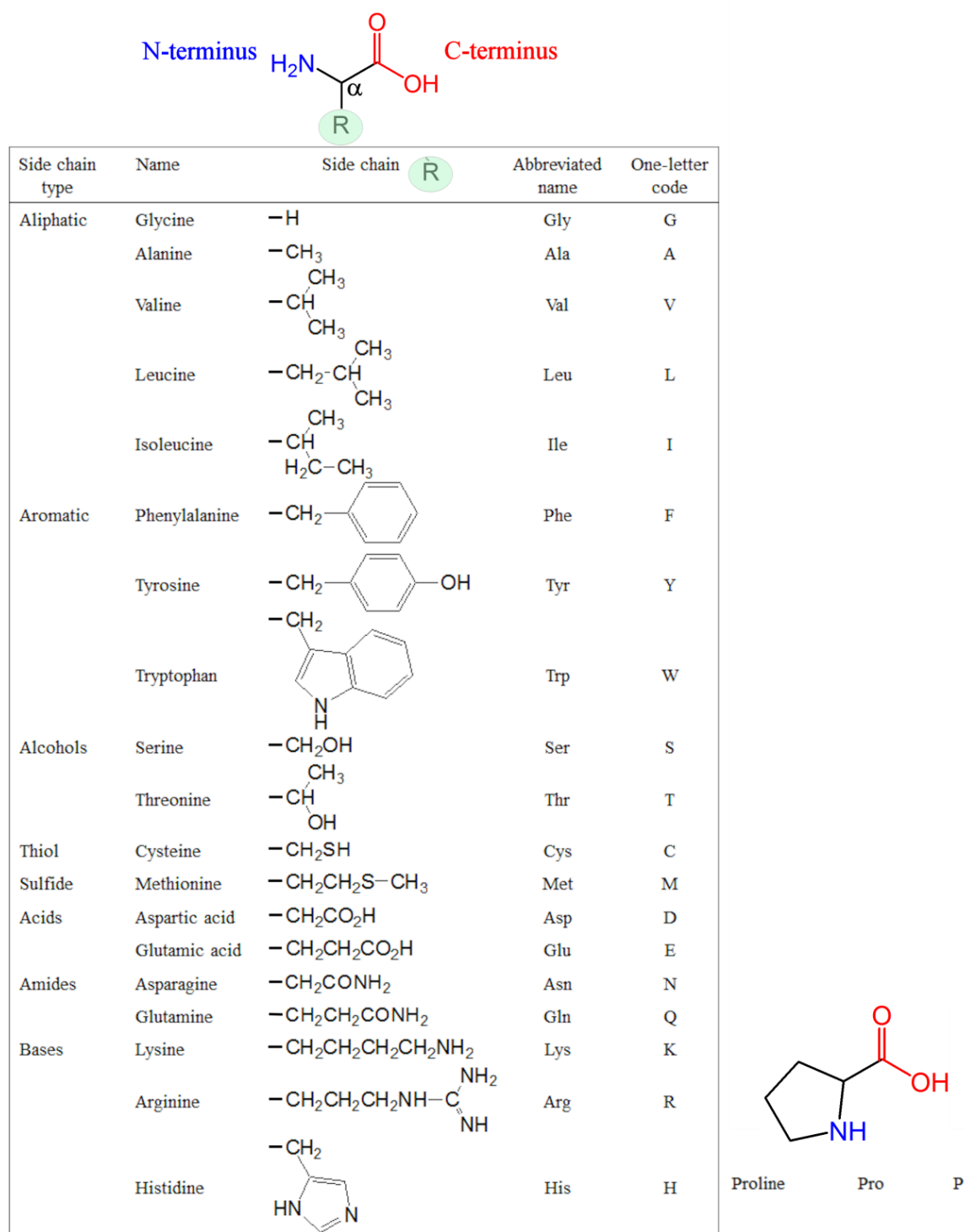
Figure 28: Presentation of the building blocks of peptide chains: the 20 L-α-amino. The amino acids are sorted by side chain functions and each are given with their abbreviated name and their one letter code. L-Proline, the only one made of a secondary amine, is represented separetly.

Peptides and proteins are not just randomly coiled chains of amino acids; spatial organisations are critical characteristics for their activity and function. To assess the complex structure of proteins, their structure is described at four levels of organisation: primary, secondary, tertiary and quaternary structure (Figure 29).[166] The primary structure is defined by the amino acid sequence, always given from the N-terminus to the

C-terminus (in view of being unambiguous about the start and the end of a sequence). The secondary structure gives the conformation of the peptide backbone into regular structural domains such as α-helices and β-sheets. The relationship of the different domains of the secondary structure and the interactions of the amino acid substituent groups (R) are given by the tertiary structure: the complete three-dimensional structure of the polypeptide chain. A full protein can consist of several polypeptide chains, these chains being able to form inter- or intra-chain covalent connections, like disulphide bridges, or be chemically modified (acetylation, hydroxylation, carboxylation…), but non-amino acid components such as minerals, lipids and carbohydrates can also be components of proteins. The quaternary structure describes the interactions of all these different protein components.
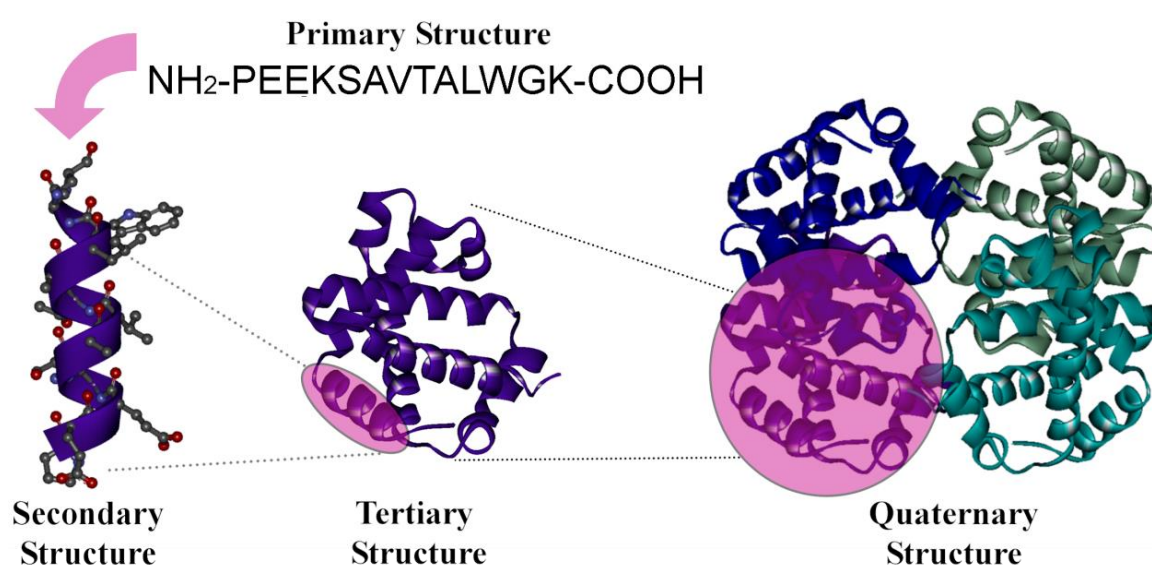
Figure 29: Representation of the four levels of organisation of a protein: primary, secondary tertiary and quaternary structure; example of the crystallographic structure of human deoxyhaemoglobin.[167]

While protein tertiary and quaternary structures are mostly determined by X-ray crystallography[168-170] (structures accessible in the protein data bank (PDB)),[171] other complementary techniques facilitate the evaluation of the structural organisation on various levels. Primary structures can be investigated by peptide sequencing techniques,[166,172,173] these are well established protocols mostly based on mass spectrometry analyses. Circular dichroism (CD) is a technique often used to explore the secondary or tertiary arrangement of proteins since different chromophores found in peptide chains can give rise to CD signals.[174,175] The usual regular structures found in peptides (α-helix, β-turn…) display well-known specific CD signals in the far UV region (240-180 nm; see Figure 30). The study of this region of the electromagnetic spectra, characteristic of the peptide bond absorption, allow the overall secondary structure content of a protein to be assessed. Furthermore, CD spectra in the near UV region (320-260 nm) are representative of the

aromatic amino acids' side chains environment and their study can give information about the tertiary structure of proteins.
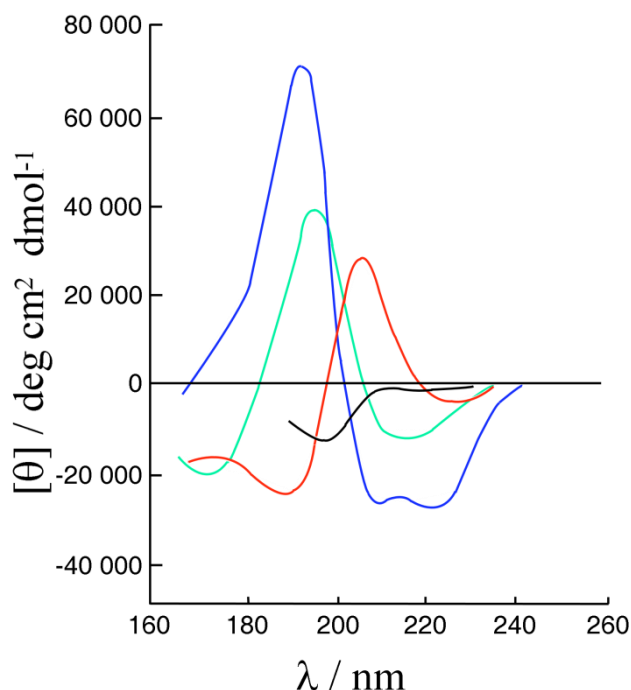
Figure 30: CD spectra of the far UV region and examples of characteristic signals of specific secondary structure: α-helix (blue), anti-parallel β-sheet (cyan) and type I β-turn (red). In black is presented an example of irregular structure signal.

[1]H Nuclear magnetic resonance (NMR) spectroscopy also permits the exploration of the tertiary structure of proteins and gives further insight on the protein structure in near-physiological conditions[173,176,177] – since NMR data can be recorded in solution, parameters such as the pH, the temperature and the salt concentration can be altered to mimic biological environment. Three complementary 2D experiments are widely used to explore the structure of proteins: COSY, TOCSY and NOESY (Figure 31). In the 2D COSY spectra only signals of protons which are two to three bonds apart are visible. The cross peaks due to the coupling of the H_N and H_α protons are of special importance since the ^3J coupling constant between them can be used to determine the torsion angle of the protein backbone (secondary structure). The TOCSY experiment which correlates all protons of a same spin system allows the amino acid composition to be determined. It can then be compared to the NOESY experiment to investigate how the amino acids are linked to each other and obtain the primary structure of the protein. The NOESY experiment also correlates protons which are distant in the amino acid sequence but close in space giving precious information to explore the tertiary structure of proteins.
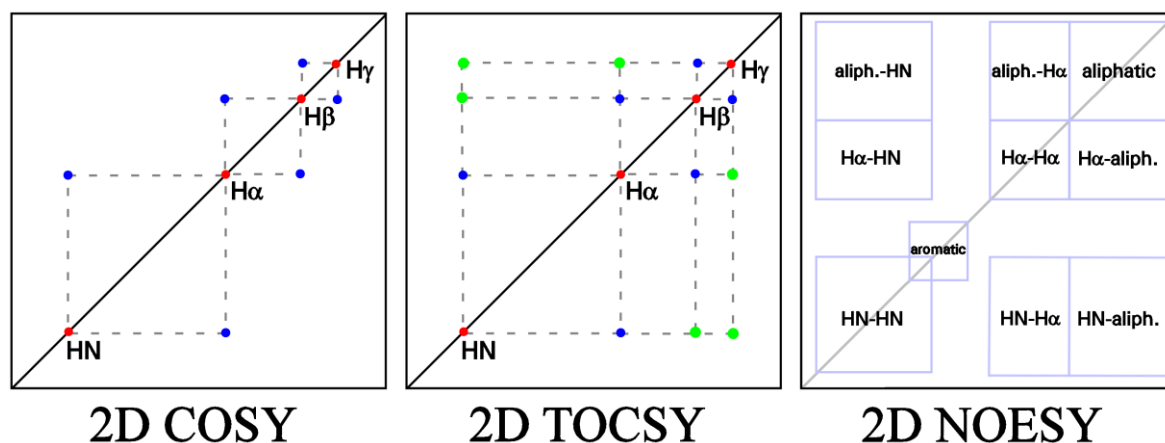
Figure 31: Schematic representation of the information given by each ^{1}H-^{1}H 2D NMR experiment commonly used for peptide structure determination.

The combination of all these structural studies at different scale and in different media brings a better insight on the structure-function relationship of proteins.

1.3.2 Chemical synthesis of peptides

Understanding the relationship between the structures of peptides and their biological activity was a key element to be able to reliably use them in pharmacology or material sciences. Synthetic peptides offer the possibility of substituting one or several amino acids by another or even by unnatural amino acids; the synthesis of numerous analogues to a same sequence can then permit the identification of active sites or the role of an amino acid in the organisation of a chain. The creation of a reliable method for their synthesis was therefore a crucial step for their use in therapeutics and peptide-based materials.

Peptide bonds are easily formed by the reaction of amines with activated carboxylic acids (derivatives which have been extensively developed[178]), however, since amino acids are at least bi-functional units (or more depending on the side chain) and peptides are made of the repetition of these units, the control of which functionalities are reacting is a fundamental point for the chemical synthesis of peptides. This control is obtained by the use of temporary protecting groups, whose role is to deactivate the functions that should not react; these protecting groups are only temporary and, when required, can be removed to retrieve the original reactivity.[179] Peptides are thus synthesised in a stepwise fashion punctuated by amide formation and function deprotection. Since several functions may necessitate protection simultaneously but not necessarily be activated all at once, orthogonal protecting systems have been developed to offer a better selectivity on the function deprotected.[179]

Another major requirement for efficient peptide synthesis is that the amide couplings should be as complete as possible. The reason for this is that, as illustrated in Figure 32, the overall yield decreases rapidly with the number of addition cycle; for steps yields of 90% the overall yield for a peptide of 25 residues being even less than 10%. The completion of each addition steps is critical since changing or omitting just a single amino acid in a key position in a peptide can significantly alter its activity and function.
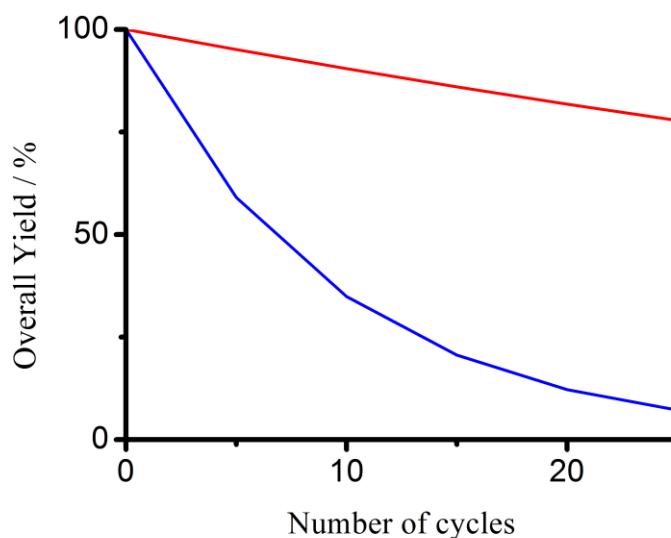
Figure 32: Impact of the step yield on the overall yield. Yield for each coupling cycle: 90% (blue), 99% (red).

Originally the chemical synthesis of peptides was based on a solution synthesis approach, which required the isolation and the purification of the peptide product after each cycle leading to a time consuming and laborious process, with loss of yield even with efficient coupling steps.[180]

In 1963, R. B. Merrifield revolutionised the chemical synthesis of peptides by introducing a new synthetic protocol: the solid-phase peptide synthesis (SPPS).[181] The principle of the SPPS technique, based on the use of an insoluble and filterable cross-linked PS support, is represented in Figure 33.[163,182] In this approach, the growing peptide chain is attached to a solid support *via* its C-terminus and the peptide is synthesised stepwise from the C-terminus to the N-terminus by repetition of coupling/deprotection steps (SPPS cycle). Once the desired peptide sequence is completed, all protecting groups can be removed and the peptide cleaved from the solid support. Since reagents and side products can easily be separated from the growing peptide by filtration and washings, a large excess of reagent is used to drive each coupling step to completion and ensure the synthesis of a peptide of good purity. Another advantage of this approach is that by having the growing peptide

chain covalently attached to a solid support the solubility issues encountered in solution with protected peptide chains does not arise.
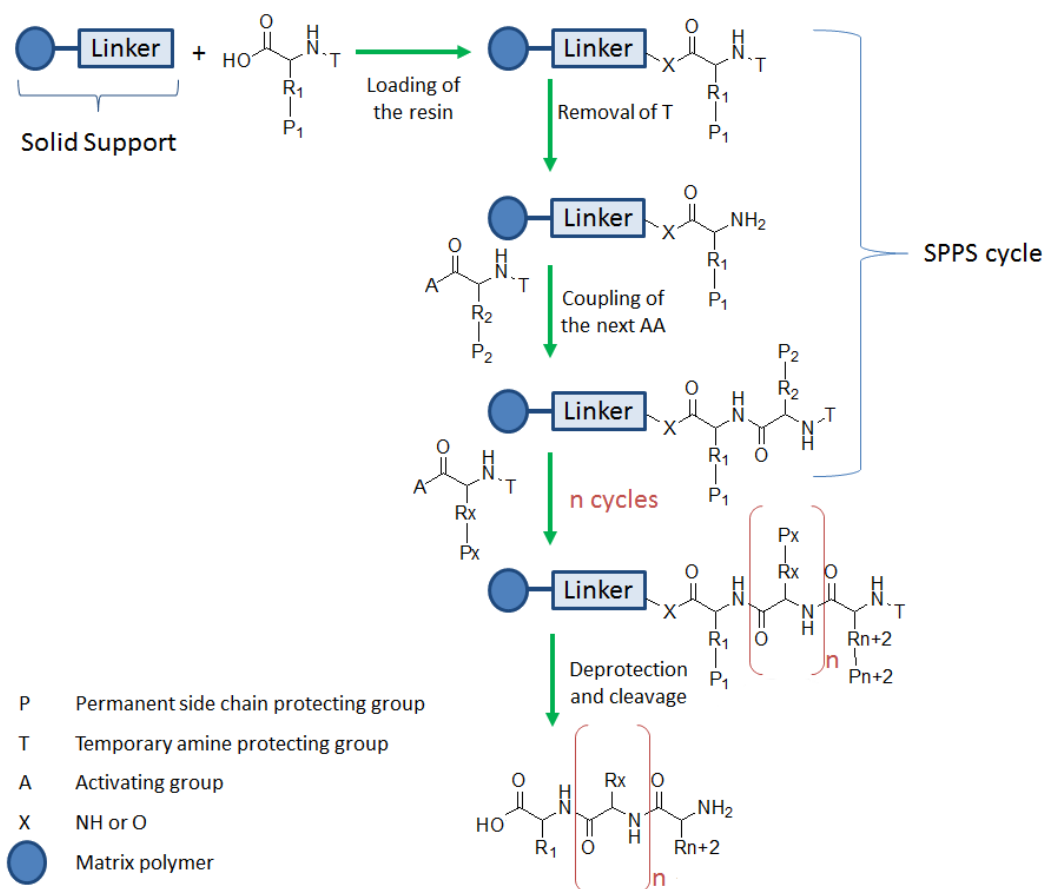
Figure 33: Schematic representation of a standard SPPS process from the resin loading to the isolation of the final product.

Since the publication of the original SPPS method by Merrifield, many aspects of the synthesis have been the object of studies and optimisations giving rise to general simple procedures[182-184] with many tuneable parameters such as the matrix polymer,[185] the linker and cleavage type,[186] the protection system[187] and the coupling reagents.[178] Since the chemical synthesis of peptides is a stepwise process which involves a lot of repetitions and cycles, and because the product is immobilised on a solid support, their synthesis was automated and peptide synthesisers are now commercially available with in-line UV detectors monitoring Fmoc deprotection to deduce each step yield and microwave reactors for faster syntheses.

1.3.3   Use of chemically synthesised peptides in material science

Peptides and proteins have unparalleled self-organisation properties and can form functional structures with unmatched characteristics which inspire chemists to create artificial molecules with similar capabilities. Recent progress in instrumentation coupled with the developments of SPPS now permit the automated synthesis of designed peptides targeting specific properties. Since proteins can act as both building scaffolds and functional entities, their use in nanotechnology could generate a large variety of smart functional materials.

The amount of work in this field is tremendous and continuously increasing, thus the hereafter description of the application of peptides in material science is not exhaustive and has for objective to give a brief overview of synthetic peptides applications; comprehensive reviews on this subject can be found in the literature.[188-190]

1.3.3.1 Aromatic short peptide derivatives

Short peptides, also called very short peptides or oligopeptides, can spontaneously associate to form discrete nanostructures such as nanotubes, nanotapes or nanofibrils.[188,191] The source of this nanoscale organisation is mostly non-covalent interactions and therefore peptide building blocks designed for these materials display groups which can be involved in these interactions (charge complementarity, amphiphile character, π–π stacking, *etc*.). Aromatic groups containing peptides, source of π–π stacking interactions, are a major type of short peptide exhibiting self-assembly behaviours. The aromatic moiety can be present in the sequence (Phe, Tyr, Trp) and/or as pendant groups attached to the peptide chain (peptide derivatives).

The design of peptide building blocks for highly ordered supramolecular architectures is often inspired by Nature. Amyloid fibrillation is the cause many diseases of unrelated origin (prion diseases, type II diabetes and Alzheimer's disease) and although the mechanism of the formation of these fibrils is not fully understood, aromatic residues found in the amyloid-related sequences may be the origin of these highly order assemblies.[192] For example, the FF motif located in diverse regions of the β-Amyloid peptide sequence could be the source of the Alzheimer's disease. When studied on its own, this di-peptide proved to form well-ordered hollow nanotubes (Figure 34), similar to amyloid fibrils, by supramolecular interactions.[193]
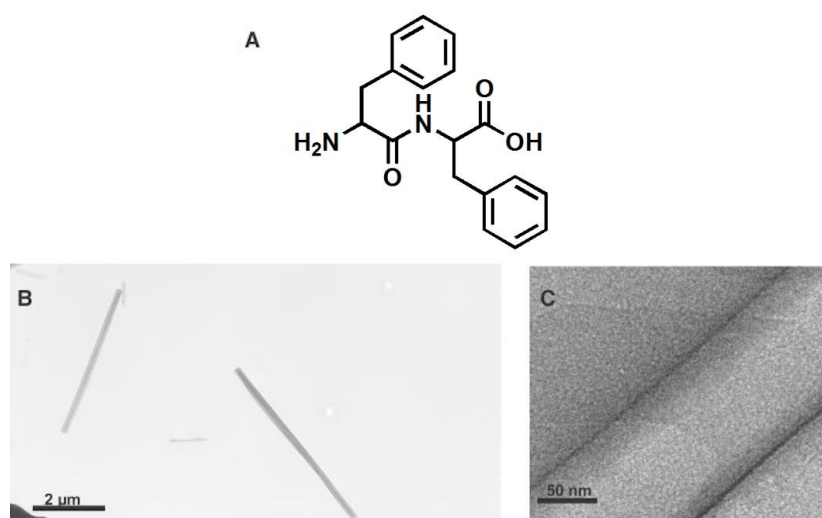
Figure 34: Self-assembly of highly organised peptide hollow nanotubes formed by the FF motif. (A) FF motif; (B) TEM images of the negatively stained nanotubes; (C) HR-TEM of the negatively stained nanotubes, visualised by field emission gun microscope. Adapted from Ref. 193 with permission from The American Association for the Advancement of Science.

These highly ordered nanostructures were then used in a "bottom-up" approach to create a nanosized material. The hollow FF fibrils were used as degradable casting mould by filling the tubes' cavities with a silver solution. This solution was then reduced to produce a silver nanowire of 20 nm diameter (Figure 35), a size that could not be reached by traditional "top-down" approaches.[193]
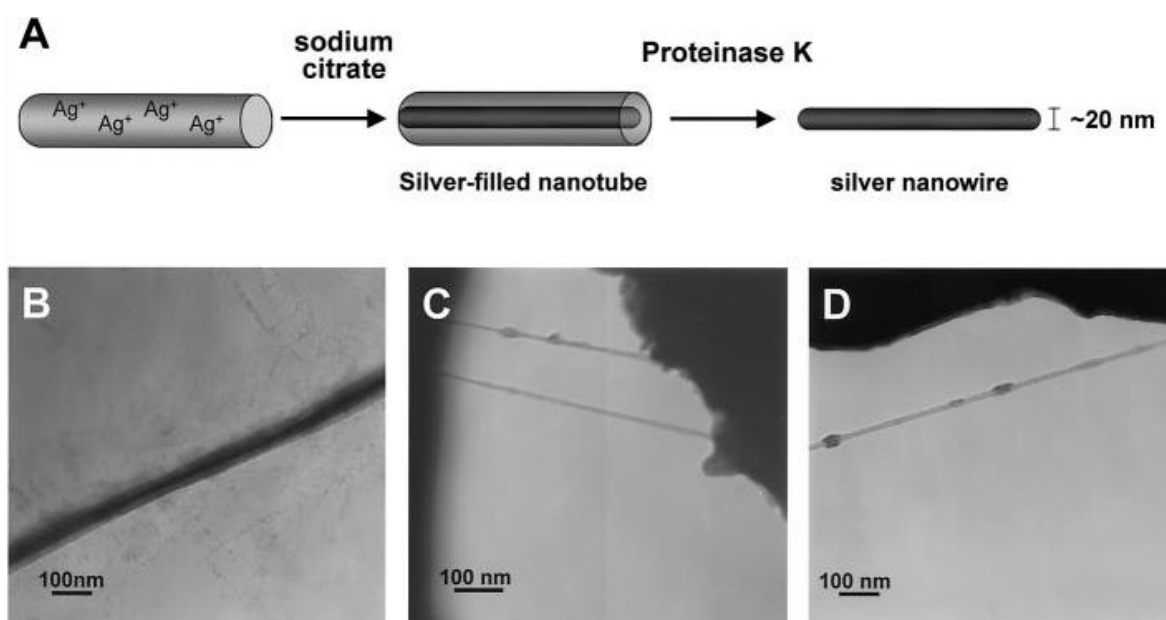
Figure 35: (A) schematic representation of the silver nanowire formation process: silver ions filling the tube cavity were reduced by treatment with sodium citrate to form a silver-filled nanotube, the peptide mould was then eliminated by enzymatic degradation. (B) TEM images of the silver-filled peptide nanotube. (C and D) TEM images of the silver nanowire obtained following this process. Reproduced from Ref. 193 with permission from The American Association for the Advancement of Science.

When functionalised with an aromatic pendant group, short peptides were revealed to act as low molecular weight gelators forming highly organised supramolecular fibrils which interact with one another to give stable self-supporting hydrogels.[194] These hydrogels are highly hydrated (more than 99% water) "solid-like" networks formed by non-covalent interactions (π–π stacking, hydrogen bonding, electrostatic interactions). Aromatic fluorenyl groups[195-198] are the most common derivatives used for hydrogel formation since their incorporation in sequences is directly obtained from peptide syntheses using 9-Fluorenylmethyloxycarbonyl (Fmoc) strategies. Their fluorescence properties also gives an mean of following the arrangement of the molecules, which permits some study of the self-assembly.[198] However, hydrogels based on other aromatic units, such as naphthalene and pyrene, have also been reported.[194]
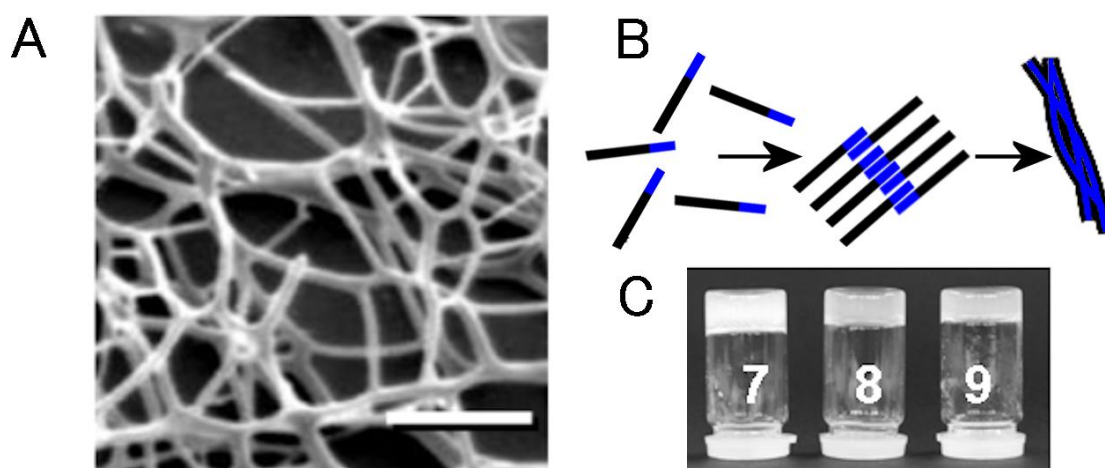
Figure 36: (A) Cryogenic scanning electron microscopy (cryoSEM) image of the nanofibrils obtained by self-assembly of the Fmoc-FF peptide derivative at pH 7. [197] Scale bar represents 1 μm. (B) Schematic representation of the proposed self-assembly mechanism to explain the fibril formation: the Fmoc groups, depicted in blue, stack through π-π interactions and assemble to form well organised nanofibers. (C) Examples of self-supporting hydrogels formed at pH 7: 7, Fmoc-FF; 8, Fmoc-FF/Fmoc-GG 50:50 mol/mol mixture; 9, Fmoc-FF/Fmoc-K 50:50 mol/mol mixture. Adapted from Ref. 197 with permission from John Wiley and Sons. [197] [197] [197]

The properties of the resulting gels are strongly dependent of the composition of the aromatic peptide derivatives. The Fmoc-FF motif demonstrated probably the most interesting behaviour since it forms gel under pH as high as 8, when most Fmoc-di-peptide only form gels at pH below 4. This motif can also be mixed with other dipeptides (50% molar ratio) to produce stable gels at pH around 7.5, proving that the Fmoc-FF improve the poor gelation properties of other dipeptides (Figure 36).[197] These properties were used to form a nanofibrous hydrogel network from Fmoc-FF and Fmoc-RGD units (a short peptide sequence known to promote cell adhesion).[199] The obtained hydrogel was mimicking

some aspects of extracellular matrices and demonstrated to permit cell adhesion, through RGD-integrin binding, as well as cell spreading and proliferation. Potentially, these hydrogels may thus be used as 3D-scaffold for *in-vitro* tissue regeneration for anchorage dependent cells.

By introducing a phosphonyl group onto the Fmoc-FF di-peptide, its self-assembly behaviour in water was totally modified: the resulting molecules acted as amphiphiles, with a hydrophobic Fmoc-FF tail and a polar phosphonyl head, which self-assembled into micelles.[198] This supramolecular arrangement could be disrupted by enzyme catalysed phosphatase to obtain highly ordered fibrils and thus a hydrogel (Figure 37). This property could lead to self-assembled materials whose arrangement is triggered by their environment.
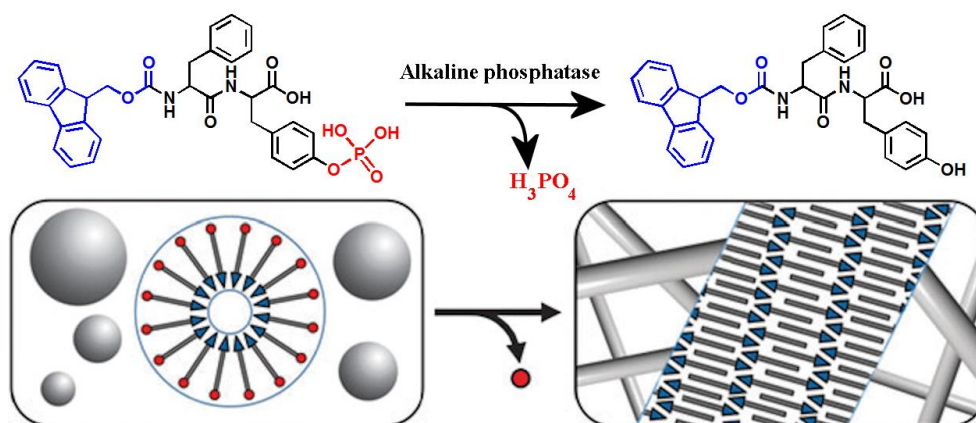
Figure 37: Schematic representation of the self-assembly rearrangement from vesicle to fibrils triggered by enzyme catalysed phosphatase.[198] Reproduced from Ref. 198 with permission from the Royal Society of Chemistry.

1.3.3.2 Controlled assembly by coiled-coil formation

Coiled-coil assemblies, which consist of several right handed α-helixes wound into a left handed superhelix, were first described in 1953 by Pauling and Corey[200] and Crick[201] (Figure 38). However, they only started generating interest with the description of the leucine zipper in 1988, as it revealed to be a source of dimerisation found in DNA binding proteins.[202]

The study of coiled-coils arrangement in natural proteins permitted the establishment of some "rules" to create these assemblies.[203,204] Only right-handed α-helices were found to form coiled-coil arrangements and a distortion of the α-helix was observed. The distorted helices possess 3.5 residues per turn, against 3.6 residues for "standard" α-helices, which allow the amino acids to occupy equivalent positions every two turns/seven residues. Their

sequences can therefore be represented as heptads repeats usually written as [*abcdefg*]$_n$. The amino acids in each position are not necessarily identical, but often present similar properties. For example in the case of a double strand: the residues at the interface between the helixes, *a* and *d*, are often non-polar and hydrophobic; charged residues are encountered in *e* and *g* positions while polar units are located in *c*, *d* and *f*. The strands can interact in a parallel or an anti-parallel fashion; the *a* and *d* residues are then lined up with *d'* and *a'* in parallel coiled-coils but with *a'* and *d'* in anti-parallel ones. Many sequences are known to form coiled-coil assemblies;[205] they have been either designed following the established rules or were part of a sequence of a natural protein.
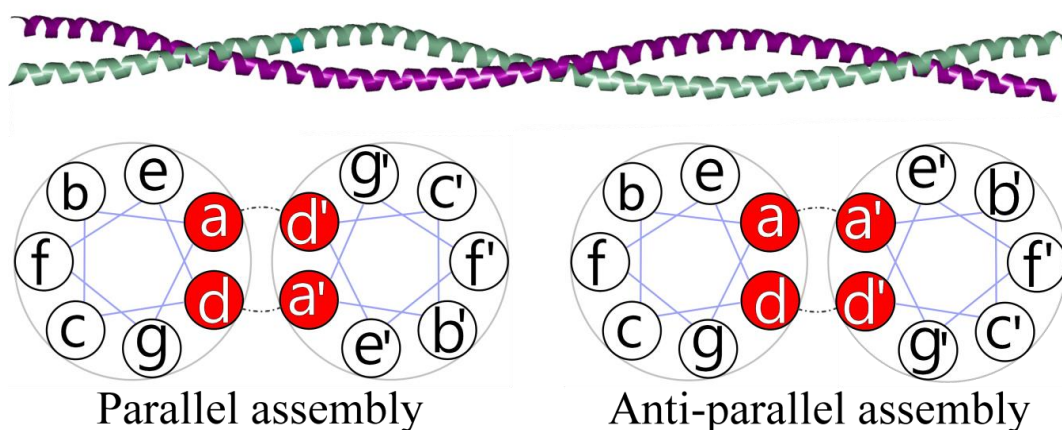
Figure 38: Example of a dimeric coiled-coil and helical wheel representing the heptads arrangements and interactions in a parallel and an anti-parallel coiled-coil. The hydrophobic interaction between *a*, *a'*, *d* and *d'* is highlighted.

This recognition process results inherently in the formation of fibrous structures and is mostly used for the rational design of self-assembling bio-compatible scaffolds.[206-208] By the use of complementary peptide sequences, which when mixed form coiled-coils, these peptide motifs have also been used in nanotechnology to reliably assemble building blocks.[209-211] For example, nanoshell (NS) functionalised with complementary sequences were found to form NS-NS complexes.[209] Due to the NS photothermal properties, it was possible to trigger the disassembly of these complexes by near IR-illumination (Figure 39).
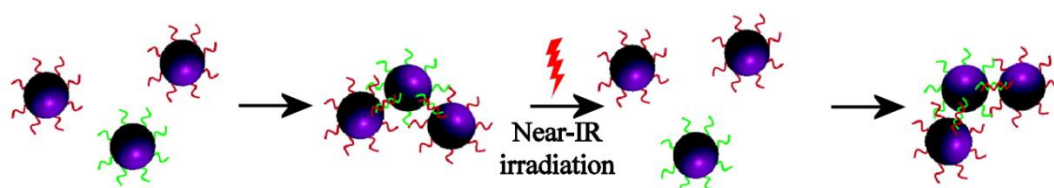
Figure 39: Controlled assembly of NS functionalised with complementary peptide sequence through coiled-coil formation. The assembly process was found to be reversible by exposition to near-IR light.[209] Adapted with permission from Ref. 209. Copyright 2007 American Chemical Society.

1.3.3.3 Peptides for therapeutic developments and cell delivery

In 1988, it was discovered that the *trans*-activator of the transcription (Tat) protein of the human immunodeficiency virus was able to cross the cellular membrane,[212] contrary to the thinking of the time that the plasma membrane was impermeable to hydrophilic molecules. Since then, many peptides have demonstrated similar behaviours, forming a class of peptides commonly called cell-penetrating peptides (CPPs) or protein transduction domains (PTDs).[213,214] CPPs are made of short sequences of no more than 30 residues and can be of three origins: natural (part of a protein), fusion of two natural sequences (chimeric peptides) or synthetic (obtained by rational design based on structure-activity studies). Sequences and origins of well-known CPPs are given in Table 3.

Table 3: origin and sequence of some well-known CPPs

Peptide	Origin	Sequence	Ref.
Protein-derived			
Penetratin	Antennapedia (43-58)	RQIKIWFQNRRMKWKK	[215]
Tat	Tat (48-60)	GRKKRRQRRRPPQ	[216]
Chimeric			
Transportan	Galamine/mastoparan	GWTLNSAGYLLGKINLKALAALAKKIL	[217]
MPG	HIV-gp41/SV40 T-antigen	GALFLGFLGAAGSTMGAWSQPKKKRKV	[218]
Synthetic			
MAP	*de novo*	KLALKLALKALKAALKLA	[219]
R_6W_3	Based on penetratin	RRWWRRWRR	[220]

Due to their cell specificity and their ability to cross the cellular membrane, CPPs are used in targeted cellular therapies as a vector to transport macromolecules at a specific site and deliver them in the cytoplasm.[221-223] Cell penetrating peptides present several benefits for the therapeutic developments inherent to their biological nature and their recognition ability: they possess a low cytotoxicity, they permit an increase of the cellular uptake, their side effects are limited and they permit lower dosage. There is almost no limitation on the type of cargo that can be delivered by CPPs, as illustrated by the large variety in size and nature that have already been the object of studies: peptides, proteins, viruses, nanoparticles, DNA, antibodies.[224]

The use of peptides in therapeutic developments is well illustrated by a recently published nanosystem comprising a tumour-specific vascular homing peptide, a pro-apoptotic

peptide, an iron oxide nanoparticle and a CPP.[225] In this system the tumour-specific vascular homing peptide (CGKRK, sequence established by phage display) acts as a recognition motif to selectively target tumour blood vessels (glioblastoma), while iRGD CPP sequence, a non-cell specific CPP, permits the nanostructure to penetrate the cell membrane. Once in the cell, the pro-apoptotic peptide ($_D$[KLAKLAK]$_2$) acts as a drug which targets the mitochondria and its effect was found to be enhanced by the iron oxide nanoparticle. This complex nanosystem, made of three peptide sequences, has proven to eradicate most tumour blood vessels present into mice, suggesting a potential clinical use for this tumour therapy and illustrate the potential complementary role of peptides in drug delivery and targeting.

2   Aims

POMs show promise in a wide range of applications such as medicine, nanotechnology and catalysis, but their poor processability, their lack of bio-specificity and their high toxicity hamper their broad use. The creation of organic-inorganic hybrid polyoxometalate systems, in which POM properties are not only combined with those of organic ligands but a synergistic effect between the two moieties can be expected, seem to be a viable route to tune the properties of the POM and, depending on the type of ligand introduced, reach novel properties.

Peptides, bio-polymeric chains of Nature's building blocks, the amino acids, offer an unmatched variety of functions and properties which are highly related to their remarkable capability of folding into extremely ordered superstructures. The evolution of the chemical synthesis of peptides now permits the design and synthesis of specific structures targeting particular arrangements and/or properties.

POMs and peptides both have remarkable properties and, in our group, we started to wonder what properties could result from of their fusion. Could the properties of peptide moieties be used to reliably organise, assemble and structure POM hybrids? Could new functions arise from the introduction of a charged metal-oxide cluster in the middle of a peptide chain? Would the incorporation of specific peptide sequences improve the bio-availability, the toxicity and the specificity of POMs? But before starting to think about answering these questions, one major point had to be addressed: how can POM-peptide hybrid materials be formed?

The covalent bond, and therefore class II hybrids were favoured, because they offer a better control at the molecular level and a greater chance of preserving the hybrid material properties from the solid to the liquid state. Among the large variety of covalent linkage available, the one *via p*-block elements was selected and more precisely, the one through tris-alkoxo groups. In the literature, as we have seen in Section 1.2.2, one hybrid POM cluster functionalised *via* Sn elements was grafted onto tri-peptide chains, but the post-functionalisation techniques employed for this synthesis are very specific to the POM building block and could not be applied to other types of POM units. To the best of our knowledge, no synthetic approach yet exists to incorporate tris-alkoxide functionalised hybrid POMs into peptide chains.

As described in Section 1.2.1.1, several POM clusters can form organic-inorganic hybrids through the incorporation of one or several tris-alkoxide ligands into their metal-oxide framework. The TRIS-based Mn-Anderson cluster was chosen as a model of TRIS-based hybrid POM on which to base the development of new methodologies, hoping that the method's applicability could then be extended to the other type of Anderson structures (*e.g.* with Fe and Cr as the heteroatom) or to the TRIS-based Lindqvist cluster or the TRIS-based Dawson $\{P_2W_{15}V_3\}$. TRIS-based Mn-Anderson clusters present several advantages which facilitate methodology developments: (i) these hybrids are very stable to air, water and light which makes them easy to handle; (ii) compounds presenting this metal-oxide core usually crystallise well (when the ligand is of reasonable size), which permits good purification and structure elucidation by X-ray crystallography; (iii) the obtained compounds can be analysed by NMR (^{1}H and ^{13}C) which is an important tool to follow the completion of a reaction and to determine the structure of synthesised products; (iv) the paramagnetic nature of the heteroatom affects the resonance of the protons of the CH_2 of the TRIS moieties in ^{1}H NMR experiments, resulting in a broad signal downfield at around 65 ppm. This signal can be used as a signature for the presence of TRIS-based Mn-Anderson clusters. Moreover, this POM hybrid offers the possibility of creating asymmetrical units that could bear different peptide chains on either side and allow the metal-oxide cluster to be part of a peptide sequence as a novel hybrid "amino acid".

To be widely applicable the methodology should be as modular as possible; the peptide part should be introduced without modification of the sequence (no activation or protection). With this goal in mind, post-functionalisation approaches were favoured to form new TRIS-based Mn-Anderson building blocks that could be synthesised and isolated in large batches and would then react with peptide chains to form POM-peptide hybrids.

To summarise, the aim of the work presented in this thesis is to establish a set of methodologies permitting the incorporation the TRIS-based Mn-Anderson cluster into peptide chains. If possible, the full potential of this hybrid POM will be explored, by its use as an asymmetrical unit inserted in the middle of a peptide backbone. A modular approach will be undertaken and general building blocks will be synthesised and introduced in peptide chains by post-functionalisation techniques. The creation of these methods should permit the study of the effect of the POM on peptides sequence functions and the self-assembly behaviour that peptide could bring to POM clusters.

3   Results and Discussion

3.1   TRIS-based Mn-Anderson building blocks modification tool box

TRIS-based Mn-Anderson clusters are robust and stable to a wide range of reaction conditions; their synthesis, either by pre-functionalisation or post-functionalisation methods, is widely documented but, to be able to fully explore the potential of this building block for covalent linkage with peptides, some synthetic parameters had to be studied – thus the construction of a "modification tool box".

As seen in the introduction (Section 1.2.1.2), synthetically obtained TRIS-based Mn-Anderson hybrids are exclusively formed as TBA salts soluble in organic solvents. The TBA cations can later be replaced through cation exchange treatments, but the synthesis of pure material by cation exchange is still a difficult task (the process often results in partially exchanged and therefore mixed cation products). While DMF soluble clusters are readily available, no straightforward procedure yet exists for the synthesis of water soluble TRIS-based Mn-Anderson compounds. Having the objective of reacting TRIS-based Mn-Anderson building blocks with peptides, compatible solubility was necessary and the first part of this chapter focuses on the synthesis of water soluble TRIS Mn-Anderson compounds.

Investigations into new methodologies to easily form amide bonds by post-functionalisation of hybrid clusters are presented herein. Acyl chloride[107] post-functionalisation of the TRIS Mn-Anderson cluster to form amide bonds was reported, but these reaction conditions are incompatible with the idea of a building block methodology (as it would require a difficult chemical modification of peptide chains).

Carboxylic acid functionalised Mn-Anderson compounds had, to our knowledge, never been reported; the pre-functionalisation protocols, mostly based on amide formation, are hardly compatible with this reactive group and no post-functionalisation method seems adequate for their introduction. For the realisation of this project the synthesis of carboxylic acid functionalised Mn-Anderson clusters, which could then react with the N-terminus of peptide chains, was crucial and is investigated in this section.

3.1.1 Synthesis of water-soluble TRIS Mn-Anderson clusters

The poor water solubility of TRIS-based Mn-Anderson compounds is mostly due to the hydrophobicity of the cation used for their synthesis: TBA. The use of smaller ammonium cations such as tetra-*n*-methylammonium (TMA), tetra-*n*-ethylammonium (TEA), tetra-*n*-propylammonium (TPA) (hereafter referred to as TXA cations, with X= M, E and P, respectively) should yield more water-soluble compounds. As cation exchange processes are messy and complicated, the investigation of the direct synthesis of TRIS Mn-Anderson clusters as TXA salts seemed a better strategy. For this purpose, the syntheses of octamolybdate clusters incorporating these cations were carried out and a novel adapted protocol for the synthesis of TXA TRIS Mn-Anderson compounds was investigated.

The work discussed in this sub-section was presented in a publication in *Dalton Transactions* in 2012.[226]

3.1.1.1 Synthesis of TXA octamolybdate salts

Three octamolybdate salts (products **1**, **2** and **3**) were synthesised by adaptation of the reported method for synthesising $(TBA)_4[\alpha\text{-}Mo_8O_{26}]$;[227] here the TBA·Br salt was replaced by TMA·Br, TEA·Br and TPA·Br, respectively. Elemental analysis of the white precipitates obtained allowed the cation ratios (organic/Na) to be determined, giving the following overall formula for each product: $(TMA)_2Na_2[Mo_8O_{26}]$ (**1**), $(TEA)_3Na_1[Mo_8O_{26}]$ (**2**) and $(TPA)_2Na_2[Mo_8O_{26}]$ (**3**), which is consistent with literature reports.[61]

	Bulk Material	Cryst. from DMF	Crystal Structures
	Compound 1 $(TMA)_2Na_2[\beta\text{-}Mo_8O_{26}]$		$(TMA)_3Na_1[\beta\text{-}Mo_8O_{26}]$ $(TMA)_4[\beta\text{-}Mo_8O_{26}]$ $Na_4[\beta\text{-}Mo_8O_{26}]$
Na_2MoO_4 + 6 M HCl (TMA, TEA, TPA, TBA)	**Compound 2** $(TEA)_3Na_1[\beta\text{-}Mo_8O_{26}]$		$(TEA)_3Na_1[\beta\text{-}Mo_8O_{26}]$ $(TEA)_4[\beta\text{-}Mo_8O_{26}]$ $(TEA)_4[\alpha\text{-}Mo_8O_{26}]$
	Compound 3 $(TPA)_2Na_2[\beta\text{-}Mo_8O_{26}]$		$(TPA)_2Na_2[\beta\text{-}Mo_8O_{26}]$ $Na_4[\beta\text{-}Mo_8O_{26}]$
	$(TBA)_4[\alpha\text{-}Mo_8O_{26}]$		$(TBA)_4[\alpha\text{-}Mo_8O_{26}]$

Figure 40: Overview of the synthesis of octamolybdate salts, highlighting that multiple crystal structures with various cation ratios and isomers are obtained from the same bulk material.

Characterisation of the POM clusters by crystallography was attempted by dissolving the bulk material obtained for **1-3** in DMF. A large amount of crystallographic data was

gathered for each compound presenting various cation ratios and isomer configurations (Figure 40 gives an overview of the structures obtained for each product). This data demonstrates that the adapted protocol yields octamolybdate clusters but the ratio of isomers configuration seems to vary within the crystalline material. Because of the close relationship between these two isomers,[61] the isomeric configuration may also vary from the bulk material to the crystalline material. The octamolybdate salts mostly crystalise as the β-isomer; examples of the crystal structures obtained are given in Figure 41. As the TXA octamolybdate configurations are only of little interest for this study, no further investigation of their structure is presented here.
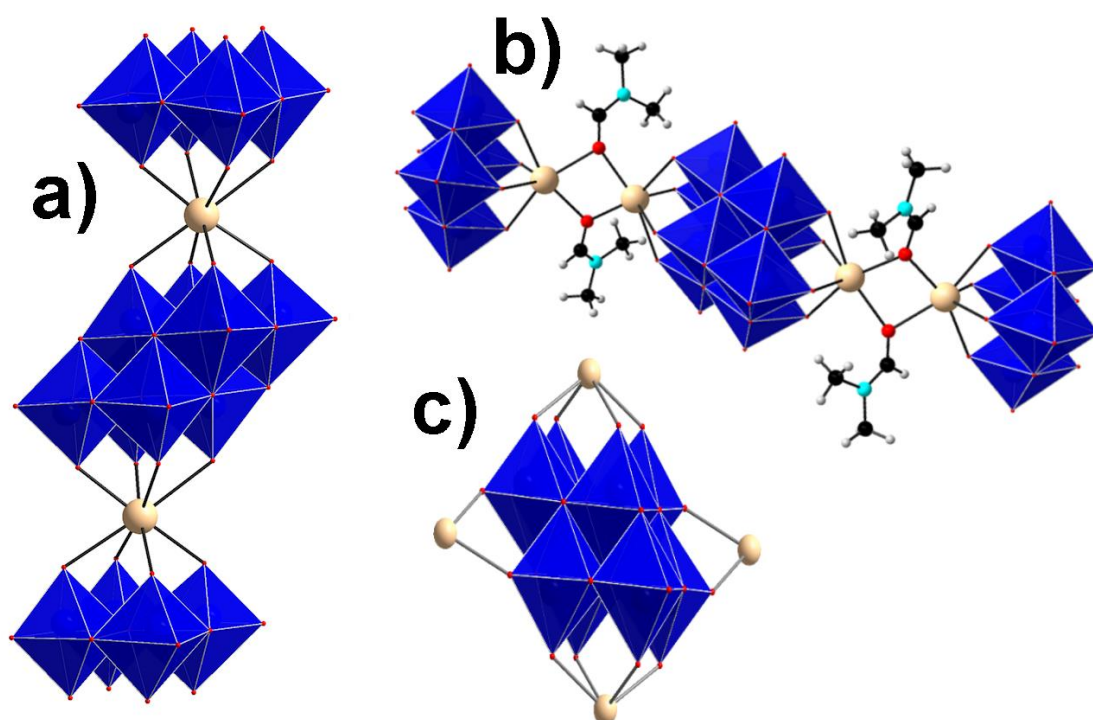
Figure 41: Crystal structures obtained for the TXA octamolybdate salts showing the different ways Na can coordinate to the terminal oxo ligands, and hence link up octamolybdate units. Structures obtained for: (a) $Na_1(TEA)_3[\beta\text{-}Mo_8O_{26}]$, (b) $Na_2(TPA)_2[\beta\text{-}Mo_8O_{26}]$, (c) $Na_4[\beta\text{-}Mo_8O_{26}]$.TXA cations are omitted for clarity. Colour scheme: Mo, blue (polyhedra); O, red; C, black; N, cyan; H, light grey; Na, beige.

Important building blocks formed immediately after the dissolution of the reagents were identified in the published ESI-MS study of the formation mechanism of the TBA TRIS Mn-Anderson cluster (see in Section 1.2.1.2 and Figure 14).[102] These building units are formed by the rearrangement of the octamolybdate cluster, $(TBA)[\alpha\text{-}Mo_8O_{26}]$, into smaller species essential for the formation of the TRIS Mn-Anderson cluster. In order to establish whether the TXA octamolybdate salts could be suitable for the synthesis of TRIS Mn-Anderson compounds, the formation of similar building blocks was investigated by ESI-MS analysis. Unlike the TBA salt, TXA salts of the octamolybdate cluster are insoluble in

MeCN, making the analysis under identical conditions difficult. Compounds **1**-**3** were thus first dissolved in a minimum amount of DMF and the resulting solution diluted with MeCN prior to analysis. The ESI-MS spectra obtained for compound **1**-**3** are given in Figure 42 along with a peak assignment table of the most intense peak envelopes.

Peak Assignment	Observed m/z	Calculated m/z
$[Mo_4O_{13}Na_1]^{1-}$	614.6	614.7
$[Mo_4O_{13}(TEA)_1]^{1-}$	721.7	722.0
$[Mo_4O_{13}(TPA)_1]^{1-}$	777.8	778.1
$[Mo_6O_{19}(TEA)_1]^{1-}$	1009.5	1009.9
$[Mo_8O_{26}(TMA)_1Na_2]^{1-}$	1304.2	1303.6
$[Mo_8O_{26}(TEA)_1Na_2]^{1-}$	1359.3	1359.7
$[Mo_8O_{26}(TPA)_1Na_2]^{1-}$	1416.4	1415.8
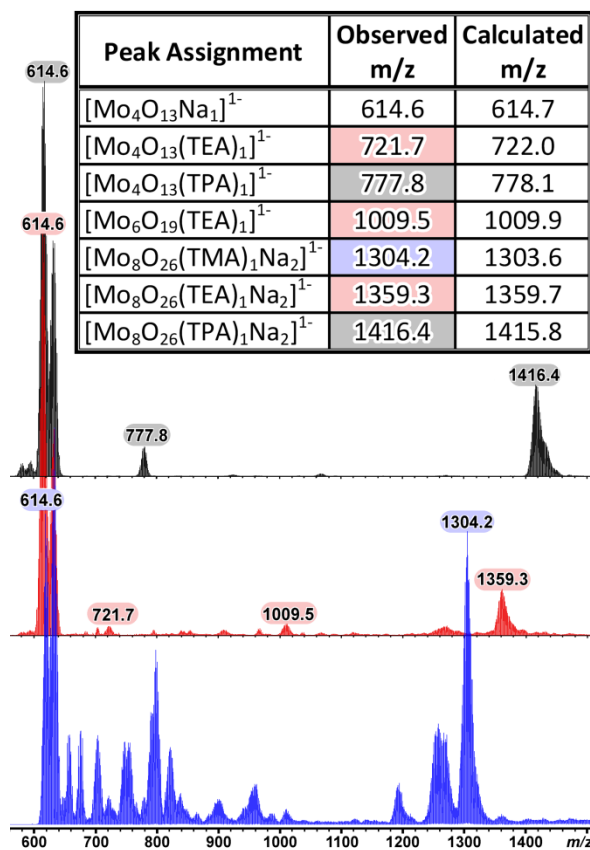
Figure 42: ESI-MS spectra obtained for compound **1** (blue), **2** (red) and **3** (black) and peak assignment table; for each compound a rearrangement into the $\{Mo_4O_{13}\}$ unit is observed.

The deviation from the original analysis conditions does not seem to affect the rearrangement of the octamolybdate cluster into the main building block, $\{Mo_4O_{13}\}$, as it is observed for each compound. The observation of this unit, identified as the first mechanistic step toward the synthesis of TRIS Mn-Anderson clusters, supported the idea that compounds **1**-**3** could be used to synthesise TRIS Mn-Anderson clusters. The investigation of this synthesis was thus explored.

3.1.1.2 Synthesis of TXA TRIS Mn-Anderson clusters

Suitable reaction conditions yielding the TRIS Mn-Anderson cluster with the novel cations had to be established, since the poor solubility of compounds **1**-**3** in MeCN could not allow the synthesis to occur in this solvent. Since TXA octamolybdates salts have greater solubility in DMF, the reaction in DMF was investigated and the synthesis of TBA TRIS

Mn-Anderson was attempted as a test reaction. The solvent was the only parameter modified in the standard protocol previously reported.[50] This reaction yielded the TBA TRIS Mn-Anderson compound and confirmed that DMF is a suitable solvent to explore the formation of TXA Mn-Anderson compounds from octamolybdate starting materials **1**-**3**.

To ensure dissolution, compounds **1**-**3** were dissolved in DMF at room temperature 30 minutes prior the addition of the Mn^{III} acetate and the TRIS ligand. After incorporation of all the reagents, the reaction mixtures were heated at 80°C for 20 h. Over the course of the reaction the colour of the mixtures changed from dark brown to orange, and brown precipitates appeared (transformations that also occur for the standard synthesis of TBA TRIS Mn-Anderson complex). The reaction mixtures were then cooled to room temperature, the precipitates removed by centrifugation and the clear orange solutions set up for crystallisation under diethyl ether (Et$_2$O) diffusion at 4 °C.
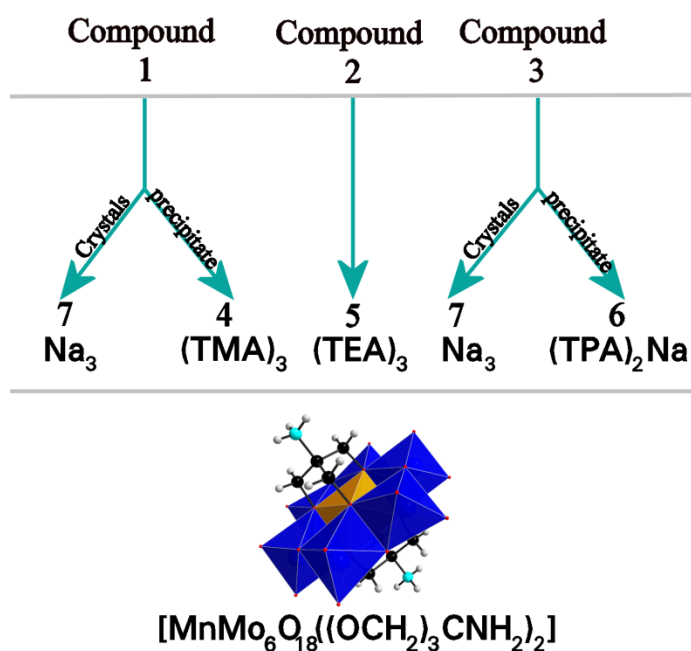
Figure 43: Schematic representation of the crystallisation pattern leading to the isolation of compounds **4**-**7**.

Solutions resulting from starting materials **1** and **3** followed the same pattern of crystallisation: Et$_2$O diffusion produced a crystalline material and a precipitate; their separation and recrystallisation from DMF yielded two different products. The original crystalline material was TRIS Mn-Anderson as a Na salt ((Na)$_3$[MnMo$_6$O$_{18}$((OCH$_2$)$_3$CNH$_2$)$_2$], **7**) while the crystals obtained from the precipitate was the TXA Mn-Anderson ((TMA)$_3$[MnMo$_6$O$_{18}$((OCH$_2$)$_3$CNH$_2$)$_2$], **4** or (TPA)$_2$(Na)[MnMo$_6$O$_{18}$((OCH$_2$)$_3$CNH$_2$)$_2$], **6**). The TEA octamolybdate salt **2**, with lower sodium content than **1** and **3**, only yielded TEA Mn-Anderson compound

$((TEA)_3[MnMo_6O_{18}((OCH_2)_3CNH_2)_2]$, **5**). An overview of the synthetic route is given in Figure 43. Interestingly, all four compounds were soluble in both water and DMF which could be a property interesting for post-functionalisation of the hybrid clusters in organic solvent followed by studies in biological media (water based). The purity of each product was confirmed by elemental analyses and the compounds were fully characterised.

^{1}H NMR analysis is an interesting tool for TRIS-based Mn-Anderson cluster characterisation due to the paramagnetic nature of the Mn^{III} central heteroatom. When analysing TRIS-based Mn-Anderson compounds, the resonance of the 12 protons located on the CH$_2$ of the TRIS moiety, closest to the paramagnetic centre, are observed as a broad peak around 65-60 ppm.[49] Broad peaks in this region were observed for all four compounds (Figure 44), giving a strong suggestion that TRIS Mn-Anderson clusters were formed.
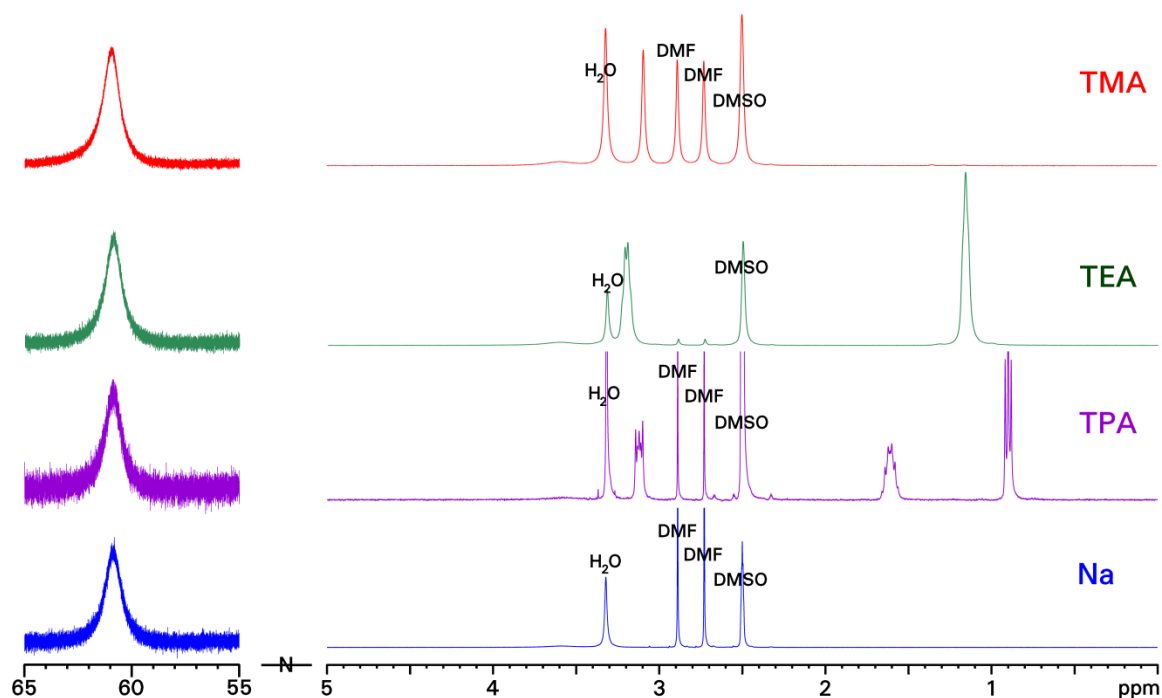
Figure 44: ^{1}H NMR spectra of the TXA TRIS Mn-Anderson compounds obtained on a 400 MHz spectrometer in deuterated DMSO; some DMF solvent peaks are observed. Colour scheme: **4**, red; **5**, green; **6**, purple; **7**, blue.

ESI-MS analyses all confirmed the successful synthesis of the TRIS Mn-Anderson compounds with the observation of fragments of the metal oxide core; peak envelopes from the ESI-MS spectra obtained for compounds **4**, **5**, **6** and **7** are shown in Figure 45, with the simulated peaks shown below in black: m/z 1303.6 corresponds to $[(TMA)_2[MnMo_6O_{18}((OCH_2)_3CNH_2)_2]]^{1-}$; m/z 1418.8 corresponds to $[(TEA)_2[MnMo_6O_{18}((OCH_2)_3CNH_2)_2]]^{1-}$; m/z 1527.8 corresponds to $[(TPA)_2[MnMo_6O_{18}((OCH_2)_3CNH_2)_2]]^{1-}$ and m/z

1201.4 corresponds to $[(Na)_2[MnMo_6O_{18}((OCH_2)_3CNH_2)_2]]^{1-}$. The ESI-MS envelope peaks obtained for TRIS-based Mn-Anderson clusters are generally more complex than their corresponding simulated patterns (as seen in Figure 45). This is due to an overlapping of envelopes of species possessing different charge states but the same m/z ratio. These species are the result of a supramolecular assembly of the hybrid POM cluster and their separation was demonstrated by the use of ion-mobility mass spectrometry (IMS/MS) in a previous report.[106]
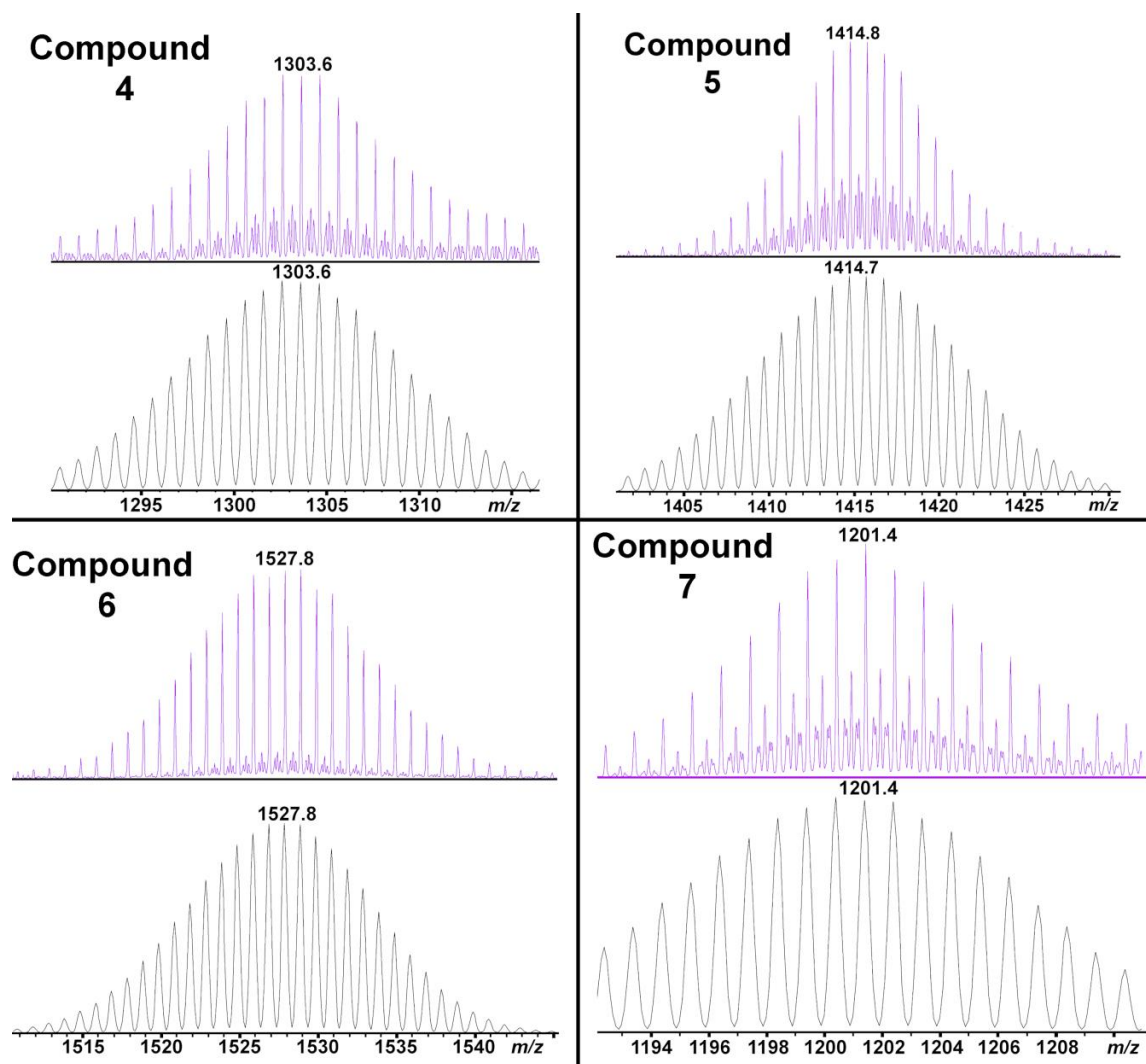
Figure 45: Representation of the main peak envelopes observed in the ESI-MS spectra of compounds **4**, **5**, **6** and **7** (purple) with the corresponding simulated pattern shown in black.

The structures of compounds **4**-**7** were determined by single crystal X-Ray diffraction. Structurally, compounds **4** and **5** are very similar to TBA TRIS Mn-Anderson structures where the compound is solely made of the POM cluster and its three cations (and solvent molecules); only unit cell data is given for these compounds. A more detailed description of the structural arrangement of compounds **6** and **7** is given as the Na cations introduce some interesting coordination patterns.

Compound **4** crystallises as orange block-shaped crystals in a monoclinic crystal system, in space group *C*2/*c*. The unit cell is *a* = 29.0498(10), *b* = 9.2853(3), *c* = 24.0873(8) Å. *β* = 102.186(3) °, the volume *V* is 6350.8(4) Å^3, and Z is 4.

Two unit cells were observed for compound **5**, depending on solvent content; the notation **5a** (1 DMF molecule) and **5b** (2 DMF molecules) is used to differentiate these structures. Compound **5a** crystallises as orange block-shaped crystals in a monoclinic crystal system, in space group *C*2/*m*. The unit cell is *a* = 15.0770(13), *b* = 23.102(2), *c* = 15.0791(14) Å. *β* = 92.336(5) °, the volume *V* is 5247.9(8) Å^3 and Z is 4. Compound **5b** crystallises as orange needle-shaped crystals in a monoclinic crystal system, in space group *C*2/*c*. the unit cell is *a* = 24.6971(16), *b* = 12.6758(8), *c* = 18.8241(10) Å. *β* = 90.641(5) °, the volume *V* is 5892.6(6) Å^3 and Z is 4.

Compound **6** crystallises as orange block-shaped crystals in an orthorhombic crystal system, in space group *Pnma*. The unit cell is *a* = 52.926(3), *b* = 27.5135(10), *c* = 9.5169(4) Å, the volume *V* is 13858.3(10) Å^3 and Z is 8. Within the unit cell two kinds of cluster arrangement coexist; the first kind consists of the "standard" TRIS Mn-Anderson structure, while the second is a TRIS Mn-Anderson coordinated to two Na atoms through terminal oxo groups, each Na atom additionally coordinates three DMF molecules (see Figure 46).
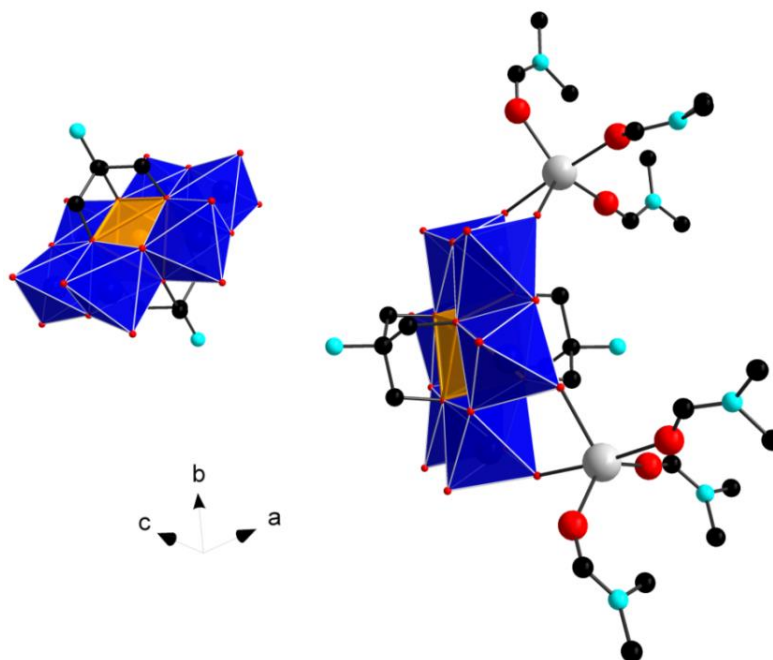
Figure 46: Polyhedral and ball-and-stick representation of the two types of TRIS Mn-Anderson cluster observed within one unit cell. TPA cations are omitted for clarity. Colour scheme: Mn, orange (polyhedra); Mo, blue (polyhedra); O, red; C, bleck; N, cyan; Na, grey.

Three unit cells were observed for compound **7** depending on solvent content; the notation **7a** (3 DMF and 5 H_2O molecules), **7b** (4 DMF and 4 H_2O molecules), **7c** (10 DMF molecules) is used to differentiate these structures. Compound **7a** crystallises as orange needle-shaped crystals in a triclinic crystal system, in space group $P\bar{1}$. The unit cell is $a = 9.1905(5)$, $b = 12.7684(6)$, $c = 12.8684(6)$ Å. $\alpha = 102.444(3)$, $\beta = 106.754(3)$, $\gamma = 110.418(3)$ °, the volume V is $1268.31(11)$ Å^3 and Z is 1. Compound **7b** crystallises as orange needle-shaped crystals in a triclinic crystal system, in space group $P\bar{1}$. The unit cell is $a = 8.6386(4)$, $b = 10.0132(5)$, $c = 14.3392(8)$ Å. $\alpha = 109.102(2)$, $\beta = 92.590(2)$, $\gamma = 93.587(2)$ °, the volume V is $1166.91(10)$ Å^3 and Z is 1. Compound **7c** crystallises as orange needle-shaped crystals in a triclinic crystal system, in space group $P\bar{1}$. The unit cell is $a = 9.5374(3)$, $b = 13.5364(5)$, $c = 28.3397(9)$ Å. $\alpha = 91.169(2)$, $\beta = 90.065(2)$, $\gamma = 109.346(2)$ °, the volume V is $3451.3(2)$ Å^3 and Z is 2. The spatial complexity of the structures decrease as the number of solvent molecules within the structure increases as more solvent molecules are coordinated to the Na atoms (see Figure 47). In **7a**, the structure which has the lowest solvent content, the TRIS Mn-Anderson clusters are arranged in a 3D array through Na coordination (8 Na coordinated to each POM cluster), while in **7c** (highest solvent content) the POM clusters are arranged in a linear 1D arrangement with only two Na atom coordinated to each POM cluster. **7b,** which possesses an intermediate solvent content, consists of a planar arrangement of POM clusters coordinated to 4 Na atoms.
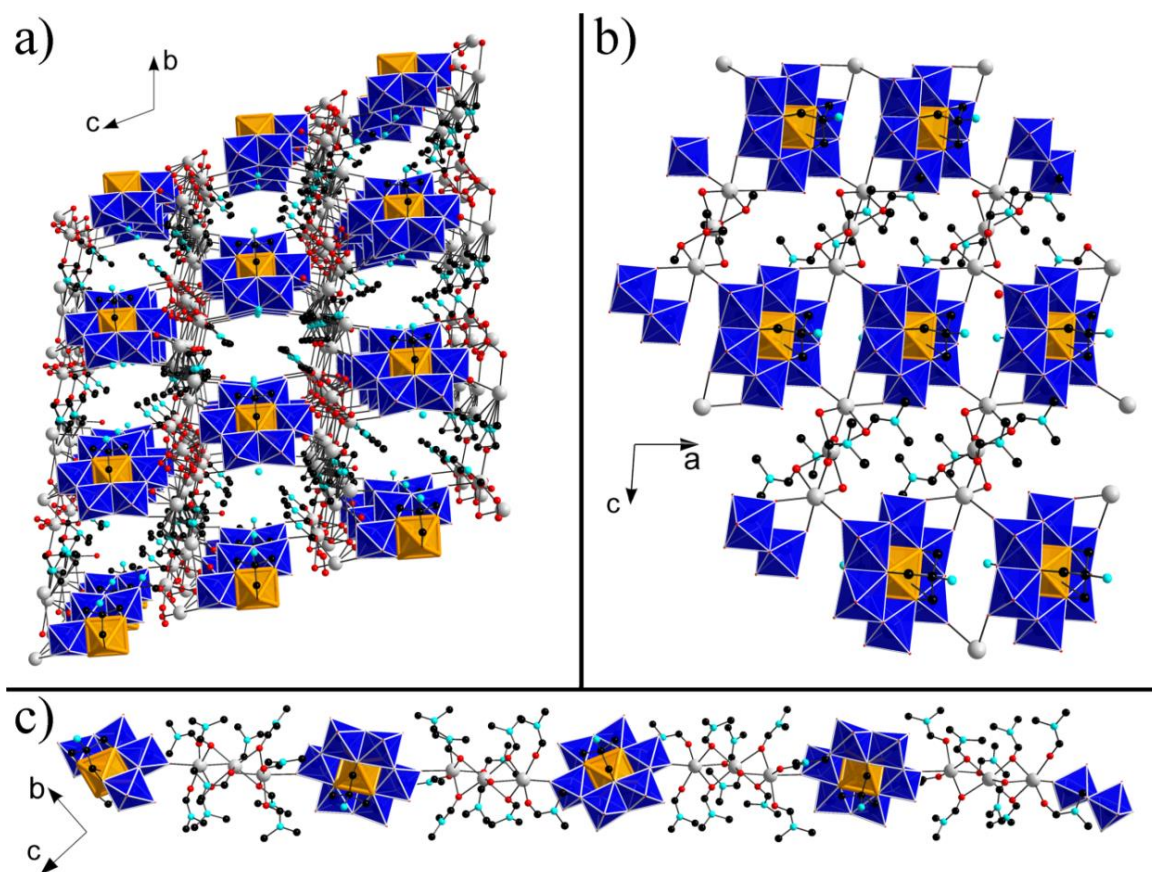
Figure 47: Polyhedral and ball-and-stick representation of the different crystal structures obtained for compound **7** differing from one another by their solvent content. (a) 3D arrangement; (b) planar arrangement; (c) linear arrangement. Colour scheme: Mn, orange (polyhedra); Mo, blue (polyhedra); O, red; C, black; N, cyan; Na, beige.

3.1.1.3 Summary

The objective of this first method of the "synthetic tool box" was to synthesise water-soluble TRIS Mn-Anderson clusters in a way which permits the circumvention of the somewhat complicated cation exchange procedures. This was made possible by the synthesis of octamolybdate salts incorporating other cations (**1**-**3**), and some small alterations to the standard synthesis protocol. This study shows the close relationship between the different octamolybdate species and their capacity to rearrange into similar building units, essentials for the formation of the TRIS Mn-Anderson clusters. The resulting hybrid compounds (**4**-**7**) are soluble in water and DMF, properties which are interesting as traditional post-functionalisation of POM clusters are carried out in organic solvents, while biological interaction studies occur in aqueous media; both could thus be explored with these new compounds.

3.1.2 Peptide bond formation *via* the C-terminus and introduction of carboxylic acid functional groups

One TRIS Mn-Anderson post-functionalisation procedure leading to amide bond formations was reported,[107] but the reaction conditions used in this method (requiring a chemical modification of the terminal carboxylic acid of peptides by acylation) was inappropriate for a modular approach. Milder reaction conditions had to be investigated in order to graft amino acids or peptide chains *via* the C-terminus in a straightforward manner.

Carboxylic acid groups can be modified to form activated intermediates in many different ways;[178] one well know activated intermediate type is the anhydride (easily formed, for example, by reaction with carbodiimide reagents) which reacts under mild conditions with amines and alcohols to form amides and esters respectively. The esterification of alcohol groups by post-functionalisation treatment of TRIS-based polyoxovanadate hybrids with anhydrides was reported,[228] however the post-functionalisation of the amine of the TRIS Mn-Anderson cluster by these reagents was never explored and is investigated here. The mild reaction conditions should allow the easy formation of peptide bonds, while the study of cyclic anhydrides could permit the insertion of carboxylic acid functional groups, a functional group never grafted to TRIS-based Mn-Anderson clusters.

Compounds discussed in this sub-section were presented in a study published in *CrystEngComm* in 2012.[229]

3.1.2.1 Peptide bond formation *via* the C-terminus

To investigate amide bond formation by treatment of the TRIS Mn-Anderson cluster by anhydrides, a couple of commercially available anhydrides presenting different organic groups was selected: propionic anhydride (reagent **A**) and benzoic anhydride (reagent **B**), see Figure 48. An excess of each anhydride (10 equiv.) was introduced in a solution of TBA TRIS Mn-Anderson compound in MeCN and the reaction was heated at 50 °C overnight. The reaction products were isolated by crystallisation under Et_2O vapour diffusion, washed with Et_2O and dried under vacuum.
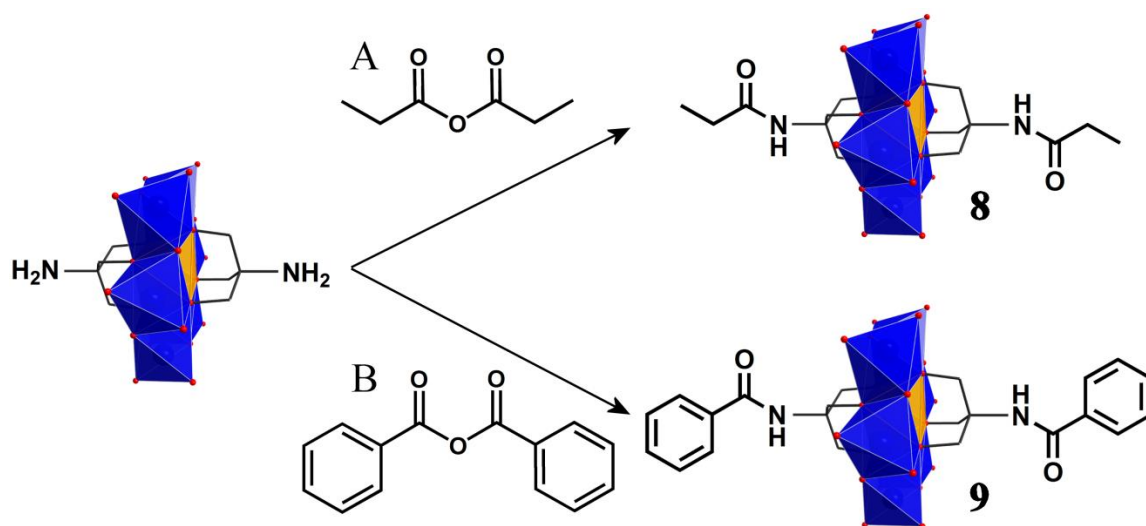
Figure 48: Anhydrides **A** and **B** used as starting material to react on the amine groups of the TRIS Mn-Anderson cluster.

Under these reaction conditions, reagents **A** and **B** yield compounds **8** ($(TBA)_3[MnMo_6O_{18}((OCH_2)_3CNHCOCH_2CH_3)_2]$) and **9** ($(TBA)_3[MnMo_6O_{18}((OCH_2)_3CNHCO(C_6H_5))_2]$) by amide bond formation on both amines of the POM cluster. The purity of the products was established by elemental analysis and the compounds were fully characterised.

^{1}H NMR analyses (spectra given in Figure 49) confirmed the structural integrity of the hybrid POMs with the observation in both products of a broad peak in the region of 60 ppm (characteristic of the incorporation of TRIS moieties into the metal-oxygen framework). In the more common ppm range (*i.e.* from 8 to 0 ppm) the characteristic resonance peak of the amine of the TRIS Mn-Anderson compound at 3.60 ppm was not observed[50] but a peak at 7.4 ppm for **8** and 7.6 for **9** attributed to the –NH of the amide was present (Figure 49). For compound **8** the integrations of the observed peaks were in agreement with the presence of three TBA cations and two –CH_2CH_3 groups (one on each ligand) with the –CH_2– observed at 2.40 ppm (4H) and the –CH_3 superimposed with the –CH_3 of the TBA at 0.94 ppm resulting in an overall integration of 42 protons (36H for TBA + 6 H for –CH3). Similarly, the integrations for compound **9** confirms the given formula and the peptide bond formations on both reactive sites; peaks attributed to the two phenyl moieties are observed at 7.77 ppm (4H) and 7.43 ppm (6H).
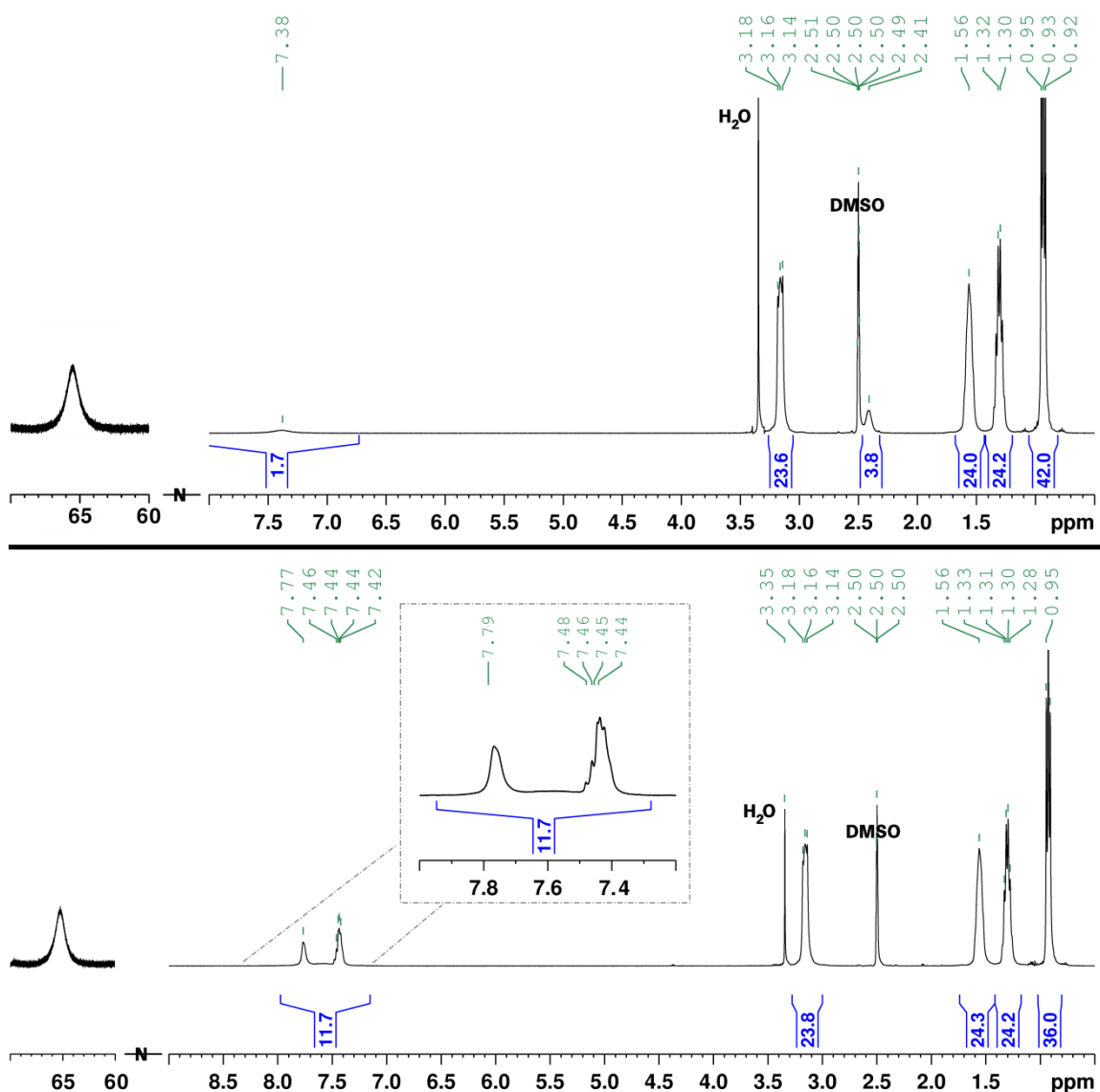
Figure 49: ^{1}H NMR spectra of compounds **8** (top) and **9** (bottom) obtained on a 400 MHz spectrometer in deuterated DMSO.

ESI-MS analyses of compounds **8** and **9** were carried out in MeCN and confirmed the identity of the products. Figure 50 shows the spectrum obtained for compound **8** in which the fragment observed at m/z 1750.99 (z = -1) was assigned as $[(TBA)_2[MnMo_6O_{18}((OCH_2)_3CNHCOCH_2CH_3)_2]]^{1-}$ (predicted: 1752.01); no peaks of the starting material or the mono-reacted species could be identified ($[(TBA)_2[MnMo_6O_{18}((OCH_2)_3CNH_2)_2]]^{1-}$ expected signal at m/z 1639.95 and $[(TBA)_2[MnMo_6O_{18}((OCH_2)_3CNHCOCH_2CH_3)((OCH_2)_3CNH_2)]]^{1-}$ expected at m/z 1695.98, respectively), attesting to the completion of the reaction and the purity of the product.
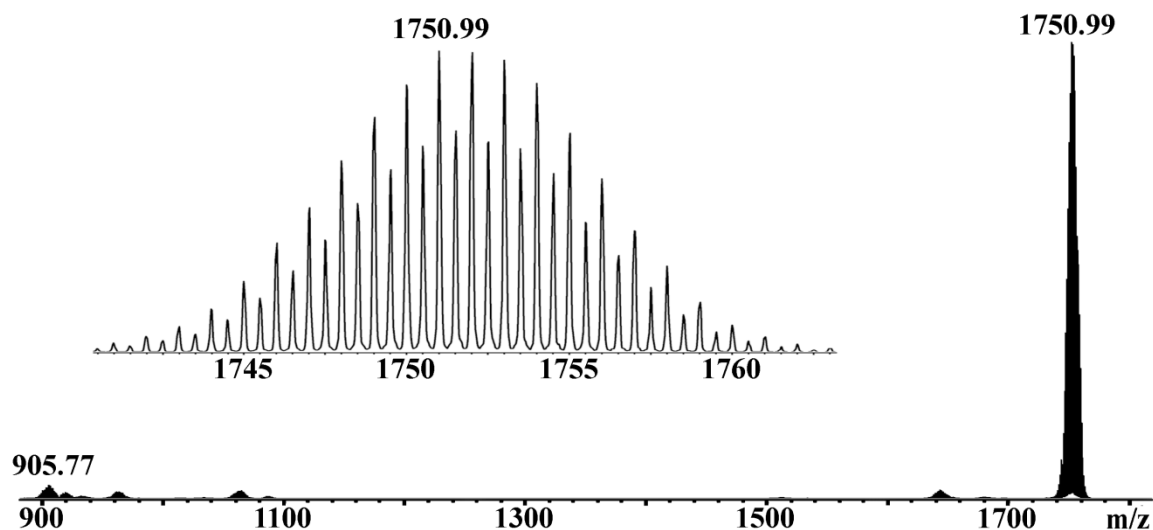
Figure 50: ESI-MS spectrum obtained for compound **8** with magnified representation of the main peak envelope at m/z 1750.99 assigned to $[(TBA)_2[MnMo_6O_{18}((OCH_2)_3CNHCOCH_2CH_3)_2]]^{1-}$.

Similarly, for compound **9** the main peak envelope observed in the spectrum (Figure 51) at m/z 1848.07 (z = -1) was assigned to $[(TBA)_2[MnMo_6O_{18}((OCH_2)_3CNHCO(C_6H_5))_2]]^{1-}$ (predicted: 1848.01); no peaks could be identified as belonging to the starting material or the mono-reacted species $([(TBA)_2[MnMo_6O_{18}((OCH_2)_3CNHCO(C_6H_5))((OCH_2)_3-CNH_2)]]^{1-}$ expected at m/z 1743.98).
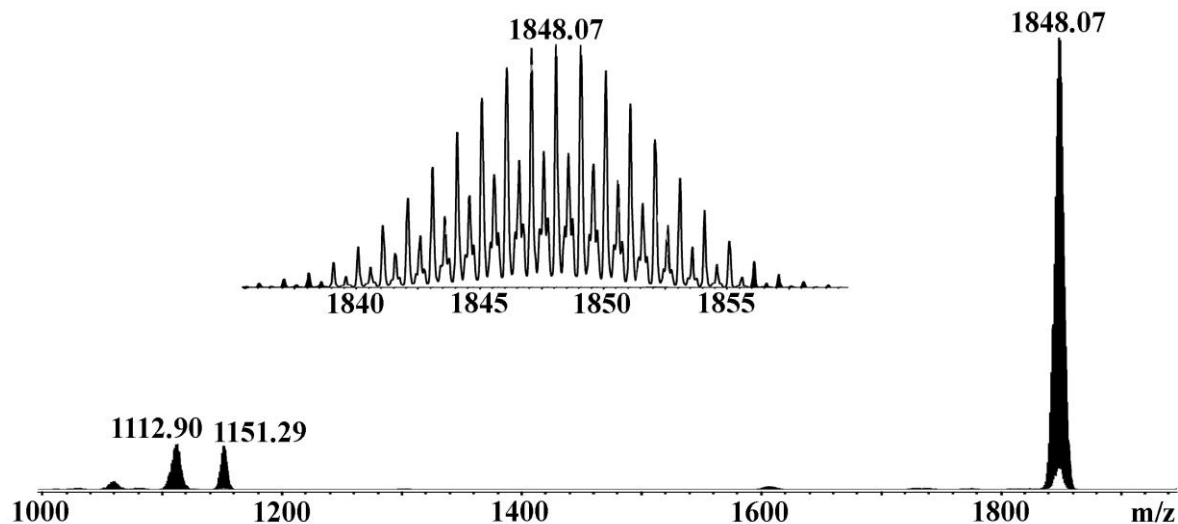
Figure 51: ESI-MS spectrum obtained for compound **8** with magnified representation of the main peak envelope at m/z 1848.07 assigned to $[(TBA)_2[MnMo_6O_{18}((OCH_2)_3CNHCO(C_6H_5))_2]]^{1-}$.

Crystal structures were obtained by single crystal X-Ray diffraction analyses. Suitable single crystals were obtained for **8** from MeCN solution while DMF was used for **9**; both solutions were exposed to Et$_2$O vapour diffusion. Compound **8** crystallises as orange block-shaped crystals in a triclinic crystal system, in space group $P\bar{1}$. The unit cell is $a =$

14.8991(11), b = 16.8272(12), c = 22.2685(17) Å, α = 73.868(4), β = 74.700(4), γ = 66.883(3) °, the volume V is 4856.2(6) Å^3 and Z is 2. The TBA cations and solvent molecules surround the hybrid POM cluster preventing them from interacting within the crystal packing (see packing diagram Figure 52a). Compound **9** crystallises as orange block-shaped crystals in an orthorhombic crystal system, in space group $Pca2_1$. The unit cell is a = 18.0293(7), b = 20.8575(8), c = 26.7597(11) Å, the volume V is 10062.9(7) Å^3 and Z is 4. The TBA cations and solvent molecules surround the hybrid POM cluster; a weak π-stacking interaction was observed between benzene units (distance measured between two centroids: 4.09 Å) creating 1D chains (see packing diagram Figure 52b). No evidence of hydrogen bonding between the aromatic group and the metal-oxygen framework was observed.
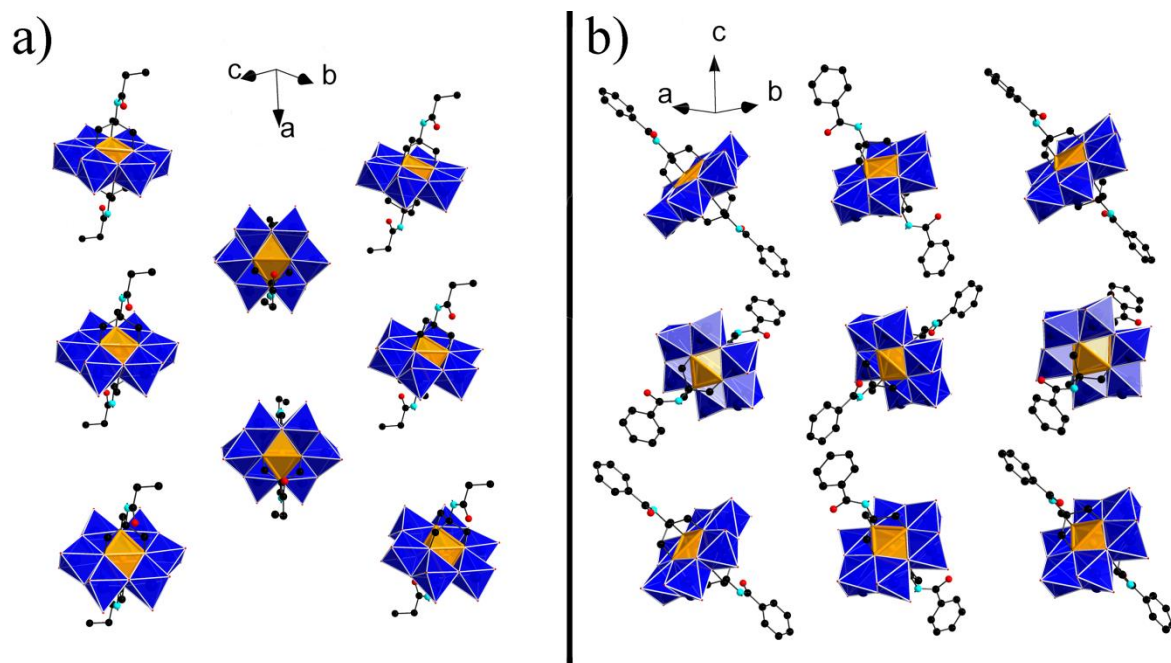
Figure 52: Polyhedral and ball-and-stick representation of a layer of the crystal packing found in compound **8** (a) and **9** (b). Colour scheme: Mn, orange (polyhedra); Mo, blue (polyhedra); O, red, C, black, N, cyan; TBA cations and solvent molecules are omitted for clarity.

These present analyses prove the formation of amide bonds by post-synthetic treatment of the TRIS Mn-Anderson cluster with an excess of anhydrides. This formation occurs at 50 °C in MeCN, reaction conditions which should be compatible with peptides.

3.1.2.2 Introduction of carboxylic acid functional groups

A modular approach to incorporate TRIS-based Mn-Anderson building units into peptide backbones requires the easy access to carboxylic acid functionalised Mn-Anderson clusters. No synthetic approach available in the literature could lead to the straightforward introduction of this functionality. The anhydride reaction reported here offers the possibility, when using cyclic anhydrides (*i.e.* activated intermediates of di-carboxylic acid molecules), of simultaneously forming an amide bond and introducing a terminal carboxylic acid functional group.

Succinic anhydride (reagent **C**, see Figure 53), a commercially available anhydride, was selected to demonstrate this post-functionalisation method. In a first attempt, ten equivalents of **C** were reacted with one equivalent of the TRIS Mn-Anderson cluster in MeCN at 50 °C, but ^{1}H NMR study of the resulting isolated product suggested that the reaction had not reached completion. It was established that the reaction reached completion when carried out in DMF at 50 °C in presence of 20 equivalents of reagent **C**. The resulting TRIS-based Mn-Anderson compound (**10**) ((TBA)$_3$[MnMo$_6$O$_{18}$((OCH$_2$)$_3$C-NHCO(CH$_2$)$_2$COOH)$_2$]) was isolated pure (purity established by elemental analysis) and fully characterised.
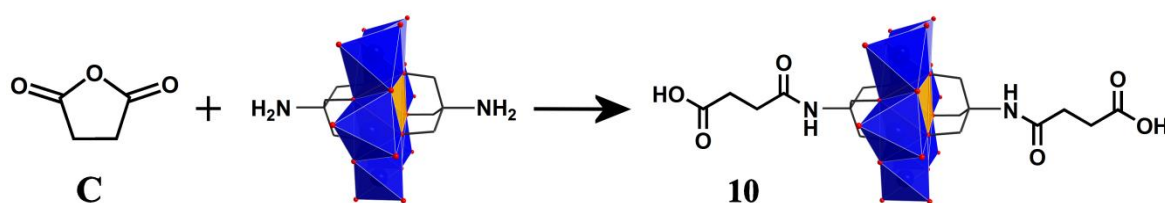
Figure 53: Reaction scheme for the synthesis of compound **10** from the reaction of reagent **C** and the TRIS Mn-Anderson building block. Colour scheme: Mn, orange (polyhedra); Mo, blue (polyhedra); O, red.

^{1}H NMR analysis confirms that the TRIS ligands were still grafted onto the metal-oxygen framework as a peak at 65 ppm was clearly observed (Figure 54). The integrations of the two peaks assigned to the two $-$CH$_2$ groups (observed at 2.37 and 2.70 ppm) and of the ones assigned to the TBA cations are consistent with the presence of two ligands and three TBA cations per cluster, which confirmed the completion of the reaction. A broad peak observed at 12.07 ppm assigned to the protons from the carboxylic acid groups confirmed the incorporation of these functional groups into the hybrid POM compound.
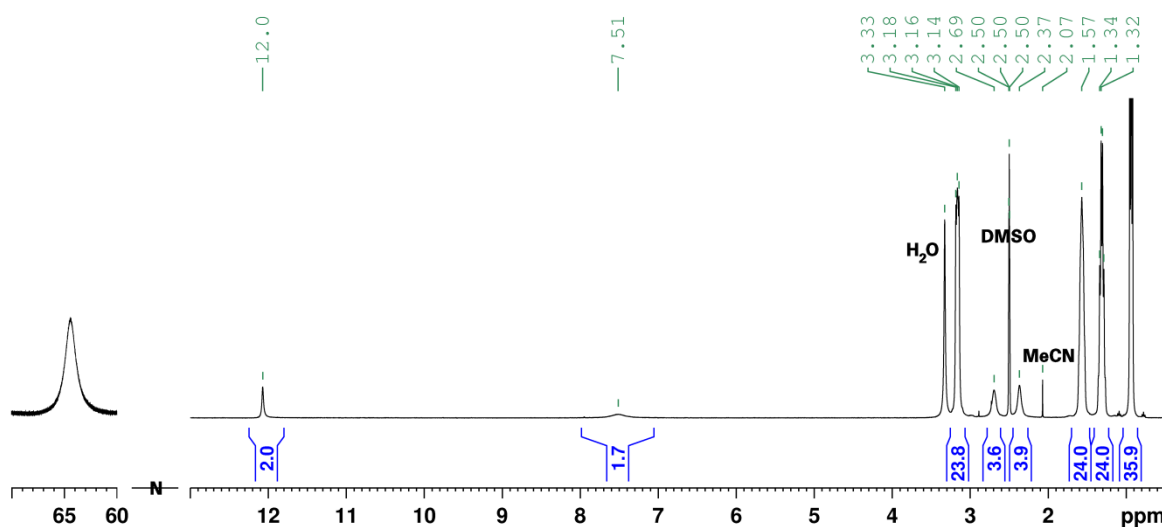
Figure 54: ^{1}H NMR spectra of compound **10** obtained on a 400 MHz spectrometer in deuterated DMSO. Residual solvent peak can be seen at $\delta = 2.07$ ppm (MeCN).

ESI-MS analysis was carried out by dissolving a small amount of the reaction product in MeCN; the obtained spectrum is shown in Figure 55. Peak envelopes observed in the spectrum correlate with the successful synthesis of compound **10**, with the main peak envelope observed at m/z 1840.09 ($z = -1$) was assigned to the anionic species $[(TBA)_2$ $[MnMo_6O_{18}((OCH_2)_3CNHCO(CH_2)_2COOH)_2]]^{1-}$ (predicted: 1839.99) and the signal observed at m/z 2081.37 ($z = -1$) to the mono deprotonated cluster $[(TBA)_3[MnMo_6O_{18}-((OCH_2)_3CNHCO(CH_2)_2COOH)((OCH_2)_3CNHCO(CH_2)_2COO)]]^{1-}$ (predicted: 2081.26). No peak could be assigned to the starting material (expected m/z 1639.95), proof of the completion of the reaction and the purity of the product **10**.
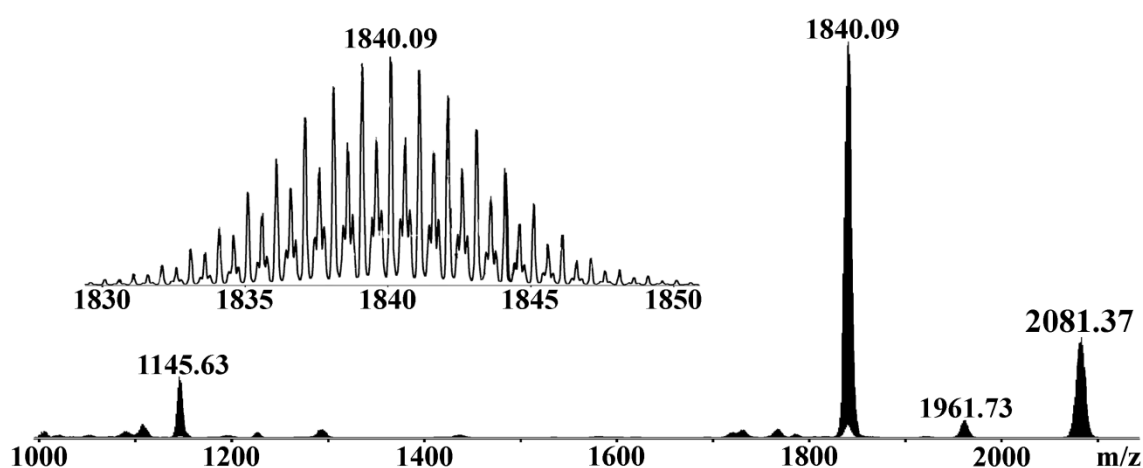

Figure 55: ESI-MS spectrum obtained for compound **10** with magnified representation of the main peak envelope at m/z 1840.09 assigned to $[(TBA)_2[MnMo_6O_{18}((OCH_2)_3CNHCO(CH_2)_2COOH)_2]]^{1-}$.

The crystal structure of compound **10** was determined by single crystal X-ray diffraction analysis of crystals grown in MeCN under Et_2O vapour diffusion. Compound **10** crystallises as orange block-shaped crystals in an orthorhombic crystal system, in space group *Pnma*. The unit cell is $a = 28.3641(5)$, $b = 23.7876(5)$, $c = 15.0216(3)$ Å, the volume V is $10135.3(3)$ Å^3 and Z is 4. The $-CH_2CH_2COOH$ moieties are highly disordered, making the analysis of the structure difficult, but no intermolecular interactions were identified within the structure (see Figure 56). The TBA cations and solvent molecules are surrounding the hybrid POM cluster, preventing most of these interactions. Within the crystal structure the aliphatic chains are highly disordered (see Figure 56). This absence of regular order is in agreement with an absence of supramolecular interactions influencing the arrangement of the organic moieties.
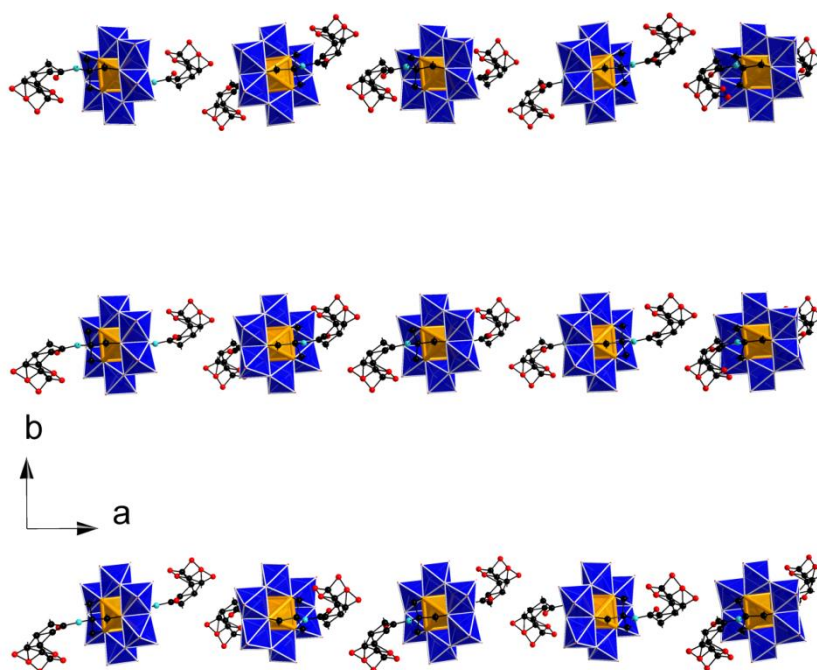

Figure 56: Polyhedral and ball-and-stick representation of a layer of the crystal packing found in compound **10**. TBA cations and solvent molecules are omitted for clarity. Colour scheme: Mn, orange (polyhedra); Mo, blue (polyhedra); O, red, C, black, N, cyan;

All characterisation of the reaction product undertaken was in agreement with the synthesis of **10**, and thus the first successful incorporation of a terminal carboxylic acid functional group on a TRIS-based Mn-Anderson cluster was achieved. The synthetic method established is simple (excess of reagent **C**, in DMF, 50 °C; product isolated in high yield and purity by crystallisation) which made this method suitable for a modular approach. This reaction makes the access of carboxylic acid functionalised Mn-Anderson clusters "as easy as" the amine functionalised one, which was important for peptide study.

3.1.2.3 Summary

The work presented in this sub-section demonstrates that anhydride reagents are a straightforward means to form amide bonds under mild reaction conditions (50 °C in MeCN or DMF) and thus represent a suitable path to introduce amino acids or peptides to hybrid Mn-Anderson clusters *via* the C-terminus. Anhydride intermediates can easily be formed by treatment of the appropriate carboxylic acid with carbodiimides,[178] reagents widely used in both peptide synthesis and post-functionalisation of POM clusters[112,126,230] which underline the compatibility of this synthetic path. Anhydrides of di-carboxylic acids offer the possibility of forming cyclic intermediates which, as demonstrated here through the succinic anhydride (reagent **C**), can react with the amine functional group of the TRIS and release a terminal carboxylic acid. Compound **10** is the first example of a carboxylic acid-functionalised TRIS-based Mn-Anderson cluster. The establishment of a straightforward method to introduce a carboxylic acid group on the POM cluster was crucial in order to be able to graft peptides onto the metal-oxide framework through the N-terminus. Since this functionality was made available, the formation of peptide bonds *via* the N-terminus could be investigated.

3.1.3 Peptide bond formation *via* the N-terminus

Since carboxylic acid functionalised Mn-Anderson clusters had been synthesized, formation of amide bonds by reaction with the N-terminus of peptides could be investigated. In our search for a modular approach, we started to explore the possibility of forming a TRIS-based Mn-Anderson intermediate that could be isolated pure and in large batches to then react with a diverse range of peptide chains.

The work presented in this section made up part of the article published in *Angewandte Chemie Int. Ed.* in 2014.[231]

3.1.3.1 Activated TRIS-based Mn-Anderson precursor synthesis

NHS ester-activation has been used in POM chemistry[126] but never with a TRIS-based system as carboxylic functions were not available; hybrid Mn-Anderson compounds covalently grafted onto a surface have been reported with NHS-activation of the surface,[230] proving the compatibility of this reagent with this POM cluster.
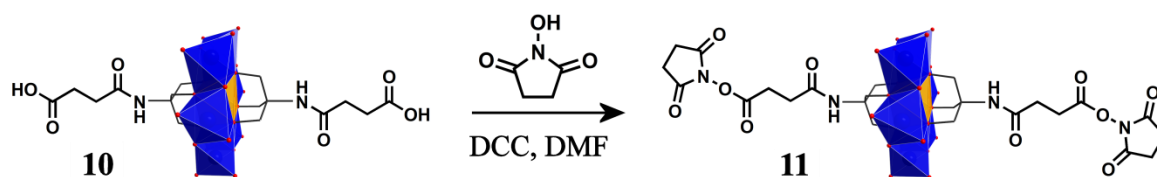
Figure 57: Reaction scheme for the synthesis of compound **11** from compound **10** by reaction with NHS with *N,N'*-Dicyclohexylcarbodiimide (DCC) as an activating agent. Colour scheme: Mn, orange (polyhedra); Mo, blue (polyhedra); O, red.

A NHS ester-activated TRIS-based Mn-Anderson precursor (**11**, $(TBA)_3[MnMo_6O_{18}$-$((OCH_2)_3CNHCO(CH_2)_2COON(COCH_2)_2)_2])$ was synthesised by treatment of compound **10** with NHS in DMF solution in the presence of *N,N'*-Dicyclohexylcarbodiimide (DCC) (Figure 57). Compound **11** was isolated in high yield (75%) by crystallisation as a pure solid (purity checked by elemental analysis).
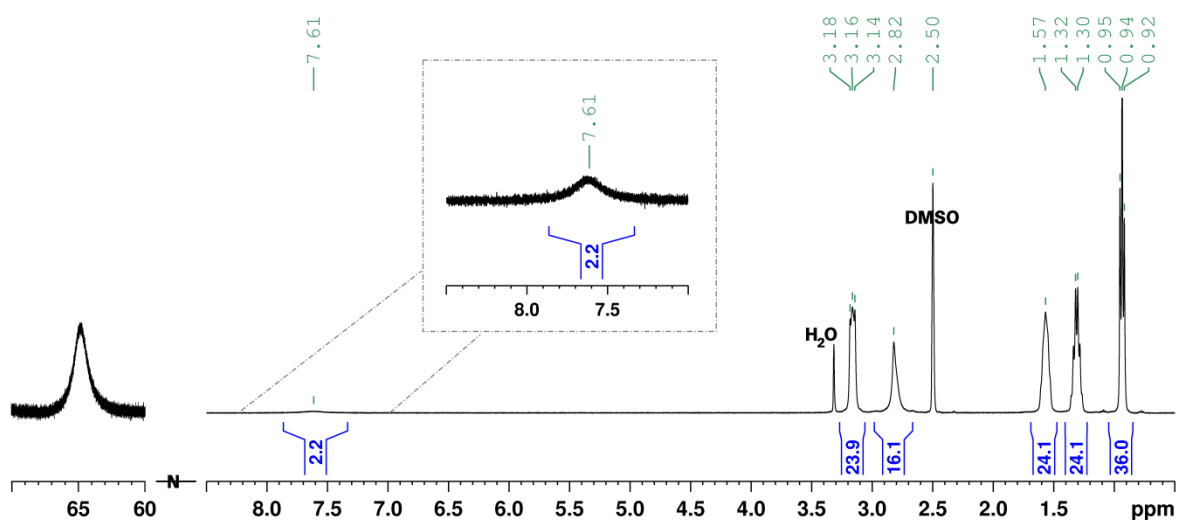
Figure 58: ^{1}H NMR spectrum of compound **11** obtained on a 400 MHz spectrometer in deuterated DMSO.

^{1}H NMR analysis showed a peak around 65 ppm characteristic of the TRIS-based ligands grafted onto the metal-oxygen framework. The analysis also confirmed the introduction of the activating groups and the formation of ester bonds (Figure 58), with the observation of a broad peak at 2.82 ppm (integrating for 16H) assigned to the 8 −CH2− groups present in the molecule and the absence of a peak at 12.07 ppm (observed for compound **10**, characteristic of the carboxylic acid group).
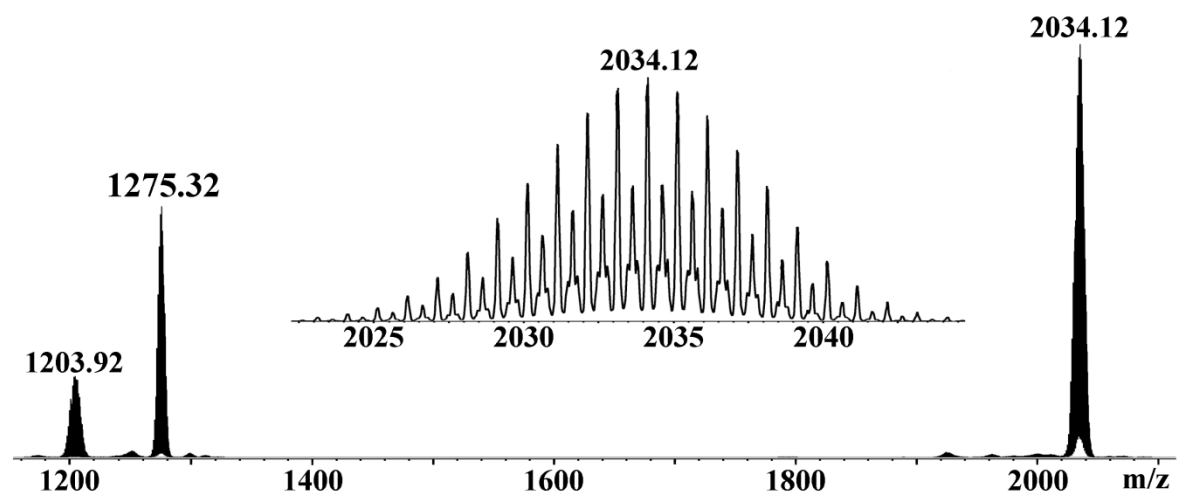

Figure 59: ESI-MS spectrum obtained for compound **11** with magnified representation of the main peak envelope at m/z 2034.12 assigned to $[(TBA)_2[MnMo_6O_{18}((OCH_2)_3CNHCO(CH_2)_2COON(COCH_2)_2)_2]]^{1-}$.

ESI-MS analysis was carried out by dissolving a small amount of the reaction product in MeCN; the obtained spectrum in shown in Figure 59. Two main peak envelopes were observed both in agreement with the proposed composition of **11**. The first peak envelope observed at m/z 1275.32 (z = -3) was assigned as a dimeric ion of the proposed compound: $[(TBA)_3[MnMo_6O_{18}((OCH_2)_3CNHCO(CH_2)_2COON(COCH_2)_2)_2]_2]^{3-}$ (predicted: 1275.25);

the second observed at *m/z* 2034.12 (z = -1) was assigned as a monomeric ion formed by the loss of one TBA cation: $[(TBA)_2[MnMo_6O_{18}((OCH_2)_3CNHCO(CH_2)_2COON-(COCH_2)_2)_2]]^{1-}$ (predicted: 2034.02).
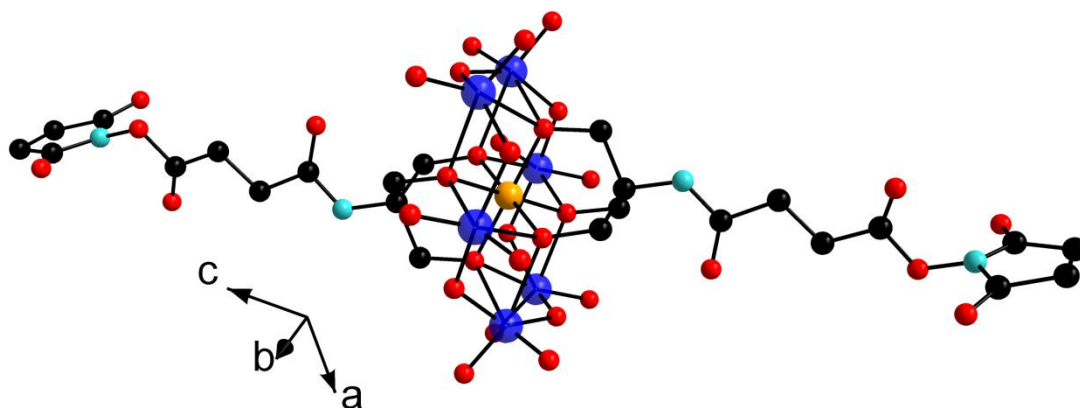
Figure 60: Ball-and-stick representation of the structure of **11** obtained by single crystal X-ray diffraction analysis of crystals grown from DMF under Et_2O vapour diffusion. TBA cations and solvent molecules are omitted for clarity. Colour scheme: Mn, orange; Mo, blue; O, red; C, black; N, cyan.

Crystal structure of compound **11** was established by single crystal X-ray diffraction analysis of crystals grown in DMF under Et_2O vapour diffusion. Compound **11** crystallises as orange block-shaped crystals in a monoclinic crystal system, in space group C2/c. The unit cell is *a* = 30.7813(16), *b* = 23.7409(12), *c* = 18.4631(10) Å, *β* = 121.095(2)°, the volume *V* is 11553.7(10) Å^3 and Z is 4. The crystal structure obtained was in agreement with the formula given for **11** and the post-functionalisation of compound **10** by the formation of an activated ester group (Figure 60).

3.1.3.2 Proof of concept

To investigate the ability of **11** to react with peptides by the formation of amide bonds, simple amino acids were first tested. Since the TRIS-based Mn-Anderson intermediate **11** is pre-activated and isolated as a pure material, no protecting group was required for the amino acid; L-glycine (Gly, G) and L-Phenylalanine (Phe, F) were therefore introduced in their native forms to generate the expected products **12** $((TBA)_3[MnMo_6O_{24}(C_{10}H_{15}N_2O_4)_2])$ and **13** $((TBA)_3[MnMo_6O_{24}(C_{17}H_{21}N_2O_4)_2])$, respectively. The reaction was carried out in stoichiometric ratios (1 equiv. of **11** for 2 equiv. of amino acid) in DMF solution at room temperature in the presence of an excess of *N,N*-diisopropylethylamine (DIPEA). The reaction was left overnight and the products, isolated by precipitation in Et_2O, were orange powders. These powders were fully analysed to investigate whether the reaction had reached completion and yielded the expected products **12** and **13**.
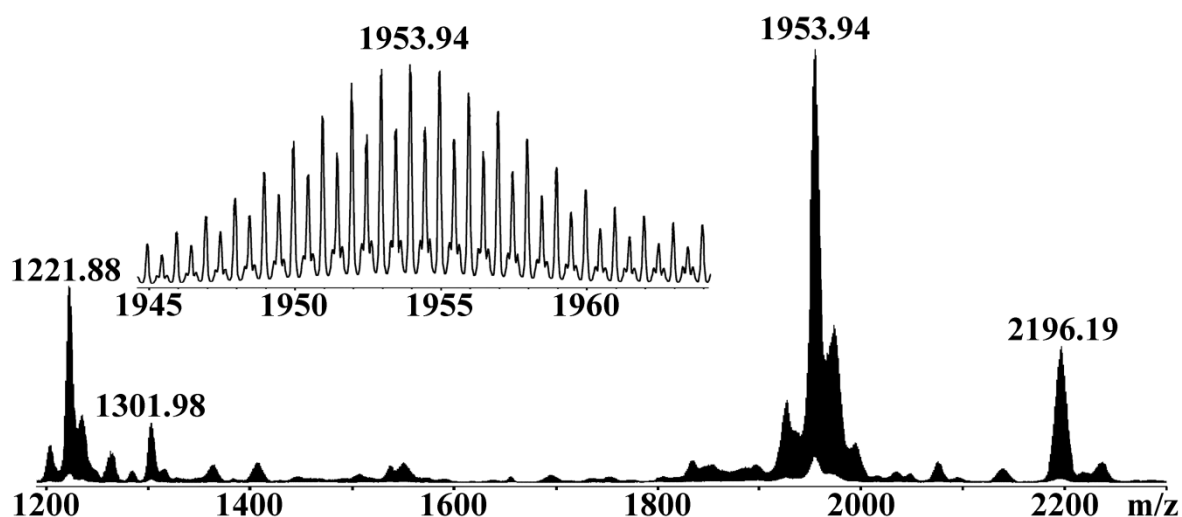
Figure 61: ESI-MS spectrum obtained for compound **12** with magnified representation of the main peak envelope at m/z 1953.94 assigned to $[(TBA)_2[MnMo_6O_{24}(C_{10}H_{15}N_2O_4)_2]]^{1-}$.

ESI-MS analyses of the reactions products, carried out by dissolving a small amount of the powders in MeCN, confirmed the identity of each compound (see Figure 61 and Figure 62). Assignments of the main peak envelopes observed are consistent with proposed formulae of compounds **12** and **13** with ligands present in their protonated and deprotonated forms and a varying number of cations. For compound **12**, anionic species such as $[(TBA)_3[MnMo_6O_{24}(C_{10}H_{15}N_2O_4)_2]_2]^{3-}$, $[(TBA)_2[MnMo_6O_{24}(C_{10}H_{15}N_2O_4)_2]]^{1-}$ and $[(TBA)_3[MnMo_6O_{24}(C_{10}H_{15}N_2O_4)(C_{10}H_{14}N_2O_4)]]^{1-}$ respectively at m/z 1221.88 (predicted: 1221.93), 1953.94 (predicted: 1954.03) and 2196.19 (predicted: 2196.31) were observed. Similarly, peak envelopes assigned to $[(TBA)_3[MnMo_6O_{24}(C_{17}H_{21}N_2O_4)_2]_2]^{3-}$ at m/z 1342.08 (predicted: 1341.99), $[(TBA)_2 [MnMo_6O_{24}(C_{17}H_{21}N_2O_4)_2]]^{1-}$ at m/z 2134.26 (predicted: 2134.12) and $[(TBA)_3[MnMo_6O_{24}(C_{17}H_{21}N_2O_4)(C_{17}H_{20}N_2O_4)]]^{1-}$ at m/z 2376.53 (predicted: 2376.40) confirmed the synthesis of **13**. Additionally, no signal could be assigned to the starting material (**11,** $[(TBA)_2[MnMo_6O_{24}(C_{12}H_{15}N_2O_5)_2]]^{1-}$ expected at m/z 1839.99) or the mono-reacted species ($[[TBA)_2[MnMo_6O_{24}(C_{10}H_{15}N_2O_4)(C_{12}H_{15}N_2O_5)_2]]^{1-}$ (predicted: 1994.02) for the reaction with Gly and $[(TBA)_2 [MnMo_6O_{24}(C_{17}H_{21}N_2O_4)(C_{12}H_{15}N_2O_5)]]^{1-}$ (predicted: 2084.07) for the reaction with Phe). The absence of starting material and mono-substituted species suggest that the reactions reached completion.
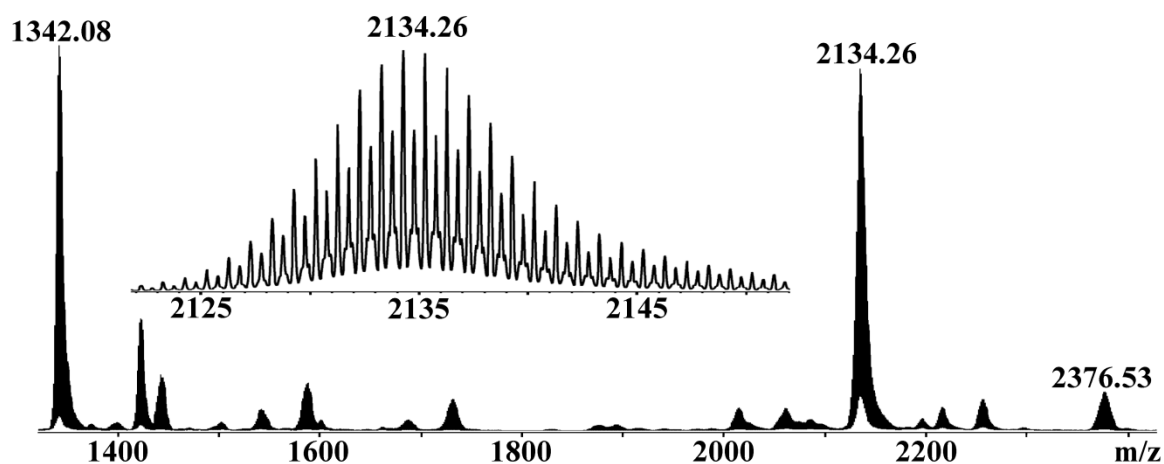
Figure 62: ESI-MS spectrum obtained for compound **13** with magnified representation of the main peak envelope at *m/z* 2134.26 assigned to $[(TBA)_2[MnMo_6O_{24}(C_{17}H_{21}N_2O_4)_2]]^{1-}$.
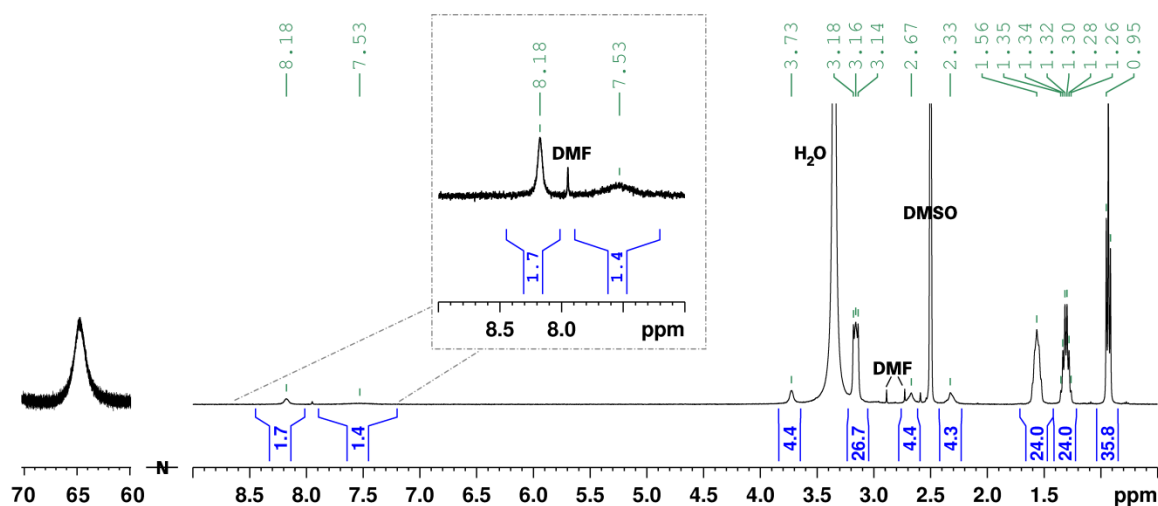

Figure 63: ^{1}H NMR spectrum of compound **12** obtained on a 400 MHz spectrometer in deuterated DMSO.

^{1}H NMR also confirmed the synthesis and isolation of the expected compounds **12** and **13**; for both compounds, a broad peak was observed in the 65 ppm region, suggesting that the metal-oxygen cluster was still intact and linked to TRIS groups. The spectra in the 14 to 0 ppm range were consistent with the structures proposed for compounds **12** and **13,** with the integrations for the TBA cations matching the ones of the two ligands. For compound **12** the resonance observed at 3.73 ppm and integrating for 4H is assigned to the $-C_{\alpha}H_2-$group of the glycine and the broad signal at 8.18 ppm is attributed to the –NH of the newly formed amide. A broad signal at 8.16 ppm is also observed for compound **13** confirming that it can be assigned to the –NH of the amide; the aromatic protons of the phenyl groups were observed as a multiplet in the region from 7.85 to 7.00 ppm. This region also corresponds to the signal observed for the amide the closest to the POM structure giving an

overall integration of 12H. The protons of the alpha carbons were observed for **13** at 4.38 ppm.
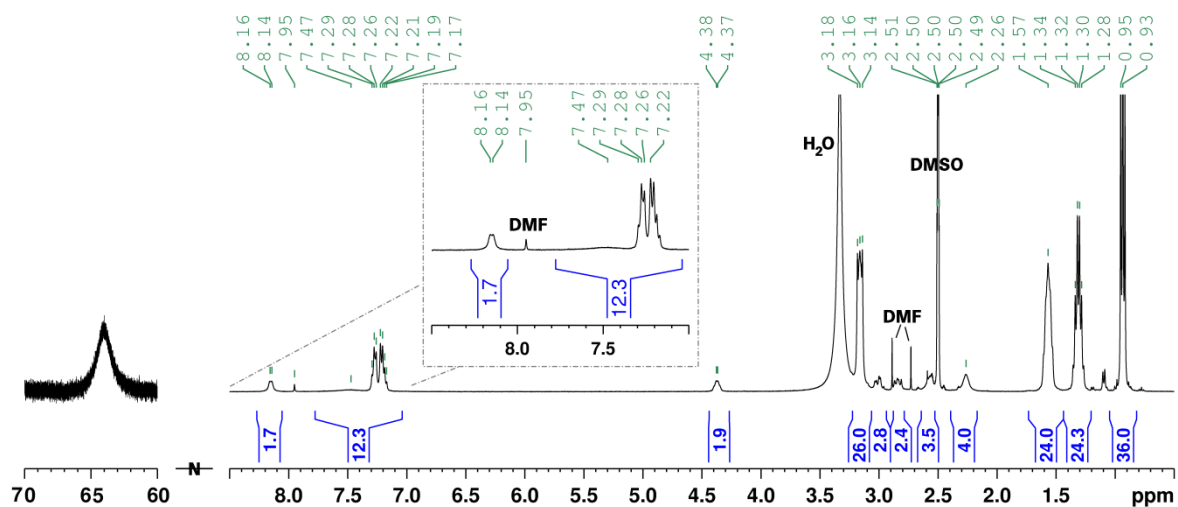
Figure 64: ^{1}H NMR spectrum of compound **13** obtained on a 400 MHz spectrometer in deuterated DMSO.

Single crystal X-ray diffraction analysis of crystals grown in DMF under Et_2O vapour diffusion was attempted for both compounds, but due to the poor quality of the crystals, suitable diffraction was only reached for compound **13**. Compound **13** crystallises as small sheet-shaped orange crystals in a monoclinic crystal system, in space group C2/c. The unit cell is a = 50.1637(14), b = 29.4838(12), c = 29.5767(12) Å, β = 124.851(3) °, the volume V is 35898(3) Å^3, and Z is 12. The structure proves the formation of an amide bond at each reactive site and the incorporation of the amino acid into the hybrid POM cluster (**Error! Reference   source   not   found.**).
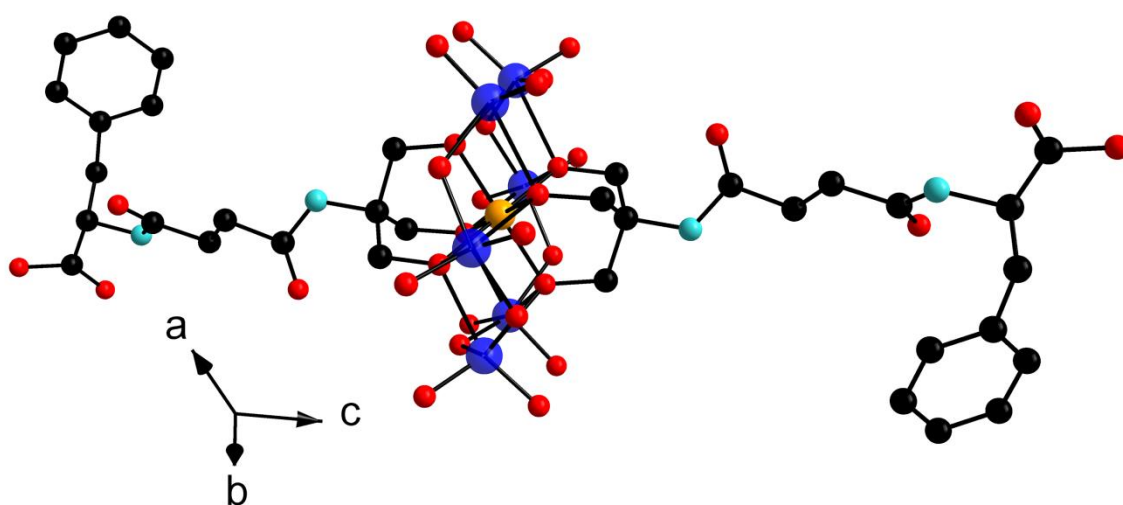

Figure 65: Ball-and-stick representation of the structure of **13** obtained by single crystal X-ray diffraction analysis of crystals grown from DMF under Et_2O vapour diffusion. TBA cations and solvent molecules are omitted for clarity. Colour scheme: Mn, orange; Mo, blue; O, red; C, black; N, cyan.

The purity of each compound was confirmed by elemental analyses (see experimental section).

These analyses demonstrate that the reaction of the precursor **11** with unmodified amino acids, Gly and Phe, in stoichiometric ratios led to the formation of peptide bonds and the desired compounds (**12** and **13** respectively), in high purity without tedious purification processes (just precipitation in Et_2O).

3.1.3.3 Summary

An NHS-activated Mn-Anderson precursor (**11**) was successfully obtained by post-functionalisation of compound (**10**) through the addition of the NHS leaving group. This precursor was isolated pure and its reactivity towards peptides tested by reaction with amino acids, Gly and Phe, yielding compound **12** and **13** respectively. The peptide bond formation reaction occurs at room temperature in DMF with the unprotected peptide in stoichiometric ratio.

This result is important for the rest of the study as it demonstrates many positive aspects of the activated precursor approach: the NHS ester/amine reaction is stoichiometric; the precursor can be produced and isolated in large batches; peptides are used in their native form; the reaction conditions are mild and well-established as compatible with biological building blocks; little variation in conditions should be required, bar the solubility demands of different peptides.

3.1.4 Section summary

In this section, important synthetic tools to make the TRIS Mn-Anderson building block compatible with peptide chemistry were developed. Solvent compatible TRIS Mn-Anderson building blocks were synthesised without the use of cation exchange processes. Reaction conditions for amide bond formation through amine and carboxylic acid additions were also established, allowing us to fully focus on the addition of peptide chains on the TRIS Mn-Anderson building block and its incorporation as a peptide sequence unit.

3.2   Incorporation of Mn-Anderson clusters as linking components

In the previous section, a NHS precursor method was tested with amino acids resulting in their incorporation on the Mn-Anderson cluster in a symmetric fashion.

The aim of this section is to further explore this method by briefly studying the introduction of TRIS-base Mn-Anderson clusters as linking components between two identical pre-synthesised peptides chains (Figure 66). The incorporated POM building block, a symmetric precursor, cannot be considered as part of the amino acid sequence. Nonetheless, interesting properties could arise from the introduction of a charged metal-oxide core between two peptide chains. This approach is also quite simple: a one pot reaction, at room temperature, with no protection or activation of the peptide chain required, and could be applied for studies in which the POM would not be required to be part of the sequence.
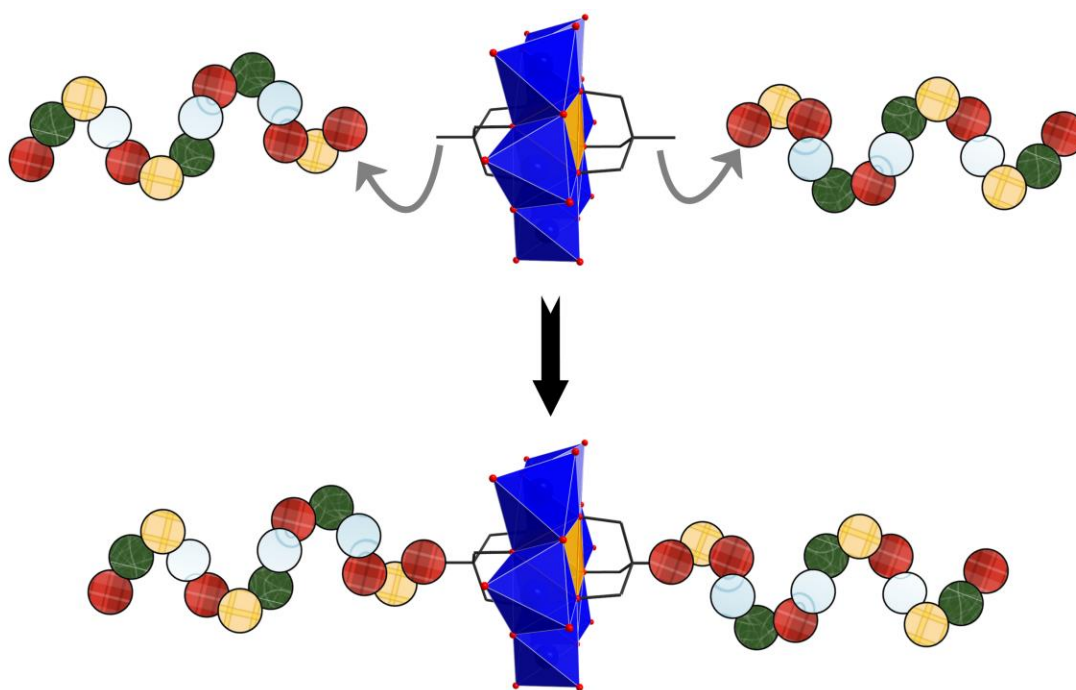
Figure 66: Schematic representation of the approach explored in this section: incorporation of the hybrid Mn-Anderson motif as a linking component between two pre-synthesised peptides.

The work presented in this section made up part of the article published in *Angewandte Chemie Int. Ed.* in 2014.[231]

3.2.1 Short peptide sequences

As the precursor methodology proved to function with amino acids, the same methodology is reported here for short peptides. Whilst simple, oligopeptides are known to display interesting self-assembly behaviour, especially di-phenylalanine (NH$_2$-Phe-Phe-OH)[193] and tri-phenylalanine (NH$_2$-Phe-Phe-Phe-OH),[232,233] which have been employed as organising motifs in many nanostructured materials.[191]

3.2.1.1 Synthesis

Compounds **14** and **15** (Figure 67) were synthesised following the established procedure, by reacting the NHS-ester activated Mn-Anderson building block (**11**) with the targeted peptides NH$_2$-Phe-Phe-OH and NH$_2$-Phe-Phe-Phe-OH respectively. **14** and **15** were isolated by simple precipitation and were then fully characterised.

14: n = 1   **15**: n = 2
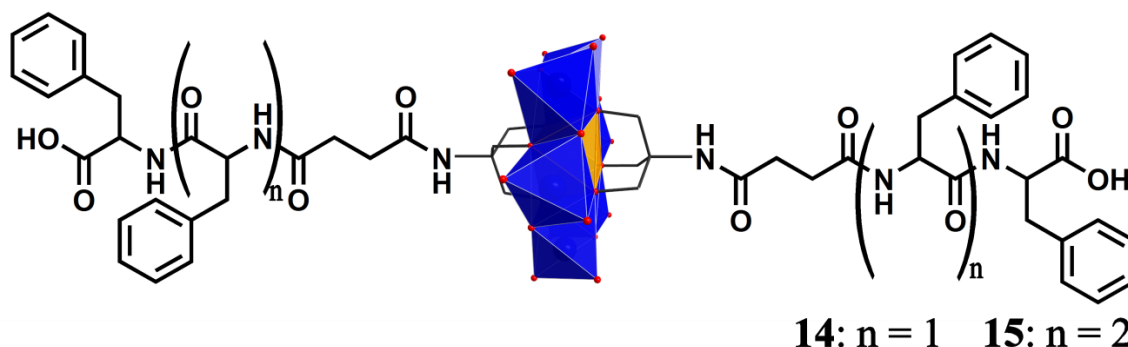
Figure 67: Schematic representation of compounds **14** and **15**. Colour scheme: Mn, orange (polyhedra); Mo, blue (polyhedra); O, red.

ESI-MS analyses proved the identities of the products isolated (Figure 68), the main peak envelopes observed being consistent with the expected general formulas of **14** and **15** ((TBA)$_3$[MnMo$_6$O$_{24}$(C$_{26}$H$_{30}$N$_3$O$_5$)$_2$] and (TBA)$_3$[MnMo$_6$O$_{24}$(C$_{35}$H$_{39}$N$_4$O$_6$)$_2$], respectively). In the ESI-MS spectrum of **14**, the four main peak envelopes observed at m/z 1538.45 (z = -3), 1618.54 (z = -4), 2430.31 (z = -1) and 2549.44 (z = -2) were assigned as [(C$_{16}$H$_{36}$N)$_3$ [MnMo$_6$O$_{24}$(C$_{26}$H$_{30}$N$_3$O$_5$)$_2$]$_2$]$^{3-}$ (predicted: 1538.41), [(C$_{16}$H$_{36}$N)$_4$[MnMo$_6$O$_{24}$(C$_{26}$H$_{30}$N$_3$O$_5$) (C$_{26}$H$_{29}$N$_3$O$_5$)]$_2$]$^{4-}$ (predicted: 1618.50), [(C$_{16}$H$_{36}$N)$_2$[MnMo$_6$O$_{24}$(C$_{26}$H$_{30}$N$_3$O$_5$)$_2$]]$^{1-}$ (predicted: 2429.26) and [(C$_{16}$H$_{36}$N)$_5$[MnMo$_6$O$_{24}$(C$_{26}$H$_{30}$N$_3$O$_5$)(C$_{26}$H$_{29}$N$_3$O$_5$)][MnMo$_6$O$_{24}$- (C$_{26}$H$_{30}$N$_3$O$_5$)$_2$]]$^{2-}$ (predicted: 2549.40), respectively. Similarly, the ESI-MS spectrum of **15** revealed four main peak envelopes at m/z 1734.61 (z = -3), 1815.04 (z = -4), 2602.90 (z = -2) and 2723.55 (z = -1) which were assigned as [(C$_{16}$H$_{36}$N)$_3$[MnMo$_6$O$_{24}$(C$_{35}$H$_{39}$N$_4$O$_6$)$_2$]$_2$]$^{3-}$ (predicted: 1734.50), [(C$_{16}$H$_{36}$N)$_4$[MnMo$_6$O$_{24}$(C$_{35}$H$_{39}$N$_4$O$_6$)(C$_{35}$H$_{38}$N$_4$O$_6$)]$_2$]$^{4-}$ (predicted:

1814.59), $[(C_{16}H_{36}N)_3H[MnMo_6O_{24}(C_{35}H_{39}N_4O_6)_2]_2]^{2-}$ (predicted: 2602.26)   and

$[(C_{16}H_{36}N)_2[MnMo_6O_{24}(C_{35}H_{39}N_4O_6)_2]]^{1-}$ (predicted: 2723.40), respectively.
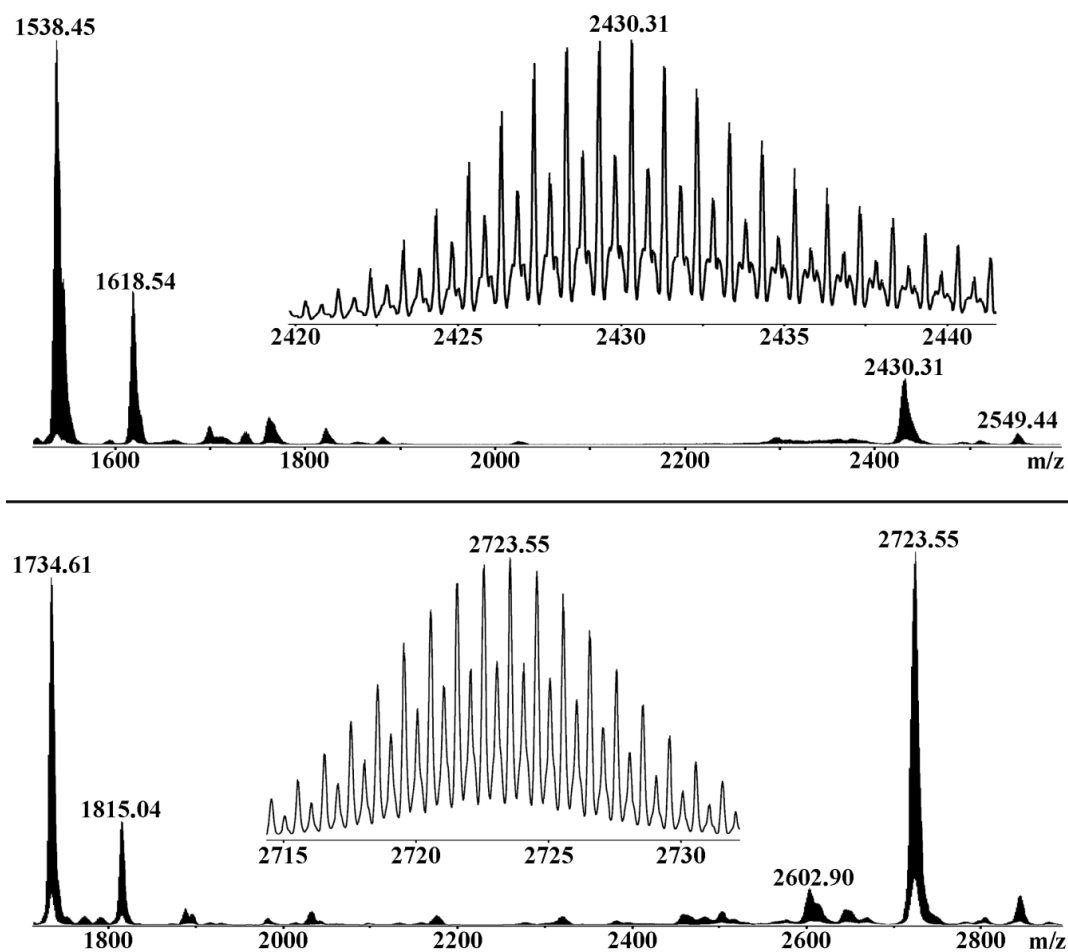
Figure 68: (Top) ESI-MS spectrum obtained for compound **14** with magnified representation of the main peak envelop at *m/z* 2430.31 assigned to $[(C_{16}H_{36}N)_2[MnMo_6O_{24}(C_{26}H_{30}N_3O_5)_2]]^{1-}$. (Bottom) spectrum obtained for compound **15** with magnified representation of the main peak envelop at *m/z* 2723.55 assigned to $[(C_{16}H_{36}N)_2[MnMo_6O_{24}(C_{35}H_{39}N_4O_6)_2]]^{1-}$.

^{1}H NMR results were also in agreement with the predicted structure of the compounds, with characteristic broad peaks observed in the 65 ppm region and the integrations of the aromatic resonances (7.85 - 6.85) matching the number of phenylalanine residues and the presence of three TBA cations (see Appendix Figure A1 and A2 for full spectra). Surprisingly, the protons of the –CH$_2$ groups of the phenylalanine side chains were not observed as well-defined peaks but very broad multiplets 3.10 to 2.50 ppm were obtained. Further investigations by COSY NMR permitted to prove that the peaks in this region are correlated to the protons of the C$_\alpha$ which appear around 4.5 ppm and present also cross peaks with the NH signal (over 8 ppm). These observations were in agreement with the assignment of the peaks in this region as the protons of the C$_\beta$ (see COSY NMR spectra Figure 69).
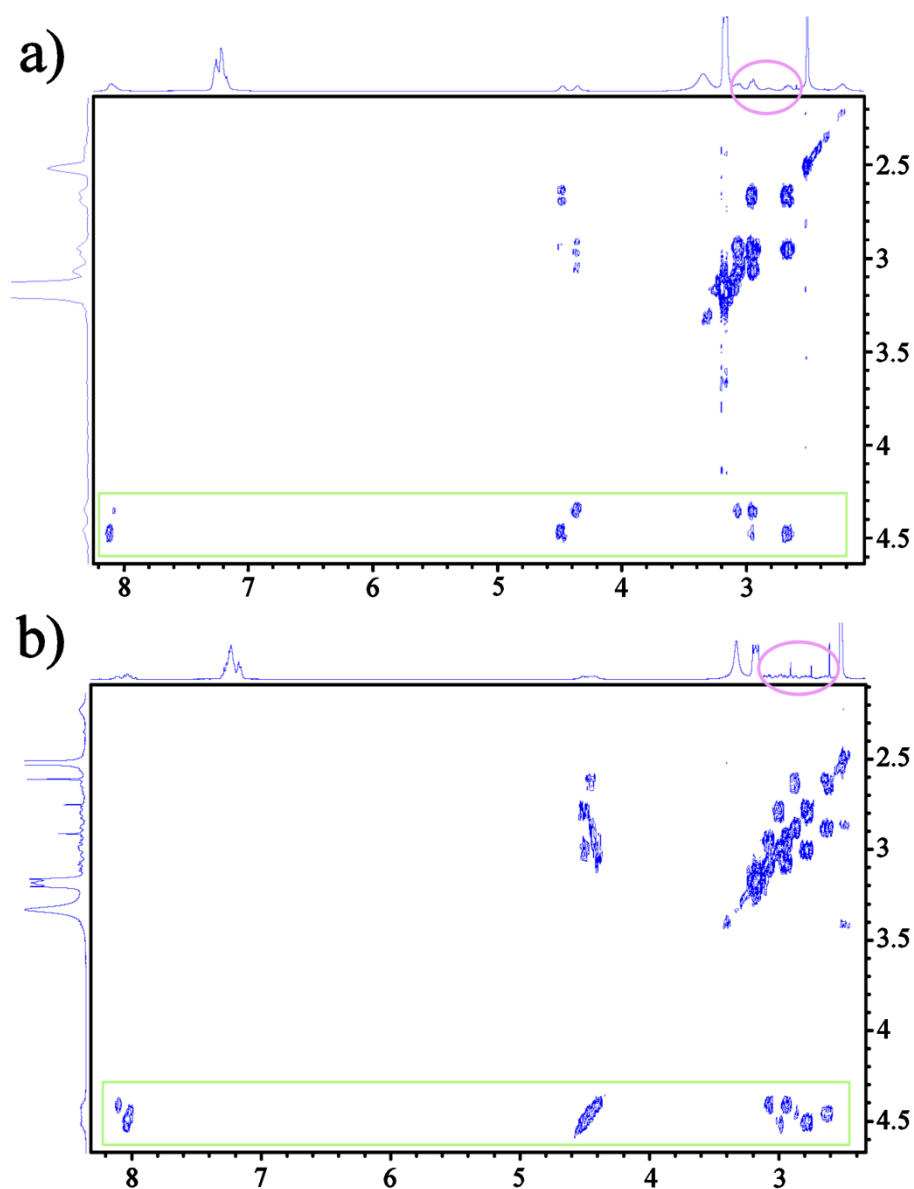
Figure 69: COSY NMR spectra of compounds **14** (a) and **15** (b) obtained on a 400 MHz spectrometer in deuterated DMSO. Correlation peaks of interest are highlighted in green; problematic region in highlighted in pink.

Purity of the samples was verified by elemental analyses and is also in agreement with the proposed formula.

These results prove that the precursor approach established is suitable to symmetrically graft oligo-peptides onto the hybrid Mn-Anderson unit without having to chemically modify the peptide chains: the NHS-activated Mn-Anderson precursor reacts with peptides in their native forms and under very mild reaction conditions. Although this technique resulted in the Mn-Anderson unit being introduced as a linking component between two peptide chains, its simplicity makes it an interesting path to functionalise POMs with peptides.

3.2.1.2 Self-assembly studies

Since Reches and Gazit discovered the self-assembling behaviour of di-phenylalanine peptides,[193] this motif was introduced in many bio-inspired nanostructured materials such as nanofibrils, nanowires, nanotubes (as seen in Section 1.3.3.1). A series of experiments to establish the self-assembly properties of the di-phenylalanine and tri-phenylalanine grafted Mn-Anderson compounds was therefore undertaken.
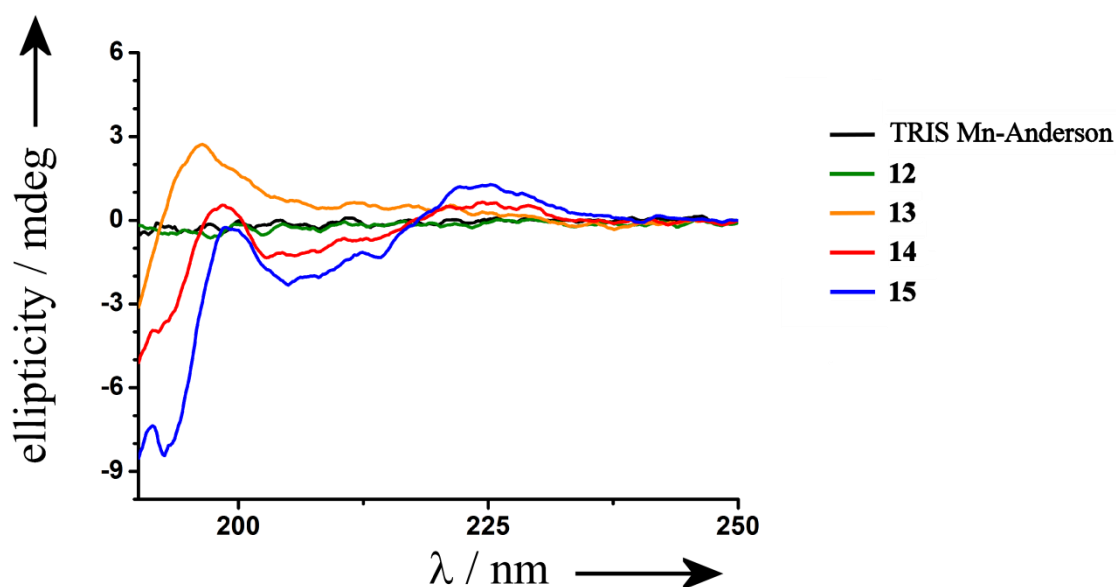
Figure 70: Far UV region CD spectra obtained for compounds **12**-**15** and TRIS Mn-Anderson in MeCN (10 μmol/L).

Self-assembly of peptides can give rise to regular secondary arrangement of the peptide chains and therefore, in some cases, characteristic CD signals may be observed (see Section 1.3.1). In order to study the self-assembly properties of the POM-peptide hybrid series, CD spectra of compounds **13**-**15** along with the Gly TRIS-based Mn-Anderson (**12**) and TRIS Mn-Anderson compounds (used as control) were recorded. As expected, the CD spectra obtained for the TRIS Mn-Anderson compound and **12** are featureless (see Figure 70), which confirms that on its own and without the appropriate ligand, TRIS-based Mn-Anderson compounds do not undergo spontaneous self-assembly. For compounds **13**-**15** CD signals were observed but were not characteristic of any regular arrangements. Interestingly, intensities of the signals increased as the number of phenylalanine residue increases (from compound **13** to **15**), suggesting stronger interactions with increasing phenylalanine chain length.

A set of measurements at various concentrations was carried out for compounds **14** and **15** to investigate the eventual concentration dependency of the interactions observed in the previous CD measurements (see Figure 71). Unfortunately, in the range of accessible concentrations (hybrid POM concentration from 0.1 to 1 mg/mL), once the CD signal were normalised, the results were near identical. This concentration independency could suggest that the observed interactions are intra-molecular ones.
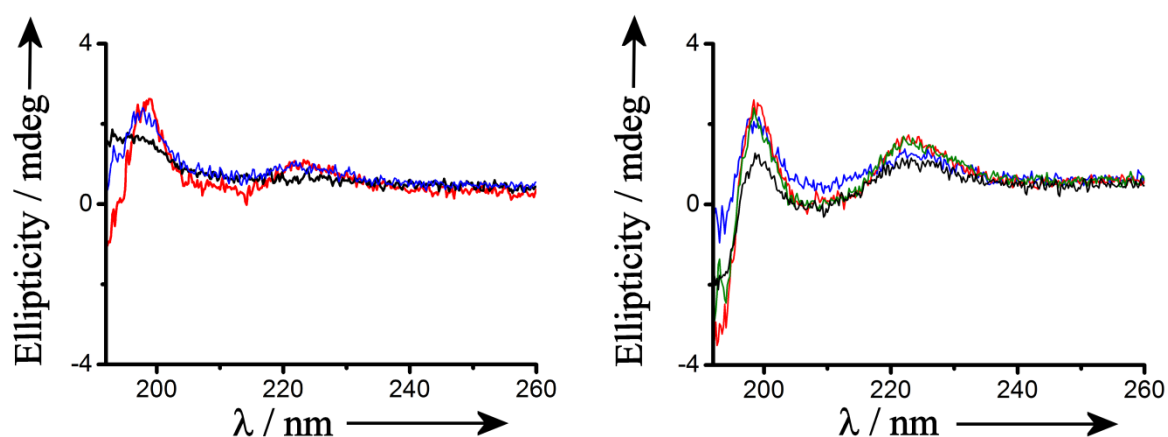
Figure 71: Normalised far UV CD spectra of compounds **14** (left) and **15** (right) in MeCN. Concentrations: 0.1 mg/mL (black), 0.5 mg/mL (blue), 0.8 mg/mL (green) and 1.0 mg/mL (red).

Organogels were obtained at much higher concentration (35 mg/mL, 13 mmol/L, 4.5 w/w%) in MeCN. For compound **15**, consisting of the tri-phenylalanine peptide, the gelation was only observed at low temperatures (-20 °C) and the gel obtained was not stable at room temperature. However, self-supporting gels which were stable at room temperature (around 20 °C) were formed upon cooling (5 °C) for solutions of **14** (Figure 72). The gel formation was a reversible process: upon heating, the solution was recovered which could then reform a gel if cooled appropriately.
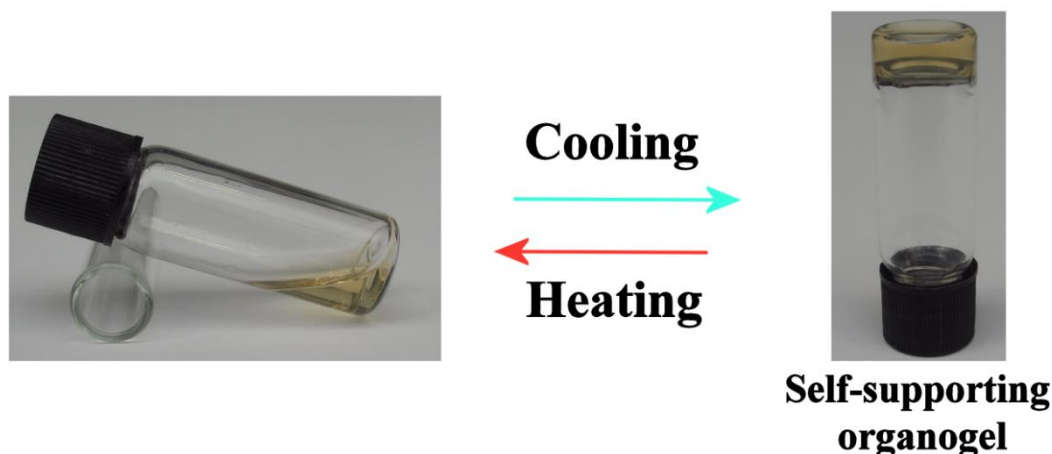
Figure 72: Self-supporting organogel stable at room temperature obtained upon cooling of an MeCN solution of **14** (4.5 w/w%). The gel formation is reversible and a solution was obtained upon heating.

With a lack of suitable techniques to fully characterise the gel, no further information concerning its structure or its properties are available. Atomic force microscopy (AFM) analysis of a drop of solution after cooling did not allow any structure elucidation, the product concentration being too high for such analysis, while dilution of the solution did not result in gel formation.

3.2.2 Long peptide sequences

To demonstrate that the NHS-precursor methodology's broad applicability reaches beyond small oligopeptides, a 15-amino acid peptide (NH$_2$-Ala-Asn-Thr-Leu-Ser-Ser-Thr-Ala-Ser-Thr-Leu-Glu-Ser-Tyr-Leu-OH, hereafter referred to as **P$_1$**) was reacted in solution with the NHS-activated Mn-Anderson building block (compound **11**). This sequence was selected for its variety of amino acids to prove that that the precursor approach is compatible with a wide range of amino acids. The resulting organic-inorganic hybrid was produced in good yields (> 80%) and fully characterised.

Purity of the isolated material was ascertained by elemental and thermogravimetric analysis (TGA) analyses and showed a small cation exchange (from TBA to sodium); both analyses are in agreement with the final formula for **16**: Na$_{0.2}$(C$_{16}$H$_{36}$N)$_{2.8}$ [MnMo$_6$O$_{24}$(C$_{74}$H$_{118}$N$_{17}$O$_{29}$)$_2$].
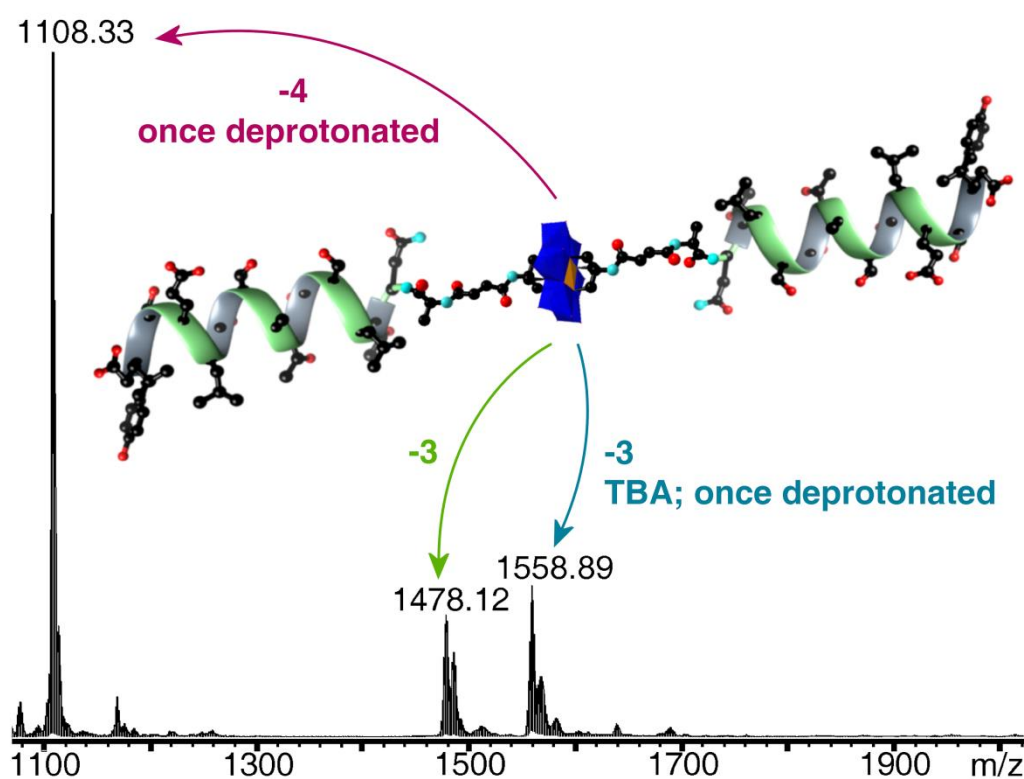
Figure 73: Mass spectrum obtained for the analysis of **16**, (Na$_{0.2}$(C$_{16}$H$_{36}$N)$_{2.8}$[MnMo$_6$O$_{24}$(C$_{74}$H$_{118}$N$_{17}$O$_{29}$)$_2$]); all major peaks are consistent with the desired product. **16** is represented in the case of the whole peptide chain adopting an *α*-helix arrangement.

The identity of the product was confirmed by ESI-MS, with all the main peak envelopes observed being consistent with the proposed structure with the peptide ligand in protonated and deprotonated forms, and varying cation mixes (see Figure 73). Peak envelopes

observed at m/z 1108.33 (z = -4), 1478.12 (z = -3), 1485.44 (z = -3) and 1558.89 (z = -3) were assigned as $[[MnMo_6O_{24}(C_{74}H_{118}N_{17}O_{29})(C_{74}H_{117}N_{17}O_{29})]]^{4-}$ (predicted: 1108.23), $[[MnMo_6O_{24}(C_{74}H_{118}N_{17}O_{29})_2]]^{3-}$ (predicted: 1477.97), $[Na[MnMo_6O_{24}(C_{74}H_{118}N_{17}O_{29})(C_{74}H_{117}N_{17}O_{29})]]^{3-}$ (predicted: 1485.30) and $[(C_{16}H_{36}N)[MnMo_6O_{24}(C_{74}H_{118}N_{17}O_{29})(C_{74}H_{117}N_{17}O_{29})]]^{3-}$ (predicted: 1558.73), respectively. 2D NMR further confirmed the isolation of the target compound (see Figure 75), with full identification of peptide chains' components, proving the chain to remained intact, and an NH signal clearly observed from the first alanine residue of P_1 (for the free amine no signal would have been detected).
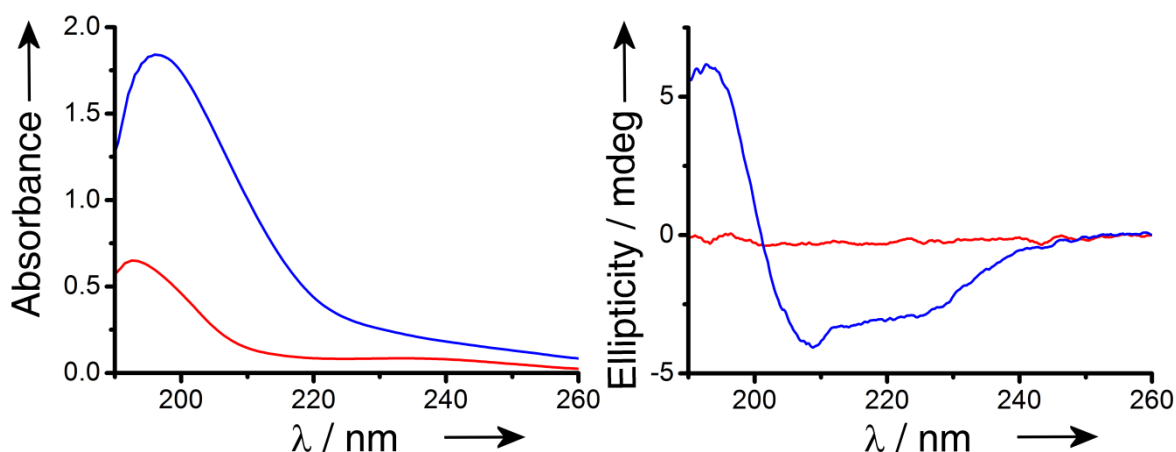
Figure 74: UV (left) and CD (right) spectra obtained for compound **16** (blue) and P_1 (red) in the far UV region; measured on saturated solution (around 10^{-5} mol/L) in MeCN.

Compound **16** is a well-defined covalent POM-peptide hybrid of unprecedented scale and can be seen as a POM cluster having been incorporated as a linker between two peptide chains of 15 amino acids each. Since the different structural motifs found in peptides exhibit distinct CD spectral features, and the overall secondary structure content of a protein can be assessed by the study in the far UV region (see Section 1.3.1), CD was chosen to investigate the new hybrid's secondary structure. Given its size and sequence, P_1 alone was not expected to manifest any regular secondary structure, it was not established if the presence of the charged metal-oxide cluster would give rise to a specific folding of the peptide ligand. UV and CD spectra were acquired for both **16** and P_1 in MeCN (Figure 74). As expected, each compound presents a UV signal characteristic of the peptide bond adsorption (from 190 nm to 250 nm). While the CD spectrum of P_1 in this region is featureless as anticipated, that of **16** is dominated by a signal characteristic of an α-helix arrangement (see Section 1.3.1 and Figure 30), with two troughs at 208 nm and 222 nm.
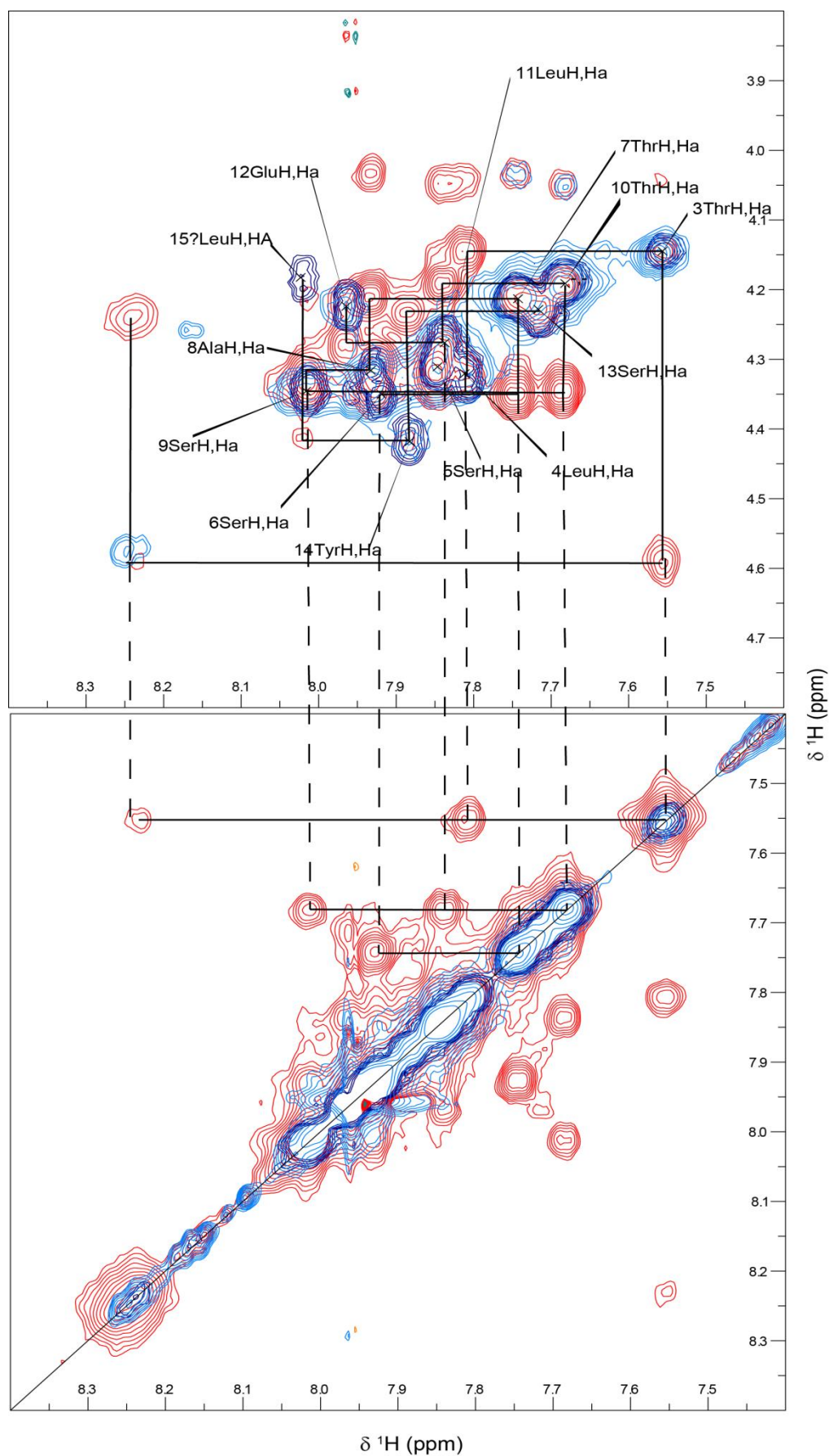
Figure 75: Expanded Ha-HN and HN-HN regions of the 2D homonuclear spectra of **16** in DMSO illustrating the inter-residue NOE connectivities. The spectra shown are magnitude COSY (dark blue), TOCSY (light blue) and NOESY (red) and were recorded at 500 MHz.

It is not clear if this feature results from a regular secondary structure in part of the molecule, or if the cluster inclusion leads to the entire peptide chain adopting a helical arrangement. Unfortunately the limited solubility of **16** in MeCN did not permit further investigation for this structure in a 2D NMR study; no peak characteristic of α-helices was observed during such a study in DMSO (unsurprising, DMSO being a more competitive solvent than MeCN). Further characterisation of the source of the CD signal in **16** is difficult considering the low solubility of the compound, nonetheless, its observation highlights how the incorporation of the POM cluster into proteins/peptides can result in significant new structural features.

3.2.3 Section summary

In this section, the NHS-ester activated Mn-Anderson building block (**11**; synthesised in previous section) was successfully reacted with a series of peptides of different length and composition without activation or protection of the peptides in a one-pot fashion. This variety of peptide chains introduced and the simplicity of the reaction conditions demonstrate the broad applicability of this NHS-precursor approach.

In this approach the POM cluster is only introduced as a linking unit between two identical peptide chains and not as part of a sequence. However, its relative simplicity could permit peptide directed POM self-assembly studies or investigations of charged metal-oxide clusters effects on peptide chain folding, as illustrated through compounds **14**-**16**.

3.3   Tackling the isolation issue of asymmetric hybrid Mn-Anderson clusters

Using the methodologies discussed in Section 3.1.3 TRIS-based Mn-Anderson units were successfully incorporated as linking components between two identical peptide chains, both grafted through the N-terminus. In order for the POM cluster to be incorporated into the backbone of a peptide sequence with one side linked to an amine and the other to an acid, the synthesis of asymmetric clusters was essential (Figure 76).
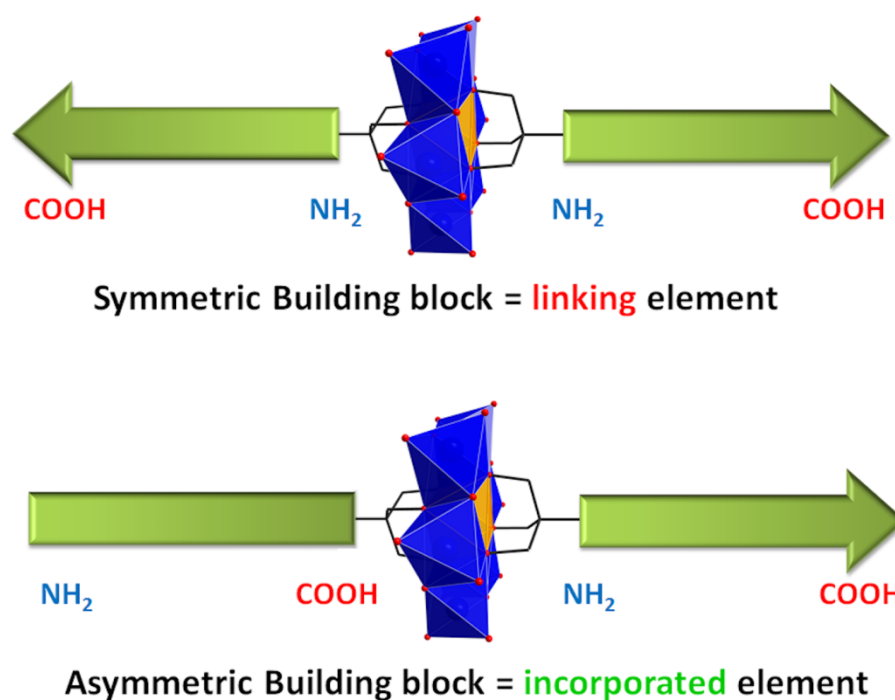
Figure 76: Schematic representation of the peptide grafting strategies available with TRIS-based Mn-Anderson building blocks. Symmetric building blocks can only be used as linking components between two peptide chains (top) while asymmetric building blocks could potentially lead to the incorporation of the POM into the backbone of a peptide sequence (bottom).

The work presented in this section was presented in a publication in *Chemical Science* in 2013;[234] further details related to the analytical results are given in this section.

3.3.1 Isolation of asymmetric TRIS-based Mn-Anderson – A problem to be solved

TRIS-based Mn-Anderson POMs are interesting clusters as they present two ligands grafted to their structure, one on each side of the planar arrangement formed by the metal-oxygen framework. This feature offers the possibility, when two different ligands are used during the formation of the hybrid cluster, of forming asymmetric clusters with a different ligand at each biding site. Unfortunately, during this synthesis two unwanted symmetrical by-products are also obtained and the one pot reaction results in a mixture of the three possible clusters present in statistical ratios (Figure 77). Methods to isolate the asymmetric cluster from the by-products by fractional crystallisation have been reported[112-115] but are efficient for only a narrow set of ligands and hard to adapt when attempting a novel kind of functionality.
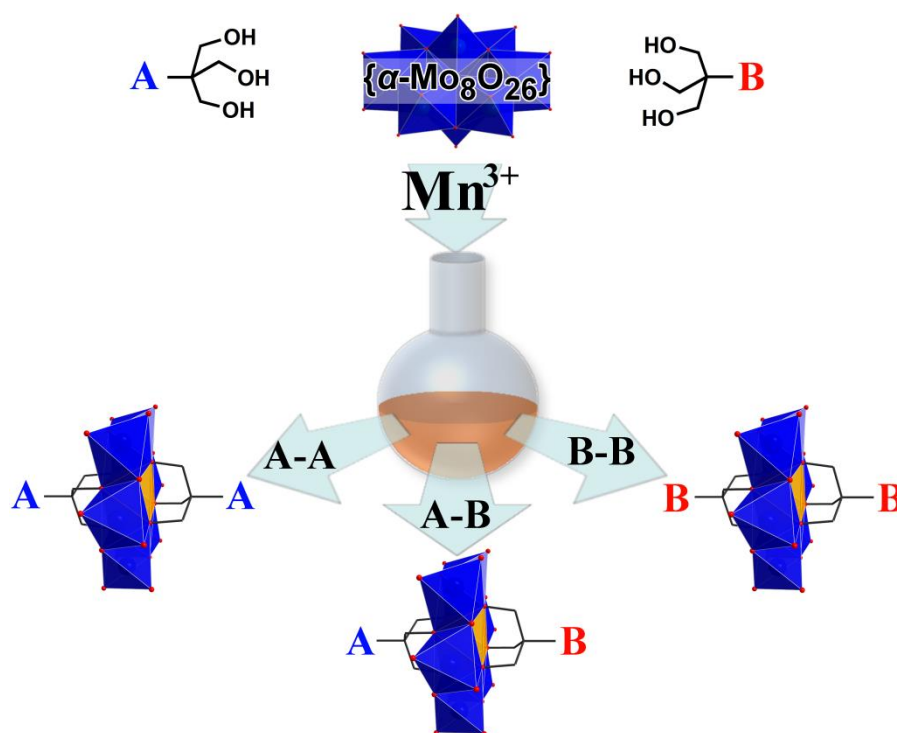
Figure 77: Schematic representation of the one pot reaction yielding an asymmetric TRIS-based Mn-Anderson cluster and two symmetric by-products. Colour scheme: Mn, orange (polyhedra); Mo, blue (polyhedra); O, red.

Before being able to pursue the peptide incorporation project, the isolation issues of asymmetric clusters had to be addressed and the results of the investigations are presented herein. A modular approach would require a reliable, simple and robust method to isolate pure asymmetric building units in good yields.

3.3.2 Implementation of a novel robust methodology

Liquid chromatography (LC) is a powerful technique which allows the analytical and preparative separation of materials from mixtures by exploiting the competitive interactions of the molecules with the stationary and mobile phases of a column. While extensively used in organic chemistry, LC is barely mentioned in hybrid POM chemistry. One attempt to purify a symmetrically grafted Mn-Anderson compound *via* normal phase chromatography was published by W. Wang *et al.*,[235] but lead to an undesired cation exchange process (protonation of the cluster, which creates solubility issues) and poor yields. This inconvenience resulted in them later reporting a post-functionalisation method which did not require further purification and writing: "the ability to circumvent chromatographic purification is extremely important […]".[109] Since reverse phase LC has been successfully applied to the resolution of various charged metal complexes,[236-238] investigations on whether it could be used to resolve, and hence purify, hybrid Mn-Anderson mixtures were carried out.

3.3.2.1 Exploration of LC resolution of hybrid Mn-Anderson mixtures – study of a model compound

In order to separate an asymmetric Mn-Anderson compound from the two corresponding unwanted symmetric by-products, the affinities of the two ligands for the stationary phase must be significantly different, yielding an asymmetric product of intermediate affinity – therefore, as a model compound, an Anthracene-TRIS/TRIS Mn-Anderson compound $((TBA)_3[MnMo_6O_{24}(C_{19}H_{16}NO)(C_4H_8N)]$, **17**) was chosen. The fluorescent Anthracene-TRIS ligand, a very hydrophobic moiety (strongly retained by RP media), could be used to form modular polymers[239] or be further functionalized by Diels-Alder reactions.[138,240] The TRIS ligand, a far less hydrophobic moiety (less strongly retained by RP media), could be further modified by established post-functionalisation techniques or used as an anchorage point for covalently functionalising surfaces. The asymmetric compound was formed following the published one pot pre-functionalisation reaction set up[49,113] where the two tris-alkoxide ligands are reacted with $(TBA)_4[\alpha\text{-}Mo_8O_{26}]$ and manganese acetate in a refluxing solution of MeCN. This reaction leads to the formation of the asymmetric product (**17**) along with two unwanted symmetric by-products: TRIS Mn-Anderson and Anthracene Mn-Anderson $(TBA)_3[MnMo_6O_{24}(C_{19}H_{16}NO)_2]$ (Figure 78). These products were all collected together as a mixture, from here on referred to as the crude mixture.
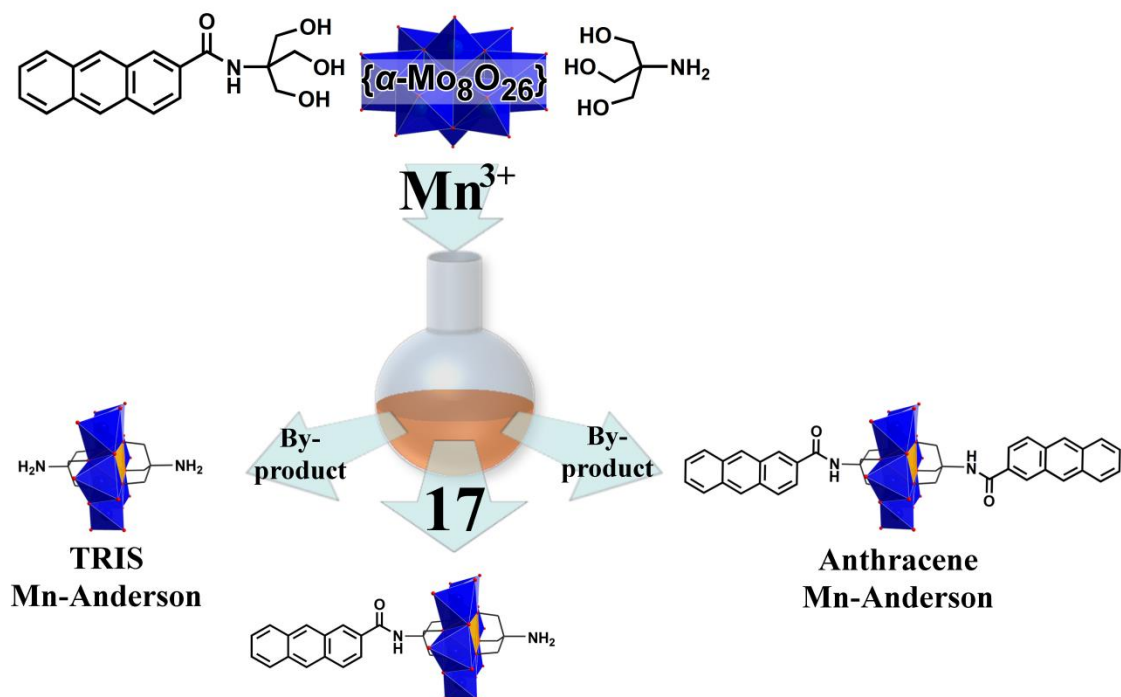
Figure 78: Schematic representation of the one pot pre-functionalisation reaction yielding asymmetric Anthracene-TRIS/TRIS Mn-Anderson compound (**17**) and two symmetric by-products: TRIS Mn-Anderson and Anthracene Mn-Anderson. Colour scheme: Mn, orange (polyhedra); Mo, blue (polyhedra); O, red.

Test separation of the crude mixture was first performed on an analytical scale using standard C_{18} RP-HPLC columns eluted with a gradient of 0.05 M ammonium acetate (pH = 6.7 - 6.9) /MeCN (A/B) solvent mixture and revealed three peaks (Figure 79a): the first one (0.85 minutes) is the least hydrophobic product, while the two subsequent products (10.22 and 11.25 min) have higher affinities for the column, being more hydrophobic. This was confirmed by comparison with analysis under the same conditions of pure samples of the symmetric by-products, synthesised following the standard protocol for symmetric synthesis.[50] As expected, each pure compound produced a single peak, with TRIS Mn-Anderson barely retained on the column (matching the 0.85 min peak in the crude mixture; see Figure 79b) and the Anthracene Mn-Anderson compound (synthesised by adaptation of a reported procedure;[49] synthesis given in the experimental section) exhibiting a high affinity for RP media (matching the 11.25 min peak in the crude mixture, see Figure 79c). The remaining peak could thus be reasonably assigned as the asymmetric product (**17**), which as expected displayed an intermediate affinity for the RP media.
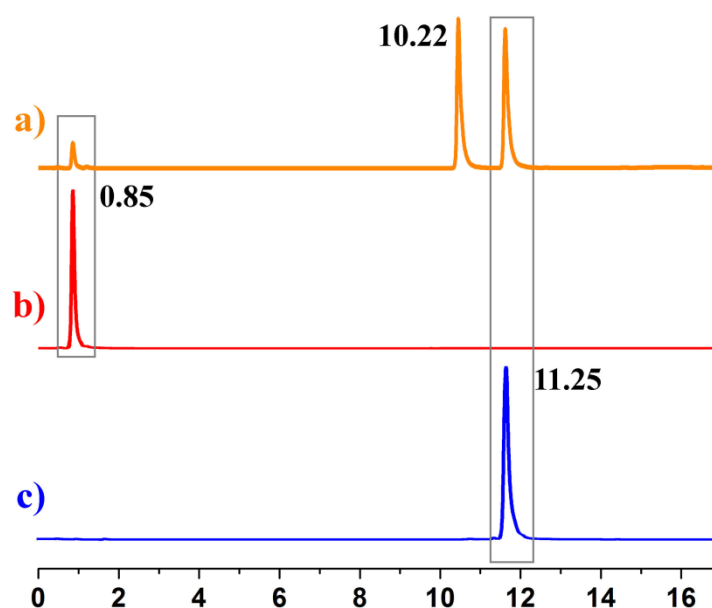
Figure 79: RP-HPLC chromatograms obtained on an analytical scale of the crude mixture (a), the symmetrically pure TRIS Mn-Anderson (b) and the symmetrically pure Anthracene Mn-Anderson (c). Peaks assigned to the same compound are highlighted in grey.

This analytical RP-HPLC method was then adapted to a preparative scale using standard commercially available C_{18} silica flash columns. Due to the poor solubility of the crude material in solvent A, it was introduced by a 'dry loading' method (adsorbed on celite, 20wt%) and the fraction of solvent B at the beginning of the gradient was increased to ensure prompt transfer from the celite adsorbant onto the RP-silica column (ensuring separation by affinity, not solubility). Elution was detected by UV and an evaporative light scattering detector (ELSD), giving the chromatograms shown in Figure 80: the sharp peaks observed in RP-HPLC are very much broadened, but are still manifested as three distinct regions (**I**, **II** and **III**).
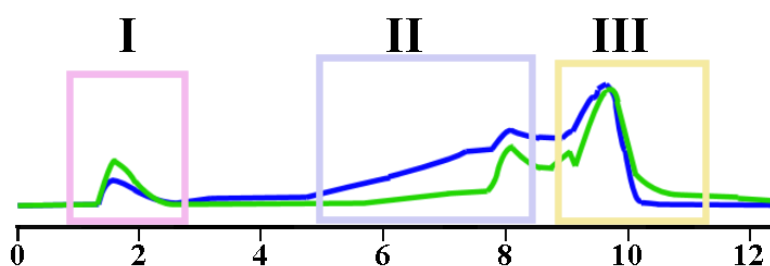
Figure 80: Chromatograms of the crude mixture separation on a preparative scale. Regions highlighted (**I**, **II** and **III**) correspond to the three products of reaction being eluted pure; in region **II** compound **17** is eluted pure. UV at $\lambda = 254$ nm: blue line; ELSD: green line.

Eluent corresponding to each region was collected (denoted as solution **I**, **II** and **III**) and analysed by ESI-MS and RP-HPLC using the previously established conditions allowing

the confirmation of the identity and the purity of the products eluted (ESI-MS spectra along with RP-HPLC chromatograms for each solution are given in Figure 81). The ESI-MS analysis of **II** confirmed the presence of the asymmetric Mn-Anderson product **17**, as several of the observed peaks can be assigned to fragments from the Anthracene-TRIS/TRIS Mn-Anderson cluster (Figure 81 and Table 4), while no peaks could be assigned to fragments of the symmetric by-products. RP-HPLC analysis of **II** confirmed its purity: only one peak was observed (at 10.17 minutes, corroborating the assignment in the analytical separation), with both symmetric by-product peaks absent. Similarly, ESI-MS and RP-HPLC analyses of solutions **I** and **II** confirmed their identities as pure symmetric products (TRIS and Anthracene Mn-Anderson, respectively).
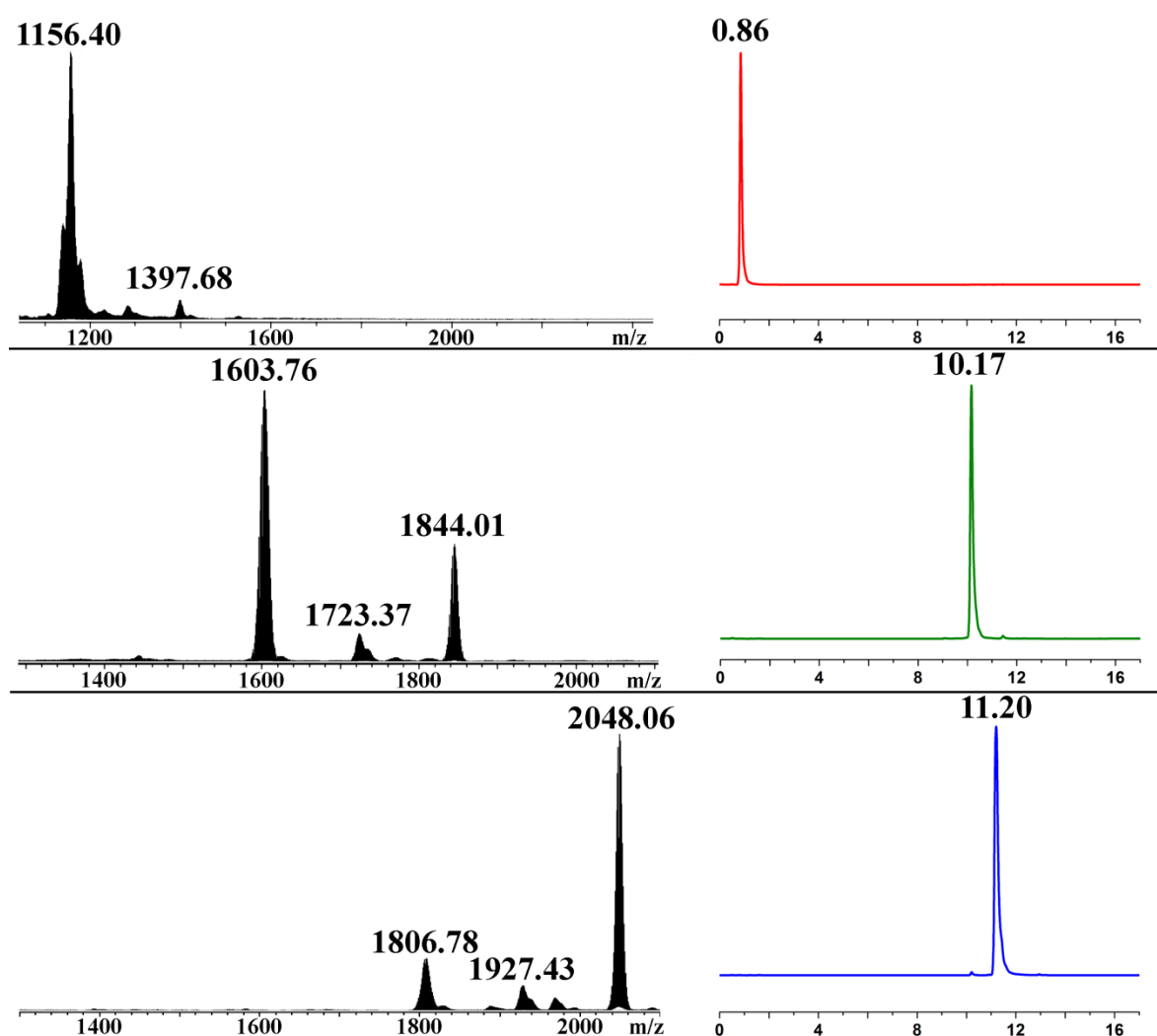
Figure 81: ESI-MS spectra (left) and RP-HPLC chromatogram (right) obtained by analysis of the eluent collected for each region (top, red) region **I**; (middle, green) region **II** in which is found compound **17**; (bottom, blue) region **III**. Assignment table of the main peak envelopes observed in the ESI-MS spectra is given in Table 4.

Table 4: Assignment table of the main peak envelopes observed during ESI-MS analyses of solution **I** (red), **II** (green) and **III** (blue); see Figure 81.

Formula assigned	z	m/z calculated
$[MnMo_6O_{24}(C_4H_8N)_2]H_2$	-1	1156.40
$[MnMo_6O_{24}(C_4H_8N)_2](C_{16}H_{36}N)_1H$	-1	1397.68
$[MnMo_6O_{24}(C_{19}H_{16}NO)(C_4H_8N)](C_{16}H_{36}N)_1H$	-1	1602.73
$[MnMo_6O_{24}(C_{19}H_{16}NO)(C_4H_8N)]_2(C_{16}H_{36}N)_3H$	-2	1723.37
$[MnMo_6O_{24}(C_{19}H_{16}NO)_2](C_{16}H_{36}N)_1H$	-1	1806.79
$[MnMo_6O_{24}(C_{19}H_{16}NO)(C_4H_8N)](C_{16}H_{36}N)_2$	-1	1844.01
$[MnMo_6O_{24}(C_{19}H_{16}NO)_2]_2(C_{16}H_{36}N)_3H$	-2	1927.43
$[MnMo_6O_{24}(C_{19}H_{16}NO)_2]_3(C_{16}H_{36}N)_5H$	-3	1967.64
$[MnMo_6O_{24}(C_{19}H_{16}NO)_2](C_{16}H_{36}N)_2$	-1	2048.07

To isolate **17**, solution **II** was collected and an excess of TBA bromide was added to ensure that **17** was isolated as a pure TBA salt (during ESI-MS analysis some protonated fragments were observed leading to the suspicion that some minor cation exchange may occur in solution). The MeCN was evaporated leaving an aqueous solution from which an orange precipitate forms; this precipitate was crystallised from MeCN under slow Et_2O diffusion to yield pure compound **17**.

Resulting crystals were analysed by single crystal X-ray crystallography, which demonstrated the typical Mn-Anderson organisation of the POM framework and the asymmetric feature of the compound with the TRIS ligand on one side of the metal-oxygen framework and the Anthracene-TRIS ligand on the other (Figure 82). The structure determination also confirmed the isolation of the POM as a TBA salt with the clear observation of three TBA cations per cluster. Compound **17** crystallises as orange block shaped crystals in a monoclinic crystal system, in space group $P2_1/c$. The unit cell is $a = 27.455(3)$, $b = 29.007(3)$, $c = 24.974(2)$ Å. $\beta = 94.450(5)$ °, the volume V is 19 829(3) Å^3 and Z is 8.
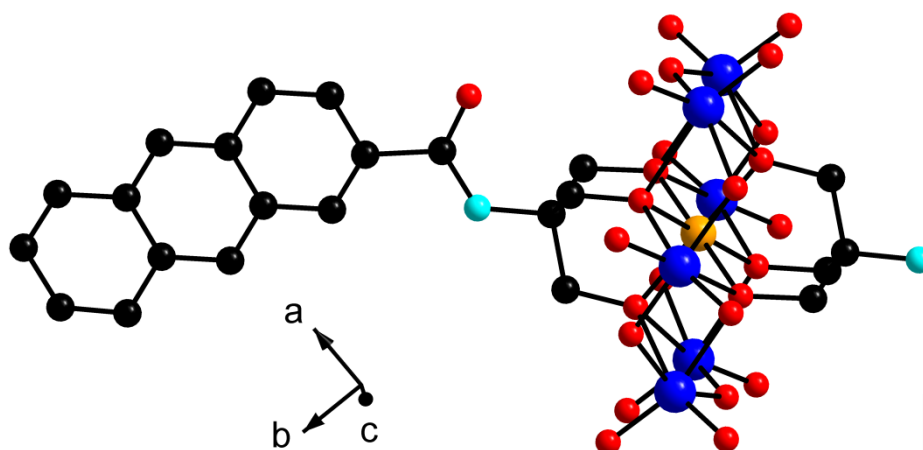
Figure 82: Ball-and-stick representation of the structure of **17** obtained by single crystal X-ray diffraction analysis of crystals grown from MeCN under Et_2O vapour diffusion. TBA cations and solvent molecules are omitted for clarity. Colour scheme: Mn, orange; Mo, blue; O, red; C, black; N, cyan.

Elemental analysis of the isolated dried powder was consistent with the proposed formula of **17** and the purity of the isolated compound was further proved by RP-HPLC analysis, and the presence of a unique signal at 10.21 min assigned to the asymmetric compound (given in the appendix Figure A3 and A4). ESI-MS analysis in MeCN is in agreement with the given structure of **17** and the absence of by-products (spectra and assignment table given in Figure A5 and Table A1).

^{1}H NMR analysis of the isolated material is in agreement with the asymmetric character of the hybrid cluster with the integrations assigned to one anthracene ligand (aromatic region and NH of the amide from 8.6 to 7.5 ppm integrating for 10H) matching the presence of three TBA cations (Figure 83).
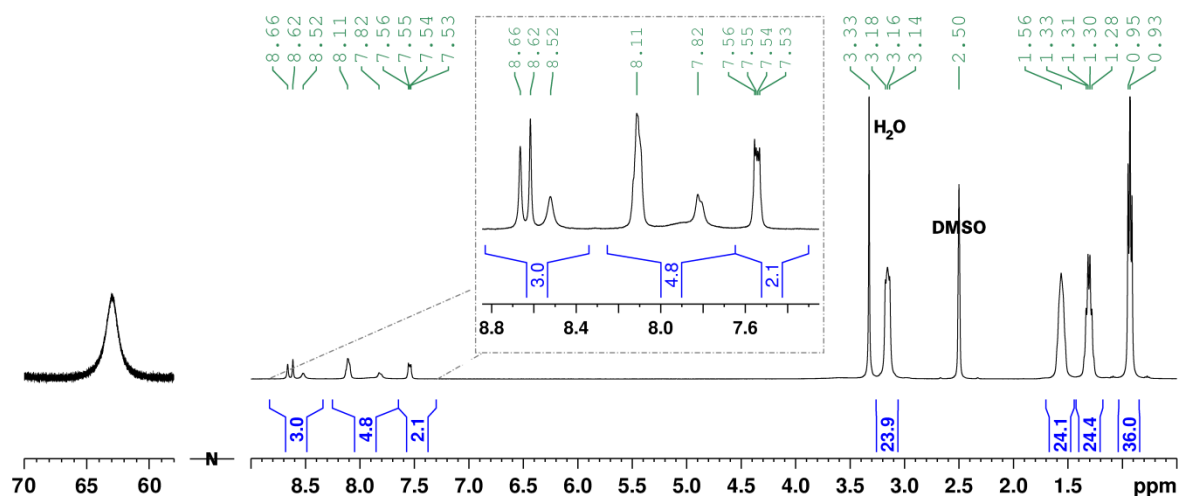
Figure 83: ^{1}H NMR spectra of compound **17** after isolation by chromatography obtained on a 400 MHz spectrometer in deuterated DMSO.

The separation by flash chromatography and the isolation of compound **17** is highly reproducible. Figure A6 (Appendix) shows chromatograms for repetition of the same separation under the same conditions producing comparable yields and purity. The efficiency of the separation, repeatability of the result, and the simplicity of the workup, make this chromatographic method suitable for the isolation of **17**. Nevertheless, a widely applicable method should be valid for a variety of pendant groups, so a study of its applicability was carried out for other asymmetric Mn-Anderson clusters.

3.3.2.2 Exploration of the robustness of the LC-methodology – Post-functionalisation approaches

To investigate whether the chromatographic methodology would be broadly applicable, two other ligand systems were studied under the same conditions as those established for compound **17**. In literature reports, asymmetric hybrid Mn-Anderson compounds have only been synthesised *via* pre-functionalisation routes, so the formation of asymmetric Mn-Anderson compounds using different post-functionalisation approaches was investigated. Here, the crude mixtures were synthesised by modification of the TRIS Mn-Anderson building block using the reactive amine groups grafted on the POM as anchorage points to introduce more complex ligands. The use of a general precursor allows the circumvention of the ligand synthesis step and the direct access of certain functional groups which might make free ligands difficult to isolate (*e.g.* carboxylic acids).

The crude mixture of compound **18** was produced by reacting the preformed TRIS Mn-Anderson cluster with two different anhydrides: palmitic and succinic (Figure 84). These ligands were selected firstly for their different hydrophobicities as well as other properties. Clusters with the hydrophobic palmitic ligand have been proven to form self-assembled amphiphilic features,[107] while the succinic anhydride introduces a carboxylic acid group on the cluster (see Section 0), which could subsequently be used as an anchorage point for further post-functionalisation. The reaction conditions were briefly refined to give the asymmetric compound as the major product. It was found that 4 equivalents of succinic anhydride and 2 equivalents of the palmitic anhydride (compared to the TRIS Mn-Anderson compound) lead to compound **18** ($(TBA)_3[MnMo_6O_{24}(C_{20}H_{38}NO)(C_8H_{12}NO_3)]$) as the major product.
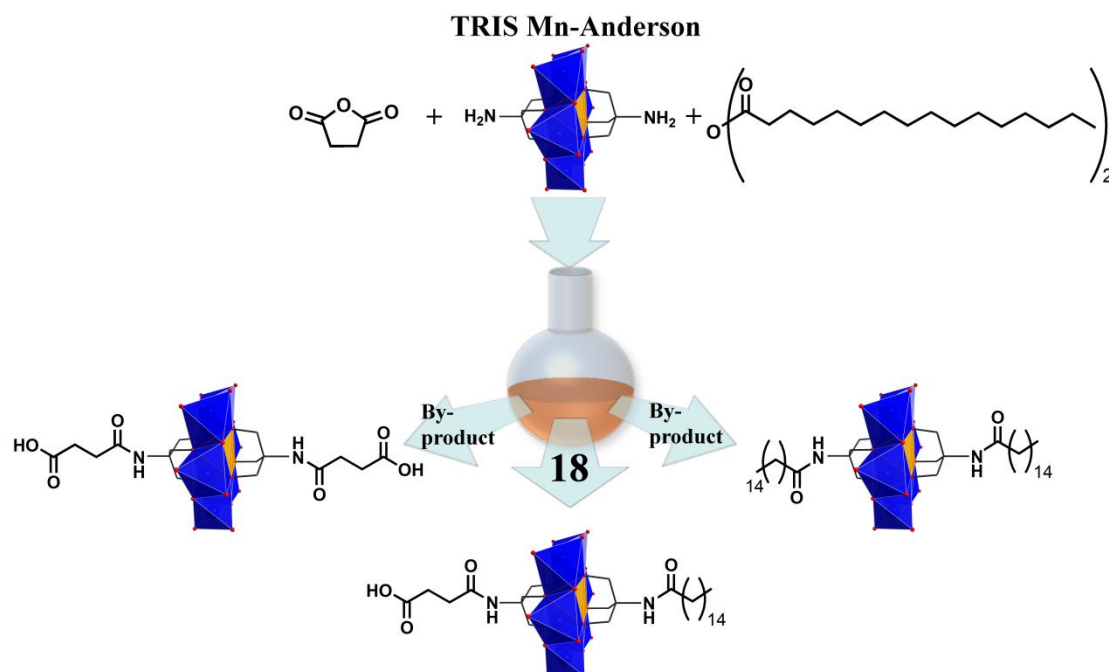
Figure 84: Schematic representation of the one-pot post-functionalisation reaction yielding asymmetric TRIS-based Mn-Anderson compound (**18**) and two symmetric by-products. Colour scheme: Mn, orange (polyhedra); Mo, blue (polyhedra); O, red.

The synthesis of the crude mixture of compound **19** was adapted from a reported procedure where palmitoyl chloride was used to react with both amines forming a symmetrically grafted Mn-Anderson amphiphile.[107] Here, the number of equivalents of palmitoyl chloride was reduced to obtain asymmetric compound **19** ($(TBA)_3[MnMo_6O_{24}(C_{20}H_{38}NO)$ $(C_4H_8N)]$) as the major product (Figure 85) but, as for other synthetic procedures, two symmetric by-products are also present in the reaction mixture (not represented on the figure).
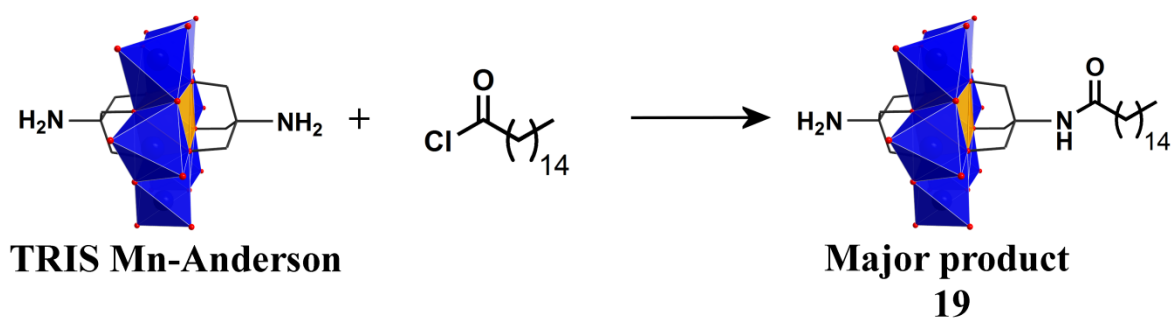
Figure 85: Schematic representation of the one pot post-functionalisation reaction, yielding asymmetric TRIS-based Mn-Anderson compound (**19**) as the major product and two symmetric by-products (not represented). Colour scheme: Mn, orange (polyhedra); Mo, blue (polyhedra); O, red.

The mother liquors of both reactions were directly adsorbed on celite and purified using the chromatographic methodology established for compound **17**. As for compound **17**, the chromatograms of compounds **18** and **19** consisted of three distinct regions with the middle one corresponding to the asymmetric product (Figure 86). Compounds **18** and **19** were both isolated as pure TBA salts using the same work up as that established for the isolation of compound **17**.
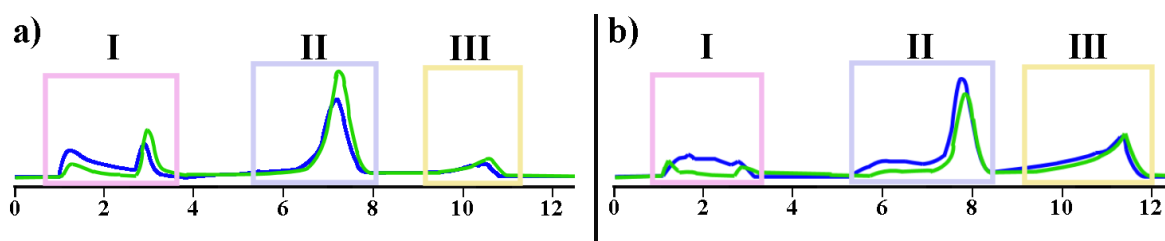
Figure 86: Chromatograms of the crude mixture separations on a preparative scale. Regions highlighted (**I**, **II** and **III**) correspond to the three products of reaction being eluted pure. (a) Crude mixture yielding **18**; (b) crude mixture yielding **19**. UV at $\lambda = 254$ nm: blue line; ELSD: green line.

The identity of the isolated compounds was established by ESI-MS and ^{1}H NMR analyses. In the ESI-MS spectrum of both products, only peak envelopes assigned to the corresponding asymmetric clusters were observed (Figure 87). In the spectrum obtained for compound **18**, the signals observed at m/z 1978.19 (z = -1), 2098.83 (z = -2) and 2220.46 (z = -1) are assigned respectively to the mono-charged species $[(TBA)_2[MnMo_6O_{24}(C_{20}H_{38}NO)(C_8H_{12}NO_3)]]^{1-}$ (predicted: 1978.20), the doubly-charged dimer $[(TBA)_5[MnMo_6O_{24}(C_{20}H_{38}NO)(C_8H_{12}NO_3)][MnMo_6O_{24}(C_{20}H_{38}NO)(C_8H_{11}NO_3)]]^{2-}$ (predicted: 2098.84) and the mono-deprotonated cluster $[(TBA)_2[MnMo_6O_{24}(C_{20}H_{38}NO)(C_8H_{11}NO_3)]]^{1-}$ (predicted: 2220.48). For compound **19** two mono-charged species with different cations $[(TBA)H[MnMo_6O_{24}(C_{20}H_{38}NO)(C_4H_8N)]]^{1-}$ and $[(TBA)_2[MnMo_6O_{24}(C_{20}H_{38}NO)(C_4H_8N)]]^{1-}$ are observed respectively at m/z 1635.90 (predicted: 1636.90) and 1878.18 (predicted: 1878.18). The obtained NMR spectra (Figure A7 and A8) are in agreement with the isolation of asymmetric Mn-Anderson clusters as pure TBA salts with the observation of the characteristic peak in the 60 ppm region and the integrations of the resonances assigned to the ligands matching the ones of the three TBA cations.
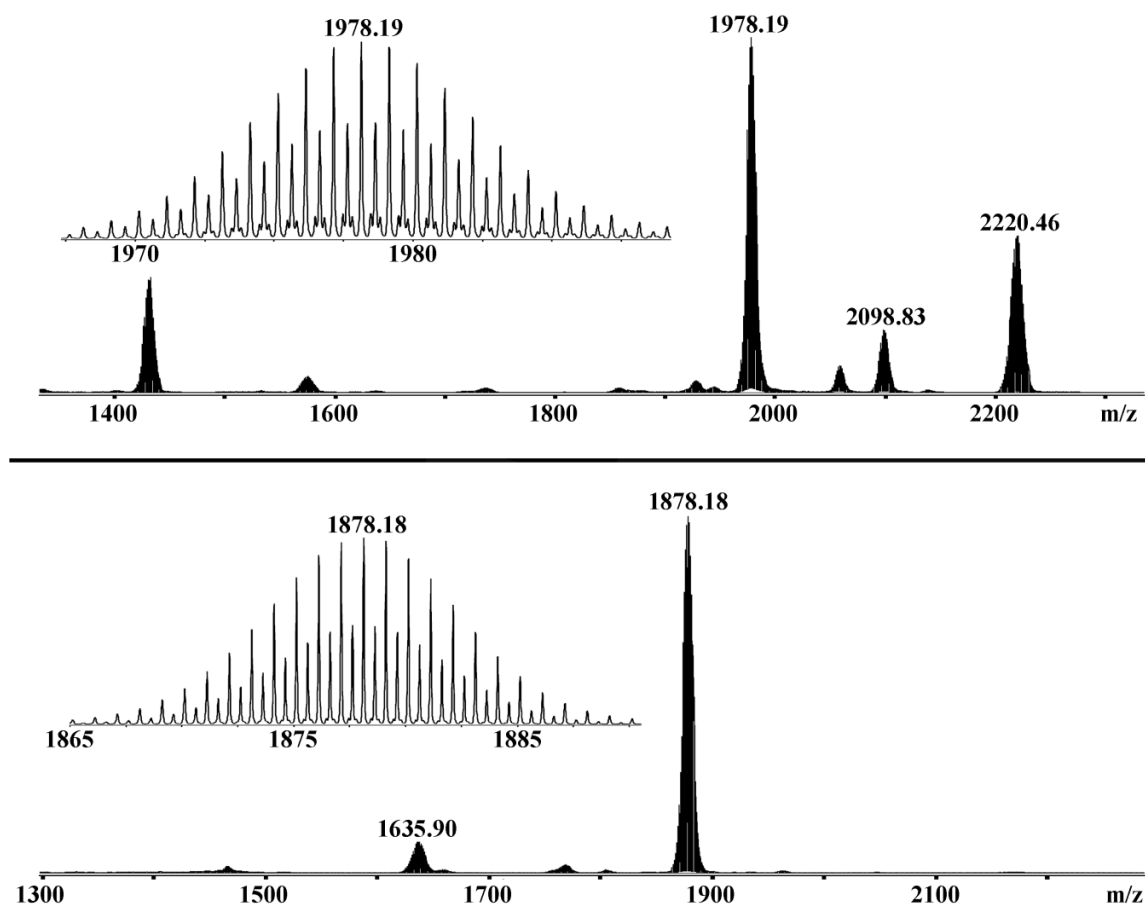
Figure 87: ESI-MS spectra obtained for compound **18** (top) and **19** (bottom) with respective magnified representations of the main peak envelopes (at m/z 1978.19 assigned to $[(TBA)_2[MnMo_6O_{24}(C_{20}H_{38}NO)(C_8H_{12}NO_3)]]^{1-}$ and m/z 1878.18 assigned to $[(TBA)_2[MnMo_6O_{24}(C_{20}H_{38}NO)(C_4H_8N)]]^{1-}$).

Purity was checked by elemental analyses for both compounds and analytical RP-HPLC was also used to give further insight into the purity and the identity of each isolated product. As shown in Figure 88, only one compound, the one of intermediate affinity, is present, giving a single signal on the chromatograms.
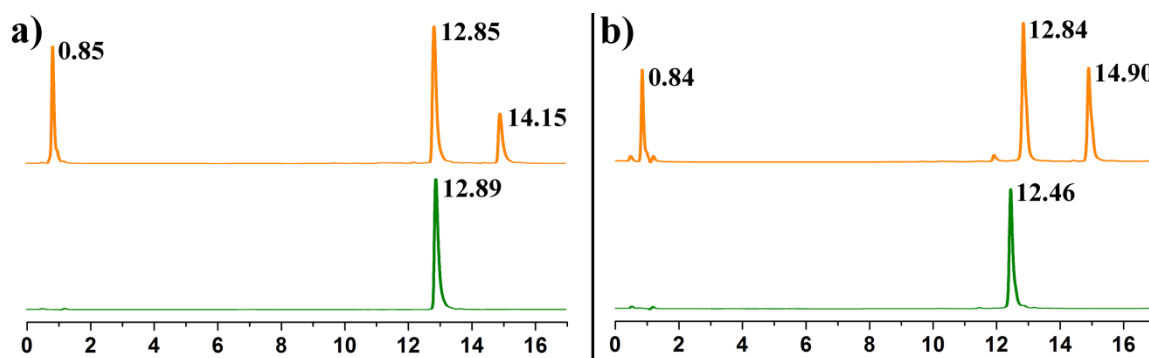
Figure 88: RP-HPLC chromatograms obtained before and after resolution of the crude mixtures by preparative chromatography. (a) Synthesis of compound **18**; (b) synthesis of compound **19**. Crude mixture before chromatography: orange line (top); pure compound after isolation by chromatography: green line (bottom).

The isolation of compound **18** and **19** following the same methodology as that established for compound **17**, without any alterations, demonstrates that this method can be reliably applied to purify a range of asymmetric hybrid Mn-Anderson clusters, so long as the ligands have sufficiently different affinities for RP media. However, to entirely eradicate the asymmetric isolation 'issue', thereby allowing full focus on the design and study of the asymmetric compounds rather than their separation, resolution of Mn-Anderson clusters with different ligands of similar affinity for the RP media must also be addressed.

3.3.3 Precursor approach to the asymmetric synthesis - A "universal" asymmetric Mn-Anderson building unit

The chromatographic methodology presented herein uses the differences of affinity for the RP stationary phase of the three compounds present in the crude mixture. Compounds **17** to **19** all have one hydrophilic and one hydrophobic ligand, hence the reaction mixtures are readily resolved. However, if two similarly-hydrophobic ligands were used, this method would not give sufficient resolution for a preparative separation (*i.e.* asymmetric products with two hydrophobic or two hydrophilic ligands would not be separated from their symmetric by-products). To overcome this issue, the idea of an asymmetric compound that could be isolated using the present chromatographic methodology and could then be used as a "universal" precursor for the synthesis of asymmetric Mn-Anderson compounds arose. Such a compound should have a reactive site which can be modified easily by post-functionalisation techniques and a protected site that can be deprotected by simple reaction steps compatible with the metal-oxide core.

3.3.3.1 Design of the "universal" precursor

The Fmoc,[241] group used for the protection of amines, which can be removed under mild conditions potentially compatible with the POM cluster (treatment with a solution of piperidine), is extremely hydrophobic, making it an appealing candidate for the protection of a "universal" precursor. Thus, an Fmoc protected TRIS ligand was synthesised following a reported procedure[242] and used to form an Fmoc-TRIS/TRIS Mn-Anderson compound (**20**, $(TBA)_3[MnMo_6O_{24}(C_{19}H_{18}NO_2)(C_4H_8N)]$), *via* a pre-functionalisation approach. The reaction mixture was easily resolved using the chromatographic method (Figure 89) and the asymmetric compound **20** was isolated.
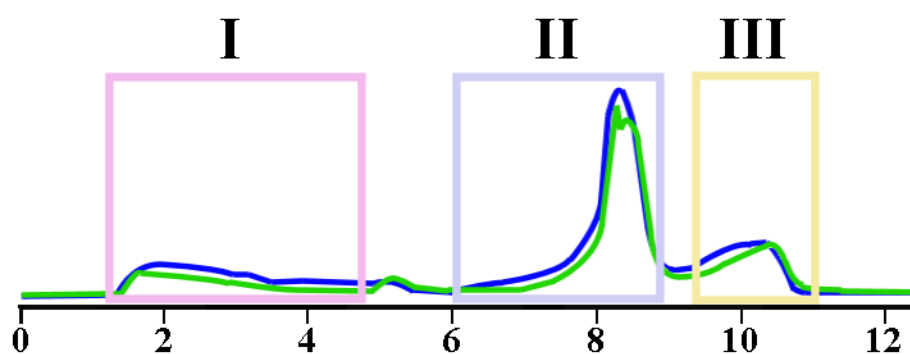
Figure 89: Chromatograms of the crude mixture separation on a preparative scale. Regions highlighted (**I**, **II** and **III**) correspond to the three products of reaction being eluted pure; in region **II** compound **20** is eluted pure. UV at $\lambda = 254$ nm: blue line; ELSD: green line.

The purity of the isolated product was controlled by elemental and RP-HPLC analyses. In the RP-HPLC chromatogram (Figure A9 and A10) a single peak is observed at 10.27 min, retention time which correlates with the central peak observed during the RP-HPLC analysis of the reaction mixture and assigned as the asymmetric POM.

ESI-MS and ^{1}H NMR analyses both confirmed the identity of the compound isolated and the absence of symmetric by-product within the obtained material. During ESI-MS analysis (Figure 90), the two main peak envelopes observed at m/z 1620.73 ($z = -1$) and 1862.02 ($z = -1$) are assigned respectively to the species $[(TBA)H[MnMo_6O_{24}(C_{19}H_{18}NO_2)(C_4H_8N)]]^{1-}$ (predicted: 1620.74) and $[(TBA)_2[MnMo_6O_{24}(C_{19}H_{18}NO_2)(C_4H_8N)]]^{1-}$ (predicted: 1862.02). Signals of the symmetric by-products would be expected at m/z 1639.95 for $[(TBA)_2[MnMo_6O_{24}(C_4H_8N)_2]]^{1-}$ and at m/z 2085.09 for $[(TBA)_2[MnMo_6O_{24}(C_{19}H_{18}NO_2)_2]]^{1-}$, but are not observed. ^{1}H NMR analysis confirmed the isolation of a TRIS-based Mn-Anderson compound with the observation of the characteristic broad peak in the 60 ppm region (spectra given in the Appendix Figure A11). Furthermore, the integrations of the Fmoc protected TRIS ligand moiety are in agreement with the asymmetric feature of the molecule and the presence of three TBA cations.
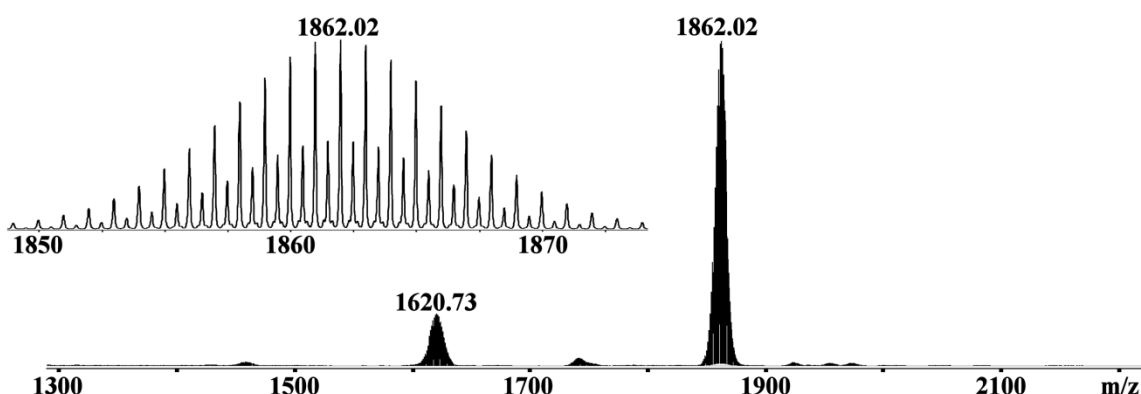
Figure 90: ESI-MS spectrum obtained for compound **20** with magnified representation of the main peak envelope at m/z 1862.02 assigned to $[(TBA)_2[MnMo_6O_{24}(C_{19}H_{18}NO_2)(C_4H_8N)]]^{1-}$.

The structure of **20** was obtained by single crystal X-ray crystallography, confirming the Fmoc protection of one amine of the TRIS Mn-Anderson cluster (Figure 91). Compound **20** crystallises as orange block shaped crystals in an orthorhombic crystal system, in space group *Pnma*. The unit cell is $a = 28.257(2)$, $b = 21.8128(16)$, $c = 16.5796(14)$ Å, the volume V is 10219.1(14) Å^3 and Z is 4. The Fmoc moiety is equally disordered between two positions within the crystal structure as shown in Figure 91.
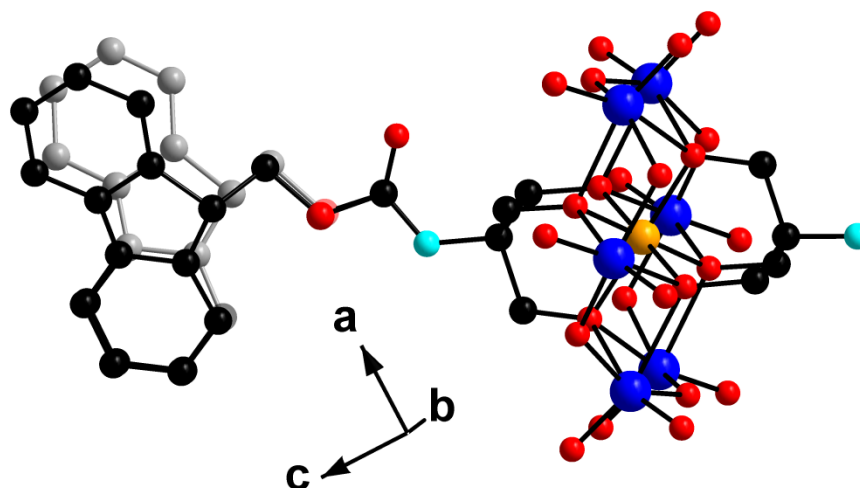
Figure 91: Ball-and-stick representation of the crystal structure obtained for the Fmoc-TRIS/TRIS Mn-Anderson compound (**20**). Colour scheme: Mn (orange); Mo (blue); O (red); C (black); N (cyan). Disorder is shown as 50 % opacity, TBA cations and solvent molecules are omitted for clarity.

3.3.3.2 Proof of concept

To illustrate the idea that compound **20** could be used as a "universal" asymmetric precursor to synthesise practically any asymmetric organic-inorganic Mn-Anderson cluster, it was used to synthesise **21** ((TBA)$_3$[MnMo$_6$O$_{24}$(C$_7$H$_{12}$NO)(C$_4$H$_8$N)]), an asymmetric Propylamide/TRIS Mn-Anderson compound which could not previously be isolated using the chromatographic methodology, since neither the symmetric nor the asymmetric compounds are sufficiently hydrophobic to be retained on the column. A two-step synthesis was designed to yield **21** (Figure 92); **20** was first reacted with 10 equivalents of propionic anhydride and the intermediate product isolated by crystallisation to remove the excess of acid. Before proceeding to the next step of the synthesis, ESI-MS analysis of the isolated compound was carried out to verify that the intermediate species had been successfully produced (the ESI-MS spectrum obtained is given in the Appendix Figure A12). Signals observed during this analysis were in agreement with the expected structure of the intermediate and no peak envelopes could be assigned to the starting material (see assignment table), proving the completion of the reaction.
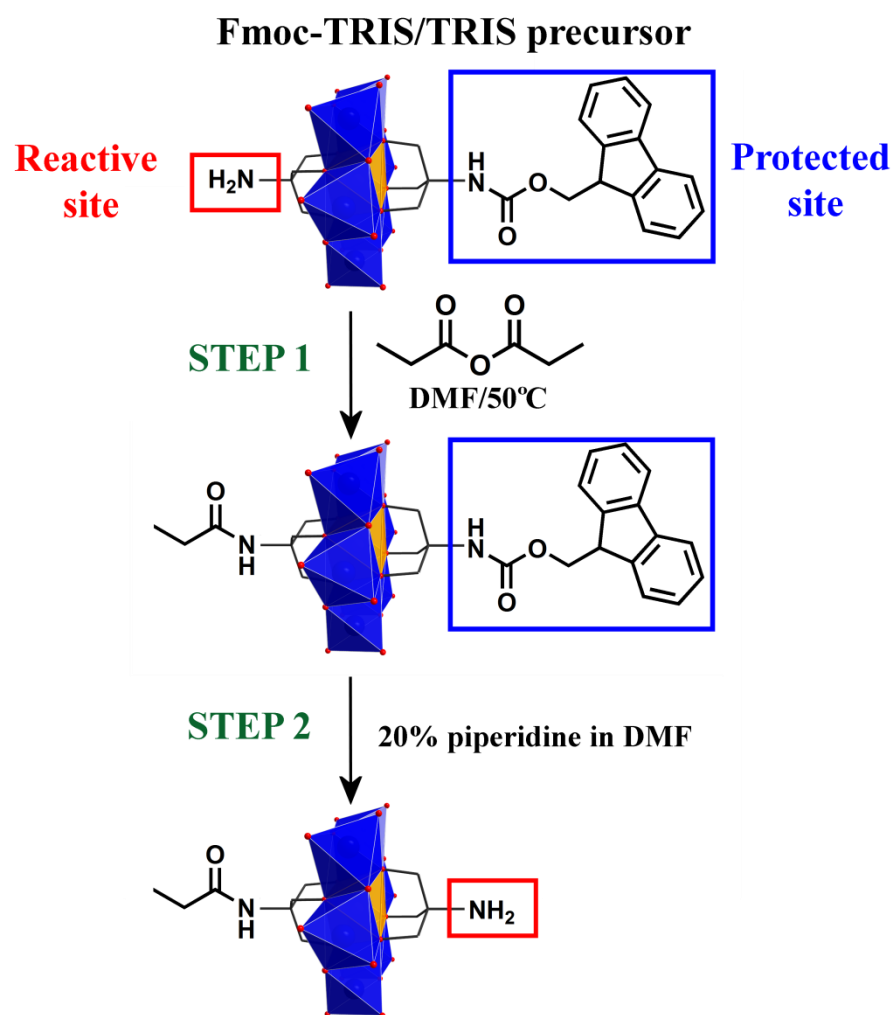
Figure 92: Schematic representation of the synthetic route for the synthesis of **21** by post-functionalisation of the "universal" asymmetric Mn-Anderson precursor (**20**). Colour scheme: Mn, orange (polyhedra); Mo, blue (polyhedra); O, red.

The intermediate product was then treated with a 20% solution of piperidine in DMF to remove the Fmoc group and the resulting material was isolated by crystallisation with Et_2O diffusion.

Crystal structure of the obtained product was determined by single crystal X-ray crystallography analysis. Compound **21** crystallises as orange flat sheet shaped crystals in an orthorhombic crystal system, in space group *Pcca*. The unit cell is a = 23.3192(17), b = 28.200(2), c = 30.215(2) Å, the volume V is 19 869(3) Å^3 and Z is 8. The structure, analogous to that of TRIS-based Mn-Anderson compounds, proves that the POM cluster is stable to the reaction conditions used during the post-functionalisation and that the addition of a propylamide group on the reactive site and the deprotection of the amine function were successful (Figure 93).
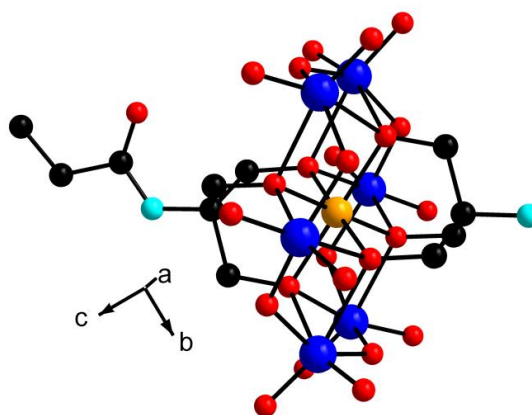
Figure 93: Ball-and-stick representation of the crystal structure obtained for the Propylamide/TRIS Mn-Anderson compound (**21**). Colour scheme: Mn (orange); Mo (blue); O (red); C (black); N (cyan). TBA cations and solvent molecules are omitted for clarity.

Identity of the product was further investigated by ESI-MS and ^{1}H NMR analyses. All peak envelopes observed in the ESI-MS spectrum could be assigned to ionic fragments of **21** (Figure 94). No starting material or intermediate product could be observed during this analysis (signals expected at *m/z* 1862.02 (z = -1) and 1918.05 (z = -1) for the starting material and the intermediate product, respectively). Main peak envelopes displayed in the spectrum at *m/z* 1453.44 (z = -1), 1586.05 (z = -2) and 1695.68 (z = -1) could be assigned respectively as [(TBA)H[MnMo$_6$O$_{24}$(C$_7$H$_{12}$NO)(C$_4$H$_8$N)]]$^{1-}$ (predicted: 1453.70), [(TBA)$_3$-Na[MnMo$_6$O$_{24}$(C$_7$H$_{12}$NO)(C$_4$H$_8$N)]$_2$]$^{2-}$ (predicted: 1586.33) and [(TBA)$_2$[MnMo$_6$O$_{24}$-(C$_7$H$_{12}$NO)(C$_4$H$_8$N)]]$^{1-}$ (predicted: 1695.98). ^{1}H NMR analysis clearly proved the successful deprotection of the amine group, with no aromatic proton signal observed in the spectra, and the stability of the hybrid POM cluster (observation of the broad peak in the 60 ppm region; Figure A13). The peak integrations are in agreement with the asymmetric feature of the cluster (*i.e.* the presence of only one propylamide-TRIS ligand) with the observation of a broad peak at 7.37 ppm integrating for 1H (assigned to the proton of the

amide) and the integrations of the propyl group matching the ones of the three TBA cations.
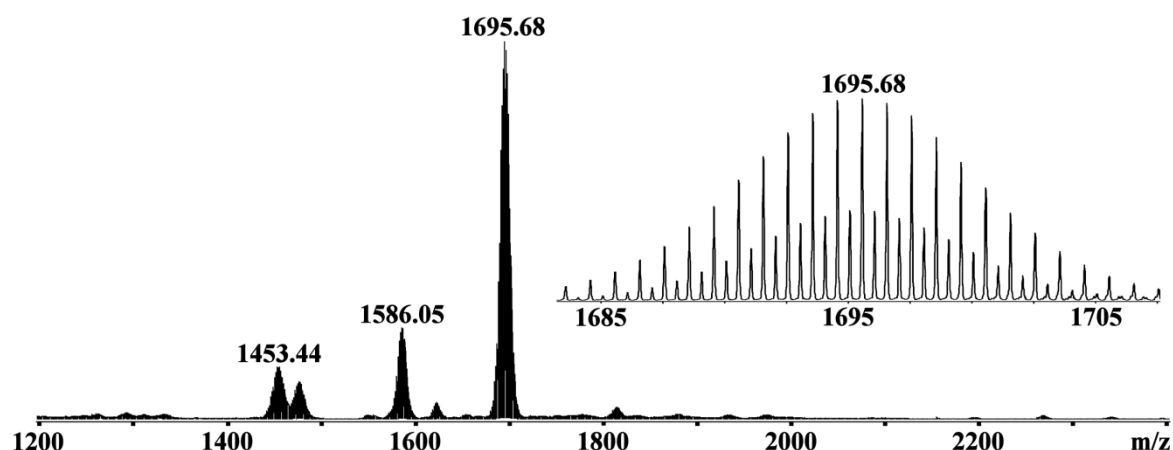
Figure 94: ESI-MS spectrum obtained for compound **21** with magnified representation of the main peak envelope at *m/z* 1695.68 assigned to $[(TBA)_2[MnMo_6O_{24}(C_7H_{12}NO)(C_4H_8N)]]^{1-}$.

The purity of the synthesised asymmetric compound **21** was verified by elemental analysis.

All these analyses revealed that the amine was fully deprotected while the hybrid Mn-Anderson remained intact and as a pure TBA salt. **20** can therefore be considered a "universal" asymmetric Mn-Anderson precursor (barring unstable or reactive groups) since its structure allows for the formation and isolation of practically any other asymmetric Mn-Anderson compound by a succession of post-functionalisation steps.

3.3.4   Section summary

A reliable chromatographic methodology which drastically simplifies the isolation of asymmetric Mn-Anderson compounds, providing a difference in affinity for RP media between the two ligands was established. Where this condition is not met, the difficulty can be overcome by post-functionalisation of a synthesised "universal" asymmetric Mn-Anderson precursor (**20**). This suite of approaches should allow the routine isolation of practically any asymmetric Mn-Anderson compound, as illustrated by the diversity of the new compounds (**17**-**21**) presented in this section.

The isolation issues hampering the synthesis of asymmetric TRIS-based Mn-Anderson clusters being now resolved, the incorporation of the cluster into peptide backbones can be fully explored.

3.4   Incorporation of Mn-Anderson clusters into peptide backbones.

In the work presented in Section 3.2, a symmetric Mn-Anderson building unit was introduced as a linking component between two identical pre-synthesised peptide chains. Having now achieved the isolation of asymmetric clusters (Section 3.3), the integration of hybrid Mn-Anderson clusters into peptide backbones, with an amine on one side and an acid group on the other side, can be explored.

Much of the unique characteristics of chemically-synthesised peptides is derived from the stepwise modular nature of their synthesis. The aim of this section is to explore the incorporation of the metal-oxide building block directly during the synthesis of a peptide as conveniently as any other amino acid (Figure 95). This approach would give a great flexibility to investigate molecular recognition motifs, catalytically active or structurally important proteins.
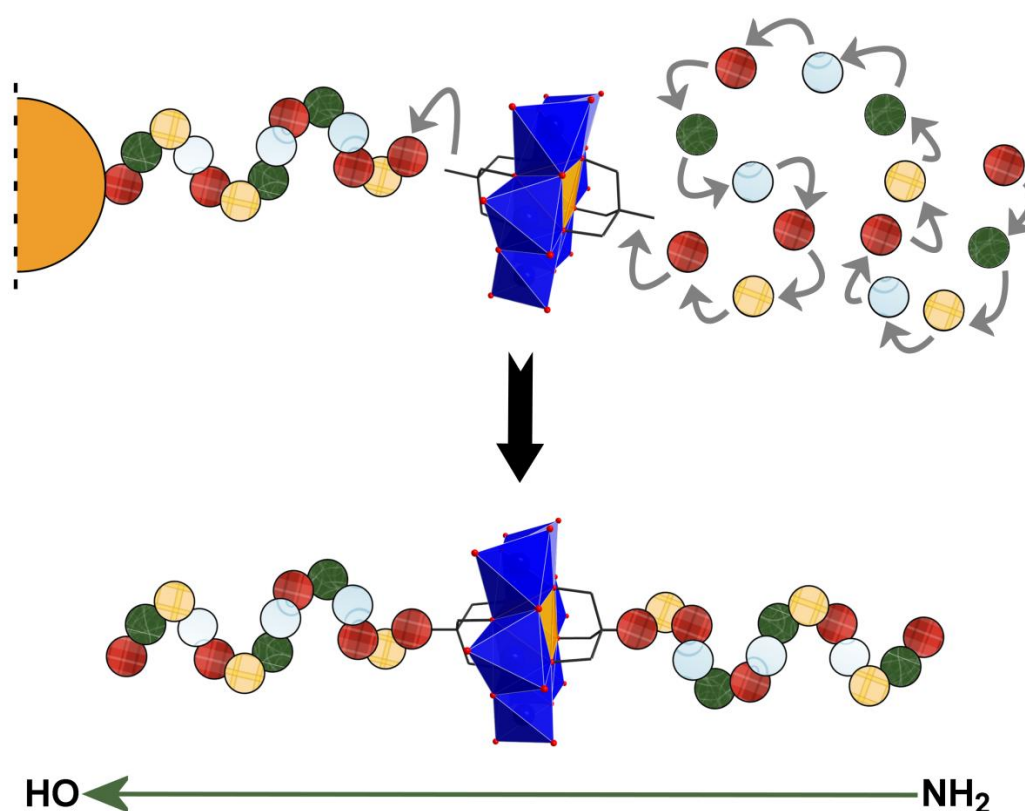
Figure 95: Schematic representation of the approach explored in this section: incorporation of the hybrid Mn-Anderson motif as an unnatural amino acid unit into a growing peptide chain during SPPS.

The work presented in this section made up part of the article published in *Angewandte Chemie Int. Ed.* in 2014.[231]

3.4.1 Synthesis of a hybrid POM amino acid

The first step before using hybrid POM amino acids in solid phase peptide synthesis (SPPS) protocols was the isolation of a hybrid amino acid building block itself, so that it could easily be synthesised in large batches. With the methodologies developed in Section 3.1 and the universal asymmetric building block designed and developed in Section 3.3.3 (compound **20**), all the components were present to synthesise the first hybrid POM amino acid.

Compound **22**, an NHS ester-activated acid/Fmoc-protected amine Mn-Anderson cluster, $(TBA)_3[MnMo_6O_{24}(C_{12}H_{15}N_2O_5)(C_{19}H_{18}NO_2)]$, was synthesised *via* the two-step post-functionalisation of compound **20** (Figure 96). **20** was first treated by an excess of succinic anhydride to introduce an acid carboxylic function which was then activated by an ester formation through treatment with DCC and NHS (post-functionalisation reactions developed in Section 3.1).
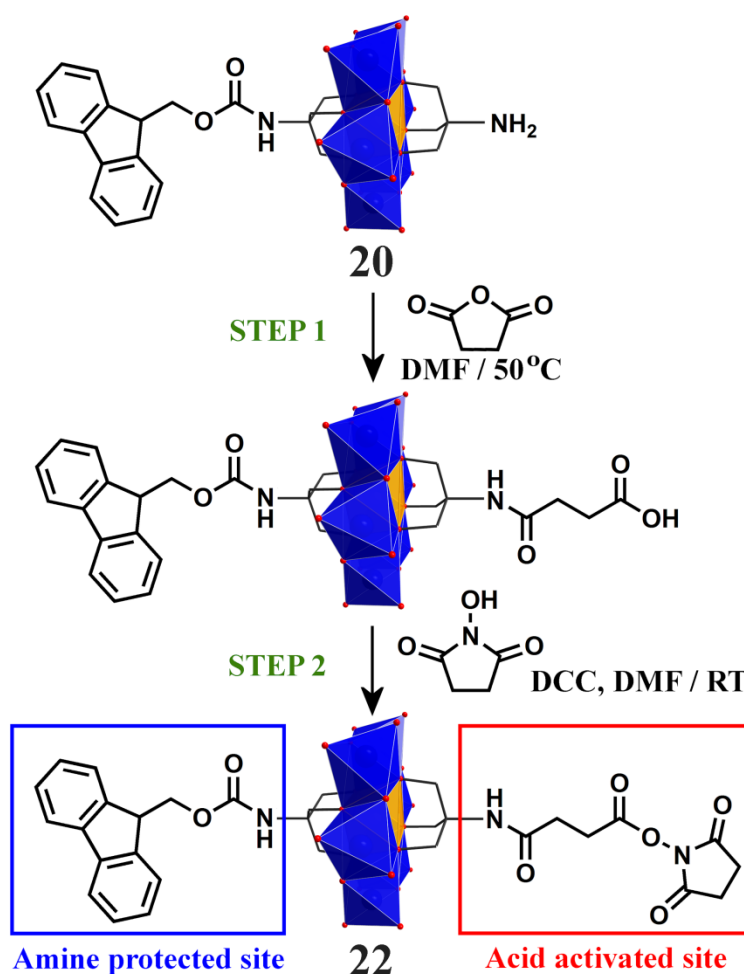
Figure 96: Schematic representation of the two-step synthesis yielding compound **22**, an NHS ester-activated acid/Fmoc-protected amine asymmetric Mn-Anderson cluster. Colour scheme: Mn, orange (polyhedra); Mo, blue (polyhedra); O, red.
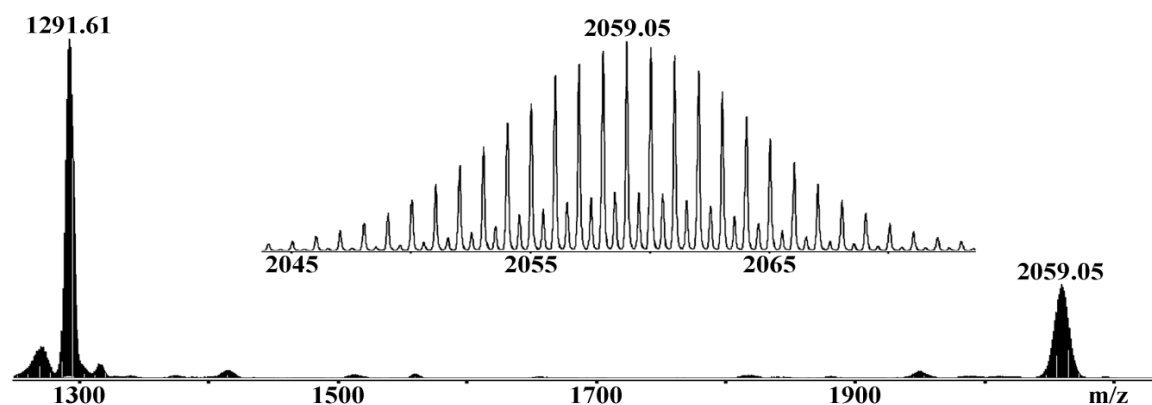
Figure 97: ESI-MS spectrum obtained for compound **22** with magnified representation of the main peak envelope at m/z 2059.05 (z = -1) assigned to $[(TBA)_2[MnMo_6O_{24}(C_{12}H_{15}N_2O_5)(C_{19}H_{18}NO_2)]]^{1-}$.

The product was analysed by elemental analysis to confirm its purity, while ESI-MS and ^{1}H NMR techniques were employed to confirm its identity. During ESI-MS analysis, two main peak envelopes were observed both in agreement with the proposed formula of product **22** (Figure 97). The first signal at m/z 1291.61 (z = -3) was assigned as $[(C_{16}H_{36}N)_3[MnMo_6O_{24}(C_{12}H_{15}N_2O_5)(C_{19}H_{18}NO_2)]_2]^{3-}$ (predicted: 1291.94) while the peak envelope at m/z 2059.05 (z = -1) was identified as $[(C_{16}H_{36}N)_2[MnMo_6O_{24}(C_{12}H_{15}N_2O_5)(C_{19}H_{18}NO_2)]]^{1-}$ (predicted: 2059.05). ^{1}H NMR also confirmed the synthesis of the expected product. The characteristic broad peak in the 65 ppm region was observed, and the resonances integrations in the 9 - 0 ppm region are in agreement with its asymmetric character as well as the presence of three TBA cations (Figure 98). Resonances from 7.9 to 7.3 ppm (integrating in total for 8H) are attributed to the aromatic protons of the Fmoc group (8H) while the broad peak observed at 2.83 ppm integrating for 8H is assigned to the two $-CH_2$ of the NHS group and the two $-CH_2$ resulting from the addition of the succinic anhydride (8 protons in total).
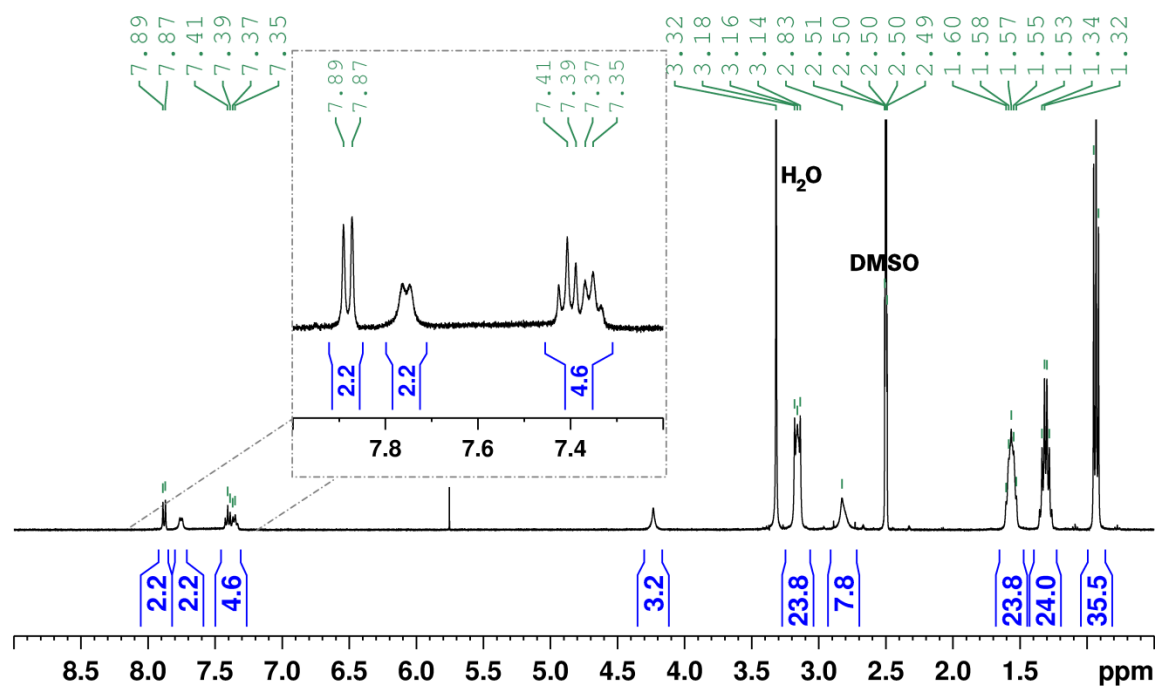
Figure 98: ^{1}H NMR spectra of compound **22** obtained on a 400 MHz spectrometer in deuterated DMSO (contains 0.03 % (v/v) TMS).

Growth of single crystals was attempted by slow Et$_2$O diffusion into DMF solution of **22**, but the quality of the crystals obtained (thin needle-shaped) was too poor for single crystal X-ray crystallographic analysis.

The hybrid amino acid building block could be synthesised in large batches, high yield (>85 %) and good purities, making it an excellent building block to use for the study of POM-peptide hybrid synthesis.

3.4.2 Making solid phase peptide synthesis (SPPS) compatible with hybrid POM amino acids

Before starting the synthesis of a POM-peptide hybrid many parameters had to be tested to verify the compatibility of the POM cluster with the reaction conditions of the different steps of SPPS. The three main points to investigate were: i) How can the POM-peptide hybrid synthesised be cleaved from the solid support without damaging the metal-oxide cluster? ii) How can the Mn-Anderson building block unit be coupled to the solid support? iii) How can the peptide synthesis continue after the incorporation of the Mn-Anderson residue?

Test reactions were thus carried out to study the parameters that would allow the synthesis of a POM-peptide hybrid chain (including retrieving it from the solid support). A small amount of material was used for each test (typically 10 - 20 mg) and ESI-MS analysis was used to check results in a binary manner (working/not working).

3.4.2.1 Choice of the solid support, the linker and cleavage conditions

The choice of the solid support, the linker and the cleavage conditions were key aspects that required careful consideration, given the somewhat low compatibility of the hybrid with SPPS reagents (sensitivity of the POM to acids, oxidant, reductant and strong bases). Examples of hybrid POMs immobilised[80,230,243] and post-functionalised[244] on a solid support are present in the literature, but solid phase was never used as an intermediate state, and no method yet exists to retrieve the hybrid POMs from the support.

Out of the range of solid supports available, a polyethylene glycol (PEG) grafted PS resin was considered, for broader reactivity than standard PS supports, due to a reduced steric hindrance and an amphiphilic character;[245] furthermore previous efforts in our group had suggested that standard PS resins may not be compatible with hybrid clusters.

The goal was to select a linker which could be cleaved in conditions compatible with the POM cluster as if this step was unsuccessful any attempt of synthesis would have been pointless. Peptide synthesis protocols usually involves an orthogonal protecting group strategy with a step-by-step construction of the peptide under basic conditions (Fmoc removed by piperidine), followed by a final deprotection and cleavage under acidic conditions (with reagents such as trifluoroacetic acid (TFA) or hydrofluoric acid (HF) being commonly employed).[187] These cleavage reaction conditions, especially the use of

strong acids, would not be compatible with the metal-oxide core; investigations had to be carried out to find a linker that could be cleaved under mild conditions.

Of the somewhat narrow range of linker chemistries meeting these requirements, the trityl linker (triphenylmethyl, Trt) was considered (Figure 99). This linker is easier to handle than photo-cleavable linkers (photosensitive) and its cleavage was established under very mild conditions (solution of 20% 1,1,1,3,3,3-hexafluoro-2-propanol (HFIP) in DCM).[246]
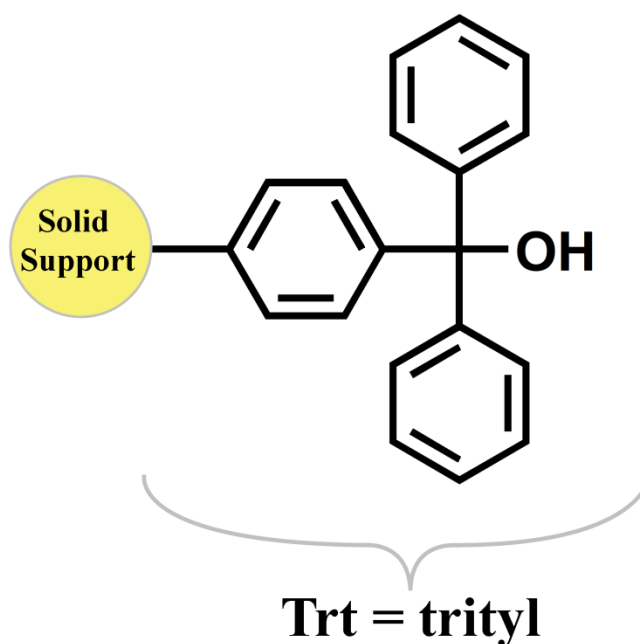
Figure 99: Schematic representation of a trityl (Trt) linker grafted on a solid support.

A test reaction (**Test A**) was conducted to see if TRIS-based Mn-Anderson clusters would be stable under the cleavage conditions used for the trityl linker. The TRIS Mn-Anderson compound was treated with the cleavage mixture for 1 h at room temperature and the resulting product was isolated after evaporation of the solvent. ESI-MS analyses were realised on the starting material and the isolated product to investigate the stability of the hybrid POM under these conditions (spectra given in Figure 100). The mass spectrum of the isolated product after treatment did not show any signs of degradation of the metal-oxide cluster (by comparison with the spectrum recorded for the starting material before treatment) and the peak envelopes observed were characteristic of the TRIS Mn-Anderson cluster.[102] The four main peak envelopes observed at m/z 689.91 (z = -1), 706.67 (z = -1), 1397.58 (z = -1) and 1639.85 (z = -1) were assigned to $[(C_{16}H_{36}N)[Mo_3O_{10}]]^{1-}$ (predicted: 689.95), $[MnMo_3O_{14}(C_4H_8N)_2]^{1-}$ (predicted: 706.72), $[(C_{16}H_{36}N)H-[MnMo_6O_{24}(C_4H_8N)_2]]^{1-}$ (predicted: 1397.68) and $[(C_{16}H_{36}N)_2[MnMo_6O_{24}(C_4H_8N)_2]]^{1-}$ (predicted: 1639.95), respectively.
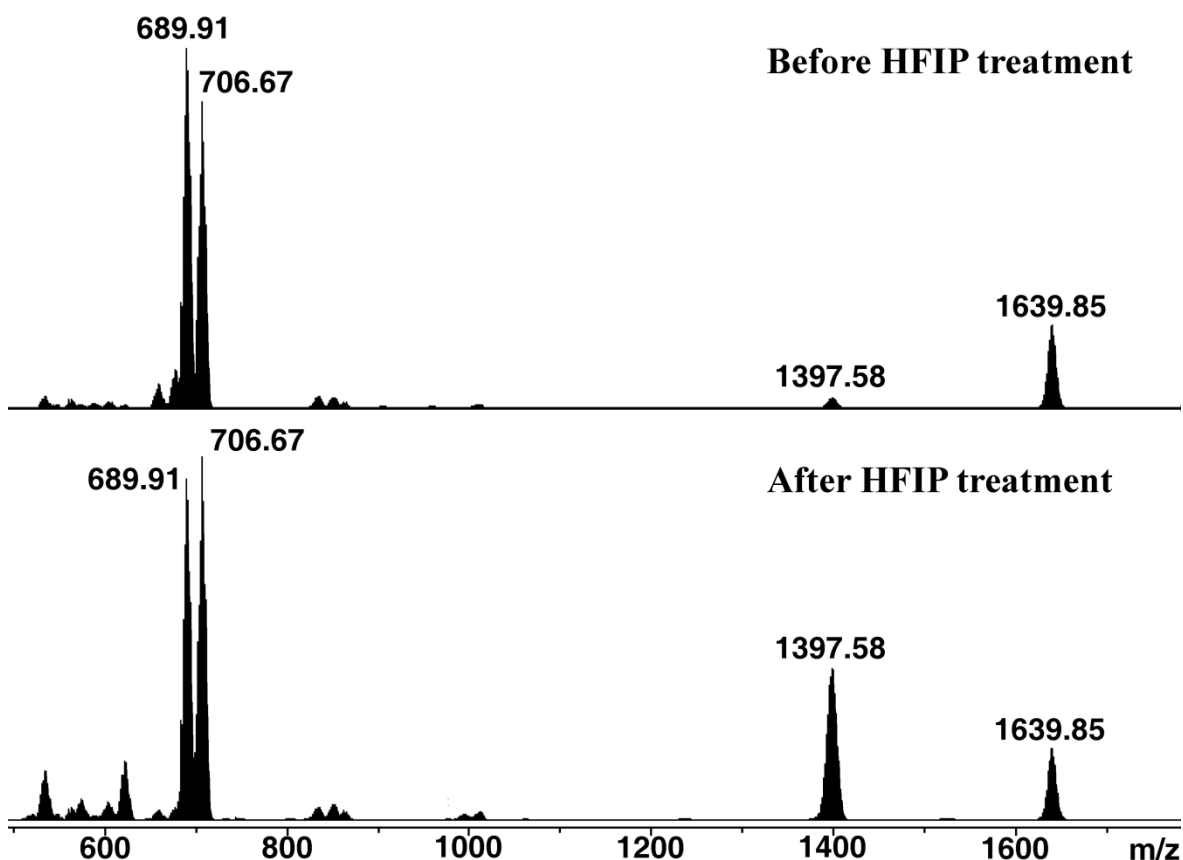
Figure 100: ESI-MS spectra obtained for **Test A**. (Top) analysis of the starting material, TRIS Mn-Anderson compound before treatment with HFIP; (bottom) analysis of the isolated compound after treatment with HFIP. The difference in peak intensity can be attributed to a variation of the concentration of the samples.

This test suggests that TRIS-based Mn-Anderson compounds are stable under the cleavage conditions of the trityl group and therefore this linker, grafted on a PEG grafted PS support, could be a good candidate for the SPPS protocol.

3.4.2.2 Addition of the hybrid POM amino acid to a growing peptide chain

The elaboration of a SPPS protocol adapted to the hybrid amino acid required the study of the reaction conditions under which the unnatural amino acid building block could be grafted to a growing peptide on a solid support (Figure 101). For the test reactions a Tentagel® S Trt resin preloaded with one alanine residue was used; the alanine unit acts as a control to verify that the hybrid POM was grafted at the expected reacting site. Without this residue it would be difficult to know whether the cleaved product was coupled to the solid support or was only interacting electrostatically with the polymer matrix.
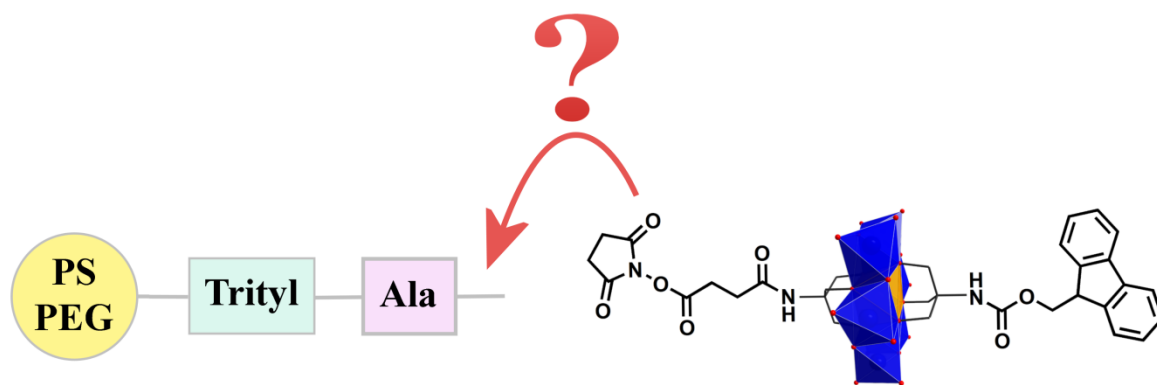
Figure 101: Schematic representation of the SPPS parameter studied in the present series of test.

The first attempt of the addition of compound **22** to the solid support was accomplished by mixing the functionalised resin with 3 equiv. of the pre-activated hybrid Mn-Anderson amino acid (**22**) in DMF for 1 h and in the presence of DIPEA (**Test B**). An hour after addition, the reagents were removed from the reaction vessel and the resin was washed with some solvent. The solid support, originally pale yellow, maintained this colour after completion of **Test B**. Since TRIS-based Mn-Anderson compounds have a strong characteristic orange colour, this absence of colour change seemed to suggest that the reaction did not occur. Another test was therefore carried out with similar conditions, however reagents were left to react for 2 h (**Test C**). At the end of **Test C** no colour change was observed.

In a last attempt, the first resin from **Test B** that had already been in presence of the reagent mixture for 1 h was re-used and left to react overnight with a newly made reaction mixture (equivalent to a double coupling: one of 1 h and second one of 16 h; **Test D**). Once the liquid phase was removed by vacuum and the resin washed with solvent, a bright orange coloured solid support was observed. In order to establish if the hybrid Mn-Anderson cluster was grafted at the expected reactive site (the amine of the alanine residue), the solid support was treated with the cleaving mixture (20% HFIP in DCM). The resulting orange solution was collected by filtration (the resin return to its original pale yellow colour) and the product was isolated by removal of the solvent. ESI-MS analysis was carried out in MeCN (Figure 102); the expected product has the general formula $(TBA)_3[MnMo_6O_{24}(C_{19}H_{18}NO_2)(C_{11}H_{17}N_2O_4)]$. Three main peak envelopes at m/z 1551.52 ($z = -1$), 1791.80 ($z = -1$) and 2033.08 ($z = -1$) were observed and could be assigned as $[H_2[MnMo_6O_{24}(C_{19}H_{18}NO_2)(C_{11}H_{17}N_2O_4)]]^{1-}$ (predicted: 1550.52), $[H(C_{16}H_{36}N)[MnMo_6O_{24}(C_{19}H_{18}NO_2)(C_{11}H_{17}N_2O_4)]]^{1-}$ (predicted: 1791.80), $[(C_{16}H_{36}N)_2[MnMo_6O_{24}(C_{19}H_{18}NO_2)(C_{11}H_{17}N_2O_4)]]^{1-}$ (predicted: 2033.08).
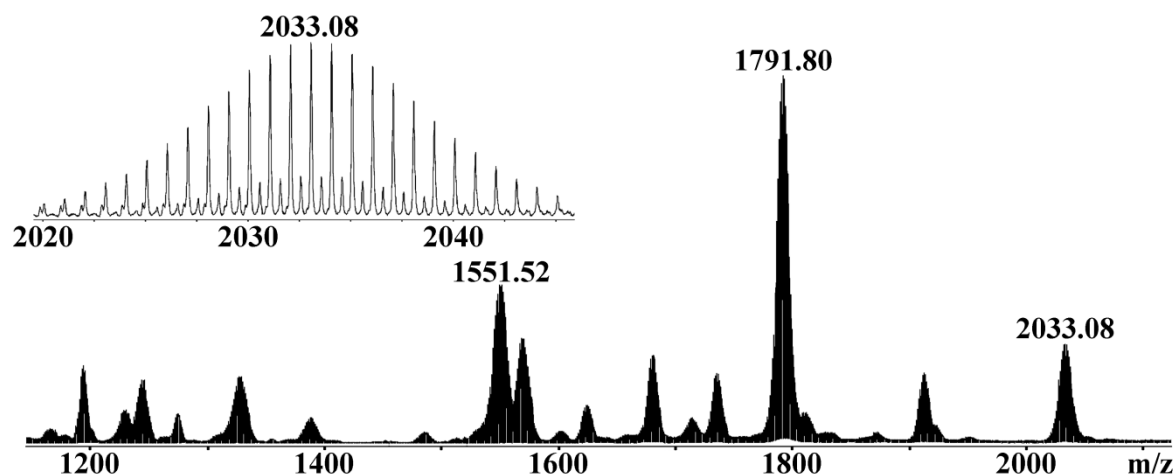
Figure 102: ESI-MS spectrum of the isolated product obtained in **Test D** with magnified representation of the main peak envelope at *m/z* 2033.08 assigned to $[(TBA)_2[MnMo_6O_{24}(C_{19}H_{18}NO_2)(C_{11}H_{17}N_2O_4)]]^{1-}$.

The main signals observed during the analysis were consistent with the expected compound formula, proving that compound **22** reacted as expected with the amine group of alanine; the reaction conditions used in **Test D** are thus appropriate for the use of **22** in our SPPS protocol. The fact that the coupling can be followed by the naked eye, as the characteristic bright orange colour of the hybrid Mn-Anderson cluster is retained on the solid support, is an interesting feature which is used hereafter as a rough means to follow the subsequent tests.

In an attempt to optimise or at the very least reduce the reaction time required for this coupling, additional tests were carried out; the two most significant are presented herein. **Test E** was reduced to a single coupling of 16 h; the resulting solid support was of a pale yellow colour suggesting an absence of reaction (a bright orange colour was obtained only when a second coupling of 16 h was completed). For **Test F**, the solid support was treated with a double coupling of 1h and then 7 h and a light orange resin was isolated, colour suggesting that the reaction did not reach completion. Although not exhaustive, this series of tests suggests that the double coupling is important for this reaction and that the reaction is a slow process (which may be due to interactions between the matrix polymer and the charged POM species).

In order to establish whether the activation of the amino acid TRIS-based Mn-Anderson by NHS ester groups was important, another kind of coupling reaction was investigated (**Test G**). *N,N,N',N'*-Tetramethyl-*O*-(1*H*-benzotriazol-1-yl)uronium hexafluorophosphate (HBTU) with DIPEA, a more common coupling reagent mixture,[178] was used with the un-activated   acid/Fmoc   protected   TRIS-based   Mn-Anderson   cluster

$((TBA)_3[MnMo_6O_{24}(C_8H_{12}NO_3)(C_{19}H_{18}NO_2)])$. After 1 h of treatment the solid support still maintained its pale yellow colour. This colour was also observed after a double coupling of 16 h and the reaction was considered unsuccessful. This test highlights the importance of the NHS activated precursor methodology developed in this study.

Other coupling reagent mixtures are available, but the exhaustive study of the different coupling methods is beyond the scope of this work. For the under construction SPPS protocol, the Mn-Anderson amino acid (**22**) will be introduced into growing peptide chains following the reaction conditions established in **Test D**.

3.4.2.3 Reaction conditions after the introduction of the hybrid POM amino acid

After the introduction of the hybrid POM amino acid into the growing peptide chain, reaction conditions to carry on the peptide synthesis had to be established. In the following tests, the solid support was functionalised with the hybrid amino acid by following the reaction conditions established in **Test D**, the Fmoc protection was removed by treatment with piperidine and the reaction conditions for the addition of an amino acid were tested (using the Fmoc-Phe-OH unit; Figure 103). Two different synthetic paths were considered: the first one was using a common SPPS protocol (HBTU/DIPEA, **Test H**) and the second was to use DIC as an activating agent to form anhydrides *in situ* (which would correspond to the same type of reaction established in Section 3.1.2.1; **Test I**).
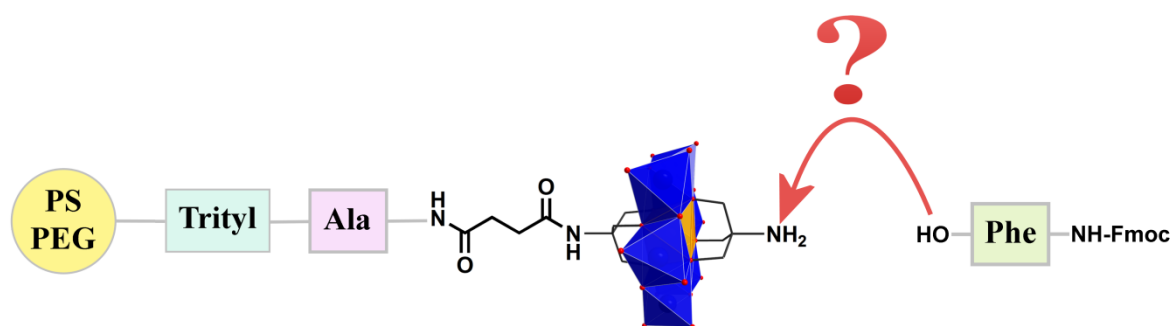
Figure 103: Schematic representation of the SPPS parameter studied in this series of tests

The activating reagent mixtures and the Fmoc-Phe-OH amino acid had to be introduced in large excess for these tests, otherwise the small scale at which these tests were carried out would imply either a small volume of solution (which could not fully cover the solid support) or a low concentration (which may have influenced the reactivity and therefore the results of the tests). Both tests were realised as double coupling and each coupling were carried out for 1 h. The resulting products were then cleaved, isolated and analysed by ESI-MS.

The expected product has the general formula $(TBA)_3[MnMo_6O_{24}(C_{28}H_{27}N_2O_3)$ $(C_{11}H_{17}N_2O_4)]$. ESI-MS analysis from **Test H** revealed two main peak envelopes at *m/z* 1327.49 (z = -1) and 1412.56 (z = -1 but also involving dimers of z= -2) which could not be assigned to the expected product or the starting material, the product of this test remains unidentified (Figure 104a). Two main peak envelopes at m/z 1698.63 (z = -1) and 1938.88 (z = -1) which could be assigned as $[H_2[MnMo_6O_{24}(C_{28}H_{27}N_2O_3)(C_{11}H_{17}N_2O_4)]]^{1-}$ (predicted: 1697.59) and $[(C_{16}H_{36}N)_1H[MnMo_6O_{24}(C_{28}H_{27}N_2O_3)(C_{11}H_{17}N_2O_4)]]^{1-}$ (predicted: 1938.87) were observed during the analysis of the product of **Test I** (Figure 104b).
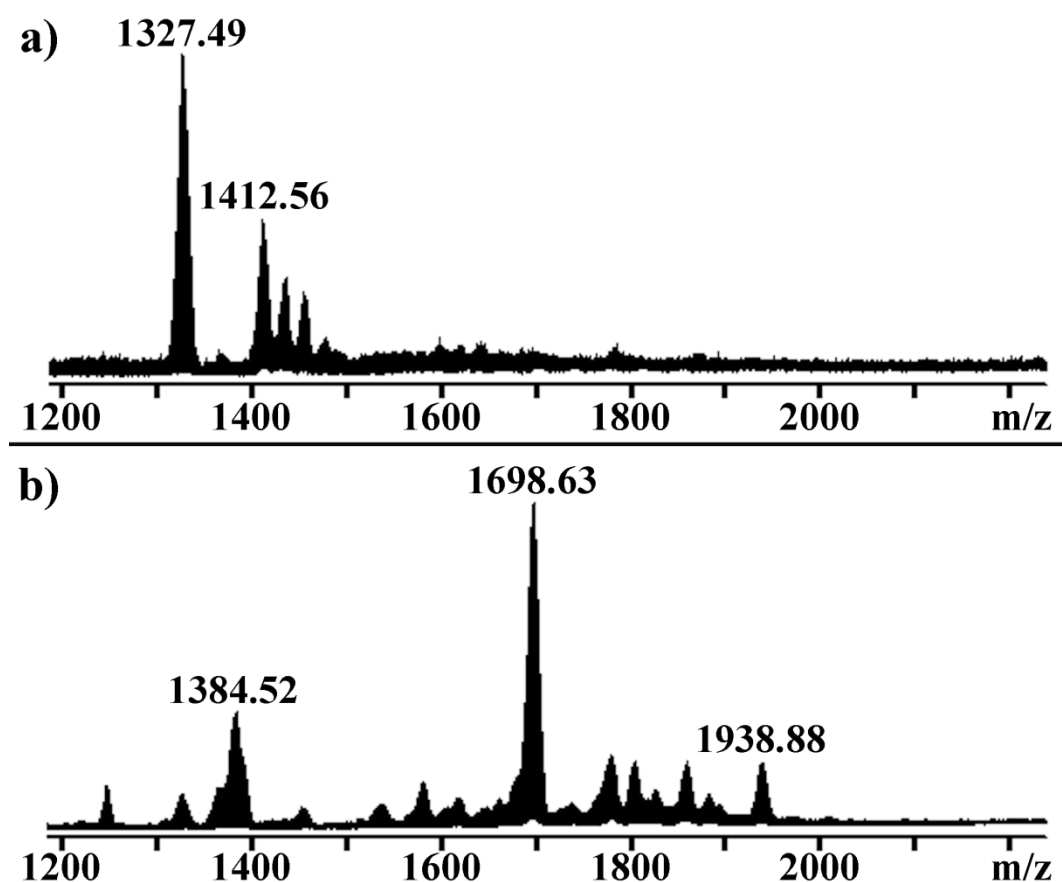
Figure 104: ESI-MS spectra obtained after isolation of the product obtained in **Test H** (a) and **Test I** (b).

Since the expected peptide-POM product was observed in the analysis of **Test I**, DIC was considered as a good candidate for our adapted SPPS protocol. The product observed in this test can be considered as the first tri-peptide synthesised with a POM amino acid.

3.4.3 Synthesis of the first POM-peptide hybrid cluster

Having established the common cluster core to be stable to SPPS conditions in isolation, a simple sequence synthesis was attempted manually: compound **23**, which can be described as NH$_2$-Val-Leu-**Hyb**-Ala-Val-Leu-Ala-OH, where '**Hyb**' denotes the hybrid amino acid residue resulting from incorporation of **22** (Figure 105).
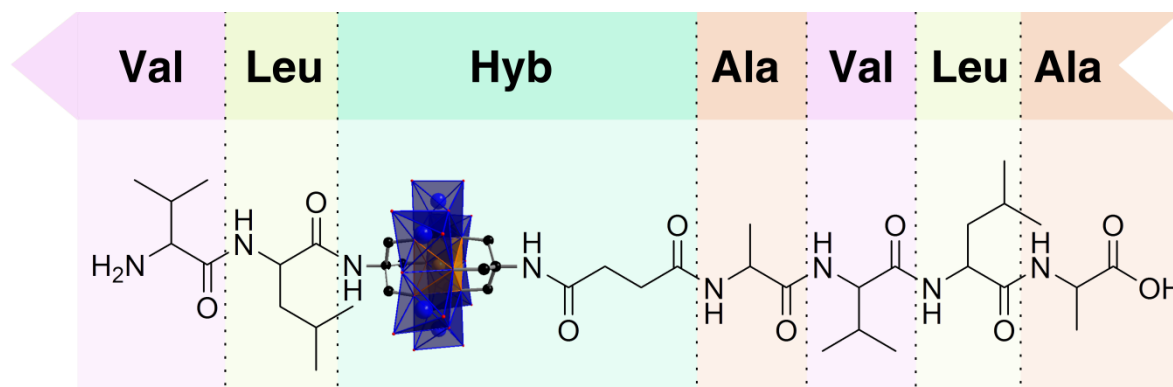
Figure 105: Representation of **23** (NH$_2$-Val-Leu-**Hyb**-Ala-Val-Leu-Ala-OH) with **Hyb** being the hybrid amino acid resulting from incorporation of **22**. The arrow indicates the addition order of the amino acids during the synthesis in an Fmoc-based solid phase synthesis.

For the section prior to the incorporation of **22** (Ala-Leu-Val), a standard SPPS protocol (5 equiv. of each amino acid and double coupling of 30 min each) using *N,N'*-diisopropylcarbodiimide (DIC) as the activating agent was employed. The hybrid amino acid (**22**) was then incorporated using a "double coupling", with a first reaction allowed to proceed for one hour, and the second overnight (same conditions than **Test D**). The excess of **22** was collected and reactivated to be re-used in the synthesis of other peptides. The same SPPS protocol was then continued for the addition of the remaining amino acids, then the resulting peptide was deprotected (treatment with a 20% piperidine solution in DMF), cleaved (20% HFIP in DCM), and isolated. ESI-MS analysis (Figure 106) was used to identify the product isolated. The expected product, compound **23**, should have the general formula (TBA)$_3$ [MnMo$_6$O$_{24}$(C$_{25}$H$_{42}$N$_5$O$_7$)(C$_{15}$H$_{28}$N$_3$O$_2$)] but peak envelopes observed at *m/z* 805.31 (z = -2) and 1611.62 (z = -1) could only be assigned as fragments consistent with NH$_2$-**Hyb**-Ala-Val-Leu-Ala-OH: [H[MnMo$_6$O$_{24}$(C$_{25}$H$_{42}$N$_5$O$_7$)(C$_4$H$_8$N)]]$^{2-}$ (predicted: 805.32) and [H$_2$[MnMo$_6$O$_{24}$(C$_{25}$H$_{42}$N$_5$O$_7$)(C$_4$H$_8$N)]]$^{1-}$ (predicted: 1611.64), respectively. This ESI-MS results showed that while the Mn-Anderson amino acid was successfully coupled to the growing peptide sequence, amino acids added subsequently had failed to react with the amine of the **Hyb** residue.
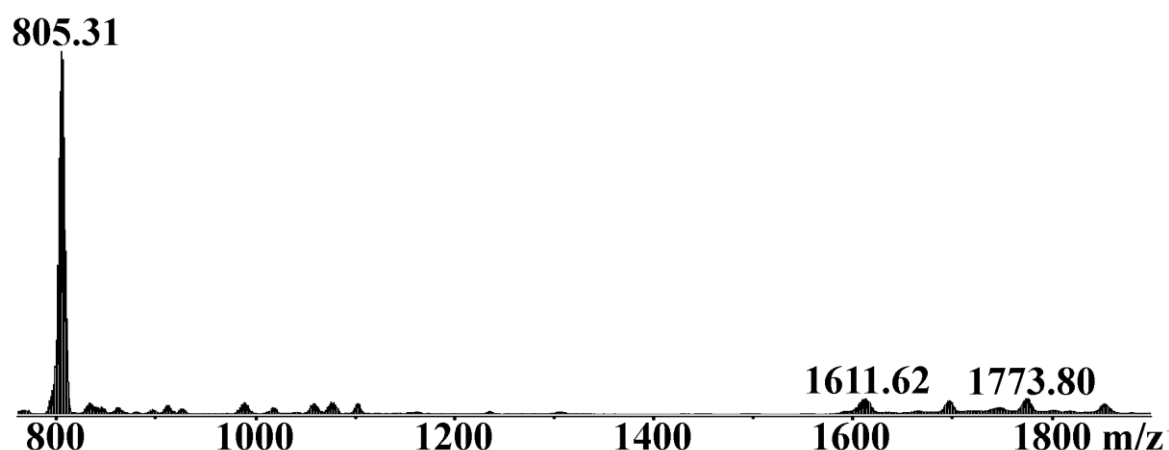
Figure 106: ESI-MS spectrum obtained after the first attempt of synthesis of compound **23**.

It was clear that, following addition of the **Hyb** residue, the coupling protocol needed to be altered to take into account the unusual reactivity of the new residue, presumably stemming from the hindered nature of TRIS –NH$_2$ group. During **Test I**, because of the small scale and the need of a sufficient reaction volume, the number of equivalents of coupling reagents was significantly higher (30 equiv. during the test). The synthesis was thus repeated and the amino acids quantities used after the introduction of the **Hyb** residue were increased six-fold; the reaction time was also increased to 3 h. The product resulting from this improved method was deprotected, cleaved, isolated and analysed by ESI-MS (Figure 107). Some major peak envelopes observed during this analysis were consistent with the proposed structure of **23**: *m/z* 911.33 (z = -2) and 2065.91 (z = -1) assigned as [H[MnMo$_6$O$_{24}$(C$_{25}$H$_{42}$N$_5$O$_7$)(C$_{15}$H$_{28}$N$_3$O$_2$)]]$^{2-}$ (predicted: 911.39) and [(C$_{16}$H$_{36}$N)H-[MnMo$_6$O$_{24}$(C$_{25}$H$_{42}$N$_5$O$_7$)(C$_{15}$H$_{28}$N$_3$O$_2$)]]$^{1-}$ (predicted: 2066.07). Other peak envelopes observed could not be identified and are probably fragments of the POM-peptide chain (no starting material or not-fully-reacted species were observed).
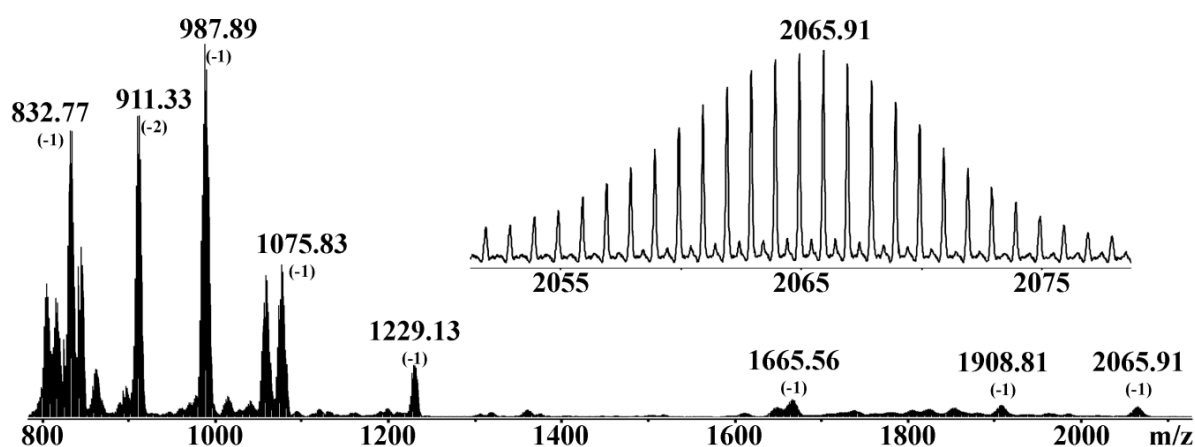
Figure 107: ESI-MS spectrum obtained after the second attempt of synthesis of compound **23** with magnified representation of the peak envelope at *m/z* 2065.91 assigned to $[(TBA)H[MnMo_6O_{24}(C_{25}H_{42}N_5O_7)(C_{15}H_{28}N_3O_2)]]^{1-}$.

Further characterisation by elemental and TGA analyses (see Section 5.4.6.2) suggested a small cation exchange occurring during the synthesis, therefore the following general formula was established for compound **23**: $(TBA)_{1.4}H_{1.6}[MnMo_6O_{24}(C_{25}H_{42}N_5O_7)(C_{15}H_{28}N_3O_2)]$.

The synthesis and the isolation of compound **23** is the proof that, using the adapted SPPS protocol and the activated POM amino acid building block (**22**), Mn-Anderson units and be introduced as unnatural amino acids into the backbone of a peptide chain. This approach outlined in this first solid-supported synthesis of POM hybrids and should find considerable application in the wider hybrid cluster field.

3.4.4 Section summary

In this section, the first amino acid hybrid POM was synthesised: compound **22** an amine-protected acid activated TRIS-based Mn-Anderson cluster. Reaction conditions permitting its use in SPPS were carefully studied through a series of test reactions (**Test A-I**). From this study, an adapted SPPS protocol was created which permit the insertion of the amino acid POM unit as part of peptide sequence, as demonstrated by the synthesis of compound **23**, the first POM-peptide hybrid ever synthesised.

4   Conclusions and Outlook

The work presented in this thesis focused on developing modular approaches that permit the introduction of polyoxometalates (POMs) in peptide chemistry. POMs and peptides both present remarkable properties which make them appealing for a wide range of applications, especially in medicine and nanotechnology. In order to study the properties that result from their fusion, reliable methods to synthesise these POM-peptide hybrid systems had to be established (Figure 108).

This work is centred on the hybrid organic-inorganic Mn-Anderson cluster, a hybrid POM first discovered by P. Gouzerh *et al*. in 2002.[49] This cluster was used as a model compound to establish robust methodologies.
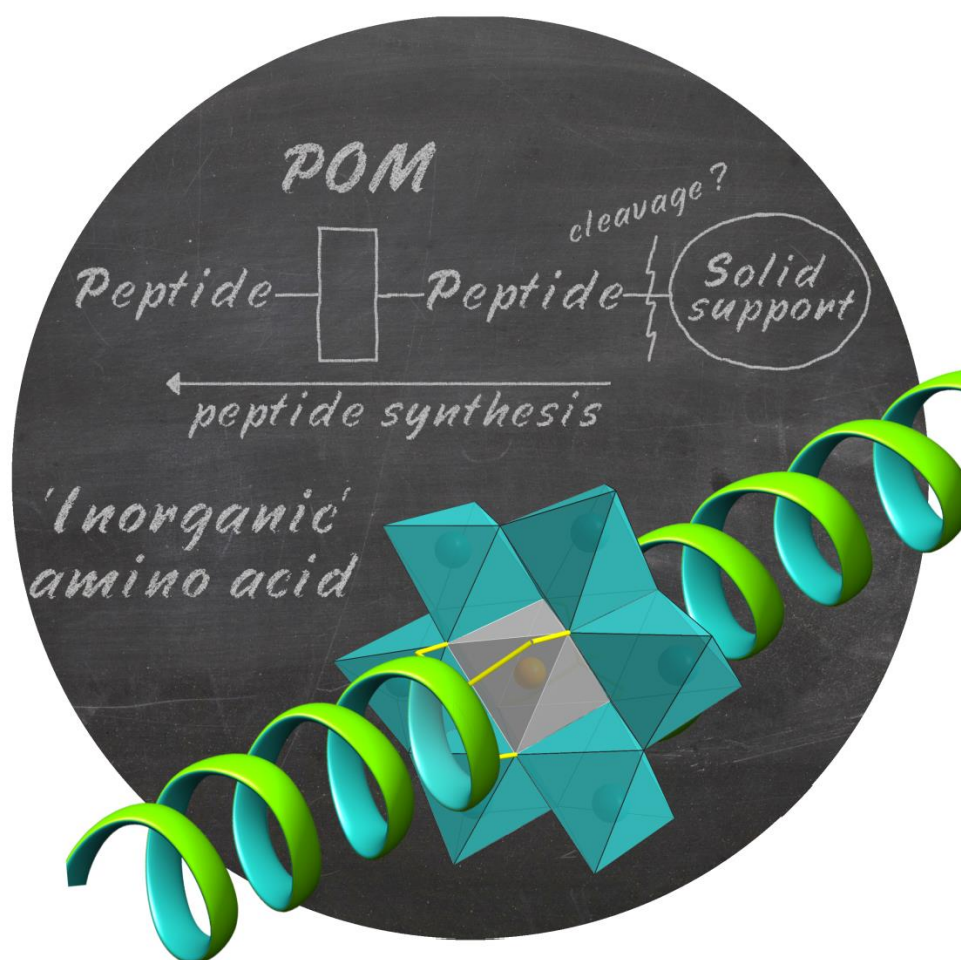
Figure 108: Cartoon representing the initial ideas and aims of this thesis along with the result, *i.e*. a TRIS-based Mn-Anderson cluster introduced into the backbone of a peptide chain.

4.1 TRIS-based Mn-Anderson building blocks modification tool box

In the first part of this thesis, a set of methodologies was established to adapt TRIS-based Mn-Anderson clusters chemistries to peptides' requirements. The variables explored included: solvent compatibility, reactivity toward amine and carboxylic acid groups, and availability of carboxylic acid functionalised clusters.

While DMF soluble clusters were readily available as TBA salts, no straightforward synthetic procedure would have led to water soluble compounds. The standard protocol for the synthesis of TRIS-based Mn-Anderson complexes consists of a one pot reaction in which $(TBA)_4[\alpha\text{-}MO_8O_{26}]$ is reacted with the TRIS ligand and Mn^{III} acetate and refluxed in MeCN yielding the hybrid cluster as a TBA salt.[50] The introduction of different counter cations can then be realised through cation exchange processes on the resultant TBA salt species.[110,111] However, these cation exchange procedures are not trivial and isolation of pure compounds by this process is achieved with difficulties. With the objective of a modular approach, water-soluble TRIS Mn-Anderson building block syntheses should be as easy as the synthesis of the TBA salt, therefore the possibility of altering the standard protocol to directly synthesise TRIS-based POM with other cations was explored.

Three octamolybdate salts $((TMA)_2Na_2[MO_8O_{26}]$, **1**; $(TEA)_3Na[MO_8O_{26}]$, **2**; $(TPA)_2Na_2[MO_8O_{26}]$, **3**) were synthesised by altering the published procedure to the synthesis of the TBA octamolybdate cluster by replacing the TBA·Br reagent for the appropriate TXA·Br (X = M, E, P, respectively). ESI-MS analyses of **1**-**3** revealed a rearrangement in solution of the POM clusters into $\{Mo_4O_{13}\}$ building units. The formation of this intermediate is known to be the first mechanistic step of the TRIS Mn-Anderson cluster formation.[102] This observation led to the synthesis of the hybrid complex. The standard protocol to synthesise the TRIS Mn-Anderson had to be modified due to the difference of solubility in TXA octamolybdate compounds compared to that of the TBA salt. The reaction solvent was thus changed to DMF and the TXA compounds were dissolved in this solvent prior to the addition of the other reagents. Four novel TRIS Mn-Anderson compounds were isolated from these reactions (Figure 109): three TXA TRIS Mn-Anderson salts $((TMA)_3[MnMo_6O_{18}((OCH_2)_3CNH_2)_2]$, **4**; $((TEA)_3[MnMo_6O_{18}((OCH_2)_3CNH_2)_2]$, **5**; $(TPA)_2(Na)[MnMo_6O_{18}((OCH_2)_3CNH_2)_2]$, **6**; formed from **1**-**3**, respectively) and a sodium species $((Na)_3[MnMo_6O_{18}((OCH_2)_3CNH_2)_2]$, **7**; obtained from **1** and **3**). Over the crystallisation process of the solution obtained for the reactions of compounds **1** and **3**, a crystalline material and precipitate were isolated. After

recrystallisation of each product the former revealed to be the Na salt species (**7**) while the precipitate recrystallised as the TXA TRIS Mn-Anderson cluster (**4** and **6**).
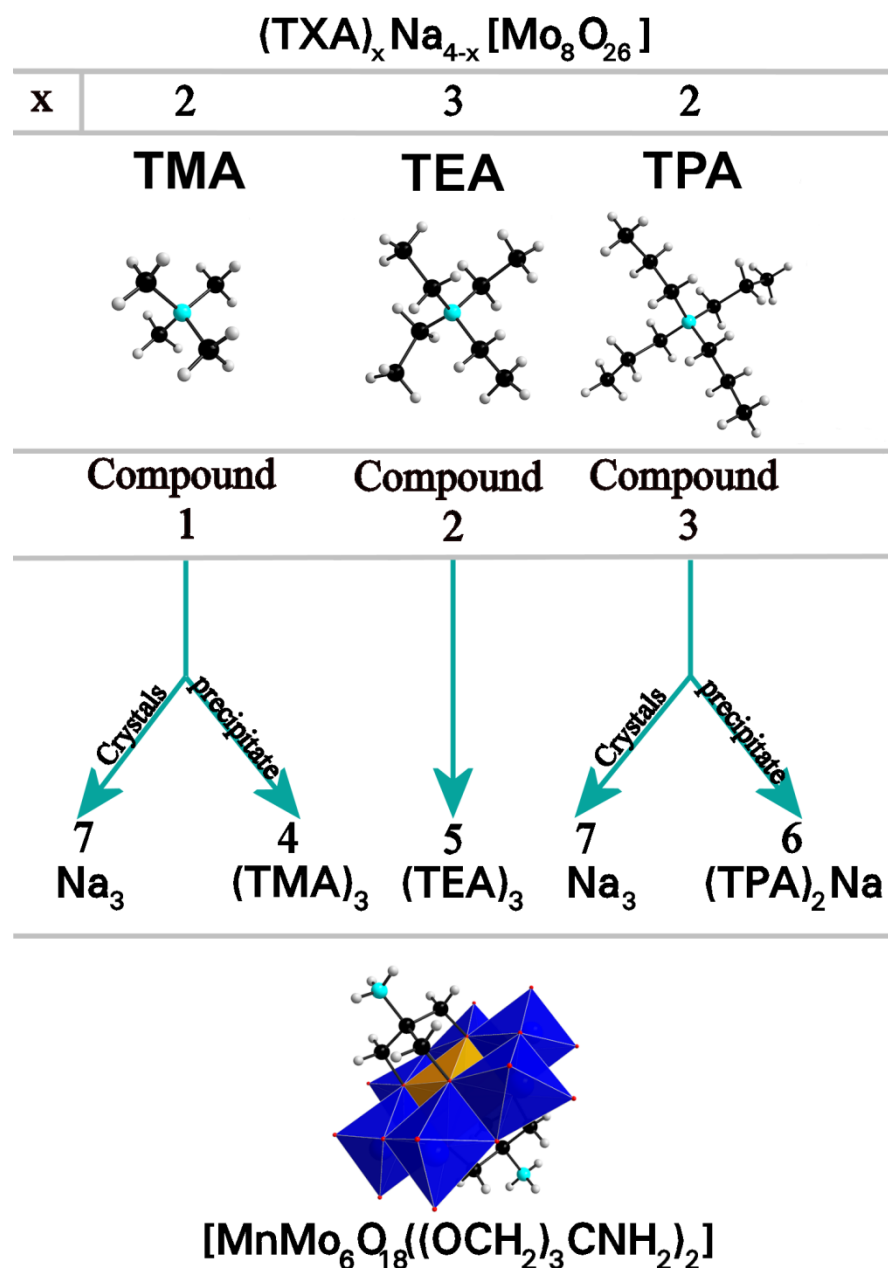
Figure 109: Overview of the synthesis and isolation pattern of compounds **4**-**7**.

These compounds are the first examples of TRIS Mn-Anderson complexes synthesised from compounds other than $(TBA)_4[\alpha\text{-}MO_8O_{26}]$ and represent an alternative to the cation exchange procedures. These clusters present interesting solubility properties from the perspective of using POM-peptides hybrids for cell targeting drugs. Their solubility in DMF permits their post-functionalisation by organic reactions while their solubility in water makes them compatible with biological studies in aqueous media.

In order to covalently link the POM cluster to peptides, the formation of peptide bonds was investigated (Figure 110). The synthesis of compounds **8** and **9** demonstrated that the use of anhydride intermediates is an efficient means to graft organic molecules to the TRIS Mn-Anderson building block in reaction conditions compatible with peptides (50 °C in DMF). Furthermore, when using cyclic anhydrides, this reaction led to the introduction of terminal carboxylic acid functional groups. This synthetic route was demonstrated through compound **10**, the first carboxylic acid functionalised Mn-Anderson cluster.
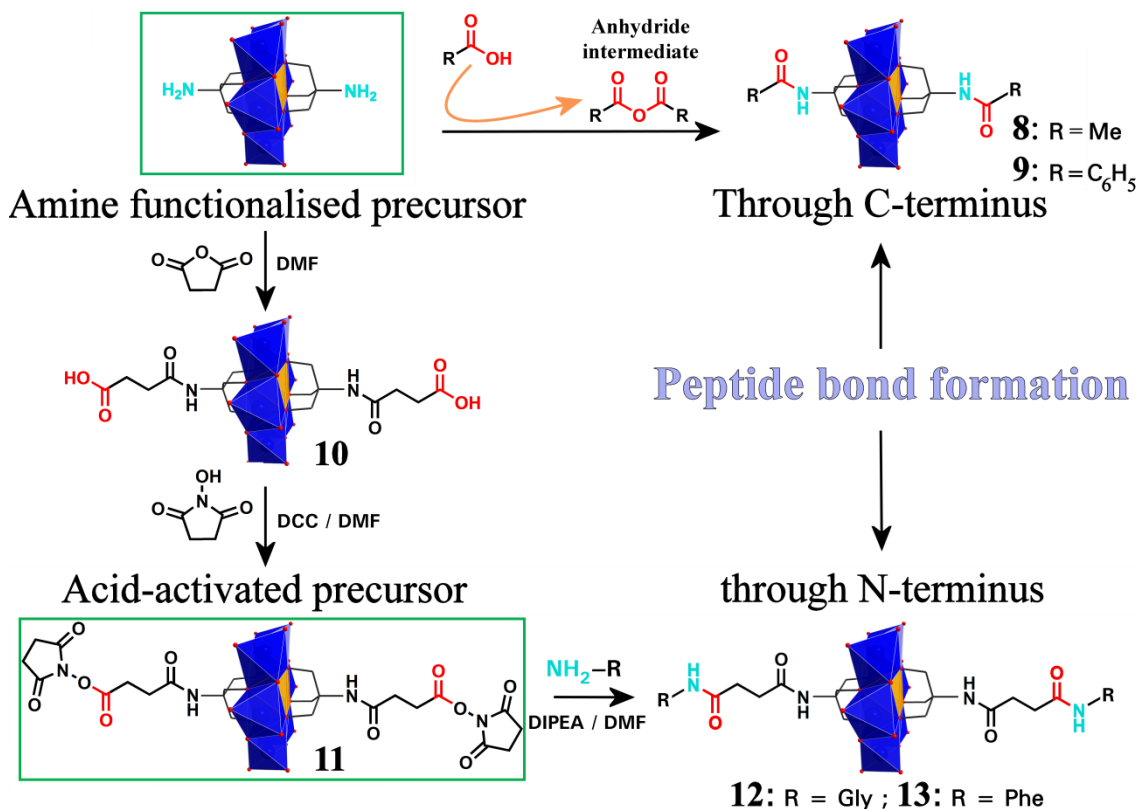
Figure 110: Overview of the strategies established in order to graft onto the POM cluster either carboxylic acid functionalised or amine functionalised ligands.

The newly obtained acid functionalised compound was then treated to form an NHS ester-activated precursor (**11**) which, as illustrated by the formation of compounds **12** and **13**, can react under mild conditions (DMF at room temperature) with the amine functional group of amino acids to form peptide bonds. This peptide bond formation methodology is highly compatible with the modular approach: the activated precursor can be synthesised in large batches to then react with various peptide chains in their native forms.

The formation of peptide bonds through the reaction with anhydride intermediates and the synthesis of an NHS-activated precursor were key steps for the incorporation of the Mn-Anderson unit into the backbone of peptides.

4.2 Incorporation of Mn-Anderson clusters as linking components

Before being able to incorporate the Mn-Anderson cluster into the backbone of a peptide, it was introduced as a linking component between two identical pre-synthesised peptide chains, where both of the peptides are attached to the POM cluster through their N-terminus. This study exploited the aforementioned NHS-activated precursor (**11**) by introducing it in the middle of two oligopeptides, the di-phenylalanine (**14**) and tri-phenylalanine (**15**), and a 15-mer (**16**). Compound **16** is a hybrid POM cluster of unprecedented scale, where the Mn-Anderson building block is introduced between two identical 15-mer chains (Figure 111).
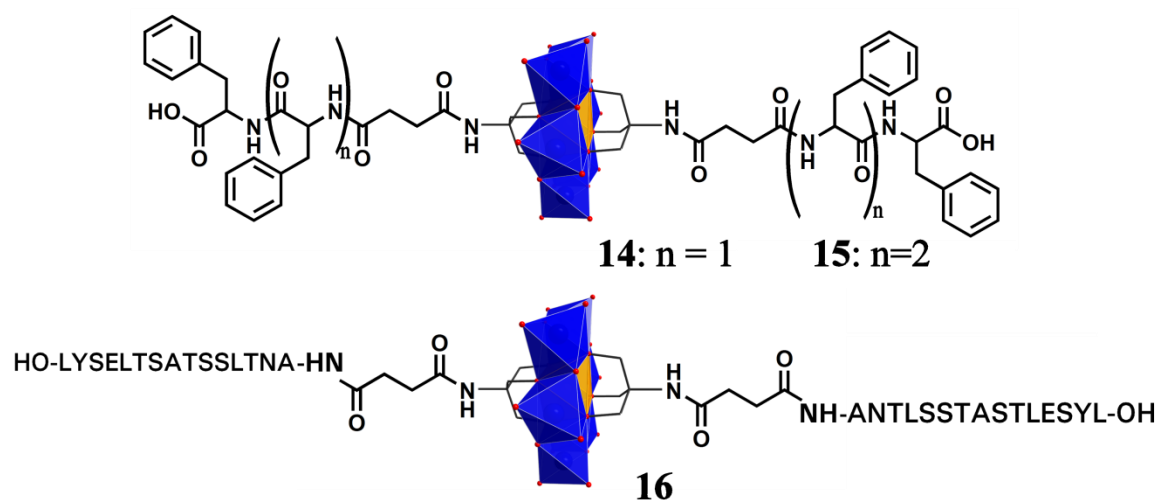
Figure 111: A variety of compounds in which the Mn-Anderson building block is introduced as a linking component between two peptide chains.

Compound **14** has demonstrated self-assembly properties induced by the peptide ligand introduced, *i.e.* a self-supporting organogel, stable at room temperature, was obtained by cooling an MeCN solution at a concentration of 4.5 w/w%. These observations validate the hypothesis that the introduction of specific peptide sequences could help tune the self-assembly properties of hybrid POM materials.

CD analysis in MeCN revealed that while the native 15-mer peptide sequence does not possess a regular structure, compound **16** adopted an α-helix arrangement. Although this analysis does not indicate if the whole molecule or only parts of it participate in the helical arrangement, this observation highlights how the incorporation of the POM cluster into proteins/peptides can result in significant new structural features.

In this approach, the POM unit is not part of a peptide sequence but the simplicity and the wide applicability of this NHS-activated precursor method makes it a good candidate for

the study of POM nanomaterial structured by peptide sequences or for the investigation of the effects of the charged metal-oxide cluster on peptide chain folding.

4.3 Tackling the isolation issue of asymmetric hybrid Mn-Anderson clusters

Until now only symmetric Mn-Anderson clusters have been synthesised, limiting the study to the introduction of the POM as a linking component between two peptide chains. To fully explore the potential of the bi-functional hybrid Mn-Anderson unit and to integrate it as part of a peptide sequence, its isolation as an asymmetric cluster had to be solved. Asymmetric clusters had been reported, but the techniques employed for their isolation were very specific to the ligand employed and could not be generally applied. To be part of a modular approach, the synthesis of asymmetric Mn-Anderson clusters had to be simple, reliable and permit the repeatable isolation of the compound in batches.
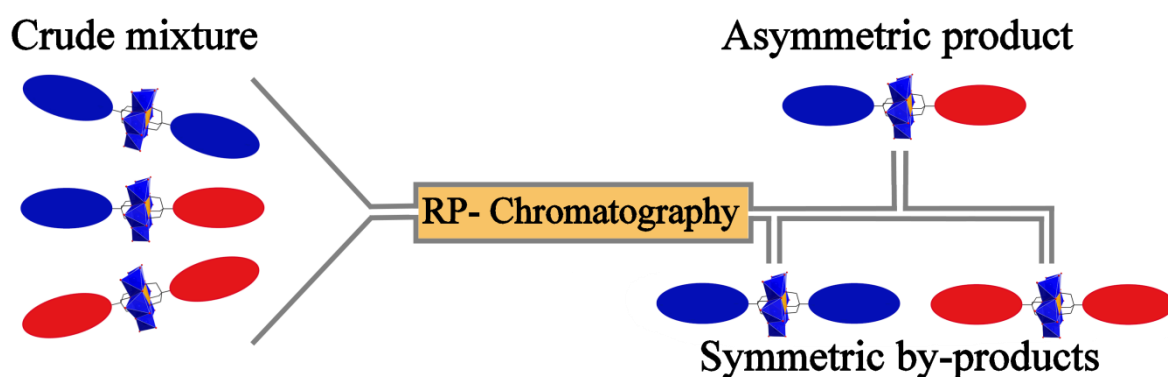
Figure 112: Schematic representation of the chromatographic method principle: the crude mixture made of the asymmetric cluster and the two symmetric by-products are separated according to their hydrophilicities on RP C18 silica columns eluted with a gradient of ammonium acetate buffer/MeCN solvent mixture. Colour Scheme: hydrophilic ligand, blue elipse; hydrophobic ligand, red elipse.

A set of methodologies was established to solve this issue. For cases where the asymmetric cluster is made of two ligands of different hydrophobicities, a chromatographic method relying on the difference of affinities for RP media of the ligands was established (Figure 112). The diversity of the asymmetric clusters isolated following this approach (**17**-**20**) proves its reliability and robustness (Figure 113).
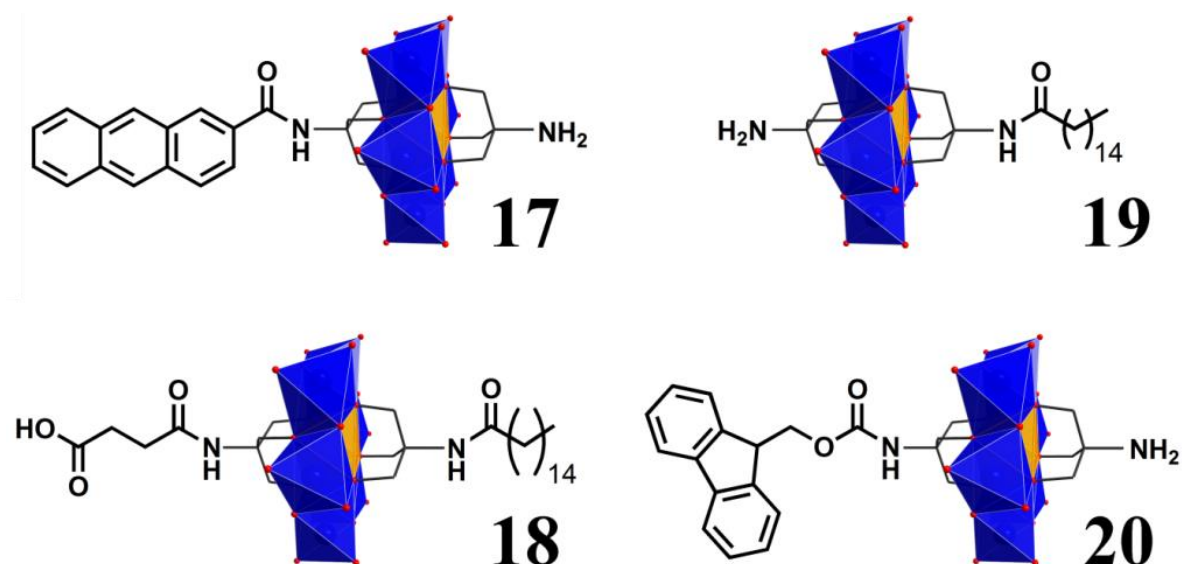
Figure 113: A variety of asymmetric clusters isolated using the chromatography approach (**17**-**20**). Each asymmetric system is made up of one hydrophobic and one hydrophilic ligand resulting in an effective separation from their symmetric by-products during RP-chromatography. Colour scheme: Mn, orange (polyhedra); Mo, blue (polyhedra); O, red.

In the case of asymmetric clusters bearing ligands of similar hydrophilicity, a post-functionalisation approach based on the modification of a "universal" asymmetric Mn-Anderson precursor (**20**) was established. This approach was demonstrated through the synthesis of **21,** an asymmetric cluster which could not have been isolated using the chromatographic approach (Figure 114).
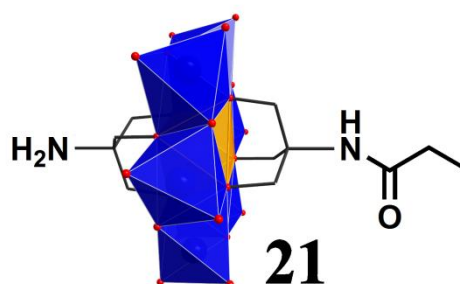
Figure 114: Asymmetric TRIS-based Mn-Anderson compound synthesised by post-synthetic modification of the asymmetric "universal" building block (**20**).

Establishing these methods means the asymmetric clusters can be reliably isolated with high purity and used as novel di-functionalised building blocks. An overview of the application of such hybrid units is given in Figure 115.
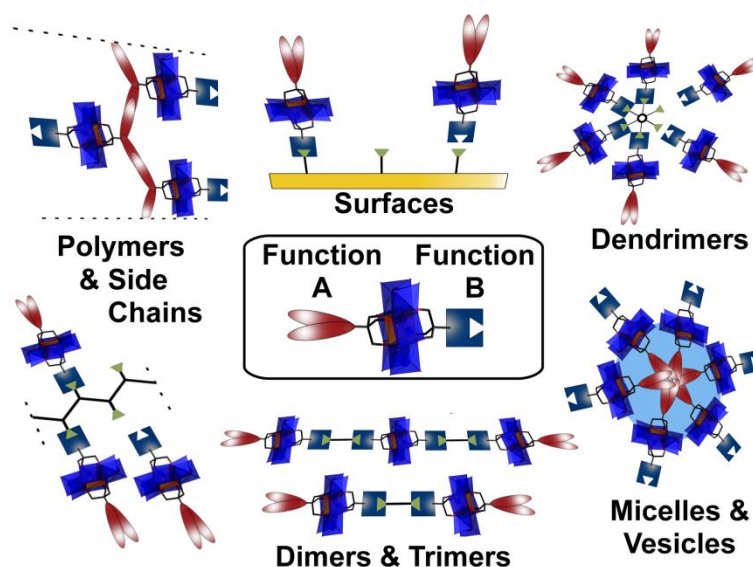
Figure 115: Schematic representation of some of the potential applications of bi-functional asymmetric Mn-Anderson compounds in material and devices. In all cases, control of reactivity either side of the metal-oxide cluster is important to achieve the desired function.

4.4   Incorporation of Mn-Anderson clusters into the peptide backbone.

In this section, the first hybrid POM amino acid was designed and isolated using the methodologies previously developed. The amino acid unit was made of the Mn-Anderson POM core functionalised on one side by an Fmoc-protected amine and by an NHS ester-activated carboxylic acid moiety on the other side (compound **22**, Figure 116).

Amine protected site   **22**   **Acid activated site**
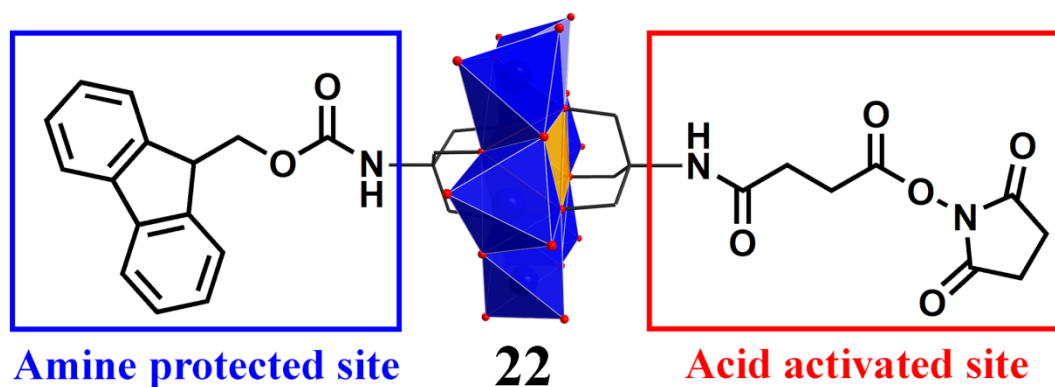
Figure 116: Amine-protected acid-activated Mn-Anderson building block (**22**).

The possibility of introducing this building block in a peptide sequence during SPPS as easily as any other amino acid was then investigated. Many aspects of SPPS protocols had to be carefully studied considering the unusual reactivity of the POM amino acid. A series of tests was thus conducted to establish each parameter individually. A PEG coated PS matrix was selected since its amphiphilic character makes it suitable for a wider range of reaction than standard PS supports. The trityl linker was found to be a suitable candidate for the SPPS adapted protocol, as TRIS-based Mn-Anderson clusters proved to be stable under its cleavage reaction conditions (HFIP 20% in DCM; **Test A**). A series of tests (**Test B-G**) were then carried out to establish the reaction conditions which would allow the hybrid amino acid building block (**22**) to be grafted on the solid support. Following these tests, it was established that the unnatural amino acid could be grafted onto the solid support if a double coupling was carried out, one lasting 1 h and a second lasting 16 h. The reaction conditions allowing the continuation of the peptide synthesis after the introduction of this unusual residue were investigated (**Test H-I**). It was found that DIC was a suitable activating agent permitting the formation of anhydride intermediates which could then react with the free amine located on the hybrid POM.

From these tests, an adapted SPPS protocol was establish (Figure 117) which permitted the synthesis of **23** (NH_2-Val-Leu-**Hyb**-Ala-Val-Leu-Ala-OH): the first peptide sequence incorporating a hybrid POM amino acid as one of its residues (**Hyb** residue).
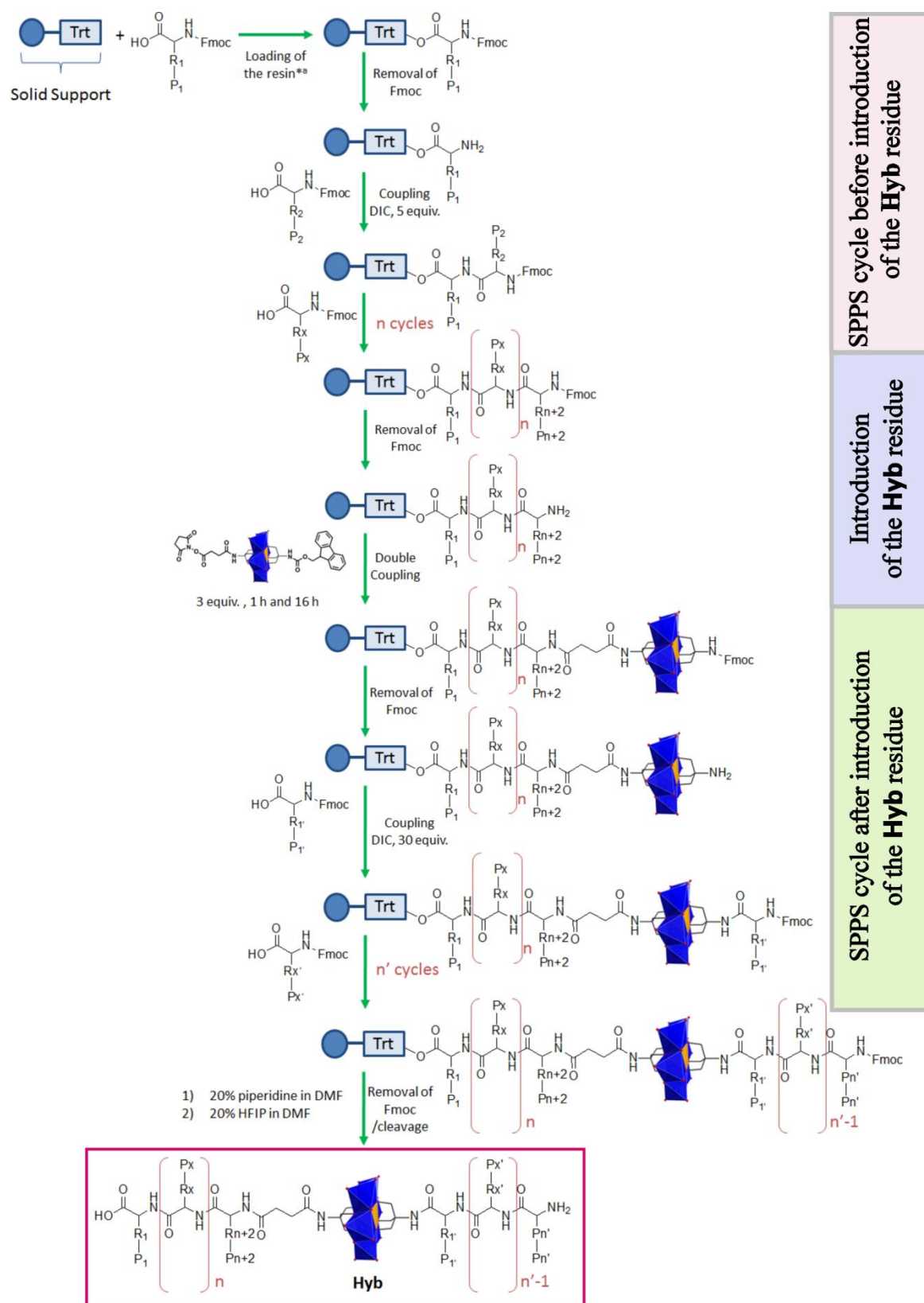
Figure 117: Schematic representation of the adapted SPPS protocol established to accommodate the unusual reactivity of the TRIS-based Mn-Anderson hybrid amino acid (**Hyb** residue).

4.5   Future work

The main goal of this thesis has been achieved: a series of methods was established which permit the introduction of the Mn-Anderson building block as part of an element of a peptide sequence. Nevertheless, many synthetic and analytic aspects of this project still require further investigation and method developments.

In the SPPS protocol, it was established that after the addition of the Mn-Anderson unit the number of equivalents of amino acid reagent used for subsequent couplings should be increased. In the synthesis of **23** the number of equivalents was thus increased to 30 equivalents to ensure reactivity, but an in-depth study should be carried out in order to optimise this step of the reaction, as this very large excess of reagent might not be needed. The compatibility of the POM cluster with side chain protecting groups and especially their cleaving conditions should also be the object of investigations as many amino acids could not be used during this work because of the reactivity of their side chain. The study of the introduction of several POM amino acids in the same sequence would also be of significant interest.

As the peptide chain gets longer, it became more difficult to assess the purity and identity of the resulting POM-peptide hybrids. New methods should thus be developed to identify and analyse these unprecedented hybrid POMs. Electrophoresis, HPLC or protein crystallisation methods could be interesting techniques to assess the purity of the synthesised hybrids.

Robust methodologies now exist to incorporate the Mn-Anderson cluster in to a peptide sequence and studies of the resulting properties that could come out of the fusion of POMs with peptides can be undertaken. Furthermore, since the POM building block can be introduced in peptide chains during their synthesis by SPPS, analogues of a sequence in which the POM is introduced at different positions could be synthesised and used to determine the effect of the charged metal-oxide cluster on peptide properties.

In this thesis, a chromatographic methodology is presented permitting the isolation of asymmetric TRIS-based Mn-Anderson clusters; it is the first time that RP chromatography has been reliably employed to purify hybrid POM compounds. Several hybrid POM clusters are di-substituted[22] (examples of which are given in Figure 118) but only the TRIS-based Mn-Anderson has been isolated as an asymmetric unit. The adaptation of this protocol should be investigated as it could lead to the purification and the isolation of other asymmetric hybrid POM systems. It is worth remembering that the asymmetric TRIS-

based hexavanadate cluster was once observed but never isolated as a pure sample.[95] Considering the technique's reliability and the isolated products' purities, this approach might reach beyond the problem of asymmetric cluster isolation and give rise to a new purification tool in the field of hybrid POM chemistry.
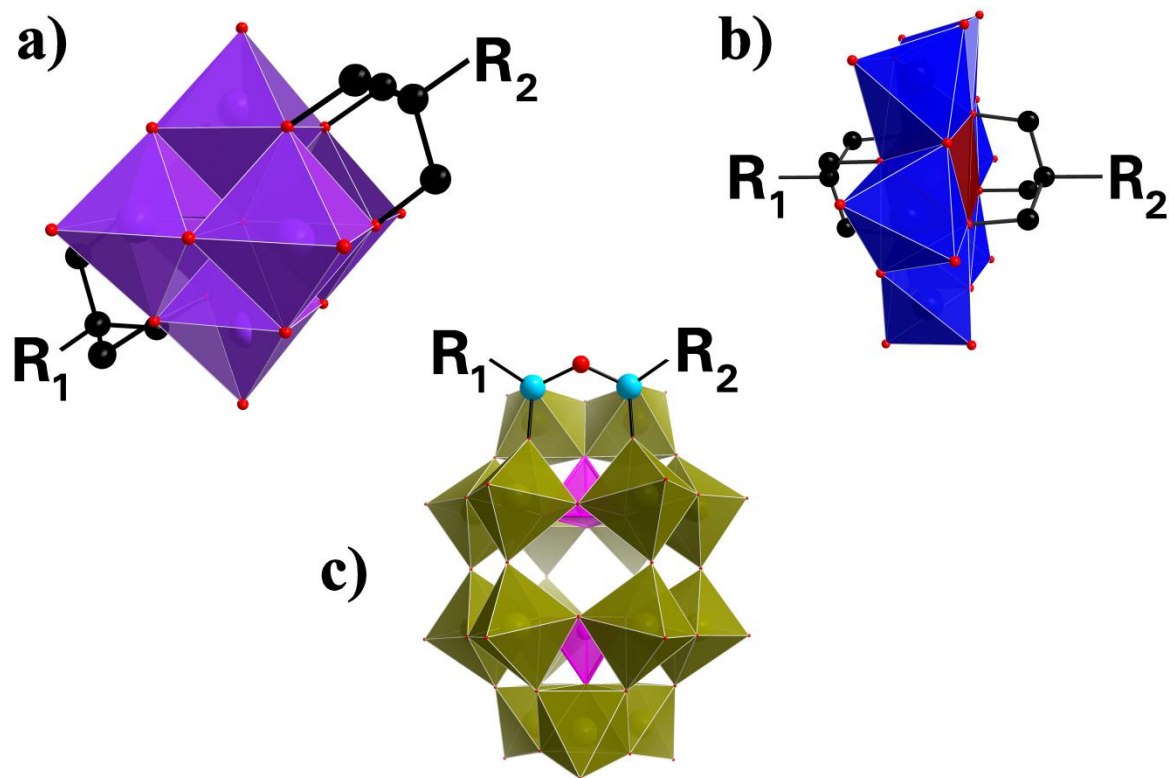
Figure 118: Examples of well-known di-functionalised hybrid POM clusters on which the asymmetric synthesis and the isolation using the chromatographic methodology could be investigated. (a) $[V_6O_{11}$-$((OCH_2)_3CR_1)((OCH_2)_3CR_2)]^{2-}$; (b) $[FeMo_6O_{18}(((OCH_2)_3CR_1)((OCH_2)_3CR_2)]^{3-}$; (c) $[P_2W_{17}O_{61}(Si_2OR_1R_2)]^{6-}$. Colour scheme: Fe, dark red (polyhedra); P, pink (polyhedra); V, purple (polyhedra); Mo, blue (polyhedra); W, green (polyhedra); O, red; C, black; Si, light blue;

5 Experimental

5.1 Materials

Unless mentioned otherwise all reagents and solvents were obtained from commercial sources and were used without further purifications. The long peptide "P_1" (NH$_2$-Ala-Asn-Thr-Leu-Ser-Ser-Thr-Ala-Ser-Thr-Leu-Glu-Ser-Tyr-Leu-OH) was purchased from PPR Ltd at a 98 % purity (HPLC trace and mass spectrometry). TBA octamolybdate (($C_{16}H_{36}N)_4[\alpha$-Mo$_8$O$_{26}]$)[227] and TBA TRIS Mn-Anderson (($C_{16}H_{36}N)_3[$Mo$_6$O$_{24}$-($C_4H_8N)_2]$)[50] starting materials were synthesised following the published procedures.

5.2 Instrumentation

Elemental Analysis

Carbon, nitrogen and hydrogen content were determined by the microanalysis services within the School of Chemistry, University of Glasgow, using an EA 1110 CHNS, CE-440 Elemental Analyser.

NMR Spectroscopy

NMR data was recorded on a Bruker Avance 400 MHz (or when indicated on a Bruker Avance 500 MHz) at T = 300 K; deuterated solvents were purchased at Goss Scientific. The peaks are denoted s = singlet, d = doublet, m = multiplet, br = broad and all coupling constants (J) are given in Hz.

Electrospray Ionisation Mass Spectroscopic Measurements

MS data for compounds **1**-**10** were carried out using a Q-trap, time-of-flight MS (MicrOTOF-Q MS) instrument equipped with an electrospray (ESI) source supplied by Bruker Daltonics Ltd. Analyses were carried out at 180 °C in MeCN and the spectrometer was calibrated with the standard tune-mix to give a precision of ca. 1.5 ppm in the region of 500-3000 m/z; The ion polarity for the MS scans recorded was negative, with the voltage of the capillary tip set at 4500 V, end plate offset at -500 V, funnel 1 RF at 400 Vpp and funnel 2 RF at 400 Vpp, hexapole RF at 400 Vpp, ion energy 5.0 eV, collision energy at 8 eV, collision cell RF at 1500 Vpp, transfer time at 100.0 μs, and the pre-pulse storage time at 10.0 μs. Each spectrum was collected for 2 min.

Measurements for compounds **11**-**23** and **Test A**-**I** were carried out at 180 °C in MeCN using a Bruker MaXis Impact instrument. The calibration solution used was Agilent ESI-L

low concentration tuning mix solution, Part No. G1969-85000, enabling calibration between approximately 50 m/z and 2000 m/z. Samples were dissolved in MeCN and introduced into the MS at a dry gas temperature of 180 °C. The ion polarity for all MS scans recorded was negative, with the voltage of the capillary tip set at 4500 V, end plate offset at -500 V, funnel 1 RF at 400 Vpp and funnel 2 RF at 400 Vpp, hexapole RF at 400 Vpp, ion energy 5.0 eV, collision energy at 15 eV, collision cell RF at 2100 Vpp, transfer time at 120.0 μs, and the pre-pulse storage time at 20.0 μs. Each spectrum was collected for 2 min.

Analysis of MS spectra was carried out using Data Analysis 4.0 software supplied by Bruker Daltonics.

Single crystal X-ray diffraction

Two different types of X-ray diffractometers were used for single crystal structure determination:

- **Bruker Apex II Quasar** charge-coupled device (CCD) detector (λ (Mo$_{K\alpha}$) = 0.71073Å) at 150(2) K, where the data reduction was performed using the Apex2 software package and structure solution.

- **Oxford Diffraction Gemini Ultra** with an ATLAS CCD detector [(λ (Cu$_{K\alpha}$) = 1.54184 Å] at 150(2) K, where the data reduction was performed using the CrysAlis software package and structure solution.

Independent of the type of X-ray diffractometer, corrections for incident and diffracted beam absorption effects were applied utilising analytical numeric absorption correction with a multifaceted crystal model,[247] or using empirical absorption correction.[248] Refinement was carried out with SHELXS-97 or -2013[249] and SHELXL-97or -2013[249] using WinGX[250] *via* a full matrix least-squares on F^2 method. For crystallographic data see Section 6.

RP-HPLC measurements

RP-HPLC measurements were performed on an Agilent 1100 Series (Agilent Technologies) equipped with a vacuum degasser, a binary pump (G1312A), a thermostated column compartment (G1316A), a standard autosampler (G1313A), and a variable wavelength detector (VWD) (G1314A). 5 μL of the samples were injected on a Phenomenex Luna® 3 μm C18(2) 100 Å, 150 x 2 mm column and eluted at 0.5 mL/min with a gradient of 0.05 M ammonium acetate (pH = 6.7 - 6.9) (**A**)/MeCN (**B**) (solvent

gradient given in Table 5). The oven temperature was set to 25 °C and elution was detected by UV (λ = 254 nm). The data recorded were processed using Bruker compass Hystar 3.2 (Bruker Daltonics) and Hyphenation Star PP software.

Table 5: Eluent composition for RP-HPLC measurements. Runlength 17.0 min.

Time (min)	**A** (%)	**B** (%)
0.0	95	5
3.0	95	5
15.0	5	95
17.0	5	95

Flash Chromatography:

Flash chromatography separations were performed on a Reveleris® iES Flash chromatography system using the Reveleris® *Navigator^{TM}* software. Before injection, columns were equilibrated for 4 min with 65:35 of A/B solvents at 18 mL/min. Samples were injected dry on Pre-packed Reveleris® C_{18} 4 g columns (two in series) by adsorption on celite (20 wt%, maximum total weight 1.8 g (*i.e.* 300 mg of compound adsorbed on 1.5 g of celite® 535 coarse)). Columns were eluted at 18 mL/min with a gradient of solvent A and B (see Table 6) and elution was detected by UV (at λ_{UV1} = 254 nm and λ_{UV2} = 350 nm) and an ELSD (carrier solvent: isopropanol).

Table 6: Eluent composition for flash chromatography. Run length 12.9 min.

Time (min)	**A** (%)	**B** (%)
0.0	65.0	35.0
2.2	65.0	35.0
11.8	5.0	95.0
12.9	5.0	95.0

UV / Vis spectroscopy:

Solvents and concentrations are given for each compound in the corresponding section.

JASCO V-670 spectrophotometer

Serial No. A007061154

Band width	2 nm
Response	Medium
Measurement range	500 - 190 nm
Data pitch	0.5 nm
Scanning speed	200 nm/min
Accumulation	1
Cell Length	1.0 cm
Temperature	20 °C

CD measurement:

JASCO J-810 spectropolarimeter

Serial No.   B029360750

Band width	1 nm
Response	2 sec
Sensitivity	Standard
Measurement range	260 - 190 nm
Data pitch	0.2 nm
Scanning speed	10 nm/min
Accumulation	3
Cell Length	0.5 cm
Temperature	20 °C

Thermogravimetric Analysis (TGA):

Thermogravimetric analysis was performed on a TA Instruments Q 500 Thermogravimetric Analyser under nitrogen flow at a typical heating rate of 5 °C/min.

5.3 Techniques

Set-up for crystallisation: each crystallisation of TRIS-based Mn-Anderson compound by slow Et_2O diffusion was set-up as followed: a 50 mL conical flask containing the product dissolved in the appropriate solvent (MeCN or DMF) was inserted into a 500 mL tub containing Et_2O (as in Figure 119).

Figure 119: Representation of the crystallisation set-up: compound solution contained in a 50 mL conical flask inserted into a 500 mL tub with Et_2O. The mother liquor is shown in orange, whilst the grey area represents the Et_2O.

Manual peptide synthesis: synthesis of compound **23** and **Test B-I** were realised using manual SPPS. The solid support on which the synthesis was realised was contained in a plastic syringe equipped with a frit column plate. Some aspects of the technique are illustrated in Figure 120.
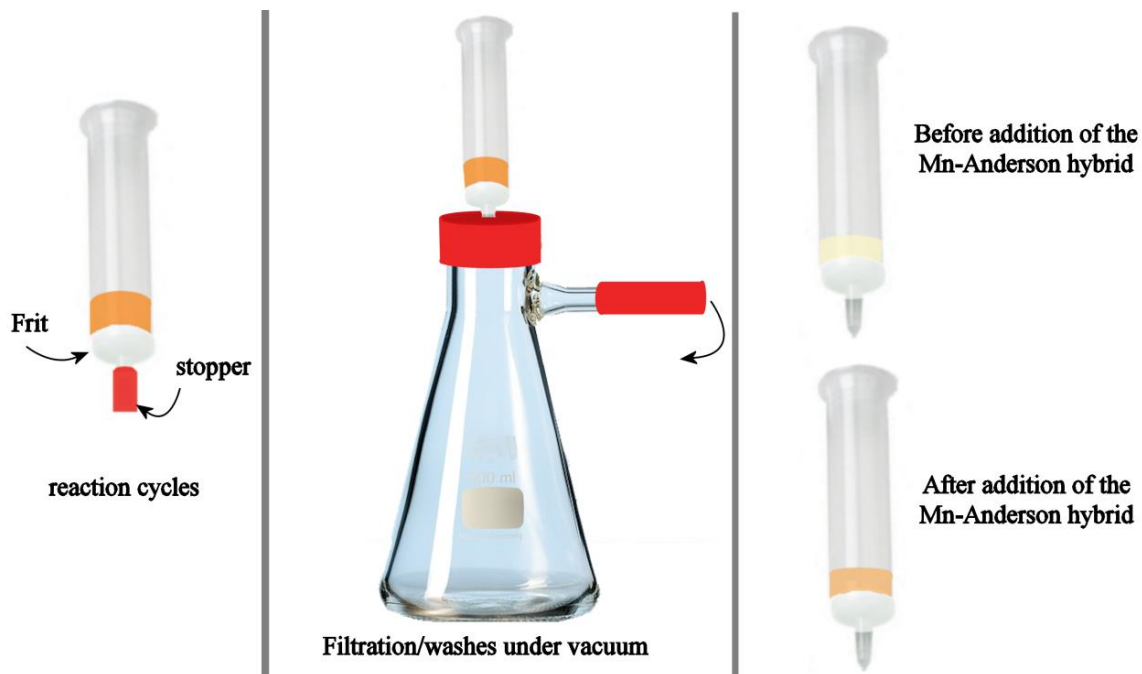
Figure 120: Representation of some key aspects of the manual peptide synthesis (left) set up for SPPS reaction cycles; (middle) set up for filtrations and washes performed using a Buchner flask linked to a vacuum pump. (right) The resin colour change: originally the resin was pale yellow, it maintained this colour until the addition of the Mn-Anderson hybrid residue. Following addition of the hybrid cluster, the solid support was of a bright orange colour.

5.4   Synthetic procedures

5.4.1   The synthesis of TXA octamolybdate salts

The synthesis of the $(TXA)_xNa_{4-x}[Mo_8O_{26}]$ were adapted from the literature procedure of $(TBA)_4[Mo_8O_{26}]$.[227] To obtain single crystals of compounds **1**-**3** for X-ray analysis the precipitates were crystallised from DMF.

5.4.1.1   Compound 1: $(TMA)_2Na_2[Mo_8O_{26}]$

Sodium molybdate dihydrate ($Na_2MoO_4 \cdot 2H_2O$, 5.0 g, 20.7 mmol) was dissolved in H_2O (12 mL) before being acidified with 6M HCl (5.05 mL). The reaction mixture was stirred vigorously for 1-2 min before a solution of TMA bromide (1.6 g, 10.4 mmol) in H_2O (10 mL) was added, resulting in the formation of a white precipitate. The reaction mixture was stirred vigorously for 10 min. The white precipitate was then collected and successively washed with H_2O (20 mL), ethanol (EtOH, 20 mL), acetone (20 mL) and Et_2O (20 mL). Compound **1**, $(N(CH_3)_4)_2Na_2[Mo_8O_{26}]$, was obtained as a white powder. **Yield**: 3.18 g, 2.31 mmol, 88 % based on Mo; **Elemental analysis:** Calc. for $C_8H_{24}Mo_8N_2Na_2O_{26}$ (1377.77 g/mol): C, 6.97; H, 1.76; N, 2.03; Found: C, 6.88; H, 1.85; N, 1.87; **ESI-MS:** peak envelopes observed at *m/z* 614.2 (z = -1) and 665.7 (z = -1) were assigned as $[Na_1[Mo_4O_{13}]]^{1-}$ (predicted: 614.55) and $[(N(CH_3)_4)[Mo_4O_{13}]]^{1-}$ (predicted: 665.65), respectively; **TGA:** The first loss is of 3.94 %, with a second loss at about 250 °C of 13.94 % (Figure 121). The theoretical value for the loss of the TMA cations is 10.76 %. If the weight-dip at about 450 °C is an artefact, then the second loss would be 12.36 %, which corresponds well with the theoretical value.
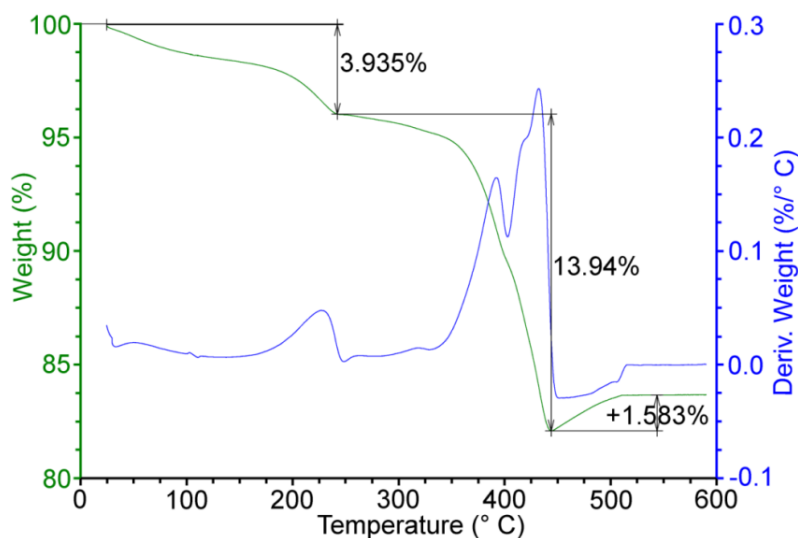
Figure 121: TGA result obtained for compound **1**

5.4.1.2 Compound 2: (TEA)$_3$Na$_1$[Mo$_8$O$_{26}$]

Compound **2** was synthesised in the same manner as compound **1**, only TMA bromide was substituted with TEA bromide (2.19 g, 10.4 mmol). The compound, (N(C$_2$H$_5$)$_4$)$_3$Na$_1$[Mo$_8$O$_{26}$], was obtained as a white powder. **Yield**: 3.73 g, 1.93 mmol, 75 % based on Mo; **Elemental analysis:** Calc. for C$_{24}$H$_{60}$Mo$_8$N$_3$Na$_1$O$_{26}$ (1597.25 g/mol): C, 18.05; H, 3.79; N, 2.63; **Found:** C, 17.79; H, 3.67; N, 2.64; **ESI-MS:** peak envelopes observed at *m/z* 614.2 (z = -1), 721.7 (z = -1) and 1574.6 (z = -1) were assigned as [Na[Mo$_4$O$_{13}$]]$^{1-}$ (predicted: 614.55), [(N(C$_2$H$_5$)$_4$)[Mo$_4$O$_{13}$]]$^{1-}$ (predicted: 721.72) and [(N(C$_2$H$_5$)$_4$)$_3$Mo$_8$O$_{26}$]$^{1-}$ (predicted: 1574.59), respectively; **TGA:** The observed loss is of 30.02% (Figure 121). The theoretical value for the loss of the TEA cations is 24.46 %. If the weight-dip at about 425 °C is an artefact, then the total loss would be 25.52 %, which corresponds well with the theoretical value.
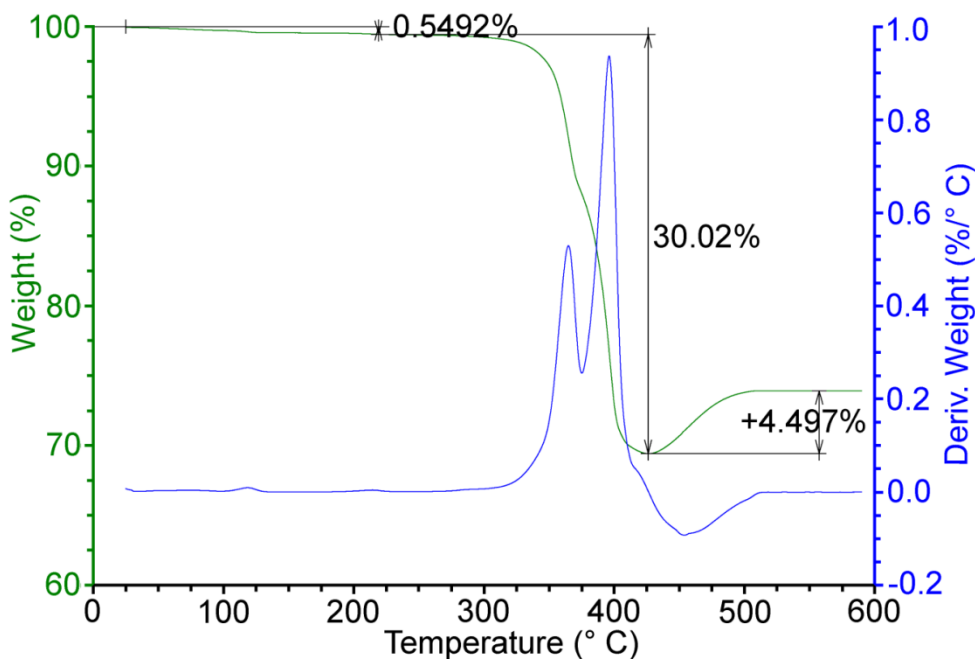
Figure 122: TGA result obtained for compound **2**

5.4.1.3 Compound 3: (TPA)$_2$Na$_2$[Mo$_8$O$_{26}$]

Compound **3** was synthesised in the same manner as compound **1**, only TMA bromide was substituted with TPA bromide (2.77 g, 10.4 mmol). The compound, (N(C$_3$H$_7$)$_4$)$_2$Na$_2$[Mo$_8$O$_{26}$], was obtained as a white powder. **Yield:** 3.63 g, 2.26 mmol, 87 % based on Mo; **Elemental analysis:** Calc. for C$_{24}$H$_{56}$Mo$_8$N$_2$Na$_2$O$_{26}$ (1602.20 g/mol): C, 17.99; H, 3.52; N, 1.75, Na 2.87; Found: C, 17.81; H, 3.45; N, 1.78, Na, 2.77; **ESI-MS:** peak envelopes observed at *m/z* 614.16 (z = -1) and 778.3 (z = -1) were assigned as [Na[Mo$_4$O$_{13}$]]$^{1-}$ (predicted: 614.55) and [(N(C$_3$H$_7$)$_4$)[Mo$_4$O$_{13}$]]$^{1-}$ (predicted: 777.78),

respectively; **TGA:** The observed loss is of 25.52% (Figure 123). The theoretical value for the loss of the TPA cations is 23.26 %. If the weight-dip at about 425 °C is an artefact, then the total loss would be 24.17 %, which corresponds well with the theoretical value.
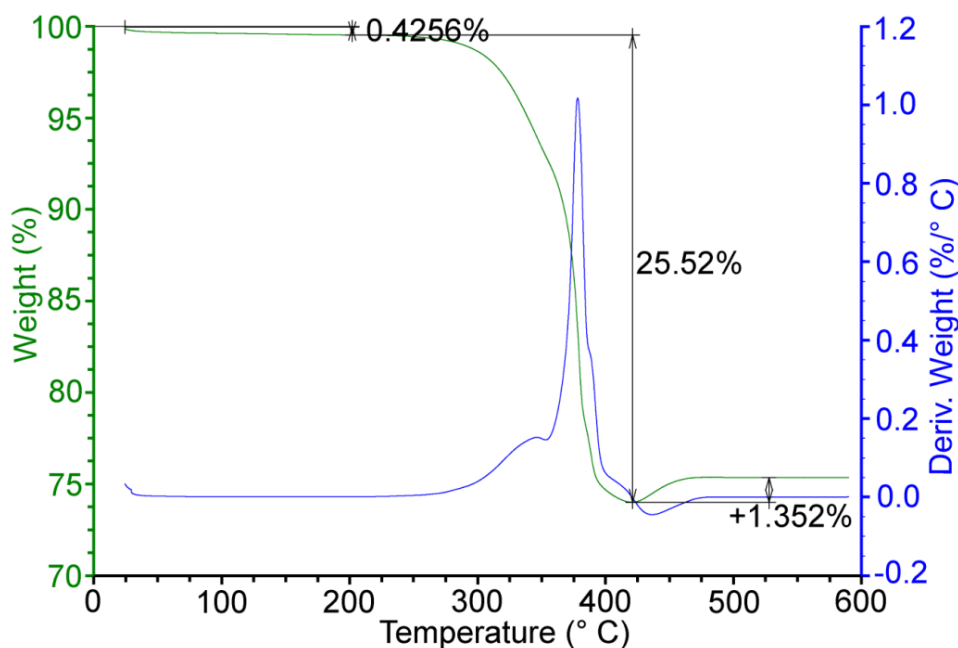
Figure 123: TGA result obtained for compound **3**

5.4.2 The synthesis of Na and TXA TRIS Mn-Anderson compounds

The compounds **4**-**7** were synthesised according to an altered literature procedure for TRIS Mn-Anderson,[50] where the $(TBA)_4[\alpha\text{-}Mo_8O_{26}]$ was substituted by compound **1**, **2** or **3**. Due to the low solubility of compounds **1**-**3** in MeCN, the reactions were carried out in DMF at 80 °C.

5.4.2.1 Compound 4 (TMA)$_3$[MnMo$_6$O$_{18}$((OCH$_2$)$_3$CNH$_2$)$_2$] and Compound 7 (Na)$_3$[MnMo$_6$O$_{18}$(OCH$_2$)$_3$CNH$_2$)$_2$]:

Compound **1** (0.430 g, 0.31 mmol) was dissolved in 60 mL of DMF at room temperature (30 min). Manganese acetate dihydrate (Mn(OAc)$_3$·2H$_2$O, 0.127 g, 0.47 mmol) and TRIS (0.131 g, 1.08 mmol) were added and the resulting solution was heated up to 80 °C for 20 h. During the reaction a brown precipitate was formed, the reaction was then cooled to room temperature and the precipitate removed. The resulting clear orange solution was set up of crystallisation at 4 °C by Et$_2$O diffusion. This crystallisation led to the formation of crystals and a precipitate. The crystalline material is compound **7**, whilst compound **4** is obtained by redissolving the precipitate in DMF and crystallised by Et$_2$O diffusion at 4 °C.

Compound 4 (N(CH$_3$)$_4$)$_3$[MnMo$_6$O$_{18}$((OCH$_2$)$_3$CNH$_2$)$_2$]: **Yield:** 9 % based on Mo; **Elemental analysis:** Calc. for C$_{20}$H$_{52}$Mn$_1$Mo$_6$N$_5$O$_{24}$ (1377.22 g/mol): C, 17.44; H, 3.81; N, 5.09; Found: C, 17.27; H, 2.90; N, 4.57; **^{1}H NMR (DMSO-d$_6$, 400 MHz)**: δ = 64.00-58.00 (m, br, 12H, CH$_2$), 3.60 (s, br, 4H, NH$_2$), 3.10 ppm (s, 36H, CH$_3$); **ESI-MS**: The peak envelope observed at *m/z* 1304.6 (z = -1) was assigned as [(N(CH$_3$)$_4$)$_2$[MnMo$_6$O$_{18}$((OCH$_2$)$_3$CNH$_2$)$_2$]]$^{1-}$ (predicted: 1302.58).

Compound 7 Na$_3$[MnMo$_6$O$_{18}$(OCH$_2$)$_3$CNH$_2$)$_2$]: Yield: 9 % based on Mo; **Elemental analysis:** Calc. for C$_8$H$_{16}$Mn$_1$Mo$_6$N$_2$Na$_3$O$_{24}$·(DMF)$_3$ (1443.04 g/mol): C, 14.15; H, 2.58; N, 4.85; Found: C, 13.68.; H, 2.63; N, 4.36; **^{1}H NMR (DMSO-d$_6$, 400 MHz):** δ = 64.00-58.00 (m, br, 12H, CH$_2$), 3.60 ppm (s, br, 4H, NH$_2$); **ESI-MS:** The peak envelope observed at *m/z* 1201.4 (z = -1) was assigned as [Na$_2$[MnMo$_6$O$_{18}$((OCH$_2$)$_3$CNH$_2$)$_2$]]$^{1-}$ (predicted: 1200.36).

5.4.2.2 Compound 5: (TEA)$_3$[MnMo$_6$O$_{18}$((OCH$_2$)$_3$CNH$_2$)$_2$]

Compound **2** (0.498 g, 0.31 mmol) was dissolved in 60 mL of DMF at room temperature (30 min). Mn(OAc)$_3$·2H$_2$O (0.127 g, 0.47 mmol) and TRIS (0.131 g, 1.08 mmol) were added and the resulting solution was heated up to 80 °C for 20 h. The reaction was then cooled down to room temperature and the clear orange solution was set up of crystallisation at 4°C by Et$_2$O diffusion. This crystallisation led to the formation of crystals and a precipitate both made of compound **5**. Compound **5** was obtained pure by redissolving separately the crystals and the precipitate in DMF and recrystallised by Et$_2$O diffusion at 4 °C. **Yield**: 27 % based on Mo; **Elemental analysis:** Calc. for C$_{32}$H$_{76}$Mn$_1$Mo$_6$N$_5$O$_{24}$ (1545.54 g/mol): C, 24.87; H, 4.96; N, 4.53; Found: C, 24.16; H, 4.73; N, 4.42; **^{1}H NMR (DMSO-d$_6$, 400 MHz)**: δ = 65.00 - 58.00 (m, br, 12H, CH$_2$), 3.60 (s, br, 4H, NH$_2$), 3.28 - 3.12 (m, 24H, CH$_2$), 1.26 - 1.00 ppm (m, 36H, CH$_3$); **ESI-MS**: The peak envelope observed at *m/z* 1414.8 (z = -1) was assigned as [(N(C$_2$H$_5$)$_4$)$_2$ [MnMo$_6$O$_{18}$((OCH$_2$)$_3$CNH$_2$)$_2$]]$^{1-}$ (predicted: 1414.70).

5.4.2.3 Compound 6 (TPA)$_3$[MnMo$_6$O$_{18}$((OCH$_2$)$_3$CNH$_2$)$_2$] and compound 7 (Na)$_3$[Mn Mo$_6$O$_{18}$((OCH$_2$)$_3$CNH$_2$)$_2$]

Compound **3** (0.500 g, 0.31 mmol) was dissolved in 60 mL of DMF at room temperature (30 min). Mn(OAc)$_3$·2H$_2$O (0.127 g, 0.47 mmol) and TRIS (0.131 g, 1.08 mmol) were added and the resulting solution was heated up to 80 °C for 20 h. The reaction was then cooled to room temperature and the resulting clear orange solution was set up of

crystallisation at 4 °C by Et$_2$O diffusion. This crystallisation led to the formation of crystals and a precipitate. The crystalline material is compound **7**, whilst compound **6** is obtained by redissolving the precipitate in DMF and crystallised by Et$_2$O diffusion at 4 °C.

Compound 6 TPA$_2$Na$_1$[MnMo$_6$O$_{18}$((OCH$_2$)$_3$CNH$_2$)$_2$]: Yield: 16 % based on Mo; **Elemental analysis:** Calc. for C$_{32}$H$_{72}$Mn$_1$Mo$_6$N$_4$Na$_1$O$_{24}$ (1550.49 g/mol): C, 24.79; H, 4.68; N, 3.61; Found: C, 24.87; H, 4.77; N, 3.91; **^{1}H NMR (DMSO-d$_6$, 400 MHz):** δ = 63.00 - 59.00 (m, br, 12H, CH$_2$), 3.60 (s, br, 4H, NH$_2$), 3.19 - 3.06 (m, 24H, CH$_2$), 1.70 - 1.53 (m, 24H, CH$_2$), 0.94 - 0.83 ppm (m, 36H, CH$_3$); **ESI-MS:** The peak envelope observed at *m/z* 1527.9 (z = -1) was assigned as [(N(C$_3$H$_7$)$_4$)$_2$[MnMo$_6$O$_{18}$((OCH$_2$)$_3$C-NH$_2$)$_2$]]$^{1-}$ (predicted: 1527.83).

Compound 7 Na$_3$[MnMo$_6$O$_{18}$((OCH$_2$)$_3$CNH$_2$)$_2$]: Yield: 17 % based on Mo; **Elemental analysis:** Calc. for C$_8$H$_{16}$Mn$_1$Mo$_6$N$_2$Na$_3$O$_{24}$ ·(DMF)$_3$ (1443.04 g/mol): C, 14.15; H, 2.58; N, 4.85; Found: C, 15.55; H, 2.24; N, 4.37; **^{1}H NMR (DMSO-d$_6$, 400 MHz):** δ = 64.00 - 58.00 (m, br, 12H, CH$_2$), 3.60 ppm (s, br, 2H, NH$_2$); **ESI-MS:** The peak envelope observed at *m/z* 1201.4 (z = -1) corresponds to [Na$_2$[MnMo$_6$O$_{18}$((OCH$_2$)$_3$CNH$_2$)$_2$]]$^{1-}$ (predicted: 1200.36).

5.4.3 Procedures for peptide bond formation *via* the C-terminus

5.4.3.1 Compound 8: (TBA)$_3$[MnMo$_6$O$_{24}$(C$_7$H$_{12}$NO)$_2$]
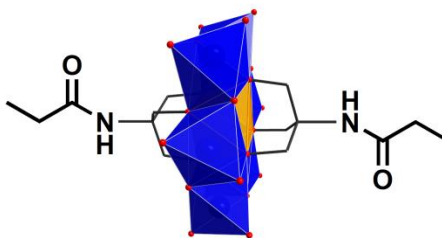
205 μL of propionic anhydride (208 mg, 1.60 mmol, 10 equiv.) were added to a MeCN solution (10 mL) of TBA TRIS Mn-Anderson starting material (300 mg, 0.16 mmol). The resulting orange clear solution was stirred for 24 h at 50 °C, then cooled down to room temperature. Product was isolated by crystallisation under slow Et$_2$O diffusion as block shaped orange crystals (obtained within a week). **Yield**: 277 mg, 0.14 mmol, 87 %; **Elemental analysis**: Calc. for C$_{62}$H$_{132}$MnMo$_6$N$_5$O$_{26}$ (1994.31 g/mol): C, 37.34; H, 6.67; N, 3.51; Found: C, 36.76; H, 6.63; N, 3.51; **^{1}H NMR (DMSO-d$_6$, 400 MHz):** δ = 67.00 - 62.00 (s, br, 12H, CH$_2$), 7.38 (br, s, 2H, NH), 3.16 (m, 24H, CH$_2$ from TBA$^+$), 2.41 (br, s, 4H, CH$_2$), 1.56 (m, 24H, CH$_2$ from TBA$^+$), 1.31 (m, 24H, CH$_2$ from TBA$^+$), 0.93 ppm (m,

42H, CH$_3$ + CH$_3$ from TBA$^+$); ^{13}**C DEPTQ NMR (DMSO-d$_6$, 100 MHz)**: δ = 57.5 (CH$_2$), 27.0 (CH$_2$), 23.1 (CH$_2$), 19.3 (CH$_2$), 13.6 (CH$_3$), 11.0 ppm (CH$_3$); **ESI-MS**: the peak envelope observed at *m/z* 1750.99 (z = -1) was assigned as [(C$_{16}$H$_{36}$N)$_2$[MnMo$_6$O$_{18}$-((OCH$_2$)$_3$CNHCOCH$_2$CH$_3$)$_2$]]$^{1-}$ (predicted: 1752.01).
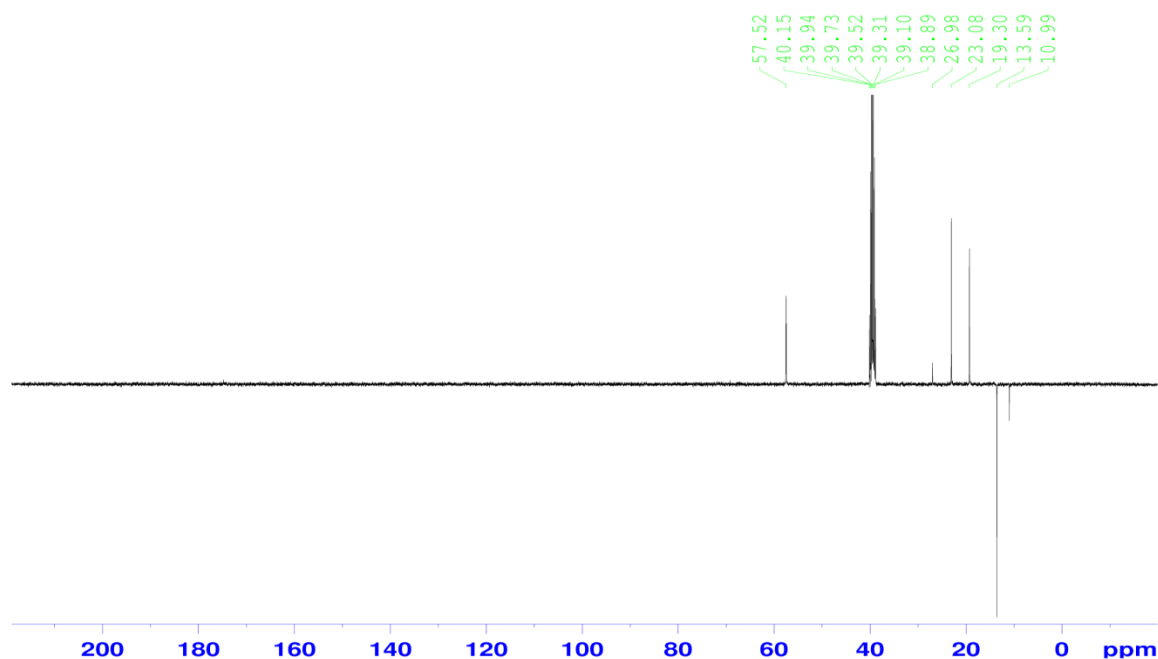
Figure 124: ^{13}C DEPTQ NMR of **8** in DMSO-d$_6$ at 100 MHz.

5.4.3.2 Compound 9: (TBA)$_3$[MnMo$_6$O$_{24}$(C$_{11}$H$_{12}$NO)$_2$]
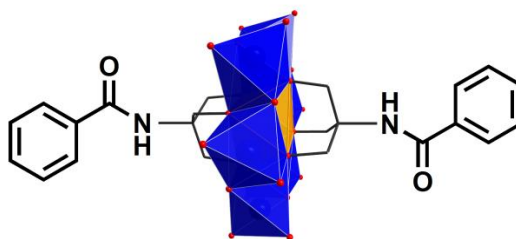
360 mg of benzoic anhydride (1.60 mmol, 10 equiv.) were added to a MeCN solution (10 mL) of TBA TRIS Mn-Anderson starting material (300 mg, 0.16 mmol). The resulting orange clear solution was stirred for 24 h at 50 °C, then cooled down to room temperature. Product was isolated by crystallisation under slow Et$_2$O diffusion as block shaped orange crystals (obtained within a week). **Yield**: 270 mg, 0.13 mmol, 79 %; **Elemental analysis**: Calc. for C$_{70}$H$_{132}$MnMo$_6$N$_5$O$_{26}$ (2090.39 g/mol): C, 40.22; H, 6.36; N, 3.35; Found: C, 40.35; H, 6.55; N, 3.40; ^{1}**H NMR (DMSO-d$_6$, 400 MHz):** δ = 67.00 - 62.00 (s, br, 12H, CH$_2$), 8.1-7.1 (m, 12H, CH + NH), 3.16 (m, 24H, CH$_2$ from TBA$^+$), 1.56 (m, 24H, CH$_2$ from TBA$^+$), 1.31 (m, 24H, CH$_2$ from TBA$^+$), 0.93 ppm (m, 36H, CH$_3$ from TBA$^+$); ^{13}**C**

DEPTQ NMR (DMSO-d$_6$, 100 MHz): δ = 132.1 (C), 131.3 (CH), 128.1 (CH), 127.6 (CH), 57.5 (CH$_2$), 23.1 (CH$_2$), 19.3 (CH$_2$), 13.6 ppm (CH$_3$); **ESI-MS**: the peak envelope observed at *m/z* 1848.07 (z = -1) was assigned as $[(C_{16}H_{36}N)_2[MnMo_6O_{18}((OCH_2)_3C\text{-}NHCO(C_6H_5))_2]]^{1-}$ (predicted: 1848.01).

5.4.3.3 Compound 10: (TBA)$_3$[MnMo$_6$O$_{24}$(C$_8$H$_{12}$NO$_3$)$_2$]
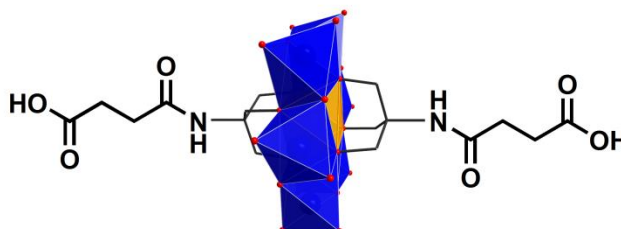
320 mg of succinic anhydride (3.20 mmol, 20 equiv.) were added to a DMF solution (10 mL) of TBA TRIS Mn-Anderson (300 mg, 0.16 mmol). The resulting orange clear solution was stirred for 24 h at 50 °C, then cooled down to room temperature. Product was isolated by crystallisation under slow Et$_2$O diffusion as block shaped orange crystals (obtained within a week). **Yield**: 291 mg, 0.14 mmol, 88 %; **Elemental analysis**: Calc. for C$_{64}$H$_{132}$MnMo$_6$N$_5$O$_{30}$ (2082.33 g/mol): C, 36.91; H, 6.39; N, 3.36; Found: C, 36.62; H, 6.53; N, 3.60; **^{1}H NMR (DMSO-d$_6$, 400 MHz):** δ = 67.00 - 62.00 (s, br, 12H, CH$_2$), 12.07 (s, 2H, COOH), 8.0 - 7.1 (s, br, 2H, NH), 3.16 (m, 24H, CH$_2$ from TBA$^+$), 2.69 (m, 4H, CH$_2$), 2.37 (m, 4H, CH$_2$), 1.57 (m, 24H, CH$_2$ from TBA$^+$), 1.31 (m, 24H, CH$_2$ from TBA$^+$), 0.94 ppm (m, 36H, CH$_3$ from TBA$^+$); **^{13}C DEPTQ NMR (DMSO-d$_6$, 100 MHz)**: δ = 57.5 (CH$_2$), 29.7 (CH$_2$), 28.4 (CH$_2$), 23.1 (CH$_2$), 19.3 (CH$_2$), 13.6 ppm (CH$_3$); **ESI-MS**: peak envelopes observed at *m/z* 1840.09 (z = -1) and 2081.37 (z = -1) were assigned as $[(C_{16}H_{36}N)_2[MnMo_6O_{18}((OCH_2)_3CNHCO(CH_2)_2COOH)_2]]^{1-}$ (predicted: 1839.99) and $[(C_{16}H_{36}N)_3[MnMo_6O_{18}((OCH_2)_3CNHCO(CH_2)_2COOH)((OCH_2)_3CNHCO(CH_2)_2COO)]]^{1-}$ (predicted: 2081.26), respectively.
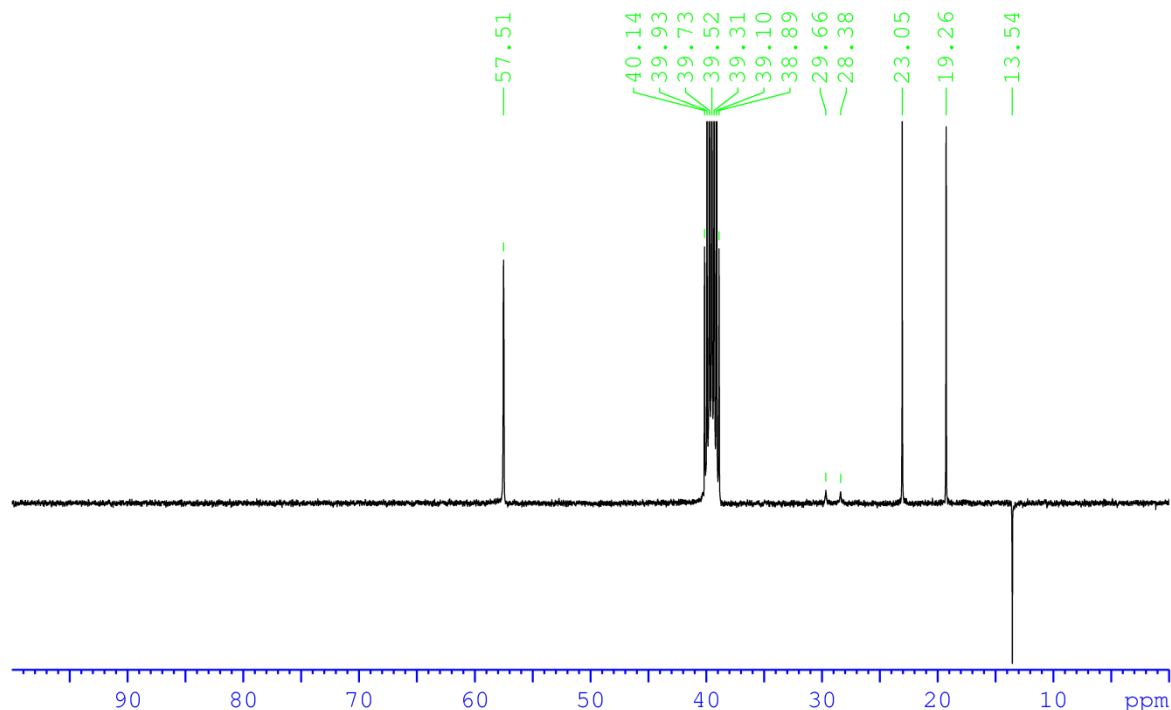
Figure 125: ^{13}C DEPTQ NMR of **10** in DMSO-d$_6$ at 100 MHz.

5.4.4 Procedures for peptide bond formation *via* the N-terminus

5.4.4.1 Compound 11: (TBA)$_3$[MnMo$_6$O$_{24}$(C$_{12}$H$_{15}$N$_2$O$_5$)$_2$]
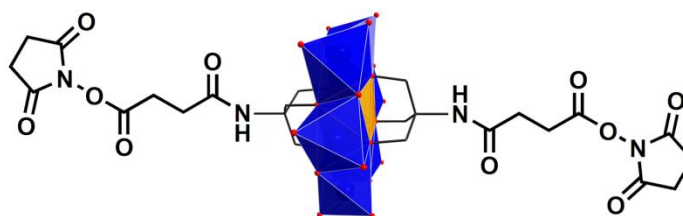
Compound **10** (2.14 g, 1.03 mmol), NHS (474 mg, 4.12 mmol, 4 equiv.) and DCC (1.27 g, 6.18 mmol, 6 equiv.) were dissolved in DMF (20 mL). The orange solution was stirred at room temperature for 24 h. A white precipitate of *N, N'*-dicyclohexylurea (DCU) forming over the time of the reaction was removed by centrifugation and the resulting bright orange solution was set up for crystallisation with Et$_2$O diffusion. Within a week, compound **11** was isolated pure as orange needle crystals suitable for X-ray diffraction analysis. For other analyses the product was recrystallised from MeCN. **Yield:** 1.77 g, 0.78 mmol, 75 %; **Elemental analysis:** Calc. for C$_{72}$H$_{138}$MnMo$_6$N$_7$O$_{34}$ (2276.47 g/mol): C, 37.99; H, 6.11; N, 4.31; Found: C, 37.80; H, 6.20; N, 4.49; ^{1}**H NMR (DMSO-d$_6$, 400 MHz):** δ = 67.00 - 62.00 (s, br, 12H, CH$_2$), 7.61 (s, br, 2H, NH), 3.16 (m, 24H, CH$_2$ from TBA$^+$), 2.82 (m, 16H, CH$_2$), 1.57 (m, 24H, CH$_2$ from TBA$^+$), 1.31 (m, 24H, CH$_2$ from TBA$^+$), 0.94 ppm (m,

36H, CH$_3$ from TBA$^+$); **^{13}C DEPTQ NMR (DMSO-d$_6$, 100 MHz):** δ = 171.0 (CO), 170.1 (CO), 168.4 (CO), 57.5 (CH$_2$), 27.5 (CH$_2$), 26.2 (CH$_2$), 25.4 (CH$_2$), 23.0 (CH$_2$), 19.2 (CH$_2$), 13.5 ppm (CH$_3$); **ESI-MS:** peak envelopes observed at *m/z* 1275.32 (z = -3) and 2034.12 (z = -1) were assigned as [(C$_{16}$H$_{36}$N)$_3$[MnMo$_6$O$_{18}$((OCH$_2$)$_3$CNH-CO(CH$_2$)$_2$COON(COCH$_2$)$_2$)$_2$]$_2$]$^{3-}$ (predicted: 1275.25) and [(C$_{16}$H$_{36}$N)$_2$[MnMo$_6$O$_{18}$-((OCH$_2$)$_3$CNHCO(CH$_2$)$_2$COON(COCH$_2$)$_2$)$_2$]]$^{1-}$ (predicted: 2034.02), respectively.
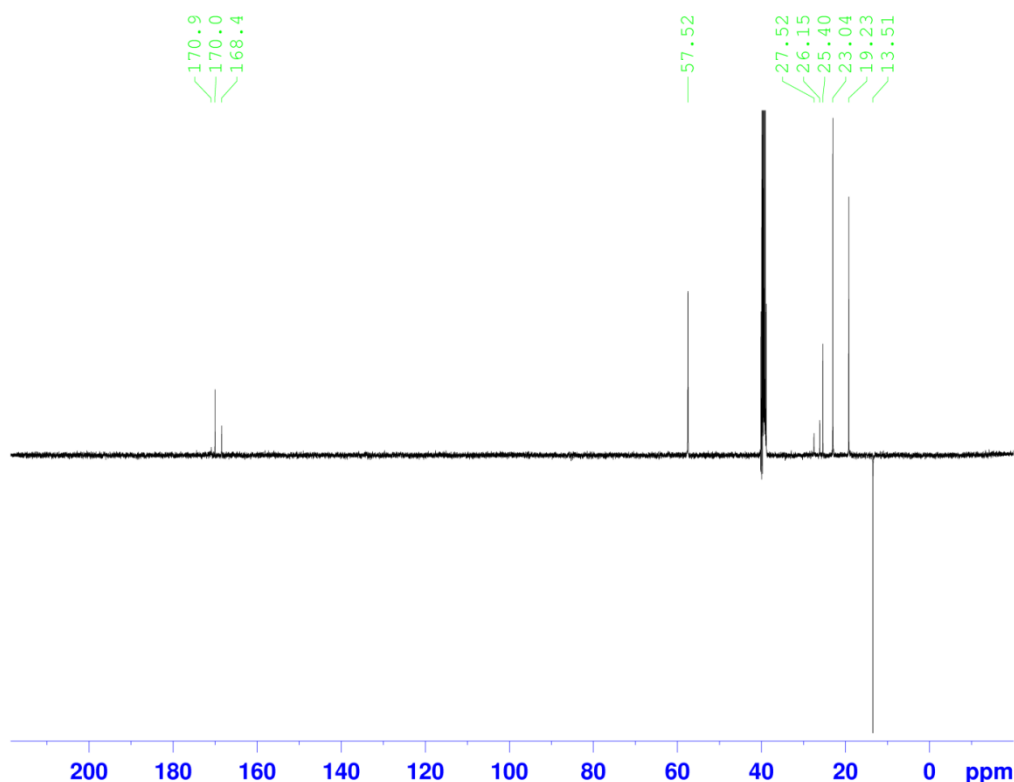
Figure 126: ^{13}C DEPTQ NMR of **11** in DMSO-d$_6$ at 100 MHz.

5.4.4.2 Compound 12: (TBA)$_3$[MnMo$_6$O$_{24}$(C$_{10}$H$_{15}$N$_2$O$_4$)$_2$]
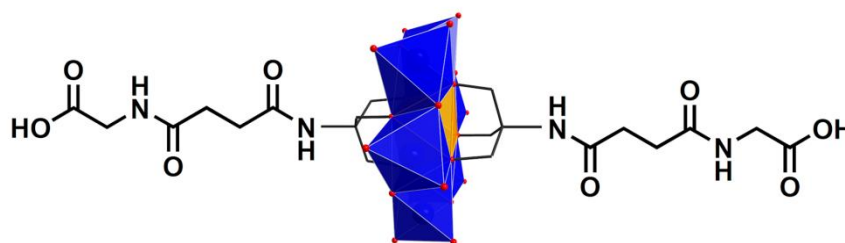
Glycine (34 mg, 0.45 mmol, 2 equiv.) and DIPEA (500 μL, 2.8 mmol) were added to a solution of compound **11** (500 mg, 0.22 mmol) in DMF (10 mL). The resulting clear orange solution was left to stir at room temperature overnight. The product was then precipitated into Et$_2$O (500 mL), collected and redissolved in MeCN to then precipitate it again in Et$_2$O. The precipitation process was repeated twice to yield to **12** in high purity.

Yield: 302 mg, 0.14 mmol, 63 %. **Elemental analysis:** Calc. for $C_{68}H_{138}MnMo_6N_7O_{32}$ (2196.43 g/mol): C, 37.18; H, 6.33; N, 4.46; Found: C, 36.97; H, 6.32; N, 4.63. **^{1}H NMR (DMSO-d$_6$, 400 MHz)**: δ = 67.0 - 62.0 (s, br, 12H, CH_2), 8.18 (s, 2H, NH), 7.53 (s, br, 2H, NH), 3.73 (m, 4H, CH_2), 3.16 (m, 24H, CH_2 from TBA$^+$), 2.67 (m, br, 4H, CH_2), 2.33 (m, br, 4H, CH_2), 1.56 (m, 24H, CH_2 from TBA$^+$), 1.30 (m, 24H, CH_2 from TBA$^+$), 0.93 ppm (m, 36H, CH_3 from TBA$^+$). **^{13}C DEPTQ NMR (DMSO-d$_6$, 100 MHz)**: δ = 57.5 (CH_2), 40.8 (CH_2), 31.3 (CH_2), 29.1 (CH_2), 23.1 (CH_2), 19.3 (CH_2), 13.5 ppm (CH_3); **ESI-MS:** peak envelopes observed at *m/z* 1221.8 (z = -3), 1953.94 (z = -1) and 2196.19 (z = -1) were assigned as $[(C_{16}H_{36}N)_3[MnMo_6O_{24}(C_{10}H_{15}N_2O_4)_2]_2]^{3-}$ (predicted: 1221.93), $[(C_{16}H_{36}N)_2$ $[MnMo_6O_{24}(C_{10}H_{15}N_2O_4)_2]]^{1-}$ (predicted: 1954.03) and $[(C_{16}H_{36}N)_3[MnMo_6O_{24}$-$(C_{10}H_{15}N_2O_4)(C_{10}H_{14}N_2O_4)_2]]^{1-}$ (predicted: 2196.31), respectively.
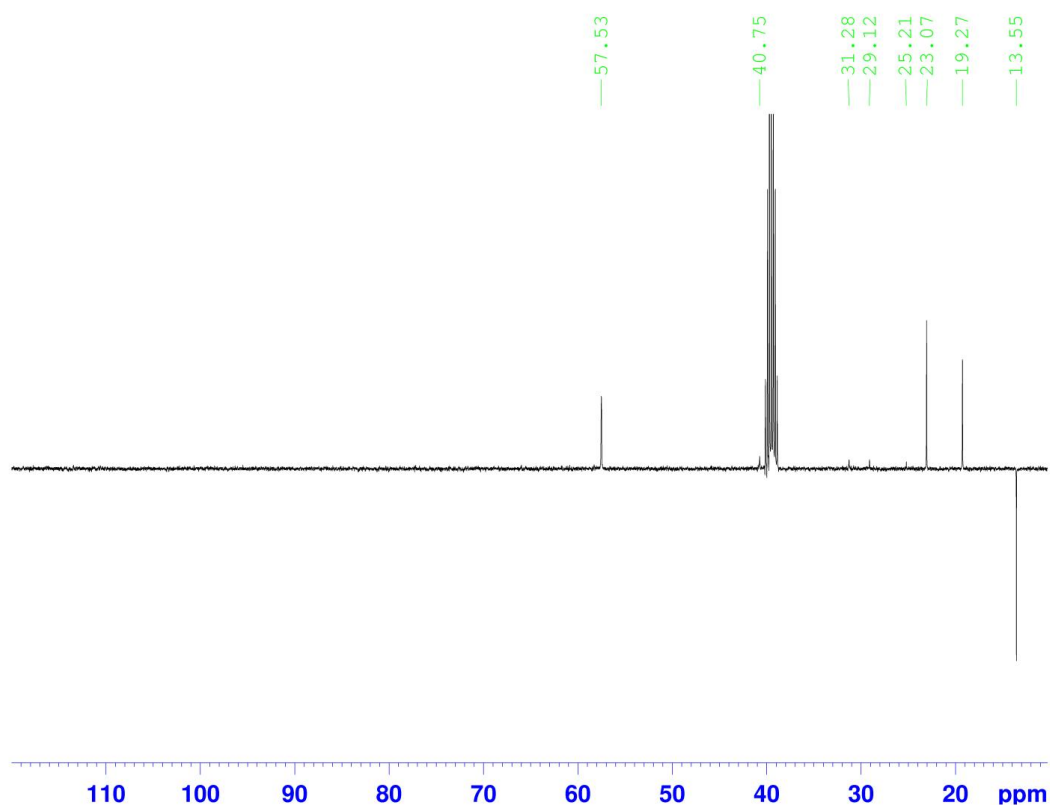
Figure 127: ^{13}C DEPTQ NMR of **12** in DMSO-d$_6$ at 100 MHz.

5.4.4.3 Compound 13: (TBA)₃[MnMo₆O₂₄(C₁₇H₂₁N₂O₄)₂]
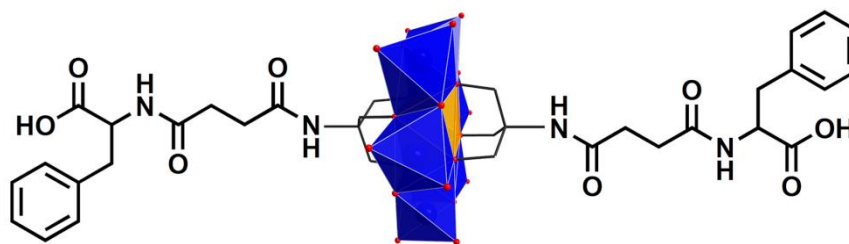
L-phenylalanine (74 mg, 0.45 mmol, 2 equiv.) and DIPEA (500 μL, 2.8 mmol) were added to a solution of compound **11** (500 mg, 0.22 mmol) in DMF (10 mL). The resulting clear orange solution was left to stir at room temperature overnight. The product was then precipitated into a Et₂O solution (500 mL), collected and redissolved in MeCN to precipitate it again in Et₂O. The precipitation process was repeated twice to yield to **13** in high purity. Single crystals suitable for X-ray diffraction were obtained by diffusion of Et₂O into a DMF solution of **13**. **Yield**: 412 mg, 0.17 mmol, 78 %; **Elemental analysis:** Calc. for $C_{82}H_{150}MnMo_6N_7O_{32}$ (2376.67 g/mol) C, 41.44; H, 6.36; N, 4.13; Found: C, 41.44; H, 6.43; N, 4.26; **¹H NMR (DMSO-d₆, 400 MHz)**: δ = 67.0 - 62.0 (s, br, 12H, CH_2), 8.16 (s, 2H, NH), 7.85 - 7.00 (m, br, 12H , NH + CH), 4.38 (s, br, 2H, CH), 3.17 (m, 24H, CH_2 from TBA⁺), 3.08 - 2.53 (m, 8H, CH_2), 2.26 (m, 4H, CH_2), 1.56 (m, 24H, CH_2 from TBA⁺), 1.30 (m, 24H, CH_2 from TBA⁺), 0.93 ppm (m, 36H, CH_3 from TBA⁺); **¹³C DEPTQ NMR (DMSO-d₆, 100 MHz)**: δ = 137.7 (C), 129.1 (CH), 128.1 (CH), 126.3 (CH), 57.5 (CH_2), 53.7 (CH), 36.83 (CH_2), 31.5 (CH_2), 29.4 (CH_2), 23.1 (CH_2), 19.2 (CH_2), 13.5 ppm (CH_3); **ESI-MS:** peak envelopes observed at *m/z* 1342.08 (z = -3), 2134.26 (z = -1) and 2376.53 (z = -1) were assigned as [(TBA)₃[MnMo₆O₂₄-(C₁₇H₂₁N₂O₄)₂]₂]³⁻ (predicted: 1341.99), [(TBA)₂ [MnMo₆O₂₄(C₁₇H₂₁N₂O₄)₂]]¹⁻ (predicted: 2134.12) and [(TBA)₃[MnMo₆O₂₄(C₁₇H₂₁N₂O₄)(C₁₇H₂₀N₂O₄)]]¹⁻ (predicted: 2376.40), respectively.
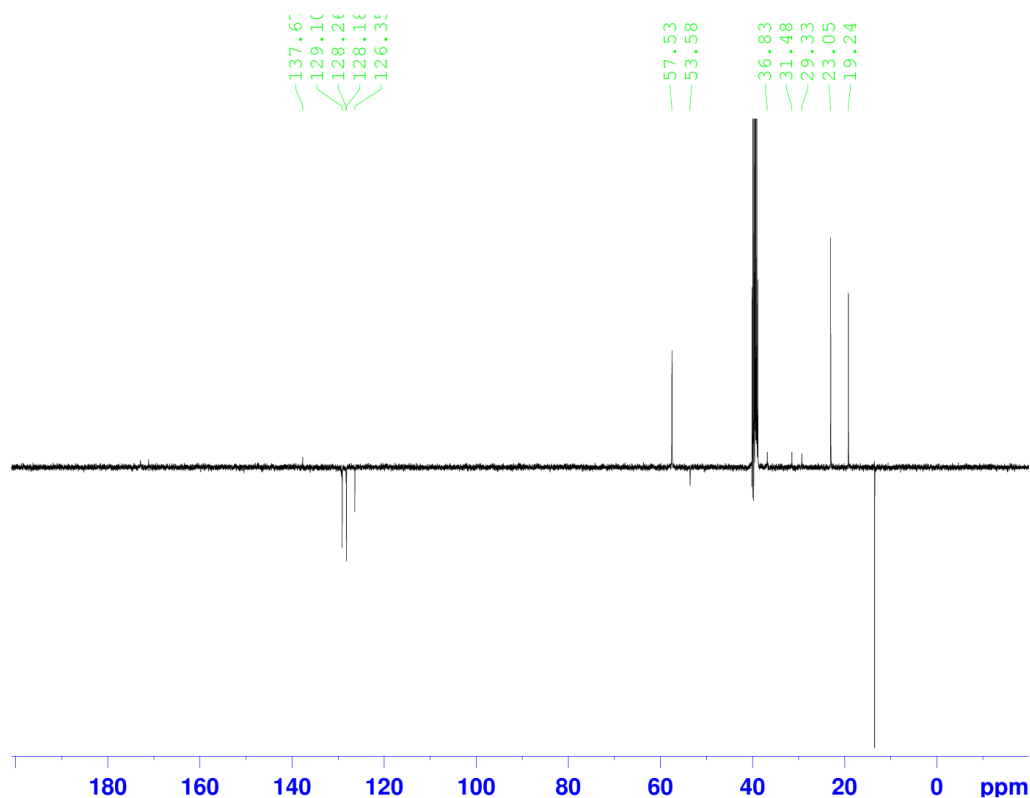
Figure 128: ^{13}C DEPTQ NMR of **13** in DMSO-d$_6$ at 100 MHz.

5.4.4.4 Compound 14: (TBA)$_3$[MnMo$_6$O$_{24}$(C$_{26}$H$_{30}$N$_3$O$_5$)$_2$]
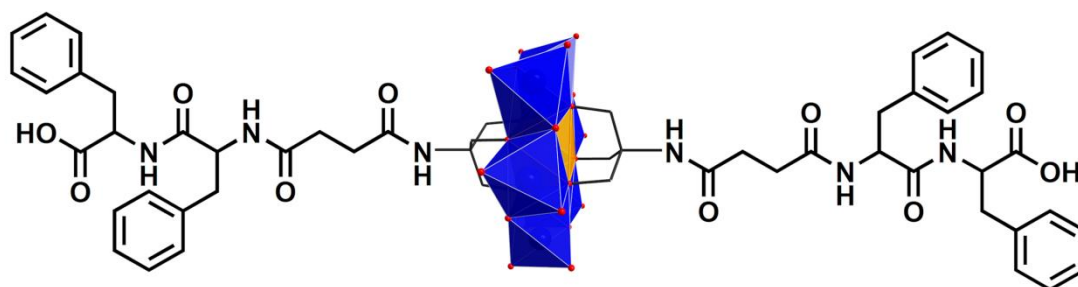
Di-L-phenylalanine (141 mg, 0.45 mmol, 2 equiv.) and DIPEA (500 μL, 2.8 mmol) were added to a solution of compound **11** (500 mg, 0.22 mmol) in DMF (10 mL). The resulting clear orange solution was left to stir at room temperature overnight The product was then precipitated into a Et$_2$O solution (500 mL), collected and redissolved in MeCN to precipitate it again in Et$_2$O. The precipitation process was repeated twice to yield to **14** in high purity. **Yield**: 401 mg, 0.15 mmol, 68 %; **Elemental analysis:** Calc. for C$_{100}$H$_{168}$MnMo$_6$N$_9$O$_{34}$ (2671.02 g/mol): C, 44.97; H, 6.34; N, 4.72; Found: C, 44.37; H, 6.43; N, 4.86. **^{1}H NMR (DMSO-d$_6$, 400 MHz)**: δ = 67.0 - 62.0 (s, br, 12H, CH$_2$), 8.08 (m, 4H, NH), 7.85 - 6.85 (m, br, 22H, NH + CH), 4.48 (s, br, 2H, CH), 4.37 (s, br, 2H, CH), 3.16 (m, 24H, CH$_2$ from TBA$^+$), 3.08 - 2.53 (m, 12H, CH$_2$), 2.22 (m, 4H, CH$_2$), 1.57 (m,

24H, CH_2 from TBA^+), 1.31 (m, 24H, CH_2 from TBA^+), 0.94 ppm (m, 36H, CH_3 from TBA^+). **^{13}C DEPTQ NMR (DMSO-d$_6$, 100 MHz)**: δ = 137.9 (C), 129.2 (CH), 129.1 (CH), 128.2 (CH), 128.0 (CH), 126.4 (CH), 57.5 (CH_2), 37.4 (CH_2), 36.6 (CH_2), 31.5 (CH_2), 29.4 (CH_2), 23.0 (CH_2), 19.2 (CH_2), 13.5 ppm (CH_3); **ESI-MS:** peak envelopes observed at *m/z* 1538.45 (z = -3), 1618.54 (z = -4), 2430.31 (z = -1) and 2549.44 (z = -2) were assigned as $[(C_{16}H_{36}N)_3[MnMo_6O_{24}(C_{26}H_{30}N_3O_5)_2]_2]^{3-}$ (predicted: 1538.41), $[(C_{16}H_{36}N)_4[MnMo_6O_{24}(C_{26}H_{30}N_3O_5)(C_{26}H_{29}N_3O_5)]_2]^{4-}$ (predicted: 1618.50), $[(C_{16}H_{36}N)_2[MnMo_6O_{24}(C_{26}H_{30}N_3O_5)_2]]^{1-}$ (predicted: 2429.26) and $[(C_{16}H_{36}N)_5[MnMo_6O_{24}(C_{26}H_{30}N_3O_5)(C_{26}H_{29}N_3O_5)][MnMo_6O_{24}(C_{26}H_{30}N_3O_5)_2]]^{2-}$ (predicted: 2549.40), respectively.

Figure 129: ^{13}C DEPTQ NMR of **14** in DMSO-d$_6$ at 100 MHz.

5.4.4.5 Compound 15: (TBA)$_3$[MnMo$_6$O$_{24}$(C$_{35}$H$_{39}$N$_4$O$_6$)$_2$]
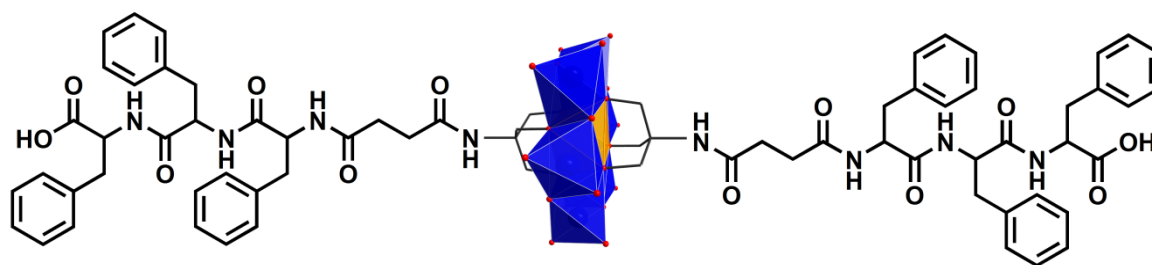
Tri-L-phenylalanine (207 mg, 0.45 mmol, 2 equiv.) and DIPEA (500 μL, 2.8 mmol) were added to a solution of compound **11** (500 mg, 0.22 mmol) in DMF (10 mL). The resulting clear orange solution was left to stir at room temperature overnight The product was then precipitated into a Et$_2$O solution (500 mL), collected and redissolved in MeCN to then precipitate it again in Et$_2$O. The precipitation process was repeated twice to yield to **15** in high purity. **Yield**: 535 mg, 0.18 mmol, 82 %; **Elemental analysis:** Calc. for C$_{118}$H$_{186}$MnMo$_6$N$_{11}$O$_{36}$ (2965.37 g/mol): C, 47.79; H, 6.32; N, 5.20; Found: C, 47.72; H, 6.44; N, 5.38; **^{1}H NMR (DMSO-d$_6$, 400 MHz)**: δ = 67.0 - 62.0 (s, br, 12H, CH$_2$), 8.20 - 8.96 (m, 6H, NH), 7.85 - 6.85 (m, br, 32H , NH + CH), 4.46 (m, br, 6H, CH), 3.16 (m, 24H, CH$_2$ from TBA$^+$), 3.08 - 2.53 (m, 16H, CH$_2$), 2.21 (m, 4H, CH$_2$), 1.57 (m, 24H, CH$_2$ from TBA$^+$), 1.31 (m, 24H, CH$_2$ from TBA$^+$), 0.94 ppm (m, 36H, CH$_3$ from TBA$^+$); **^{13}C DEPTQ NMR (DMSO-d$_6$,100 MHz)**: δ = 170.9 (CO), 137.9 (C), 137.6 (C), 129.3 (CH), 129.2 (CH), 128.2 (CH), 128.0 (CH), 126.4 (CH), 126.2 (CH), 57.5 (CH$_2$), 53.7 (CH), 37.3 (CH$_2$), 31.6 (CH$_2$), 29.4 (CH$_2$), 23.0 (CH$_2$), 19.2 (CH$_2$), 13.5 ppm (CH$_3$); **ESI-MS:** peak envelopes observed at *m/z* 1734.61 (z = -3), 1815.04 (z = -4), 2602.90 (z = -2) and 2723.55 (z = -1) were assigned as [(C$_{16}$H$_{36}$N)$_3$[MnMo$_6$O$_{24}$(C$_{35}$H$_{39}$N$_4$O$_6$)$_2$]$_2$]$^{3-}$ (predicted: 1734.50), [(C$_{16}$H$_{36}$N)$_4$[MnMo$_6$O$_{24}$(C$_{35}$H$_{39}$N$_4$O$_6$)(C$_{35}$H$_{38}$N$_4$O$_6$)]$_2$]$^{4-}$ (predicted: 1814.59), [(C$_{16}$H$_{36}$N)$_3$H [MnMo$_6$O$_{24}$(C$_{35}$H$_{39}$N$_4$O$_6$)$_2$]$_2$]$^{2-}$ (predicted: 2602.26) and [(C$_{16}$H$_{36}$N)$_2$[MnMo$_6$O$_{24}$-(C$_{35}$H$_{39}$N$_4$O$_6$)$_2$]]$^{1-}$ (predicted: 2723.40), respectively.

Figure 130: ^{13}C DEPTQ NMR of **15** in DMSO-d$_6$ at 100 MHz.

5.4.4.6 Compound 16: Na$_{0.2}$(TBA)$_{2.8}$[MnMo$_6$O$_{24}$(C$_{74}$H$_{118}$N$_{17}$O$_{29}$)$_2$]·5H$_2$O ·1.5DMF*
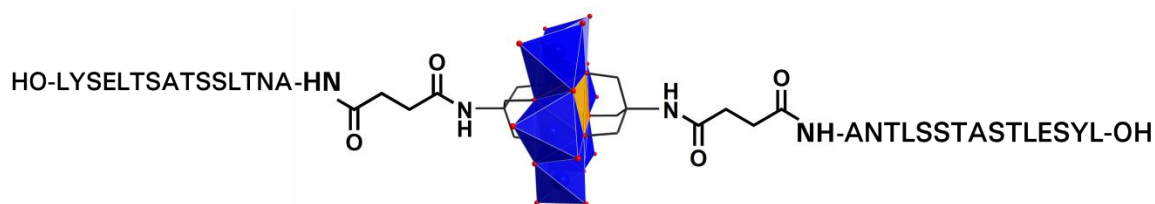
NH$_2$-Ala-Asn-Thr-Leu-Ser-Ser-Thr-Ala-Ser-Thr-Leu-Glu-Ser-Tyr-Leu-OH (**P$_1$**, 140 mg, 0.090 mmol, 2 equiv.) and DIPEA (120 μL, 0.69 mmol) were added to a solution of compound **11** (102 mg, 0.045 mmol) in dry DMF (5 mL). The resulting clear orange solution was left to stir at room temperature overnight. The solution was then exposed to Et$_2$O vapour and a precipitate formed within a few days. The precipitate (**16**) was isolated by centrifugation, washed several times with Et$_2$O and then dried. **Yield**: 193 mg, 0.036 mmol, 80 %; **Elemental analysis:** Calc. for C$_{197.3}$H$_{357.3}$MnMo$_6$N$_{38.3}$Na$_{0.2}$O$_{88.5}$ (5317.43 g/mol): C, 44.56; H, 6.77; N, 10.09; Found: C, 44.09; H, 6.73; N, 10.17;^{1}**H NMR (DMSO-d$_6$, 400 MHz)**: see Figure 132; **ESI-MS:** Peak envelopes observed at m/z 1108.33 (z = -4), 1478.12 (z = -3), 1485.44 (z = -3) and 1558.89 (z = -3) were assigned as

$[[MnMo_6O_{24}(C_{74}H_{118}N_{17}O_{29})(C_{74}H_{117}N_{17}O_{29})]]^{4-}$ (predicted: 1108.23), $[[MnMo_6O_{24}-(C_{74}H_{118}N_{17}O_{29})_2]]^{3-}$ (predicted: 1477.97), $[Na[MnMo_6O_{24}(C_{74}H_{118}N_{17}O_{29})(C_{74}H_{117}N_{17}O_{29})]]^{3-}$ (predicted: 1485.30) and $[(C_{16}H_{36}N)[MnMo_6O_{24}(C_{74}H_{118}N_{17}O_{29})(C_{74}H_{117}N_{17}O_{29})]]^{3-}$ (predicted: 1558.73), respectively; **TGA**: the loss of 3.79 % corresponds to the loss of solvent $((H_2O)_5(DMF)_{1.5}$; calculated loss: 3.8 %). The weight loss starting at 100 °C of 81.14 % corresponds to the loss of the organic cations and the ligands (theoretically 78.9 %). At about 650 °C the metal oxide starts decomposing

*Formula established from TGA analysis and elemental analysis results; Na cations were observed during ESI-MS analysis.
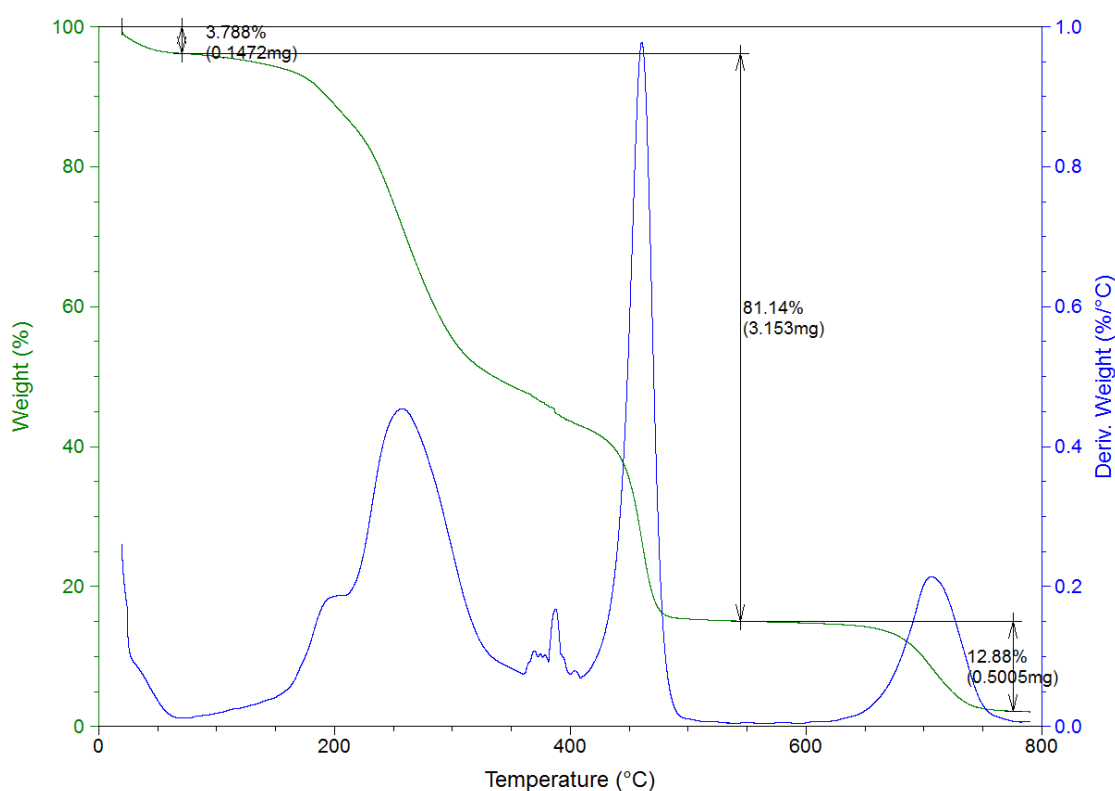
Figure 131: TGA analysis of compound **16**.

1	2	3	4	5	6	7	8	9	10	11	12	13	14	15
Ala	Asn	Thr	Leu	Ser	Ser	Thr	Ala	Ser	Thr	Leu	Glu	Ser	Tyr	Leu

	H	
1 Ala	8.17	H^a 4.25, H^{b*} 1.19
2 Asn	8.24	H^a 4.59
3 Thr	7.55	H^a 4.15, H^b 4.04, H^{g2*} 1.05
4 Leu	7.81	H^a 4.32, H^{d1*} 0.84, H^{d2*} 0.84
5 Ser	7.85	H^a 4.31, H^{b2} 3.60, H^{b3} 3.60
6 Ser	7.92	H^a 4.35, H^{ba} 3.59, H^{bb} 3.67
7 Thr	7.74	H^a 4.21, H^b 4.04, H^{g2*} 1.05
8 Ala	7.94	H^a 4.33, H^{b*} 1.24
9 Ser	8.01	H^a 4.35, H^{ba} 3.58, H^{bb} 3.64
10 Thr	7.68	H^a 4.19, H^b 4.05, H^{g2*} 1.05
11 Leu	7.84	H^a 4.28, H^{d1*} 0.83, H^{d2*} 0.83
12 Glu	7.79	H^a 4.23, H^{ba} 1.75, H^{bb} 1.91, H^{g2} 2.24, H^{g3} 2.24
13 Ser	7.72	H^a 4.23, H^{ba} 3.48, H^{bb} 3.53
14 Tyr	7.89	H^a 4.42, H^{ba} 2.71, H^{bb} 2.97, H^{d*} 7.02, H^{e*} 6.62

Figure 132: (top) Annotations used for the 2D NMR analyses of **16** and (bottom) table of resonance assignments.

5.4.5 Synthesis and isolation of asymmetric hybrid Mn-Anderson clusters

5.4.5.1 Compound 17: $(TBA)_3[MnMo_6O_{24}(C_4H_8N)(C_{19}H_{16}NO)]$
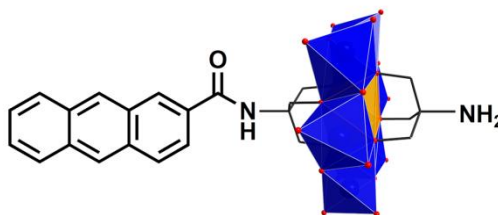
STEP 1: Synthesis of the Anthracene-TRIS ligand (adapted from a published procedure).[251]

To a solution of anthracene-2-carboxylic acid (407 mg, 1.83 mmol) and *N*-methylmorpholine (0.22 mL, 2.00 mmol) in tetrahydrofuran (10 mL) at 0 ˚C, ethylchloroformate (0.19 mL, 2.00 mmol) was added dropwise, causing a white precipitate to form. The reaction mixture was then stirred for 30 min at 0 ˚C, then filtered directly into a solution of TRIS (218 mg, 1.83 mmol) and triethylamine (0.28 mL, 2.00 mmol) in DMF (10 mL) which had been stirring for 10 min. The reaction mixture was then stirred overnight, after which solvents were removed under reduced pressure until only DMF remained. The product was crystallised by Et_2O diffusion into this DMF solution over 2 days, giving clear yellow needles. **Yield:** 428 mg, 1.32 mmol, 36 %; **Elemental analysis:** Calc. for $C_{19}H_{19}NO_4$ (325.36 g/mol): C 70.14 H 5.89 N 4.31; Found C 69.71 H 5.97 N 4.58; **¹H NMR (DMSO-d₆, 400 MHz):** δ = 8.74 (s, 1H, CH), 8.62 (s, 2H, 2CH), 8.15 (m, 3H, 3CH), 7.86 (m, 1H, CH), 7.57 (m, 3H, 2CH + NH), 4.84 (s, 3H, 3OH), 3.77 ppm (s, 6H, 3CH₂); **¹³C DEPTQ NMR (DMSO-d₆, 100 MHz):** δ = 167.3 (CO), 132.1 (C), 132.0 (C), 131.5 (C), 130.0 (C), 128.2 (CH), 128.1 (CH), 128.0 (CH), 128.0 (CH), 127.7 (CH), 126.3 (CH), 125.9 (CH), 125.9 (CH), 123.8 (CH), 62.8 (C), 60.4 ppm (CH₂).

STEP 2: Synthesis of the Anthracene-TRIS/TRIS Mn-Anderson compound (**17**)

The crude mixture was synthesised according to an adapted literature procedure.[50,113]

A mixture of $(TBA)_4[\alpha\text{-}Mo_8O_{26}]$ (765 mg, 0.36 mmol), $Mn(OAc)_3 \cdot 2H_2O$ (220 mg, 0.91 mmol), TRIS (139 mg, 0.94 mmol) and Anthracene-TRIS ligand (304 mg; 0.94 mmol) was refluxed in MeCN (15 mL) for 18 h. The resulting brown mixture was cooled down to room temperature and the precipitate removed by centrifugation to lead to a bright orange solution. The crude mixture was isolated by crystallisation by Et_2O diffusion. After three days, orange crystals were formed and isolated (crude mixture yield: 557 mg). 100 mg of

the crude mixture adsorbed on celite (500 mg) were purified *via* flash chromatography (see instrumentation for operation conditions). The purity of the fractions was established by RP-HPLC. The fractions composed exclusively of the asymmetric Anthracene-TRIS/TRIS Mn-Anderson cluster (retention time 10.4 min) were combined and a large excess of TBA bromide (500 mg; 1.55 mmol) was added to the resulting solution. MeCN was evaporated under vacuum leading to the formation of an orange precipitate in the remaining aqueous solution. This precipitate was isolated by centrifugation and then dissolved in MeCN. The solution was centrifuged to remove any insoluble material and set up for crystallisation with Et_2O diffusion. Within 3 days crystals of compound **17** were formed, dried and analysed. Single crystals suitable for X-ray diffraction were grown from DMF by slow Et_2O diffusion (needle crystal, 3 days). **Yield:** 167 mg, 0.08 mmol, 17 % based on Mo (estimated from the purification of 100 mg of the crude material); **Elemental analysis:** Calc. for $C_{71}H_{132}MnMo_6N_5O_{25}$ (2086.35 g/mol): C, 40.87; H, 6.38; N, 3.36; Found: C, 40.72; H, 6.30; N, 3.34; **^{1}H NMR (DMSO-d$_6$, 400 MHz):** δ = 66.0 - 60.0 (s, br, 6CH$_2$), 8.68 (s, 1H, CH), 8.63 (s, 1H, CH), 8.54 (s, 1H, CH), 8.15 (m, 3H, 3CH), 7.84 (m, 2H, CH + NH), 7.56 (m, 2H, 2CH), 3.17 (m, 24H, CH$_2$ from TBA$^+$), 1.58 (m, 24H, CH$_2$ from TBA$^+$), 1.32 (m, 24H, CH$_2$ from TBA$^+$), 0.95 ppm (m, 36H, CH$_3$ from TBA$^+$); **^{13}C DEPTQ NMR (DMSO-d$_6$, 100 MHz):** δ = 132.1 (C), 131.8 (C), 131.3 (C), 129.7 (C), 129.0 (CH), 128.7 (C), 128.3 (CH), 128.1 (CH), 128.0 (CH), 127.9 (CH), 127.5 (CH), 126.2 (CH), 125.7 (CH), 124.5 (CH), 57.5 (CH$_2$), 23.1 (CH$_2$), 19.2 (CH$_2$),13.5 ppm (CH$_3$); **ESI-MS**: peak envelopes observed at *m/z* 1602.71 (z = -1) and 1843.98 (z = -1) were assigned as $[(C_{16}H_{36}N)_1H[MnMo_6O_{24}(C_4H_8N)(C_{19}H_{16}NO)]]^{1-}$ (predicted: 1602.73) and $[(C_{16}H_{36}N)_2[MnMo_6O_{24}(C_4H_8N)(C_{19}H_{16}NO)]]^{1-}$ (predicted: 1844.01), respectively.
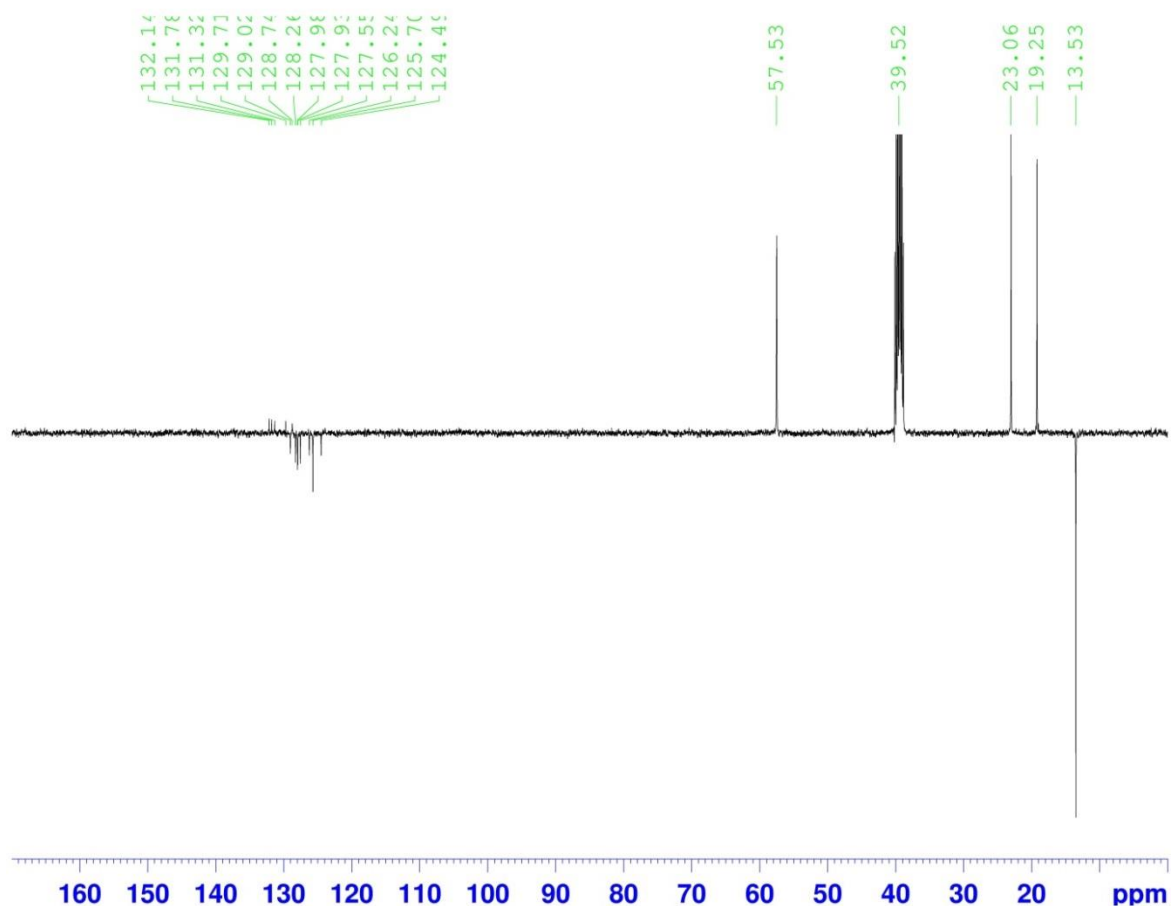
Figure 133: ^{13}C DEPTQ NMR of the Anthracene-TRIS/TRIS Mn-Anderson (**17**) in DMSO-d$_6$ at 100 MHz.

5.4.5.2 Compound 18: (TBA)$_3$[MnMo$_6$O$_{24}$(C$_{20}$H$_{38}$NO)(C$_8$H$_{12}$NO$_3$)]
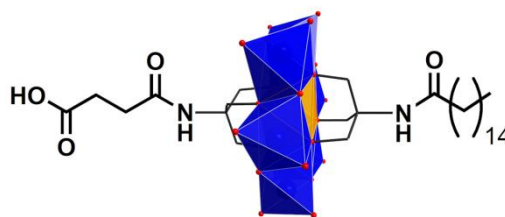
Succinic anhydride (72 mg, 0.64 mmol, 4 equiv.) and palmitic anhydride (180 mg, 0.32 mmol, 2 equiv.) were added to a solution of TRIS Mn-Anderson starting material (300 mg, 0.16 mmol) in DMF (5 mL) and left to react overnight at 50 °C. The bright orange solution was then cooled to room temperature and, without any purification, celite (1.5 g) was added and the solvent evaporated under vacuum to obtain a powder ('dry loading'). The crude material adsorbed on celite was purified by flash chromatography. The pure fractions (purity checked by RP-HPLC, retention time of interest: 12.85 min) were combined and a large excess of TBA bromide (0.5 g, 1.55 mmol) was added to the resulting light orange solution. The MeCN was evaporated under vacuum leading to the formation of an orange precipitate in the remaining aqueous solution. This precipitate was isolated by

centrifugation and then dissolved in MeCN. The solution was centrifuged to remove any insoluble material and left undisturbed for crystallisation with Et$_2$O diffusion. Within 3 days, crystals of compound **18** were formed, dried and analysed. **Yield**: 95 mg, 0.043 mmol, 27 %; **Elemental analysis:** Calc. for C$_{76}$H$_{158}$MnMo$_6$N$_5$O$_{28}$ (2220.66 g/mol): C, 41.11; H, 7.17; N, 3.15; Found: C, 41.09; H, 7.26; N, 3.26; **^{1}H NMR (DMSO-d$_6$, 400 MHz):** δ = 66.00 - 62.00 ppm (s, br, 6 CH$_2$), 11.20 (s, br, 1H, OH), 7.90 (s, br, 1H, NH), 7.32 (s, br, 1H, NH), 3.17 (m, 24H, CH$_2$ from TBA$^+$), 2.66 (s, br, 2H, CH$_2$), 2.45 - 2.24 (m, 4H, 2 CH$_2$), 1.70 - 1.15 (m, 74H, 13 CH$_2$ + 2 x CH$_2$ from TBA$^+$),0.94 (m, 36H, CH$_3$ from TBA$^+$), 0.85 ppm (m, 3H, CH$_3$); **^{13}C DEPTQ NMR (DMSO-d$_6$, 100 MHz):** δ = 57.5 (CH$_2$), 33.7 (CH$_2$), 31.2 (CH$_2$), 29.1 (CH$_2$), 29.0 (CH$_2$), 28.9 (CH$_2$), 28.8 (CH$_2$), 28.7 (CH$_2$), 26.3 (CH$_2$), 23.1 (CH$_2$), 22.0 (CH$_2$), 19.2 (CH$_2$), 13.9 (CH$_3$),13.5 ppm (CH$_3$); **ESI-MS**: peak envelopes observed at *m/z* 1978.19 (z = -1), 2098.83 (z = -2) and 2220.46 (z = -1) were assigned as [(C$_{16}$H$_{36}$N)$_2$[MnMo$_6$O$_{24}$(C$_{20}$H$_{38}$NO)(C$_8$H$_{12}$NO$_3$)]]$^{1-}$ (predicted: 1978.20), [(C$_{16}$H$_{36}$N)$_5$[MnMo$_6$O$_{24}$(C$_{20}$H$_{38}$NO)(C$_8$H$_{12}$NO$_3$)][MnMo$_6$O$_{24}$(C$_{20}$H$_{38}$NO)(C$_8$H$_{11}$NO$_3$)]]$^{2-}$ (predicted: 2098.84) and [(C$_{16}$H$_{36}$N)$_2$[MnMo$_6$O$_{24}$(C$_{20}$H$_{38}$NO)(C$_8$H$_{11}$NO$_3$)]]$^{1-}$ (predicted: 2220.48), respectively.
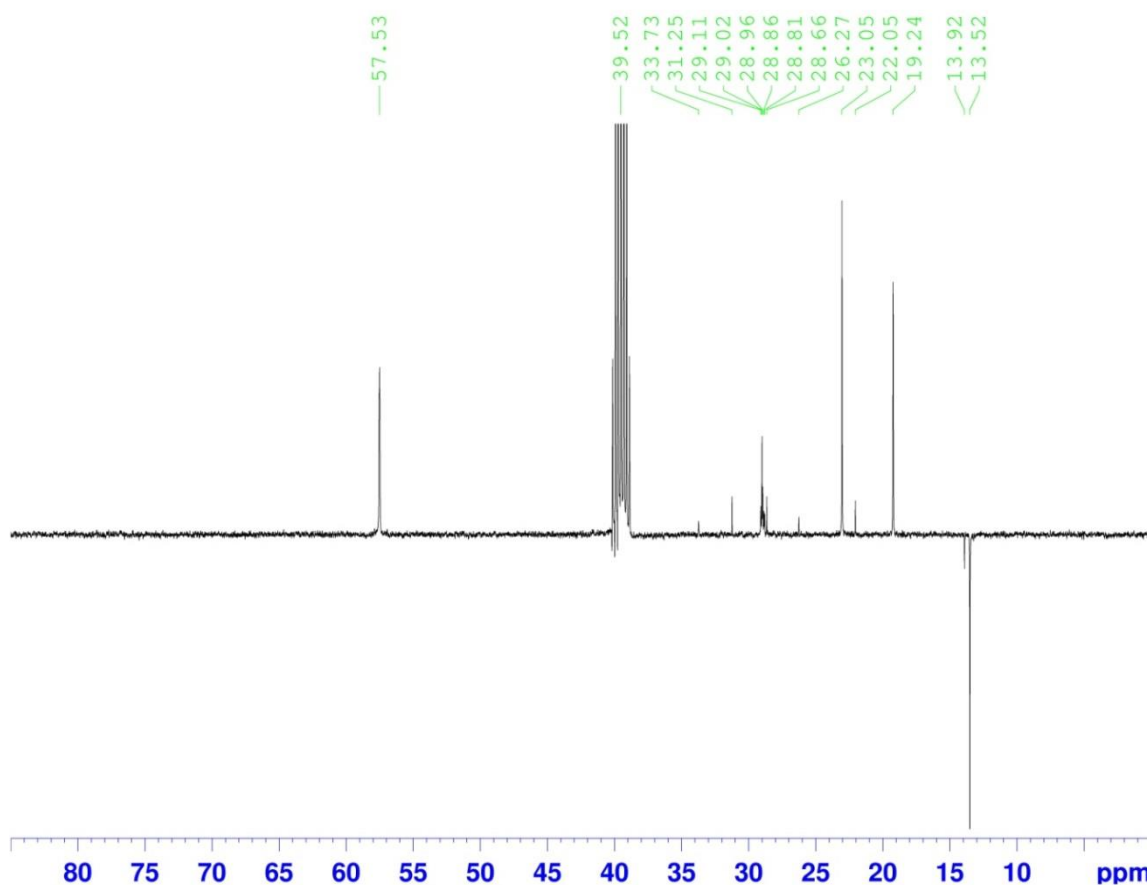
Figure 134: ^{13}C DEPTQ NMR of the Palmitic-TRIS/Succinic-Acid-TRIS Mn-Anderson (**18**) in DMSO-d$_6$ at 100 MHz

5.4.5.3 Compound 19: (TBA)$_3$[MnMo$_6$O$_{24}$(C$_{20}$H$_{38}$NO)(C$_4$H$_8$N)]
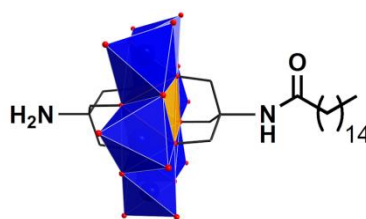
Synthesis of compound **19** was adapted from a reported synthesis.[107]

Palmitoyl chloride (63 μL, 0.21 mmol, 1.3 equiv.) was slowly added to a solution of TRIS Mn-Anderson starting material (300 mg, 0.16 mmol) and triethylamine (90 μL; 0.64 mmol) in dry MeCN (5 mL) and the resulting solution refluxed overnight. The bright orange solution was then cooled to room temperature and, without any purification, celite (1.5 g) was added and the solvent evaporated under vacuum to obtain a powder ('dry loading'). The crude material adsorbed on celite was purified by flash chromatography (see instrumentation for further details). The pure fractions (purity checked by RP-HPLC, retention time of interest: 12.84 min) were combined and a large excess of TBA bromide (0.5 g; 1.55 mmol) was added to the resulting solution. The MeCN was evaporated under vacuum leading to the formation of an orange precipitate. This precipitate was isolated from the remaining acetate buffer solution by centrifugation and then dissolved in MeCN. The resulting orange solution was centrifuged to remove any insoluble material and left for crystallisation with Et$_2$O diffusion. Within 3 days crystal of compound **19** were formed, dried and analysed. **Yield:** 100 mg, 0.05 mmol, 32 %; **Elemental analysis:** Calc. for C$_{72}$H$_{154}$MnMo$_6$N$_5$O$_{25}$ (2120.59 g/mol): C, 40.78; H, 7.32; N, 3.30; Found: C, 40.61; H, 7.40; N, 3.37; **^{1}H NMR (DMSO-d$_6$, 400 MHz):** δ = 66.0 - 61.0 (s, br, 6CH$_2$), 7.80 - 7.00 (s, br, 1H, NH), 3.80 - 3.45 (s, br, 2H, NH$_2$), 3.16 (m, 24H, CH$_2$ from TBA$^+$), 2.36 (m, 2H, CH$_2$), 1.70 - 1.15 (m, 74H, 13 CH$_2$ + 2 x CH$_2$ from TBA$^+$), 0.93 (m, 36H, CH$_3$ from TBA$^+$), 0.85 ppm (m, 3H, CH$_3$); **^{13}C DEPTQ NMR (DMSO-d$_6$, 100 MHz):** δ = 13.6 (CH$_3$), 14.0 (CH$_3$), 19.3 (CH$_2$), 22.1 (CH$_2$), 23.1 (CH$_2$), 26.3 (CH$_2$), 28.7 (CH$_2$), 28.9 (CH$_2$), 29.0 (CH$_2$), 29.1 (CH$_2$), 29.2 (CH$_2$), 31.3 (CH$_2$), 57.5 (CH$_2$); **ESI-MS:** peak envelopes observed at *m/z* 1635.90 (z = -1) and 1878.18 (z = -1) were assigned as [(C$_{16}$H$_{36}$N)H[MnMo$_6$O$_{24}$(C$_{20}$H$_{38}$NO)(C$_4$H$_8$N)]]$^{1-}$(predicted: 1636.90) and [(C$_{16}$H$_{36}$N)$_2$ [MnMo$_6$O$_{24}$(C$_{20}$H$_{38}$NO)(C$_4$H$_8$N)]]$^{1-}$ (predicted: 1878.18), respectively.
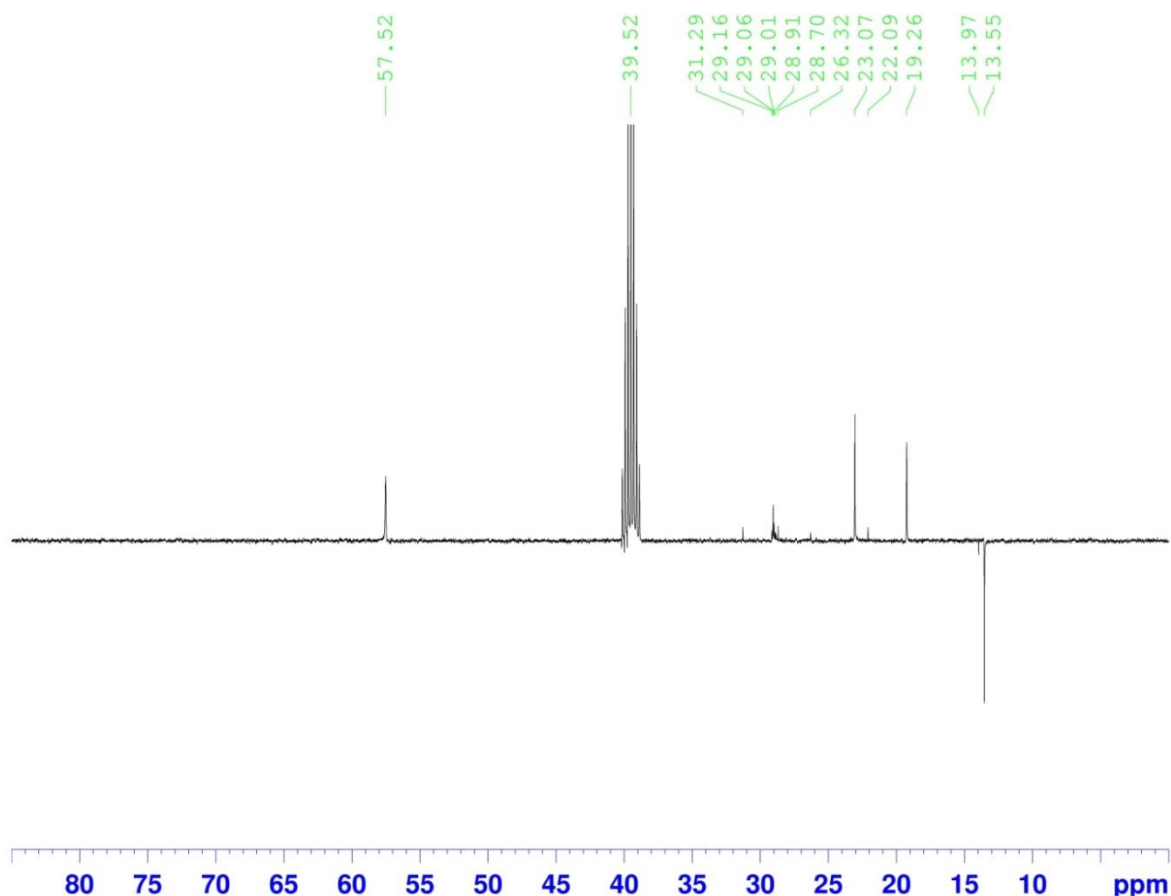
Figure 135: ^{13}C DEPTQ NMR of the Palmitic-TRIS/ TRIS Mn-Anderson (**19**) in DMSO-d$_6$ at 100 MHz

5.4.5.4 Compound 20: (TBA)$_3$[MnMo$_6$O$_{24}$(C$_{19}$H$_{18}$NO$_2$)(C$_4$H$_8$N)]

A mixture of (TBA)$_4$[α-Mo$_8$O$_{26}$] (1.53 g, 0.71 mmol), Mn(OAc)$_3$·2H$_2$O (0.44 g, 1.62 mmol), TRIS (0.28 g, 1.87 mmol) and Fmoc-TRIS[242] ((HOCH$_2$)$_3$CNH-Fmoc, 0.64 g, 1.87 mmol) was refluxed in MeCN (45 mL) for 18 h. The resulting brown mixture was cooled down to room temperature and the precipitate removed by centrifugation to lead to a bright orange solution. The crude mixture was isolated by crystallisation by Et$_2$O diffusion. After three days, orange crystals were formed and isolated (crude mixture yield: 1.40 g). 300 mg of the crude mixture adsorbed on celite (1.5 g) were purified *via* flash chromatography. The purity of the fractions was established by RP-HPLC. The fractions composed exclusively of the asymmetric Fmoc-TRIS/TRIS Mn-Anderson cluster (retention time 10.26 min) were combined and a large excess of TBA bromide (0.5 g, 1.55 mmol) was added to the resulting solution. MeCN was evaporated under vacuum leading

to the formation of an orange precipitate in the remaining aqueous solution. This precipitate was isolated by centrifugation and then dissolved in MeCN. The solution was centrifuged to remove any insoluble material and set up for crystallisation with Et_2O diffusion. Within 3 days crystals of compound **20** were formed, dried and analysed. Single crystals suitable for X-ray diffraction were grown from DMF by slow Et_2O diffusion (cubic crystal, 3 days). **Yield:** 588 mg, 0.28 mmol, 30 % based on Mo (estimated from the purification of 300 mg of the crude material; equivalent to a 60 % recovery of the asymmetric product); **Elemental analysis:** Calc. for $C_{71}H_{134}MnMo_6N_5O_{26}$ (2104.42 g/mol): C, 40.52; H, 6.42; N, 3.33; Found: C, 40.52; H, 6.45; N, 3.41; **^{1}H NMR (DMSO-d_6, 400 MHz):** δ = 65.00 - 60.00 (s, br, 6 CH_2), 7.88 (d, 2H, 2 CH, J = 7.4 Hz), 7.75 (m, 2H, 2 CH), 7.67 - 7.25 (m, 5H, 4 CH + NH), 4.23 (m, 3H, CH_2 + CH), 3.55 (s, br, 2H, NH_2), 3.16 (m, 24H, CH_2 from TBA$^+$), 1.56 (m, 24H, CH_2 from TBA$^+$), 1.31 (m, 24H, CH_2 from TBA$^+$), 0.93 ppm (m, 36H, CH_3 from TBA$^+$); **^{13}C DEPTQ NMR (DMSO-d_6, 100 MHz):** δ = 143.8 (C), 140.6 (C), 127.6 (CH), 127.1 (CH), 125.6 (CH), 120.0 (CH), 65.7 (CH_2), 57.5 (CH_2), 46.7 (CH), 23.0 (CH_2), 19.2 (CH_2), 13.5 ppm (CH_3); **ESI-MS:** peak envelopes observed at m/z 1620.73 (z = -1) and 1862.02 (z = -1) were assigned to $[(C_{16}H_{36}N)H \quad [MnMo_6O_{24}(C_{19}H_{18}NO_2)(C_4H_8N)]]^{1-}$ (predicted: 1620.74) and $[(C_{16}H_{36}N)_2[MnMo_6O_{24}-(C_{19}H_{18}NO_2)(C_4H_8N)]]^{1-}$ (predicted: 1862.02), respectively.
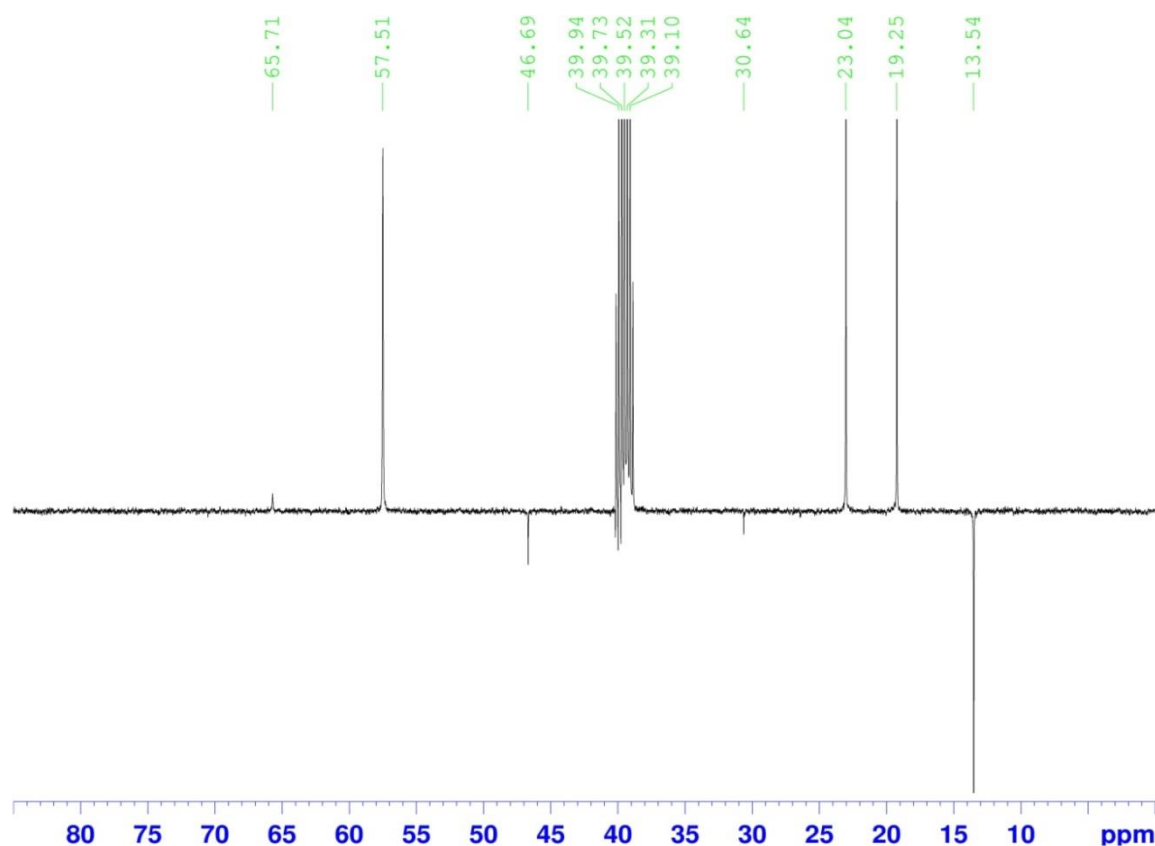
Figure 136: ^{13}C DEPTQ NMR of the Fmoc-TRIS/TRIS Mn-Anderson (**20**) in DMSO-d_6 at 100 MHz

5.4.5.5 Compound 21: (TBA)$_3$[MnMo$_6$O$_{24}$(C$_7$H$_{12}$NO)(C$_4$H$_8$N)]
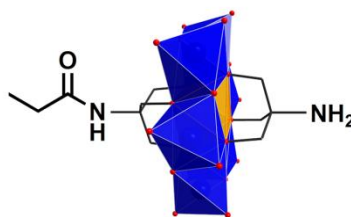
Compound **20** (50 mg, 0.03 mmol) and propionic anhydride (33 mg, 0.25 mmol, 10 equiv.) were dissolved in DMF (1 mL) and heated overnight at 50 °C. The intermediate product was isolated from the bright orange solution by crystallisation with slow Et$_2$O diffusion. A small sample of the product was analysed by ESI-MS to check the presence of the intermediate product and the absence of the POM starting material (Fig. S37). The crude material was then treated for 5 h at room temperature with a 20% piperidine solution by volume in DMF (1 mL). Solvent was evaporated under vacuum and the resulting orange powder washed twice with Et$_2$O. The orange product was dissolved in MeCN and diffusion of Et$_2$O into the MeCN solution resulted in the formation of crystals of pure compound **21** within 4 days. **21** was isolated, dried and analysed. Crystals suitable for X-ray diffraction were grown from DMF with slow Et$_2$O diffusion. **Yield**: 43 mg, 0.02 mmol, 88 %; **Elemental analysis:** Calc. for C$_{59}$H$_{128}$MnMo$_6$N$_5$O$_{25}$ (1938.24 g/mol): C, 36.56; H, 6.66; N, 3.61; Found: C, 36.41; H, 6.69; N, 3.66; **^{1}H NMR (DMSO-d$_6$, 400 MHz):** δ = 65.00 - 60.00 (s, br, 12H, 6 CH$_2$), 7.37 (s, br, 1H, NH), 3.53 (s, br, 2H, NH$_2$), 3.16 (m, 24H, CH$_2$ from TBA$^+$), 2.40 (m, 2H, CH$_2$), 1.57 (m, 24H, CH$_2$ from TBA$^+$),1.31 (m, 24H, CH$_2$ from TBA$^+$), 0.94 ppm (m, 39H, CH$_3$ + CH$_3$ from TBA$^+$); **^{13}C DEPTQ NMR (DMSO-d$_6$, 100 MHz):** δ = 57.5 (CH$_2$), 27.0 (CH$_2$), 23.1 (CH$_2$), 19.2 (CH$_2$), 13.5 (CH$_3$), 10.9 ppm (CH$_3$); **ESI-MS:** peak envelopes observed at *m/z* 1453.44 (z = -1), 1586.05 (z = -2) and 1695.68 (z = -1) were assigned as [(C$_{16}$H$_{36}$N)H[MnMo$_6$O$_{24}$(C$_7$H$_{12}$NO)(C$_4$H$_8$N)]]$^{1-}$ (predicted: 1453.70), [(C$_{16}$H$_{36}$N)$_3$Na[MnMo$_6$O$_{24}$(C$_7$H$_{12}$NO)(C$_4$H$_8$N)]$_2$]$^{2-}$ (predicted: 1586.33) and [(C$_{16}$H$_{36}$N)$_2$[MnMo$_6$O$_{24}$(C$_7$H$_{12}$NO)(C$_4$H$_8$N)]]$^{1-}$ (predicted: 1695.98), respectively.
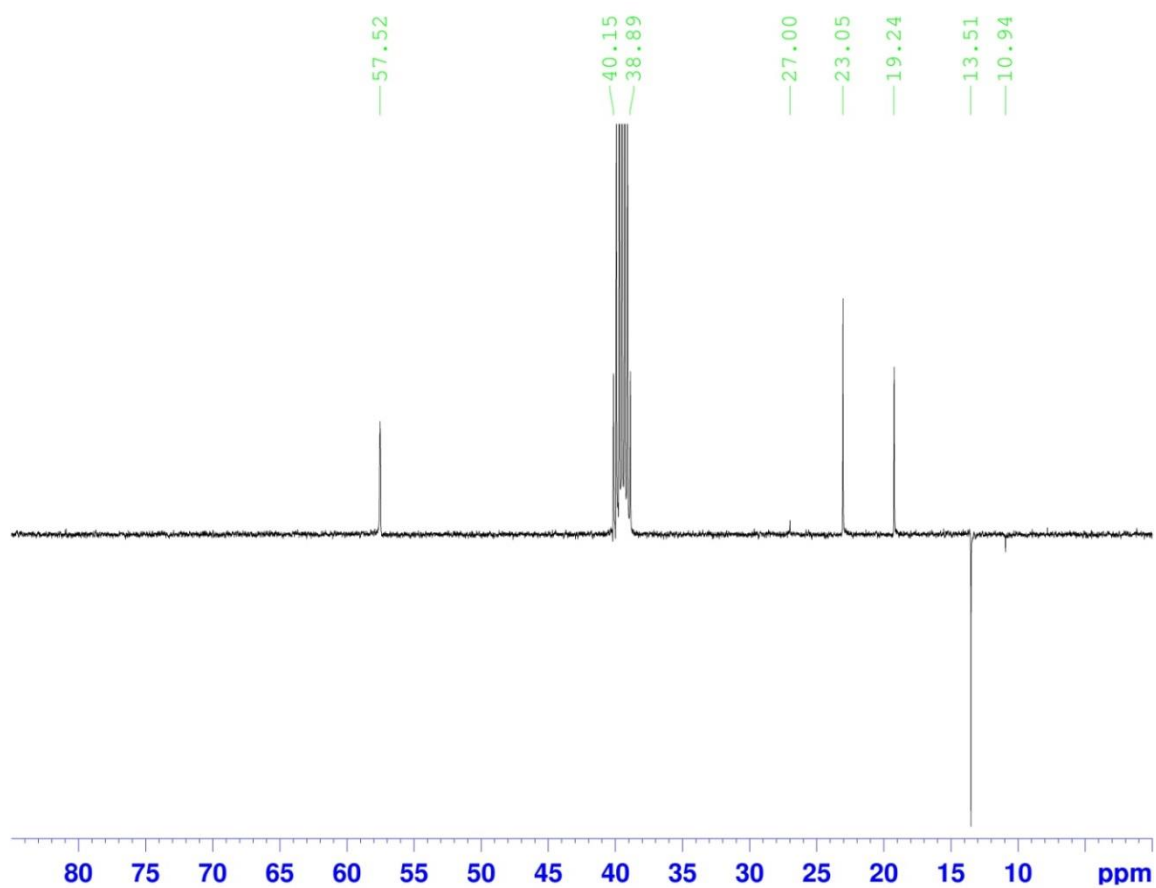
Figure 137: ^{13}C DEPTQ NMR of the propylamide-TRIS/TRIS Mn-Anderson (**21**) in DMSO-d$_6$ at 100 MHz

5.4.6 Synthesis and use of the amino acid hybrid Mn-Anderson building block

5.4.6.1 Compound 22: (TBA)$_3$[MnMo$_6$O$_{24}$(C$_{12}$H$_{15}$N$_2$O$_5$)(C$_{19}$H$_{18}$NO$_2$)]
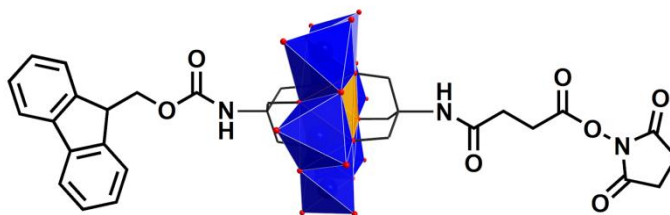
Fmoc-TRIS/TRIS Mn-Anderson compound (**20**, 545 mg, 0.26 mmol) was reacted overnight with 20 equiv. of succinic anhydride (518 mg, 5.18 mmol) in DMF (5 mL) at 50 °C. The resulting bright orange solution was cooled to room temperature and the intermediate product isolated by crystallisation with Et$_2$O at room temperature. The resulting orange crystals were isolated, washed with Et$_2$O, dried and subsequently treated with NHS (120 mg, 1.04 mmol, 4 equiv.) and DCC (322 mg, 1.56 mmol, 6 equiv.) in DMF (5 mL) at room temperature. As the reaction occurs a white precipitate of DCU appears and the mixture was stirred overnight. The white precipitate of DCU was then removed by centrifugation and the bright orange solution was exposed to Et$_2$O vapour for several days. **Yield:** 520 mg, 0.23 mmol, 88 %; **Elemental analysis:** Calc. for C$_{79}$H$_{141}$MnMo$_6$N$_6$O$_{31}$ (2301.56 g/mol): C, 41.23; H, 6.17; N, 3.65; Found: C, 40.70; H, 6.21; N, 3.84; **^{1}H NMR (DMSO-d$_6$, 400 MHz)**: δ = 67.0 - 62.0 (s, br, 12H, CH$_2$), 7.88 (m, 2H, 2 CH), 7.75 (m, 2H, 2 CH), 7.45 - 7.25 (m, 4H, 4 CH),4.23 (s, br, 3H, CH$_2$ + CH), 3.16 (m, 24H, CH$_2$ from TBA$^+$), 2.90 - 2.70 (m, br, 8H, CH$_2$), 1.57 (m, 24H, CH$_2$ from TBA$^+$), 1.30 (m, 24H, CH$_2$ from TBA$^+$), 0.93 ppm (m, 36H, CH$_3$ from TBA$^+$); **^{13}C DEPTQ NMR (DMSO-d$_6$, 100 MHz)**: δ = 170.1 (CO), 143.9 (C), 140.6 (C), 127.6 (CH), 127.2 (CH), 125.7 (CH), 120.0 (CH), 57.5 (CH$_2$), 46.7 (CH), 25.4 (CH$_2$), 29.1 (CH$_2$), 19.2 (CH$_2$), 13.5 ppm (CH$_3$); **ESI-MS**: peak envelopes observed at *m/z* 1291.61 (z = -3) and 2059.05 (z = -1) were assigned as [(C$_{16}$H$_{36}$N)$_3$[MnMo$_6$O$_{24}$(C$_{12}$H$_{15}$N$_2$O$_5$)(C$_{19}$H$_{18}$NO$_2$)]$_2$]$^{3-}$ (predicted: 1291.94) and [(C$_{16}$H$_{36}$N)$_2$[MnMo$_6$O$_{24}$(C$_{12}$H$_{15}$N$_2$O$_5$)(C$_{19}$H$_{18}$NO$_2$)]]$^{1-}$ (predicted: 2059.05), respectively.
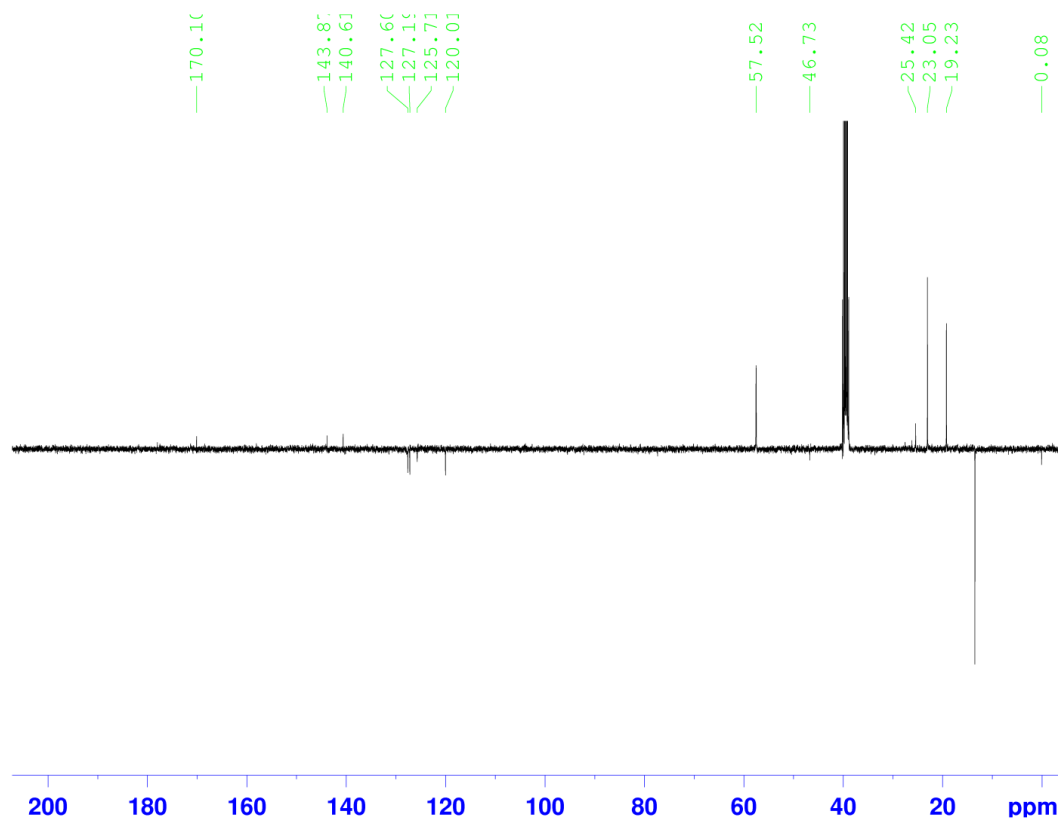
Figure 138: ^{13}C DEPTQ NMR of **22** in DMSO-d$_6$ (contains 0.03 % (v/v) TMS) at 100 MHz.

5.4.6.2 Compound 23: (TBA)$_{1.4}$H$_{1.6}$[MnMo$_6$O$_{24}$(C$_{25}$H$_{42}$N$_5$O$_7$)(C$_{15}$H$_{28}$N$_3$O$_2$)] · 0.7DMF*
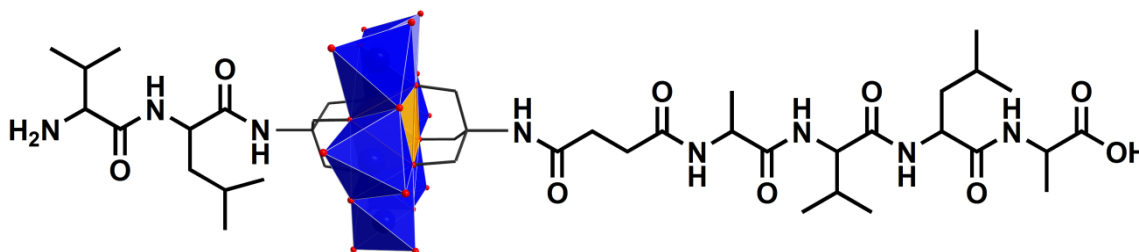
*Formula established from TGA analysis and elemental analysis results.

The synthesis of **23** can be divided into three parts: peptide synthesis before addition of the Mn-Anderson amino acid, addition of the Mn-Anderson amino acid and peptide synthesis after addition of the Mn-Anderson amino acid.

Resin preparation:

1. 150 mg (0.027 mmol, 1 equiv.) of Tentagel® S Trt-Ala-Fmoc resin (0.18 mmol/g) was weighed into a plastic syringe with a frit column plate.

2. 1.0 mL of DCM were added to the dried resin, the mixture was stirred gently for 1 min, and left for resin swelling for 15 min. Solvent was then removed by vacuum filtration.

3. 1.0 mL of DMF were added to the swelled resin, the mixture was stirred gently for 1 min and the solvent removed by vacuum filtration.

Part 1: peptide synthesis before addition of the Mn-Anderson amino acid (**Hyb**)

Deprotection/coupling cycle:

4. <u>Fmoc removal step:</u> 1.0 mL of 20% piperidine/DMF (vol/vol) was added, the mixture was stirred gently for 1 min and the solution was removed by vacuum filtration. 1.0 mL of the same solution was added again, the mixture was stirred gently for 1 min, left to react for 10 min and the solution was removed by vacuum filtration.

5. <u>Washing step:</u> 1.0 mL of DMF was added, the mixture was stirred for 30 s, the solvent was then removed by vacuum filtration. This step was repeated 6 times.

6. <u>Addition step:</u> a DMF (1 mL) solution of Fmoc-Leu-OH (48 mg, 0.135 mmol, 5 equiv.) with DIC (25 μL, 0.16 mmol, 6 equiv.) was added (mixture made 15 min before addition), the resulting mixture was stirred gently for 1 min and left to react for 30 min. The solution was then removed by vacuum filtration and the addition step was repeated once.

7. <u>Washing step:</u> 1.0 mL of DMF was added, the mixture was stirred for 30 s, and the solvent was then removed by vacuum filtration. This step was repeated 6 times.

8. The deprotection/coupling cycle was repeated for each subsequent amino acid (*i.e.* Fmoc-Val-OH (46 mg, 0.135 mmol, 5 equiv.) and Fmoc-Ala-OH (42 mg, 0.135 mmol, 5 equiv.))

Part 2: Addition of the Mn-Anderson amino acid (**Hyb**)

1. <u>Fmoc removal step:</u> 1.0 mL of 20% piperidine/DMF (vol/vol) was added, the mixture was stirred gently for 1 min and the solution was removed by vacuum filtration. 1.0 mL of the same solution was added again, stirred gently for 1 min, left to react for 10 min and then removed by vacuum filtration.

2. <u>Washing step:</u> 1.0 mL of DMF was added, the mixture was stirred for 30 s, and the solvent was then removed by vacuum filtration. This step was repeated 6 times.

3. <u>Addition step:</u> a DMF (1 mL) solution of **22** (0.081 mmol, 186 mg, 3 equiv.) and DIPEA (180 μL, 1.03 mmol) were added, the resulting mixture was stirred gently

for 1 min and left to react for 1 h. The solution was then removed by vacuum filtration and the addition step was repeated once but this time the reaction was left overnight.

4. <u>Washing step:</u> 1.0 mL of DMF was added, the mixture was stirred for 30 s, and the solvent was then removed by vacuum filtration. This step was repeated 6 times.

Part 3: peptide synthesis after addition of the Mn-Anderson amino acid (**Hyb**).

Deprotection/coupling cycle:

1. <u>Fmoc removal step:</u> 1.0 mL of 20% piperidine/DMF (vol/vol) was added, stirred gently for 1 min and removed by vacuum filtration. 1.0 mL of the same solution was added again, stirred gently for 1 min, left to react for 10 min and removed by vacuum filtration.

2. <u>Washing step:</u> 1.0 mL of DMF was added, the mixture was stirred for 30 s, and the solvent was then removed by vacuum filtration. This step was repeated 6 times.

3. <u>Addition step:</u> a DMF (1 mL) solution of Fmoc-Leu-OH (286 mg, 0.81 mmol, 30 equiv.) with DIC (125 μL, 0.81 mmol, 30 equiv.) (mixture made 15 min before addition) was added, the resulting mixture was stirred gently for 1 min and left to react for 3h. The solution was then removed by vacuum filtration and the addition step was repeated once.

4. <u>Washing step:</u> 1.0 mL of DMF was added, the mixture was stirred for 30 s, and the solvent was then removed by vacuum filtration. This step was repeated 6 times.

5. The deprotection/coupling cycle was repeated for the subsequent amino acid (*i.e.* Fmoc-Val-OH (275 mg, 0.81 mmol, 30 equiv.))

Cleavage/Product isolation:

1. <u>Washing step:</u> 1.0 mL of DCM was added, the mixture was stirred for 30 s, the solvent was then removed by vacuum filtration. This step was repeated 3 times.

2. 2.5 mL of 20% HFIP/DCM (vol/vol) was added, the mixture was stirred for 2 min, left to react for 10 min and the solution was collected by vacuum filtration.

3. 1.0 mL of DCM was added, the mixture was stirred for 30 s, and the solution was then collected by vacuum filtration.

4. <u>IMPORTANT washing step:</u> 1.0 mL of DMF was added, the mixture was stirred for 30 s, and the solution was then collected by vacuum filtration. This step was repeated once.

[This step is particularly important since the peptide product is only partially soluble in DCM. For other peptides different solvent might need to be considered depending on solubility.]

5. The solutions collected were combined and the solvent evaporated under reduced pressure.

6. The resulting orange product was cleaned with cold Et_2O (about 10 mL) and dried.

Analyses:

Yield: 42 mg, 0.019 mmol, 70 %; **Elemental analysis:** Calc. for for $C_{64.5}H_{126.9}MnMo_6N_{10.1}O_{33.7}$ (2213.82 g/mol): C, 34.99; H, 5.78; N, 6.39; Found: C, 34.95; H, 5.77; N, 6.39; **ESI-MS**: peak envelopes observed at *m/z* 911.33 (z = -2) and 2065.91 (z = -1) were assigned as $[H[MnMo_6O_{24}(C_{25}H_{42}N_5O_7)(C_{15}H_{28}N_3O_2)]]^{2-}$ (predicted: 911.39) and $[(C_{16}H_{36}N)H[MnMo_6O_{24}(C_{25}H_{42}N_5O_7)(C_{15}H_{28}N_3O_2)]]^{1-}$ (predicted: 2066.07), respectively; **TGA**: The loss of 2.51% corresponds to the loss of solvent $((DMF)_{0.7};$ calculated loss: 2.3%). The weight loss starting at 100°C of 66.38% corresponds to the loss of the organic cations and the ligands (theoretically 56.2%). At about 650°C the metal oxide cluster starts decomposing.
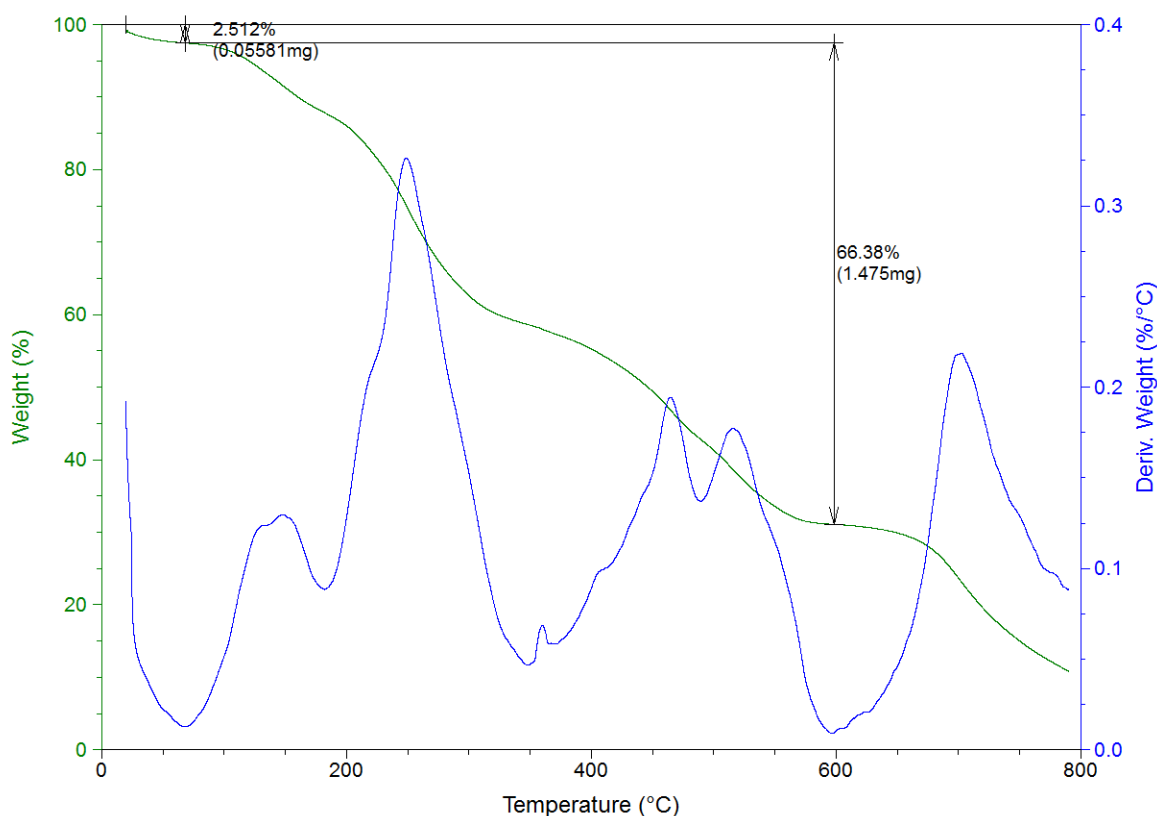
Figure 139: TGA analysis of compound **23**.

5.4.7 Control compound for the chromatography methodology: $(TBA)_3[MnMo_6O_{24}(C_{19}H_{16}NO)_2]$:
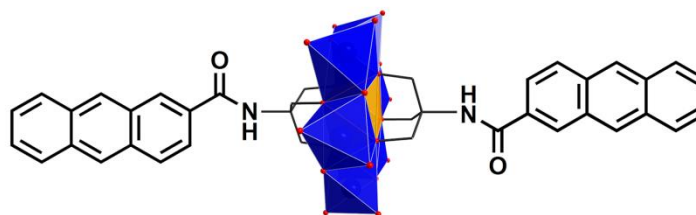
A mixture of $(TBA)_4[\alpha\text{-}Mo_8O_{26}]$ (400 mg, 0.19 mmol), $Mn(OAc)_3 \cdot 2H_2O$ (74 mg, 0.28 mmol) and Anthracene-TRIS ligand (213 mg; 0.66 mmol) was refluxed in MeCN (20 mL) for 16 h. The resulting brown mixture was cooled down to room temperature and the precipitate removed by centrifugation to lead to a bright orange solution. The crude mixture was isolated by crystallisation by Et_2O diffusion. After three days, orange crystals were formed, isolated and analysed. Single crystals suitable for X-ray diffraction were grown from MeCN by slow Et_2O diffusion (square crystal, 3 days). **Yield:** 200 mg, 0.09 mmol, 36 % based on Mo; **Elemental analysis:** Calc. for $C_{86}H_{140}MnMo_6N_5O_{26} \cdot CH_3CN$ (2331.68 g/mol): C, 45.33; H, 6.18; N, 3.60; Found: C, 45.22; H, 6.17; N, 3.81; **^{1}H NMR (DMSO-d_6, 400 MHz):** δ = 67.0 - 62.0 (s, br, $6CH_2$), 8.68 (s, 2H, 2CH), 8.63 (s, 2H, 2CH), 8.55 (s, 2H, 2CH), 8.12 (m, 6H, 6CH), 7.84 (m, 4H, 2CH + 2NH), 7.56 (m, 4H, 4CH), 3.15 (m, 24H, CH_2 from TBA^+), 1.56 (m, 24H, CH_2 from TBA^+), 1.30 (m, 24H, CH_2 from TBA^+), 0.93 ppm (m, 36H, CH_3 from TBA^+); **^{13}C DEPTQ NMR (DMSO-d_6, 100 MHz):** δ = 167.9 (CO), 132.2 (C), 131.8 (C), 131.3 (C), 129.7 (C), 129.1 (CH), 128.7 (C), 128.3 (CH), 128.0 (CH), 127.9 (CH), 127.6 (CH), 126.3 (CH), 125.7 (CH), 124.5 (CH), 57.5 (CH_2), 23.1 (CH_2), 19.3 (CH_2), 13.5 ppm (CH_3); **ESI-MS**: peak envelopes observed at m/z 1805.75 (z = -1) and 2048.04 (z = -1) were assigned as $[(C_{16}H_{36}N)_1H[MnMo_6O_{24}(C_{19}H_{16}NO)_2]]^{1-}$ (predicted: 1806.79) and $[(C_{16}H_{36}N)_2[MnMo_6O_{24}(C_{19}H_{16}NO)_2]]^{1-}$ (predicted: 2048.07), respectively.

5.5   Test reactions for the elaboration of the SPPS protocol

5.5.1   Cleavage conditions - stability to HFIP (Test A)

A sample of TRIS Mn-Anderson compound was analysed by ESI-MS in MeCN before and after treatment with the solution mix.

For the analysis after treatment 25 mg of compound were stirred for 1 h in 1 mL of a solution of 20 % HFIP in DCM (vol/vol). The solvent was then evaporated and the resulting orange powder dissolved in MeCN for ESI-MS analysis. **ESI-MS:** peak envelopes observed at m/z 689.91 (z = -1), 706.67 (z = -1), 1397.58 (z = -1) and 1639.85 (z = -1) were assigned as $[(C_{16}H_{36}N)[Mo_3O_{10}]]^{1-}$ (predicted: 689.95), $[(C_{16}H_{36}N)_2 [Mo_3O_{14}(C_4H_8N)]]^{1-}$ (predicted: 706.71), $[(C_{16}H_{36}N)H[MnMo_6O_{24}(C_4H_8N)_2]]^{1-}$ (predicted: 1397.67) and $[(C_{16}H_{36}N)_2[MnMo_6O_{24}(C_4H_8N)_2]]^{1-}$ (predicted: 1639.95), respectively.

5.5.2   Addition of the hybrid POM amino acid to a growing peptide chain

Tests B-**G** were realised on a commercial Tentagel® S Trt-Ala-Fmoc resin (0.18 mmol/g). The following steps were realised before the actual test reaction:

Resin preparation:

1. 25 mg (0.0045 mmol, 1 equiv.) of Tentagel® S Trt-Ala-Fmoc resin was weighed into a plastic syringe with a frit column plate.
2. 1.0 mL of DCM were added to the dried resin, the mixture was stirred gently for 1 min, and left for resin swelling for 15 min. Solvent was then removed by vacuum filtration.
3. 1.0 mL of DMF were added to the swelled resin, the mixture was stirred gently for 1 min and the solution removed by vacuum filtration.

Deprotection:

1. <u>Fmoc removal step:</u> 1.0 mL of 20% piperidine/DMF (vol/vol) was added, the mixture was stirred gently for 1 min and the solution removed by vacuum filtration. 1.0 mL of the same solution was added again, stirred gently for 1 min, left to react for 10 min and removed by vacuum filtration.
2. <u>Washing step:</u> 1.0 mL of DMF was added, the mixture was stirred for 30 s, the solvent was then removed by vacuum filtration. This step was repeated 6 times.

5.5.2.1 Test B

Coupling:

1. <u>Reaction:</u> a DMF (200 μL) solution of **22** (0.0135 mmol, 31 mg, 3 equiv.) and DIPEA (30 μL, 0.17 mmol) were added, the resulting mixture was stirred gently for 1 min and left to react for 1 h. The solvent was then removed by vacuum filtration.
2. <u>Washing step:</u> 1.0 mL of DMF was added, the mixture was stirred for 30 s, the solvent was then removed by vacuum filtration. This step was repeated 6 times.

Result: a pale yellow solid support was obtained.

5.5.2.2 Test C

Coupling:

1. <u>Reaction:</u> a DMF (200 μL) solution of **22** (0.0135 mmol, 31 mg, 3 equiv.) and DIPEA (30 μL, 0.17 mmol) were added, the resulting mixture was stirred gently for 1 min and left to react for 2 h. The solvent was then removed by vacuum filtration.
2. <u>Washing step:</u> 1.0 mL of DMF was added, the mixture was stirred for 30 s, the solvent was then removed by vacuum filtration. This step was repeated 6 times.

Result: a pale yellow solid support was obtained.

5.5.2.3 Test D

Solid support obtained at the end of **Test B** was used and a second coupling was carried out:

 Second coupling:

3. <u>Reaction:</u> a DMF (200 μL) solution of **22** (0.0135 mmol, 31 mg, 3 equiv.) and DIPEA (30 μL, 0.17 mmol) were added, the resulting mixture was stirred gently for 1 min and left to react for 16 h. The solvent was then removed by vacuum filtration.
4. <u>Washing step:</u> 1.0 mL of DMF was added, the mixture was stirred for 30 s, the solvent was then removed by vacuum filtration. This step was repeated 6 times.

Result: a bright orange solid support was obtained.

Cleavage/Product isolation:

1. Washing step: 1.0 mL of DCM was added, the mixture was stirred for 30 s, the solvent was then removed by vacuum filtration. This step was repeated 3 times.

2. 500 μL of 20% HFIP/DCM (vol/vol) was added, the mixture was stirred for 2 min, left to react for 10 min and the solution was collected by vacuum filtration.

3. 1.0 mL of DCM was added, the mixture was stirred for 30 s, and the solution was then collected by vacuum filtration.

4. The solutions collected were combined and the solvent evaporated under reduced pressure.

ESI-MS analysis: peak envelopes observed at m/z 1551.52 (z = -1), 1791.80 (z = -1) and 2033.08 (z = -1) were assigned as $[H_2[MnMo_6O_{24}(C_{19}H_{18}NO_2)(C_{11}H_{17}N_2O_4)]]^{1-}$ (predicted: 1550.52), $[(C_{16}H_{36}N)H[MnMo_6O_{24}(C_{19}H_{18}NO_2)(C_{11}H_{17}N_2O_4)]]^{1-}$ (predicted: 1791.80) and $[(C_{16}H_{36}N)_2[MnMo_6O_{24}(C_{19}H_{18}NO_2)(C_{11}H_{17}N_2O_4)]]^{1-}$ (predicted: 2033.08), respectively.

5.5.2.4 Test E

Coupling:

1. Reaction: a DMF (200 μL) solution of **22** (0.0135 mmol, 31 mg, 3 equiv.) and DIPEA (30 μL, 0.17 mmol) were added, the resulting mixture was stirred gently for 1 min and left to react for 16 h. The solvent was then removed by vacuum filtration.

2. Washing step: 1.0 mL of DMF was added, the mixture was stirred for 30 s, the solvent was then removed by vacuum filtration. This step was repeated 6 times.

Result: a pale yellow solid support was obtained.

5.5.2.5 Test F

Coupling:

1. Reaction: a DMF (200 μL) solution of **22** (0.0135 mmol, 31 mg, 3 equiv.) and DIPEA (30 μL, 0.17 mmol) were added, the resulting mixture was stirred gently for 1 min and left to react for 1 h. The solvent was then removed by vacuum filtration. A double coupling was carried out with an identical reagent mixture and was left to react for 7h. The solvent was then removed by vacuum filtration.

2. Washing step: 1.0 mL of DMF was added, the mixture was stirred for 30 s, the solvent was then removed by vacuum filtration. This step was repeated 6 times.

Result: a pale orange solid support was obtained.

5.5.2.6 Test G

Coupling:

1. Reaction: a DMF (200 μL) solution of the un-activated acid/Fmoc protected TRIS-based Mn-Anderson cluster ((TBA)$_3$[MnMo$_6$O$_{24}$(C$_8$H$_{12}$NO$_3$)(C$_{19}$H$_{18}$NO$_2$)]; 0.0135 mmol, 30 mg, 3 equiv.) with HBTU (0.018 mmol, 6.6 mg, 4 equiv.) and DIPEA (30 μL, 0.17 mmol) were added, the resulting mixture was stirred gently for 1 min and left to react for 1 h. The solvent was then removed by vacuum filtration. A double coupling was carried out with an identical reagent mixture and was left to react for 16 h. The solvent was then removed by vacuum filtration.
2. Washing step: 1.0 mL of DMF was added, the mixture was stirred for 30 s, the solvent was then removed by vacuum filtration. This step was repeated 6 times.

Result: a pale yellow solid support was obtained.

5.5.3 Addition of amino acids after the introduction of the hybrid POM amino acid

A Tentagel® S Trt-Ala resin coupled to one Mn-Anderson amino acid synthesised under the same conditions than the ones exposed in **Test D** was used for the following tests. Prior to reaction the Mn-Anderson amino acid residue immobilised on the solid support had to be deprotected:

1. Fmoc removal step: 1.0 mL of 20% piperidine/DMF (vol/vol) was added, the mixture was stirred gently for 1 min and the solution was removed by vacuum filtration. 1.0 mL of the same solution was added again, the mixture was stirred gently for 1 min, left to react for 10 min and removed by vacuum filtration.
2. Washing step: 1.0 mL of DMF was added, the mixture was stirred for 30 s, and the solvent was then removed by vacuum filtration. This step was repeated 6 times.

5.5.3.1 Test H

Coupling:

3. Reaction: a DMF (200 μL) solution of Fmoc-Phe-OH (0.135 mmol, 52 mg, 30 equiv.) with HBTU (0.18 mmol, 66 mg, 4 equiv.) and DIPEA (60 μL, 0.34 mmol)

were added (mixture made 15 min before addition), the resulting mixture was stirred gently for 1 min and left to react for 1 h. The solvent was then removed by vacuum filtration. A double coupling was carried out with an identical reagent mixture and was left to react for 16 h. The solvent was then removed by vacuum filtration.

5. Washing step: 1.0 mL of DMF was added, the mixture was stirred for 30 s, the solvent was then removed by vacuum filtration. This step was repeated 6 times.

Cleavage/Product isolation:

5. Washing step: 1.0 mL of DCM was added, the mixture was stirred for 30 s, the solvent was then removed by vacuum filtration. This step was repeated 3 times.

6. 500 μL of 20% HFIP/DCM (vol/vol) was added, the mixture was stirred for 2 min, left to react for 10 min and the solution was collected by vacuum filtration.

7. 1.0 mL of DCM was added, the mixture was stirred for 30 s, and the solution was then collected by vacuum filtration.

8. The solutions collected were combined and the solvent evaporated under reduced pressure.

ESI-MS results: two main peak envelopes at *m/z* 1327.49 (z = -1) and 1412.56 (z = -1 but also involving dimers of z = -2) which could not be assigned to the expected product or the starting material were observed, the product of this test still remains unidentified. The expected product has the general formula $(C_{16}H_{36}N)_3[MnMo_6O_{24}(C_{28}H_{27}N_2O_3)(C_{11}H_{17}N_2O_4)]$.

5.5.3.2 Test I

Coupling:

4. Reaction: a DMF (200 μL) solution of Fmoc-Phe-OH (0.135 mmol, 52 mg, 30 equiv.) and DIC (21 μL, 0.135 mmol, 30 equiv.) (mixture made 15 min before addition) was added, the resulting mixture was stirred gently for 1 min and left to react for 3 h. The solvent was then removed by vacuum filtration and the addition step repeated once.

6. Washing step: 1.0 mL of DMF was added, the mixture was stirred for 30 s, the solvent was then removed by vacuum filtration. This step was repeated 6 times.

Cleavage/Product isolation:

9. <u>Washing step:</u> 1.0 mL of DCM was added, the mixture was stirred for 30 s, the solvent was then removed by vacuum filtration. This step was repeated 3 times.

10. 500 μL of 20% HFIP/DCM (vol/vol) was added, the mixture was stirred for 2 min, left to react for 10 min and the solution was collected by vacuum filtration.

11. 1.0 mL of DCM was added, the mixture was stirred for 30 s, and the solution was then collected by vacuum filtration.

12. The solutions collected were combined and the solvent evaporated under reduced pressure.

ESI-MS results:

Two main peak envelopes at m/z 1698.63 (z = -1) and 1938.88 (z = -1) were assigned as $[H_2[MnMo_6O_{24}(C_{28}H_{27}N_2O_3)(C_{11}H_{17}N_2O_4)]]^{1-}$ (predicted: 1697.59) and $[(C_{16}H_{36}N)_1H-[MnMo_6O_{24}(C_{28}H_{27}N_2O_3)(C_{11}H_{17}N_2O_4)]]^{1-}$ (predicted: 1938.87). The expected product has the general formula $(C_{16}H_{36}N)_3[MnMo_6O_{24}(C_{28}H_{27}N_2O_3)(C_{11}H_{17}N_2O_4)]$.

6   Crystallographic Section

Single crystal X-ray diffraction data for compounds **1**-**11**, **13**, **17**, **20** and **21** are presented in this thesis. Structures were solved using Patterson or Direct methods with SHELXS-97[249] or SIR-92 using WinGX[250] routines. Refinement was accomplished by full matrix least-squares on F^2 *via* SHELXL-97.[249] All non-hydrogen atoms were refined anisotropically unless stated otherwise. Hydrogen atom positions were calculated using standard geometric criteria and refined using a riding model. All data manipulation and presentation steps were performed using WinGX. Due to the large amount of tabulated data this section only presents the refinement details of each structure. Supplementary data deposited with this thesis can be obtained from the University of Glasgow. The following quantities are given in the information for each structure and were calculated as follows:

$$\text{Goodness-of-fit (GooF)} = \left(\sqrt{\sum \frac{w(F_0^2 - F_c^2)^2}{(n-p)}} \right)$$

$$\text{Weighting scheme } w = \frac{1}{[\sigma^2(F_0)^2 + (AP)^2 + (BP)]}$$

With $P = \dfrac{[\max(I_{obs,O}) + 2F_c^2]}{3}$, and *p*: number of parameters; *n*: number of data; A, B: weighting scheme parameters

$$R1 = \frac{\sum || F_0 | - | F_c ||}{\sum | F_o |}$$

$$wR2 = \sqrt{\frac{\sum[w(F_0^2 - F_c^2)^2]}{\sum w(F_0^2)^2}}$$

$$R(\text{int}) = \frac{\sum |F_0^2 - F_c^2 (mean)|}{\sum |F_0^2|}, \text{ where both summation involve reflections for which more}$$

than one symmetry equivalent is averaged.

6.1 Crystal data and structure refinement for compound 1a

Empirical formula	$C_{18}H_{50}Mo_8N_5NaO_{28}$
Formula weight	1575.14
Temperature	150(2) K
Wavelength	1.54178 Å
Crystal system, space group	Monoclinic, $P2_1/c$
Unit cell dimensions	$a = 9.4649(4)$ Å $\quad \alpha = 90\,°$
	$b = 20.3666(8)$ Å $\quad \beta = 93.236(3)\,°$
	$c = 11.6803(4)$ Å $\quad \gamma = 90\,°$
Volume	2248.00(15) Å^3
Z, Calculated density	2, 2.327 Mg/m^3
Absorption coefficient	18.591 mm^{-1}
F(000)	1528
Crystal size	0.11 x 0.07 x 0.04 mm
Theta range for data collection	4.37 to 57.50 °
Limiting indices	-10<=h<=9, -22<=k<=21, -12<=l<=12
Reflections collected / unique	12277 / 3055 [R(int) = 0.0523]
Completeness to theta = 57.50	99.3 %
Absorption correction	Analytical
Max. and min. transmission	0.5234 and 0.2342
Refinement method	Full-matrix least-squares on F2
Data / restraints / parameters	3055 / 0 / 249
Goodness-of-fit on F2	1.102
Final R indices [I>2sigma(I)]	R1 = 0.0714, wR2 = 0.2541
R indices (all data)	R1 = 0.0793, wR2 = 0.2598
Largest diff. peak and hole	3.18 and -1.36 e.Å^{-3}

6.2   Crystal data and structure refinement for compound 1b

Empirical formula	$C_{28}H_{76}Mo_8N_8O_{30}$
Formula weight	1772.49
Temperature	150(2) K
Wavelength	0.71073 Å
Crystal system, space group	Monoclinic, $P2_1/n$
Unit cell dimensions	$a = 10.8532(5)$ Å $\alpha = 90\,°$
	$b = 25.1978(14)$ Å $\beta = 116.657(3)\,°$
	$c = 11.7908(6)$ Å $\gamma = 90\,°$
Volume	2881.8(3) Å^3
Z, Calculated density	2, 2.043 Mg/m^3
Absorption coefficient	1.770 mm^{-1}
F(000)	1752
Crystal size	0.20 x 0.10 x 0.05 mm
Theta range for data collection	2.09 to 26.00 °
Limiting indices	-13<=h<=13, -28<=k<=31, 14<=l<=14
Reflections collected / unique	22348 / 5667 [R(int) = 0.0766]
Completeness to theta = 26.00	99.9 %
Absorption correction	Empirical
Max. and min. transmission	0.9167 and 0.7185
Refinement method	Full-matrix least-squares on F2
Data / restraints / parameters	5667 / 16 / 335
Goodness-of-fit on F2	1.003
Final R indices [I>2sigma(I)]	R1 = 0.0423, wR2 = 0.0832
R indices (all data)	R1 = 0.0795, wR2 = 0.0982
Largest diff. peak and hole	0.78 and -0.90 e.Å^{-3}

6.3   Crystal data and structure refinement for compound 2a

Empirical formula	$C_{24}H_{60}Mo_8N_3NaO_{26}$
Formula weight	1597.26
Temperature	150(2) K
Wavelength	0.71073 Å
Crystal system, space group	Monoclinic, $P2_1$
Unit cell dimensions	$a = 10.9912(10)$ Å $\alpha = 90\,°$
	$b = 22.757(2)$ Å $\beta = 98.239(4)\,°$
	$c = 18.7179(15)$ Å $\gamma = 90\,°$
Volume	4633.5(7) Å^3
Z, Calculated density	4, 2.290 Mg/m^3
Absorption coefficient	2.187 mm^{-1}
F(000)	3120
Crystal size	0.15 x 0.12 x 0.10 mm
Theta range for data collection	1.42 to 25.00 °
Limiting indices	-13<=h<=12, 0<=k<=27, 0<=l<=22
Reflections collected / unique	8838 / 8838 [R(int) = 0.0000]
Completeness to theta = 25.00	87.5 %
Absorption correction	Empirical
Max. and min. transmission	0.8110 and 0.7350
Refinement method	Full-matrix least-squares on F2
Data / restraints / parameters	8838 / 2 / 611
Goodness-of-fit on F2	1.080
Final R indices [I>2sigma(I)]	R1 = 0.0778, wR2 = 0.1685
R indices (all data)	R1 = 0.1095, wR2 = 0.1941
Largest diff. peak and hole	1.81 and -1.77 e.Å^{-3}

6.4 Crystal data and structure refinement for compound 2b

Empirical formula	$C_{38}H_{94}Mo_8N_6O_{28}$
Formula weight	1850.71
Temperature	150(2) K
Wavelength	0.71073 Å
Crystal system, space group	Monoclinic, $P2_1/c$
Unit cell dimensions	$a = 12.6794(7)$ Å $\quad \alpha = 90\,°$
	$b = 11.9967(6)$ Å $\quad \beta = 95.176(3)\,°$
	$c = 20.8920(11)$ Å $\quad \gamma = 90\,°$
Volume	3164.9(3) $Å^3$
Z, Calculated density	2, 1.942 Mg/m^3
Absorption coefficient	1.613 mm^{-1}
F(000)	1848
Crystal size	0.10 x 0.10 x 0.06 mm
Theta range for data collection	1.96 to 26.00 °
Limiting indices	-15<=h<=12, -14<=k<=14, -25<=l<=25
Reflections collected / unique	42348 / 6210 [R(int) = 0.0485]
Completeness to theta = 26.00	99.6 %
Absorption correction	Empirical
Max. and min. transmission	0.9094 and 0.8553
Refinement method	Full-matrix least-squares on F2
Data / restraints / parameters	6210 / 0 / 378
Goodness-of-fit on F2	1.050
Final R indices [I>2sigma(I)]	R1 = 0.0286, wR2 = 0.0687
R indices (all data)	R1 = 0.0393, wR2 = 0.0760
Largest diff. peak and hole	0.68 and -0.96 e.$Å^{-3}$

6.5 Crystal data and structure refinement for compound 3a

Empirical formula	$C_{30}H_{70}Mo_8N_4Na_2O_{28}$
Formula weight	1748.40
Temperature	150(2) K
Wavelength	0.71073 Å
Crystal system, space group	Triclinic, $P\bar{1}$
Unit cell dimensions	$a = 13.1358(11)$ Å $\alpha = 65.365(3)$ °
	$b = 20.1210(15)$ Å $\beta = 89.772(4)$ °
	$c = 23.1313(17)$ Å $\gamma = 88.935(4)$ °
Volume	5556.3(7) Å^3
Z, Calculated density	4, 2.090 Mg/m^3
Absorption coefficient	1.844 mm^{-1}
F(000)	3440
Crystal size	0.18 x 0.15 x 0.10 mm
Theta range for data collection	1.55 to 25.80 °
Limiting indices	-16<=h<=16, -24<=k<=24, -28<=l<=28
Reflections collected / unique	75354 / 21097 [R(int) = 0.0305]
Completeness to theta = 25.80	98.7 %
Absorption correction	Empirical
Max. and min. transmission	0.8371 and 0.7326
Refinement method	Full-matrix least-squares on F2
Data / restraints / parameters	21097 / 67 / 1314
Goodness-of-fit on F2	1.108
Final R indices [I>2sigma(I)]	R1 = 0.0340, wR2 = 0.0787
R indices (all data)	R1 = 0.0407, wR2 = 0.0825
Largest diff. peak and hole	1.51 and -0.94 e.Å^{-3}

6.6 Crystal data and structure refinement for compound 3b

Empirical formula	$C_{51}H_{119}Mo_8N_5O_{27}$
Formula weight	2002.03
Temperature	150(2) K
Wavelength	0.71073 Å
Crystal system, space group	Orthorhombic, *Pccn*
Unit cell dimensions	$a = 21.2892(12)$ Å $\quad \alpha = 90\,°$
	$b = 22.0626(10)$ Å $\quad \beta = 90\,°$
	$c = 16.7364(8)$ Å $\quad \gamma = 90\,°$
Volume	7861.0(7) Å^3
Z, Calculated density	4, 1.692 Mg/m^3
Absorption coefficient	1.304 mm^{-1}
F(000)	4048
Crystal size	0.09 x 0.08 x 0.07 mm
Theta range for data collection	1.80 to 26.00 $°$
Limiting indices	-13<=h<=25, -24<=k<=27, -20<=l<=19
Reflections collected / unique	32104 / 7648 [R(int) = 0.0360]
Completeness to theta = 26.00	98.9 %
Absorption correction	Empirical
Max. and min. transmission	0.9142 and 0.8916
Refinement method	Full-matrix least-squares on F2
Data / restraints / parameters	7648 / 2 / 418
Goodness-of-fit on F2	1.059
Final R indices [I>2sigma(I)]	R1 = 0.0276, wR2 = 0.0610
R indices (all data)	R1 = 0.0391, wR2 = 0.0688
Largest diff. peak and hole	1.04 and -0.55 e.Å^{-3}

6.7   Crystal data and structure refinement for compound 3c

Empirical formula	$C_{18}H_{42}Mo_8N_6Na_4O_{32}$
Formula weight	1714.06
Temperature	150(2) K
Wavelength	0.71073 Å
Crystal system, space group	Monoclinic, $P2_1/n$
Unit cell dimensions	$a = 12.236(2)$ Å $\alpha = 90\,°$
	$b = 13.609(2)$ Å $\beta = 99.455(7)\,°$
	$c = 14.868(2)$ Å $\gamma = 90\,°$
Volume	2442.2(7) Å^3
Z, Calculated density	2, 2.331 Mg/m^3
Absorption coefficient	2.117 mm^{-1}
F(000)	1656
Crystal size	0.16 x 0.10 x 0.04 mm
Theta range for data collection	2.00 to 25.80 °
Limiting indices	-14<=h<=14, -16<=k<=12, -18<=l<=16
Reflections collected / unique	18549 / 4691 [R(int) = 0.0278]
Completeness to theta = 25.80	99.9 %
Max. and min. transmission	0.9201 and 0.7281
Refinement method	Full-matrix least-squares on F2
Data / restraints / parameters	4691 / 10 / 352
Goodness-of-fit on F2	1.065
Final R indices [I>2sigma(I)]	R1 = 0.0182, wR2 = 0.0420
R indices (all data)	R1 = 0.0218, wR2 = 0.0442
Largest diff. peak and hole	0.351 and -0.450 e.Å^{-3}

6.8 Crystal data and structure refinement for compound 4

Empirical formula	$C_{29}H_{73}MnMo_6N_8O_{27}$
Formula weight	1596.53
Temperature	150(2) K
Wavelength	1.54184 Å
Crystal system, space group	Monoclinic, $C2/c$
Unit cell dimensions	$a = 29.0498(10)$ Å $\quad \alpha = 90\,°$
	$b = 9.2853(3)$ Å $\quad \beta = 102.186(3)\,°$
	$c = 24.0873(8)$ Å $\quad \gamma = 90\,°$
Volume	6350.8(4) Å^3
Z, Calculated density	4, 1.670 Mg/m^3
Absorption coefficient	11.617 mm^{-1}
F(000)	3184
Crystal size	0.14 x 0.10 x 0.05 mm
Theta range for data collection	3.75 to 54.31 °
Limiting indices	-30<=h<=30, -9<=k<=9, -25<=l<=25
Reflections collected / unique	15048 / 3874 [R(int) = 0.0720]
Completeness to theta = 54.31	99.6 %
Absorption correction	Analytical
Max. and min. transmission	0.5943 and 0.2931
Refinement method	Full-matrix least-squares on F2
Data / restraints / parameters	3874 / 0 / 299
Goodness-of-fit on F2	1.053
Final R indices [I>2sigma(I)]	R1 = 0.0744, wR2 = 0.2050
R indices (all data)	R1 = 0.1125, wR2 = 0.2425
Largest diff. peak and hole	1.60 and -0.97 e.Å^{-3}

6.9   Crystal data and structure refinement for compound 5a

Empirical formula	$C_{35}H_{83}MnMo_6N_6O_{25}$
Formula weight	1618.65
Temperature	150(2) K
Wavelength	0.71073 Å
Crystal system, space group	Monoclinic, $C2/m$
Unit cell dimensions	$a = 15.0770(13)$ Å $\alpha = 90\,°$
	$b = 23.102(2)$ Å $\beta = 92.336(5)\,°$
	$c = 15.0791(14)$ Å $\gamma = 90\,°$
Volume	5247.9(8) Å^3
Z, Calculated density	4, 2.049 Mg/m^3
Absorption coefficient	1.708 mm^{-1}
F(000)	3248
Crystal size	0.19 x 0.12 x 0.07 mm
Theta range for data collection	1.61 to 26.00 °
Limiting indices	-18<=h<=18, -28<=k<=28, -17<=l<=18
Reflections collected / unique	19081 / 5245 [R(int) = 0.0293]
Completeness to theta = 26.0	99.1 %
Absorption correction	Empirical
Max. and min. transmission	0.8898 and 0.7374
Refinement method	Full-matrix least-squares on F2
Data / restraints / parameters	5245 / 0 / 333
Goodness-of-fit on F2	1.032
Final R indices [I>2sigma(I)]	R1 = 0.0456, wR2 = 0.1279
R indices (all data)	R1 = 0.0605, wR2 = 0.1447
Largest diff. peak and hole	1.41 and -1.29 e.Å^{-3}

6.10 Crystal data and structure refinement for compound 5b

Empirical formula	$C_{38}H_{90}MnMo_6N_7O_{26}$
Formula weight	1691.75
Temperature	150(2) K
Wavelength	0.71073 Å
Crystal system, space group	Monoclinic, $C2/c$
Unit cell dimensions	$a = 24.6971(16)$ Å $\alpha = 90$ °
	$b = 12.6758(8)$ Å $\beta = 90.641(5)$ °
	$c = 18.8241(10)$ Å $\gamma = 90$ °
Volume	5892.6(6) Å^3
Z, Calculated density	4, 1.907 Mg/m^3
Absorption coefficient	1.527 mm^{-1}
F(000)	3408
Crystal size	0.28 x 0.06 x 0.05 mm
Theta range for data collection	2.81 to 25.73 °
Limiting indices	-30<=h<=30, -15<=k<=15, -22<=l<=22
Reflections collected / unique	23531 / 5603 [R(int) = 0.0756]
Completeness to theta = 25.73	99.6 %
Absorption correction	Analytical
Max. and min. transmission	0.9276 and 0.6744
Refinement method	Full-matrix least-squares on F2
Data / restraints / parameters	5603 / 0 / 358
Goodness-of-fit on F2	1.054
Final R indices [I>2sigma(I)]	R1 = 0.0453, wR2 = 0.0885
R indices (all data)	R1 = 0.0802, wR2 = 0.1075
Largest diff. peak and hole	0.87 and -0.80 e.Å^{-3}

6.11   Crystal data and structure refinement for compound 6

Empirical formula	$C_{41}H_{93}MnMo_6N_7NaO_{27}$
Formula weight	1769.79
Temperature	150(2) K
Wavelength	0.71073 Å
Crystal system, space group	Orthorhombic, *Pnma*
Unit cell dimensions	$a = 52.926(3)$ Å $\alpha = 90\,°$
	$b = 27.5135(10)$ Å $\beta = 90\,°$
	$c = 9.5169(4)$ Å $\gamma = 90\,°$
Volume	13858.3(10) Å^3
Z, Calculated density	8, 1.696 Mg/m^3
Absorption coefficient	1.309 mm^{-1}
F(000)	7136
Crystal size	0.16 x 0.10 x 0.05 mm
Theta range for data collection	1.07 to 21.97 °
Limiting indices	-55<=h<=37, -22<=k<=28, -8<=l<=10
Reflections collected / unique	33040 / 8660 [R(int) = 0.0780]
Completeness to theta = 21.97	99.9 %
Absorption correction	Empirical
Max. and min. transmission	0.9374 and 0.8179
Refinement method	Full-matrix least-squares on F2
Data / restraints / parameters	8660 / 0 / 586
Goodness-of-fit on F2	1.024
Final R indices [I>2sigma(I)]	R1 = 0.0812, wR2 = 0.2093
R indices (all data)	R1 = 0.1221, wR2 = 0.2301
Largest diff. peak and hole	1.55 and -0.92 e.Å^{-3}

6.12   Crystal data and structure refinement for compound 7a

Empirical formula	$C_{17}H_{47}MnMo_6N_5Na_3O_{32}$
Formula weight	1533.15
Temperature	150(2) K
Wavelength	0.71073 Å
Crystal system, space group	Triclinic, $P\bar{1}$
Unit cell dimensions	$a = 9.1905(5)$ Å $\alpha = 102.444(3)$ °
	$b = 12.7684(6)$ Å $\beta = 106.754(3)$ °
	$c = 12.8684(6)$ Å $\gamma = 110.418(3)$ °
Volume	1268.31(11) Å^3
Z, Calculated density	1, 2.007 Mg/m^3
Absorption coefficient	1.792 mm^{-1}
F(000)	750
Crystal size	0.12 x 0.10 x 0.04 mm
Theta range for data collection	1.77 to 25.73 °
Limiting indices	-10<=h<=11, -15<=k<=15, -15<=l<=15
Reflections collected / unique	18023 / 4820 [R(int) = 0.0469]
Completeness to theta = 25.73	99.3 %
Absorption correction	Empirical
Max. and min. transmission	0.9318 and 0.8137
Refinement method	Full-matrix least-squares on F2
Data / restraints / parameters	4820 / 0 / 321
Goodness-of-fit on F2	1.018
Final R indices [I>2sigma(I)]	R1 = 0.0570, wR2 = 0.1543
R indices (all data)	R1 = 0.0775, wR2 = 0.1719
Largest diff. peak and hole	2.66 and -1.58 e.Å^{-3}

6.13   Crystal data and structure refinement for compound 7b

Empirical formula	$C_{20}H_{52}MnMo_6N_6Na_3O_{32}$
Formula weight	1588.23
Temperature	150(2) K
Wavelength	0.71073 Å
Crystal system, space group	Triclinic, $P\bar{1}$
Unit cell dimensions	$a = 8.6386(4)$ Å $\alpha = 109.102(2)$ °
	$b = 10.0132(5)$ Å $\beta = 92.590(2)$ °
	$c = 14.3392(8)$ Å $\gamma = 93.587(2)$ °
Volume	1166.91(10) Å^3
Z, Calculated density	1, 2.260 Mg/m^3
Absorption coefficient	1.953 mm^{-1}
F(000)	780
Crystal size	0.14 x 0.06 x 0.02 mm
Theta range for data collection	2.16 to 25.99 °
Limiting indices	-10<=h<=10, -12<=k<=12, -17<=l<=15
Reflections collected / unique	16581 / 4556 [R(int) = 0.0270]
Completeness to theta = 25.99	99.3 %
Absorption correction	Empirical
Max. and min. transmission	0.9620 and 0.7716
Refinement method	Full-matrix least-squares on F2
Data / restraints / parameters	4556 / 14 / 356
Goodness-of-fit on F2	1.034
Final R indices [I>2sigma(I)]	R1 = 0.0202, wR2 = 0.0494
R indices (all data)	R1 = 0.0246, wR2 = 0.0524
Largest diff. peak and hole	0.48 and -0.69 e.Å^{-3}

6.14 Crystal data and structure refinement for compound 7c

Empirical formula	$C_{38}H_{86}MnMo_6N_{12}Na_3O_{34}$
Formula weight	1954.74
Temperature	150(2) K
Wavelength	0.71073 Å
Crystal system, space group	Triclinic, $P\bar{1}$
Unit cell dimensions	$a = 9.5374(3)$ Å $\quad \alpha = 91.169(2)$ °
	$b = 13.5364(5)$ Å $\quad \beta = 90.065(2)$ °
	$c = 28.3397(9)$ Å $\quad \gamma = 109.346(2)$ °
Volume	3451.3(2) Å^3
Z, Calculated density	2, 1.881 Mg/m^3
Absorption coefficient	1.344 mm^{-1}
F(000)	1960
Crystal size	0.12 x 0.10 x 0.06 mm
Theta range for data collection	0.72 to 26.00 °
Limiting indices	-11<=h<=11, -16<=k<=16, -34<=l<=34
Reflections collected / unique	50838 / 13543 [R(int) = 0.0254]
Completeness to theta = 26.00	99.8 %
Absorption correction	Empirical
Max. and min. transmission	0.9237 and 0.8553
Refinement method	Full-matrix least-squares on F2
Data / restraints / parameters	13543 / 0 / 852
Goodness-of-fit on F2	1.037
Final R indices [I>2sigma(I)]	R1 = 0.0244, wR2 = 0.0655
R indices (all data)	R1 = 0.0266, wR2 = 0.0670
Largest diff. peak and hole	0.69 and -0.60 e.Å^{-3}

6.15 Crystal data and structure refinement for compound 8

Empirical formula	$C_{72}H_{147}MnMo_6N_{10}O_{26}$
Formula weight	2199.58
Temperature	150(2) K
Wavelength	0.71073 Å
Crystal system, space group	Triclinic, $P\bar{1}$
Unit cell dimensions	$a = 14.8991(11)$ Å $\quad \alpha = 73.868(4)$ °
	$b = 16.8272(12)$ Å $\quad \beta = 74.700(4)$ °
	$c = 22.2685(17)$ Å $\quad \gamma = 66.883(3)$ °
Volume	4856.2(6) Å^3
Z, Calculated density	2, 1.504 Mg/m^3
Absorption coefficient	0.946 mm^{-1}
F(000)	2268
Crystal size	0.14 x 0.09 x 0.06 mm
Theta range for data collection	1.61 to 26.00 °
Limiting indices	-17<=h<=18, -20<=k<=20, -27<=l<=27
Reflections collected / unique	69193 / 19055 [R(int) = 0.0296]
Completeness to theta = 26.00	99.7 %
Absorption correction	Empirical
Max. and min. transmission	0.9454 and 0.8789
Refinement method	Full-matrix least-squares on F2
Data / restraints / parameters	19055 / 3 / 1018
Goodness-of-fit on F2	1.046
Final R indices [I>2sigma(I)]	R1 = 0.0287, wR2 = 0.0677
R indices (all data)	R1 = 0.0385, wR2 = 0.0750
Largest diff. peak and hole	0.76 and -0.84 e.Å^{-3}

6.16   Crystal data and structure refinement for compound 9

Empirical formula	$C_{79}H_{153}MnMo_6N_8O_{29}$
Formula weight	2309.67
Temperature	150(2) K
Wavelength	0.71073 Å
Crystal system, space group	Orthorhombic, $Pca2_1$
Unit cell dimensions	$a = 18.0293(7)$ Å $\alpha = 90\,°$
	$b = 20.8575(8)$ Å $\beta = 90\,°$
	$c = 26.7597(11)$ Å $\gamma = 90\,°$
Volume	10062.9(7) Å^3
Z, Calculated density	4, 1.525 Mg/m^3
Absorption coefficient	0.919 mm^{-1}
F(000)	4768
Crystal size	0.16 x 0.06 x 0.04 mm
Theta range for data collection	2.13 to 24.82 °
Limiting indices	-21<=h<=21, -24<=k<=24, -31<=l<=31
Reflections collected / unique	69503 / 16825 [R(int) = 0.1339]
Completeness to theta = 24.82	99.0 %
Absorption correction	Empirical
Max. and min. transmission	0.9642 and 0.8669
Refinement method	Full-matrix least-squares on F2
Data / restraints / parameters	16825 / 42 / 827
Goodness-of-fit on F2	1.056
Final R indices [I>2sigma(I)]	R1 = 0.0823, wR2 = 0.1817
R indices (all data)	R1 = 0.1592, wR2 = 0.2247
Largest diff. peak and hole	0.98 and -1.02 e.Å^{-3}

6.17 Crystal data and structure refinement for compound 10

Empirical formula	$C_{68}H_{138}MnMo_6N_7O_{30}$
Formula weight	2164.43
Temperature	150(2) K
Wavelength	0.71073 Å
Crystal system, space group	Orthorhombic, *Pnma*
Unit cell dimensions	$a = 28.3641(5)$ Å $\quad \alpha = 90\,°$
	$b = 23.7876(5)$ Å $\quad \beta = 90\,°$
	$c = 15.0216(3)$ Å $\quad \gamma = 90\,°$
Volume	10135.3(3) Å^3
Z, Calculated density	4, 1.418 Mg/m^3
Absorption coefficient	0.908 mm^{-1}
F(000)	4448
Crystal size	0.27 x 0.18 x 0.17 mm
Theta range for data collection	2.94 to 25.69 °
Limiting indices	-31<=h<=34, -28<=k<=28, -18<=l<=18
Reflections collected / unique	78055 / 9622 [R(int) = 0.0627]
Completeness to theta = 25.69	99.8 %
Absorption correction	Analytical
Max. and min. transmission	0.8610 and 0.7917
Refinement method	Full-matrix least-squares on F2
Data / restraints / parameters	9622 / 13 / 494
Goodness-of-fit on F2	1.065
Final R indices [I>2sigma(I)]	R1 = 0.0482, wR2 = 0.1211
R indices (all data)	R1 = 0.0673, wR2 = 0.1302
Largest diff. peak and hole	0.78 and -0.52 e.Å^{-3}

6.18 Crystal data and structure refinement for compound 11

Empirical formula	$C_{84}H_{166}MnMo_6N_{11}O_{38}$
Formula weight	2568.86
Temperature	150(2) K
Wavelength	0.71073 Å
Crystal system, space group	Monoclinic, $C2/c$
Unit cell dimensions	$a = 30.7813(16)$ Å $\quad \alpha = 90\,^{\circ}$
	$b = 23.7409(12)$ Å $\quad \beta = 121.095(2)\,^{\circ}$
	$c = 18.4631(10)$ Å $\quad \gamma = 90\,^{\circ}$
Volume	11553.7(10) $Å^3$
Z, Calculated density	4, 1.477 Mg/m^3
Absorption coefficient	0.815 mm^{-1}
F(000)	5312
Crystal size	0.12 x 0.10 x 0.06 mm
Theta range for data collection	1.15 to 26.00 $^{\circ}$
Limiting indices	-32<=h<=37, -29<=k<=29, -22<=l<=21
Reflections collected / unique	80717 / 11341 [R(int) = 0.0394]
Completeness to theta = 26.00	99.9 %
Absorption correction	Empirical
Max. and min. transmission	0.9527 and 0.9085
Refinement method	Full-matrix least-squares on F2
Data / restraints / parameters	11341 / 5 / 620
Goodness-of-fit on F2	1.109
Final R indices [I>2sigma(I)]	R1 = 0.0443, wR2 = 0.1275
R indices (all data)	R1 = 0.0609, wR2 = 0.1547
Largest diff. peak and hole	1.45 and -0.64 e.$Å^{-3}$

6.19 Crystal data and structure refinement for compound 13

Empirical formula	$C_{82}H_{150}MnMo_6N_7O_{32}$
Formula weight	2376.66
Temperature	150(2) K
Wavelength	0.71073 Å
Crystal system, space group	Monoclinic, $C2/c$
Unit cell dimensions	$a = 50.1637(14)$ Å $\quad \alpha = 90\,°$
	$b = 29.4838(12)$ Å $\quad \beta = 124.851(3)\,°$
	$c = 29.5767(12)$ Å $\quad \gamma = 90\,°$
Volume	35898(3) Å^3
Z, Calculated density	12, 1.319Mg/m^3
Absorption coefficient	0.777 mm^{-1}
F(000)	14688
Crystal size	0.110 x 0.090 x 0.050 mm
Theta range for data collection	0.849 to 26.000 °
Limiting indices	-61<=h<=55, -36<=k<=36, -36<=l<=36
Reflections collected / unique	246843 / 35272 [R(int) = 0.0799]
Completeness to theta = 25.242	100 %
Absorption correction	Empirical
Max. and min. transmission	n/a
Refinement method	Full-matrix least-squares on F2
Data / restraints / parameters	35272 / 54 / 992
Goodness-of-fit on F2	1.044
Final R indices [I>2sigma(I)]	R1 = 0.0839, wR2 = 0.2457
R indices (all data)	R1 = 0.1395, wR2 = 0.2650
Largest diff. peak and hole	0.99 and -0.68 e.Å^{-3}

6.20 Crystal data and structure refinement for compound 17

Empirical formula	$C_{80}H_{153}MnMo_6N_8O_{28}$
Formula weight	2305.68
Temperature	150(2) K
Wavelength	0.71073 Å
Crystal system, space group	Monoclinic, $P2_1/c$
Unit cell dimensions	$a = 27.455(3)$ Å $\quad \alpha = 90\,°$
	$b = 29.007(3)$ Å $\quad \beta = 94.450(5)\,°$
	$c = 24.974(2)$ Å $\quad \gamma = 90\,°$
Volume	19829(3) Å^3
Z, Calculated density	8, 1.545 Mg/m^3
Absorption coefficient	0.932 mm^{-1}
F(000)	9520
Crystal size	0.13 x 0.06 x 0.03 mm
Theta range for data collection	1.02 to 26.00 °
Limiting indices	-33<=h<=33, -35<=k<=35, -30<=l<=30
Reflections collected / unique	287148 / 38952 [R(int) = 0.0582]
Completeness to theta = 26.00	100 %
Absorption correction	Empirical
Max. and min. transmission	0.9726 and 0.8884
Refinement method	Full-matrix least-squares on F2
Data / restraints / parameters	38952 / 63 / 1854
Goodness-of-fit on F2	1.170
Final R indices [I>2sigma(I)]	R1 = 0.0802, wR2 = 0.1796
R indices (all data)	R1 = 0.0924, wR2 = 0.1843
Largest diff. peak and hole	1.72 and -1.08 e.Å^{-3}

6.21 Crystal data and structure refinement for compound 20

Empirical formula	$C_{80}H_{155}MnMo_6N_8O_{29}$
Formula weight	2323.70
Temperature	150(2) K
Wavelength	0.71073 Å
Crystal system, space group	Orthorhombic, *Pnma*
Unit cell dimensions	$a = 28.257(2)$ Å $\quad \alpha = 90°$
	$b = 21.8128(16)$ Å $\quad \beta = 90°$
	$c = 16.5796(14)$ Å $\quad \gamma = 90°$
Volume	10219.1(14) Å^3
Z, Calculated density	4, 1.510 Mg/m^3
Absorption coefficient	0.906 mm^{-1}
F(000)	4800
Crystal size	0.12 x 0.06 x 0.03 mm
Theta range for data collection	1.89 to 26.00 °
Limiting indices	-34<=h<=30, -26<=k<=23, -20<=l<=19
Reflections collected / unique	77882 / 10308 [R(int) = 0.0862]
Completeness to theta = 26.00	99.9 %
Absorption correction	Empirical
Max. and min. transmission	0.9733 and 0.8991
Refinement method	Full-matrix least-squares on F2
Data / restraints / parameters	10308 / 39 / 440
Goodness-of-fit on F2	1.068
Final R indices [I>2sigma(I)]	R1 = 0.0823, wR2 = 0.2554
R indices (all data)	R1 = 0.1193, wR2 = 0.2777
Largest diff. peak and hole	1.18 and -0.97 e.Å^{-3}

6.22 Crystal data and structure refinement for compound 21

Empirical formula	$C_{62}H_{135}MnMo_6N_6O_{26}$
Formula weight	2011.34
Temperature	150(2) K
Wavelength	0.71073 Å
Crystal system, space group	Orthorhombic, *Pcca*
Unit cell dimensions	$a = 23.3192(17)$ Å $\quad \alpha = 90\,^\circ$
	$b = 28.200(2)$ Å $\quad \beta = 90\,^\circ$
	$c = 30.215(2)$ Å $\quad \gamma = 90\,^\circ$
Volume	19869(3) Å^3
Z, Calculated density	8, 1.345 Mg/m^3
Absorption coefficient	0.917 mm^{-1}
F(000)	8272
Crystal size	0.12 x 0.08 x 0.05mm
Theta range for data collection	0.72 to 25.00 °
Limiting indices	-27<=h<=27, -33<=k<=31, -35<=l<=35
Reflections collected / unique	135649 / 17492 [R(int) = 0.0842]
Completeness to theta = 25.00	99.9 %
Absorption correction	Empirical
Max. and min. transmission	0.9556 and 0.8979
Refinement method	Full-matrix least-squares on F2
Data / restraints / parameters	17492 / 12 / 795
Goodness-of-fit on F2	1.076
Final R indices [I>2sigma(I)]	R1 = 0.0913, wR2 = 0.2965
R indices (all data)	R1 = 0.1506, wR2 = 0.3334
Largest diff. peak and hole	1.81 and -0.79 e.Å^{-3}

7   References

[1]   Feynman, R. P. *Eng. Sci.* **1960**, *23*, 22

[2]   http://www.nobelprize.org/nobel_prizes/chemistry/laureates/1987/

[3]   Niemeyer, C. M. *Angew. Chem. Int. Ed.* **2001**, *40*, 4128

[4]   Zhang, S. *Nat. Biotech.* **2003**, *21*, 1171

[5]   Lehn, J.-M. *Supramolecular Chemistry. Concepts and perspectives*; VCH, Weinheim, **1995**

[6]   Pope, M. T. *Heteropoly and Isopoly Oxometalates, Springer-Verlag, Berlin* **1983**

[7]   Baker, L. C. W.; Glick, D. C. *Chem. Rev.* **1998**, *98*, 3

[8]   Long, D.-L.; Burkholder, E.; Cronin, L. *Chem. Soc. Rev.* **2007**, *36*, 105

[9]   Hutin, M.; Long, D.-L.; Cronin, L. *Isr. J. Chem.* **2011**, *51*, 205

[10]   Burtseva, K. G.; Chernaia, T. S.; Sirota, M. I. *Dokl. Akad. Nauk SSSR* **1978**, *243*, 104

[11]   Berzelius, J. J. *Poggend. Ann. Phys. Chem.* **1826**, *6*, 369

[12]   Pope, M. T.; Müller, A. *Angew. Chem. Int. Ed. Engl.* **1991**, *30*, 34

[13]   Katsoulis, D. E. *Chem. Rev.* **1998**, *98*, 359

[14]   Rhule, J. T.; Hill, C. L.; Judd, D. A.; Schinazi, R. F. *Chem. Rev.* **1998**, *98*, 327

[15]   Hill, C. L.; Prosser-McCartha, C. M. *Coord. Chem. Rev.* **1995**, *143*, 407

[16]   Kozhevnikov, I. V. *Chem. Rev.* **1998**, *98*, 171

[17]   Symes, M. D.; Cronin, L. *Nature Chem.* **2013**, *5*, 403

[18]   Vilà-Nadal, L.; Mitchell, S. G.; Markov, S.; Busche, C.; Georgiev, V.; Asenov, A.; Cronin, L. *Chem. Eur. J.* **2013**, *19*, 16502

[19]   Bidan, G.; Genies, E.; Lapkowski, M. European Patent, **1989**; EP 323351 A1

[20]   Pham, M.-C.; Mostefai, M.; Lacaze, P.-C. *Synth. Met.* **1992**, *52*, 305

[21]   Bidan, G.; Fabre, B.; Lapkowski, M. World Patent, **1994**; WO 9423291 A1

[22]   Dolbecq, A.; Dumas, E.; Mayer, C. R.; Mialane, P. *Chem. Rev.* **2010**, *110*, 6009

[23]   Yan, Y.; Wu, L. *Isr. J. Chem.* **2011**, *51*, 181

[24]   Thorimbert, S.; hasenknopf, B.; Lacôte, E. *Isr. J. Chem.* **2011**, *51*, 275

[25]   Geletii, Y. V.; Yin, Q.; Hou, Y.; Huang, Z.; Ma, H.; Song, J.; Besson, C.; Luo, Z.; Cao, R.; O'Halloran, K. P.; Zhu, G.; Zhao, C.; Vickers, J. W.; Ding, Y.; Mohebbi, S.; Kuznetsov, A. E.; Musaev, D. G.; Lian, T.; Hill, C. L. *Isr. J. Chem.* **2011**, *51*, 238

[26]   Berardi, S.; Carraro, M.; Sartorel, A.; Modugno, G.; Bonchio, M. *Isr. J. Chem.* **2011**, *51*, 259

[27]   Song, Y.-F.; Tsunashima, R. *Chem. Soc. Rev.* **2012**, *41*, 7384

[28]   Proust, A.; Matt, B.; Villanneau, R.; Guillemot, G.; Gouzerh, P.; Izzet, G. *Chem. Soc. Rev.* **2012**, *41*, 7605

[29]   Miras, H. N.; Yan, J.; Long, D.-L.; Cronin, L. *Chem. Soc. Rev.* **2012**, *41*, 7403

[30]   Svanberg, L.; Struve, H. *Liebigs. Ann.* **1848**, *68*, 209

[31]   Marignac, J.-C. G. d. *Ann. Chim. & Phys.* **1864**, *4*, 1

[32]   Werner, A. *Z. Anorg. Chem.* **1893**, 267

[33]   Miolati, A.; Pizzighelli, R. *J. Prakt. Chem.* **1908**, *77*, 417

[34]   Roseinheim, A.; Jaenicke, J. *J. Prakt. Chem.* **1917**, *100*, 304

[35]   Laue, M. v. *Physikalische Zeitschrift* **1913**, *14*

[36]   Bragg, W. L. *Nature* **1913**, *90*, 410

[37]   Pauling, L. *J. Am. Chem. Soc.* **1927**, *49*, 765

[38]   Pauling, L. *J. Am. Chem. Soc.* **1929**, *51*, 2868

[39]   Keggin, J. F. *Nature* **1933**, *132*, 351

[40]   Keggin, J. F. *Proc. R. Soc.* **1934**, *144*, 0075

[41]   Anderson, J. S. *Nature* **1937**, *140*, 850

[42]   Evans, H. T. *J. Am. Chem. Soc.* **1948**, *70*, 1291

[43]   Wells, A. F. *Structural Inorganic Chemistry* **1945**, *Oxford University Press: Oxford*, 344

[44]   Dawson, B. *Acta Crystallogr.* **1953**, *6*, 113

[45]   Lindqvist, I. *Ark. Kemie* **1950**, *2*, 349

[46]   Yu, R.; Kuang, X.-F.; Wu, X.-Y.; Lu, C.-Z.; Donahue, J. P. *Coord. Chem. Rev.* **2009**, *253*, 2872

[47]   Richmond, C. J.; Miras, H. N.; Ruiz de la Oliva, A.; Zang, H.; Sans, V.; Paramonov, L.; Makatsoris, C.; Inglis, R.; Brechin, E. K.; Long, D.-L.; Cronin, L. *Nature Chem.* **2012**, *4*, 1037

[48]   Ruiz de la Oliva, A.; Sans, V.; Miras, H. N.; Yan, J.; Zang, H.; Richmond, C. J.; Long, D.-L.; Cronin, L. *Angew. Chem. Int. Ed.* **2012**, *51*, 12759

[49]   Hasenknopf, B.; Delmont, R.; Herson, P.; Gouzerh, P. *Eur. J. Inorg. Chem.* **2002**, *2002*, 1081

[50]   Marcoux, P. R.; Hasenknopf, B.; Vaissermann, J.; Gouzerh, P. *Eur. J. Inorg. Chem.* **2003**, *2003*, 2406

[51]   Fuchs, J.; Hartl, H. *Angew. Chem. Int. Ed. Eng.* **1976**, *15*, 375

[52]   Lindqvist, I. *Ark. kemie* **1950**, *2*, 349

[53]   Atovmyan, L. O.; Krasochka, O. N. *J. Struct. Chem.* **1972**, *13*, 319

[54]   Niven, M. L.; Cruywagen, J. J.; Heyns, J. B. B. *J. Chem. Soc., Dalton Trans.* **1991**, 2007

[55]   Xi, R.; Wang, B.; Isobe, K.; Nishioka, T.; Toriumi, K.; Ozawa, Y. *Inorg. Chem.* **1994**, *33*, 833

[56]   Hagrman, D.; Zubeita, C.; Rose, D. J.; Zubieta, J.; Haushalter, R. C. *Angew. Chem. Int. Ed. Engl.* **1997**, *36*, 873

[57]   Xu, J.-Q.; Wang, R.-Z.; Yang, G.-Y.; Xing, Y.-H.; Li, D.-M.; Bu, W.-M.; Ye, L.; Fan, Y.-G.; Yang, G.-D.; Xing, Y.; Lin, Y.-H.; Jia, H.-Q. *Chem. Commun.* **1999**, 983

[58]   Rarig, R. S.; Bewley, L.; Burkholder, E.; Zubieta, J. *Ind. J. Chem.* **2003**, *42A*, 2235

[59]   Allis, D. G.; Burkholder, E.; Zubieta, J. *Polyhedron* **2004**, *23*, 1145

[60]   Himeno, S.; Niiya, H.; Ueda, T. *Bull. Chem. Soc. Jpn* **1997**, *70*, 631

[61]   Klemperer, W. G.; Shum, W. *J. Am. Chem. Soc.* **1976**, *98*, 8291

[62]   Day, V. W.; Fredrich, M. F.; Klemperer, W. G.; Shum, W. *J. Am. Chem. Soc.* **1977**, *99*, 952

[63]   Masters, A. F.; Gheller, S. F.; Brownlee, R. T. C.; O'Connor, M. J.; Wedd, A. G. *Inorg. Chem.* **1980**, *19*, 3866

[64]   Evans, H. T.; Gatehouse, B. M.; Leverett, P. *J. Chem. Soc., Dalton Trans.* **1975**, 505

[65]   Fuchs, J.; Flindt, E. P. *Z. Naturforsch., Teil B: Anorg. Chem. Org. Chem.* **1979**, *34B*, 412

[66]   Perloff, A. *Inorg. Chem.* **1970**, *9*, 2228

[67]   Tsigdinos, G. A. In *Top. Curr. Chem.*; Springer Berlin Heidelberg: **1978**; Vol. 76, p 1

[68]   Lee, U. *Acta Crystallogr. C* **1994**, *50*, 1657

[69]   Drisko, G. L.; Sanchez, C. *Eur. J. Inorg. Chem.* **2012**, *2012*, 5097

[70]   Gouzerh, P.; Proust, A. *Chem. Rev.* **1998**, *98*, 77

[71]   Proust, A.; Thouvenot, R.; Gouzerh, P. *Chem. Commun.* **2008**, 1837

[72]   Coronado, E.; Giménez-Saiz, C.; Gómez-García, C. J. *Coord. Chem. Rev.* **2005**, *249*, 1776

[73]   Wilson, A. J.; Robinson, W. T.; Wilkins, C. J. *Acta Crystallogr. C* **1983**, *39*, 54

[74]   Inoue, M.; Yamase, T. *Bull. Chem. Soc. Jpn* **1995**, *68*, 3055

[75]   Knoth, W. H. *J. Am. Chem. Soc.* **1979**, *101*, 759

[76]   Mayer, C. R.; Roch-Marchal, C.; Lavanant, H.; Thouvenot, R.; Sellier, N.; Blais, J.-C.; Sécheresse, F. *Chem. Eur. J.* **2004**, *10*, 5517

[77]   Aoki, S.; Kurashina, T.; Kasahara, Y.; Nishijima, T.; Nomiya, K. *Dalton Trans.* **2011**, *40*, 1243

[78]   Xin, F.; Pope, M. T. *Organometallics* **1994**, *13*, 4881

[79]   Sazani, G.; Pope, M. T. *Dalton Trans.* **2004**, 1989

[80]   Joo, N.; Renaudineau, S.; Delapierre, G.; Bidan, G.; Chamoreau, L.-M.; Thouvenot, R.; Gouzerh, P.; Proust, A. *Chem. Eur. J.* **2010**, *16*, 5043

[81]   Zhang, J.; Xiao, F.; Hao, J.; Wei, Y. *Dalton Trans.* **2012**, *41*, 3599

[82]   Mohs, T. R.; Yap, G. P. A.; Rheingold, A. L.; Maatta, E. A. *Inorg. Chem.* **1995**, *34*, 9

[83]   Dablemont, C.; Proust, A.; Thouvenot, R.; Afonso, C.; Fournier, F.; Tabet, J.-C. *Inorg. Chem.* **2004**, *43*, 3514

[84]   Duhacek, J. C.; Duncan, D. C. *Inorg. Chem.* **2007**, *46*, 7253

[85]   Wei, Y.; Xu, B.; Barnes, C. L.; Peng, Z. *J. Am. Chem. Soc.* **2001**, *123*, 4083

[86]   B. Strong, J.; S. Haggerty, B.; L. Rheingold, A.; A. Maatta, E. *Chem. Commun.* **1997**, 1137

[87]   Strong, J. B.; Yap, G. P. A.; Ostrander, R.; Liable-Sands, L. M.; Rheingold, A. L.; Thouvenot, R.; Gouzerh, P.; Maatta, E. A. *J. Am. Chem. Soc.* **2000**, *122*, 639

[88]   Chen, Q.; Zubieta, J. *Inorg. Chem.* **1990**, *29*, 1456

[89]   Chen, Q.; Goshorn, D. P.; Scholes, C. P.; Tan, X.-L.; Zubieta, J. *J. Am. Chem. Soc.* **1992**, *114*, 4667

[90]   Khan, M. I.; Zubieta, J. *J. Am. Chem. Soc.* **1992**, *114*, 10058

[91]   Müller, A.; Meyer, J.; Bögge, H.; Stammler, A.; Botar, A. *Chem. Eur. J.* **1998**, *4*, 1388

[92]   Han, J. W.; Hardcastle, K. I.; Hill, C. L. *Eur. J. Inorg. Chem.* **2006**, *2006*, 2598

[93]   Han, J. W.; Hill, C. L. *J. Am. Chem. Soc.* **2007**, *129*, 15094

[94]   Allain, C.; Favette, S.; Chamoreau, L.-M.; Vaissermann, J.; Ruhlmann, L.; Hasenknopf, B. *Eur. J. Inorg. Chem.* **2008**, *2008*, 3433

[95]   Li, D.; Song, J.; Yin, P.; Simotwo, S.; Bassler, A. J.; Aung, Y.; Roberts, J. E.; Hardcastle, K. I.; Hill, C. L.; Liu, T. *J. Am. Chem. Soc.* **2011**, *133*, 14010

[96]   Zeng, H.; Newkome, G. R.; Hill, C. L. *Angew. Chem. Int. Ed.* **2000**, *39*, 1771

[97]   Pradeep, C. P.; Long, D.-L.; Newton, G. N.; Song, Y.-F.; Cronin, L. *Angew. Chem. Int. Ed.* **2008**, *47*, 4388

[98]   Pradeep, C. P.; Misdrahi, M. F.; Li, F.-Y.; Zhang, J.; Xu, L.; Long, D.-L.; Liu, T.; Cronin, L. *Angew. Chem. Int. Ed.* **2009**, *48*, 8309

[99]   Misdrahi, M. F.; Wang, M.; Pradeep, C. P.; Li, F.-Y.; Lydon, C.; Xu, L.; Cronin, L.; Liu, T. *Langmuir* **2011**, *27*, 9193

[100] Pradeep, C. P.; Li, F.-Y.; Lydon, C.; Miras, H. N.; Long, D.-L.; Xu, L.; Cronin, L. *Chem. Eur. J.* **2011**, *17*, 7472

[101] Li, J.; Huth, I.; Chamoreau, L.-M.; Hasenknopf, B.; Lacôte, E.; Thorimbert, S.; Malacria, M. *Angew. Chem. Int. Ed.* **2009**, *48*, 2035

[102] Wilson, E. F.; Miras, H. N.; Rosnes, M. H.; Cronin, L. *Angew. Chem. Int. Ed.* **2011**, *50*, 3720

[103] Favette, S.; Hasenknopf, B.; Vaissermann, J.; Gouzerh, P.; Roux, C. *Chem. Commun.* **2003**, 2664

[104] Song, Y.-F.; Long, D.-L.; Cronin, L. *Angew. Chem. Int. Ed.* **2007**, *46*, 3900

[105] Santoni, M.-P.; Pal, A. K.; Hanan, G. S.; Proust, A.; Hasenknopf, B. *Inorg. Chem.* **2011**, *50*, 6737

[106] Thiel, J.; Yang, D.; Rosnes, M. H.; Liu, X.; Yvon, C.; Kelly, S. E.; Song, Y.-F.; Long, D.-L.; Cronin, L. *Angew. Chem. Int. Ed.* **2011**, *50*, 8871

[107] Song, Y.-F.; McMillan, N.; Long, D.-L.; Thiel, J.; Ding, Y.; Chen, H.; Gadegaard, N.; Cronin, L. *Chem. Eur. J.* **2008**, *14*, 2349

[108] Xia, N.; Yu, W.; Wang, Y.; Han, Y.; Zheng, P.; Wang, W.; Sakaguchi, G.; Matsuda, K.; Saijo, K.; Takenaka, M.; Hasegawa, H. *Polymer* **2011**, *52*, 1772

[109] Yang, H.-K.; Su, M.-M.; Ren, L.-J.; Tang, J.; Yan, Y.-K.; Miao, W.-K.; Zheng, P.; Wang, W. *Eur. J. Inorg. Chem.* **2013**, *2013*, 1381

[110] Wang, H.; Yan, Y.; Li, B.; Bi, L.; Wu, L. *Chem. Eur. J.* **2011**, *17*, 4273

[111] Rosnes, M. H.; Musumeci, C.; Yvon, C.; Macdonell, A.; Pradeep, C. P.; Sartorio, C.; Long, D.-L.; Pignataro, B.; Cronin, L. *Small* **2013**, *9*, 2316

[112] Wang, X.-L.; Wang, Y.-L.; Miao, W.-K.; Hu, M.-B.; Tang, J.; Yu, W.; Hou, Z.-Y.; Zheng, P.; Wang, W. *Langmuir* **2013**, *29*, 6537

[113] Song, Y.-F.; Long, D.-L.; Kelly, S. E.; Cronin, L. *Inorg. Chem.* **2008**, *47*, 9137

[114] Rosnes, M. H.; Musumeci, C.; Pradeep, C. P.; Mathieson, J. S.; Long, D.-L.; Song, Y.-F.; Pignataro, B.; Cogdell, R.; Cronin, L. *J. Am. Chem. Soc.* **2010**, *132*, 15490

[115] Oms, O.; Hakouk, K.; Dessapt, R.; Deniard, P.; Jobic, S.; Dolbecq, A.; Palacin, T.; Nadjo, L.; Keita, B.; Marrot, J.; Mialane, P. *Chem. Commun.* **2012**, *48*, 12103

[116] Wu, P.; Yin, P.; Zhang, J.; Hao, J.; Xiao, Z.; Wei, Y. *Chem. Eur. J.* **2011**, *17*, 12002

[117] Zhang, J.; Huang, Y.; Zhang, J.; She, S.; Hao, J.; Wei, Y. *Dalton Trans.* **2014**, *43*, 2722

[118] Odobel, F.; Séverac, M.; Pellegrin, Y.; Blart, E.; Fosse, C.; Cannizzo, C.; Mayer, C. R.; Elliott, K. J.; Harriman, A. *Chem. Eur. J.* **2009**, *15*, 3130

[119] Bareyt, S.; Piligkos, S.; Hasenknopf, B.; Gouzerh, P.; Lacôte, E.; Thorimbert, S.; Malacria, M. *Angew. Chem. Int. Ed.* **2003**, *42*, 3404

[120] Matt, B.; Renaudineau, S.; Chamoreau, L.-M.; Afonso, C.; Izzet, G.; Proust, A. *J. Org. Chem.* **2011**, *76*, 3107

[121] Lorion, M. M.; Matt, B.; Alves, S.; Proust, A.; Poli, G.; Oble, J.; Izzet, G. *Chem. Eur. J.* **2013**, *19*, 12607

[122] Micoine, K.; Hasenknopf, B.; Thorimbert, S.; Lacôte, E.; Malacria, M. *Org. Lett.* **2007**, *9*, 3981

[123] Rieger, J.; Antoun, T.; Lee, S.-H.; Chenal, M.; Pembouong, G.; Lesage de la Haye, J.; Azcarate, I.; Hasenknopf, B.; Lacôte, E. *Chem. Eur. J.* **2012**, *18*, 3355

[124] Geisberger, G.; Gyenge, E. B.; Hinger, D.; Bösiger, P.; Maake, C.; Patzke, G. R. *Dalton Trans.* **2013**, *42*, 9914

[125] Lesage de la Haye, J.; Beaunier, P.; Ruhlmann, L.; Hasenknopf, B.; Lacôte, E.; Rieger, J. *ChemPlusChem* **2014**, *79*, 250

[126] Bareyt, S.; Piligkos, S.; Hasenknopf, B.; Gouzerh, P.; Lacôte, E.; Thorimbert, S.; Malacria, M. *J. Am. Chem. Soc.* **2005**, *127*, 6788

[127] Boglio, C.; Micoine, K.; Derat, É.; Thouvenot, R.; Hasenknopf, B.; Thorimbert, S.; Lacôte, E.; Malacria, M. *J. Am. Chem. Soc.* **2008**, *130*, 4553

[128] Micoine, K.; Hasenknopf, B.; Thorimbert, S.; Lacôte, E.; Malacria, M. *Angew. Chem. Int. Ed.* **2009**, *48*, 3466

[129] Kolb, H. C.; Finn, M. G.; Sharpless, K. B. *Angew. Chem. Int. Ed.* **2001**, *40*, 2004

[130] Becer, C. R.; Hoogenboom, R.; Schubert, U. S. *Angew. Chem. Int. Ed.* **2009**, *48*, 4900

[131] Rostovtsev, V. V.; Green, L. G.; Fokin, V. V.; Sharpless, K. B. *Angew. Chem. Int. Ed.* **2002**, *41*, 2596

[132] Tornøe, C. W.; Christensen, C.; Meldal, M. *J. Org. Chem.* **2002**, *67*, 3057

[133] Binder, W. H.; Sachsenhofer, R. *Macromol. Rapid Commun.* **2007**, *28*, 15

[134] Golas, P. L.; Matyjaszewski, K. *Chem. Soc. Rev.* **2010**, *39*, 1338

[135] Nandivada, H.; Jiang, X.; Lahann, J. *Adv. Mater.* **2007**, *19*, 2197

[136] Le Droumaguet, B.; Velonia, K. *Macromol. Rapid Commun.* **2008**, *29*, 1073

[137] Harriman, A.; Elliott, K. J.; Alamiry, M. A. H.; Pleux, L. L.; Séverac, M.; Pellegrin, Y.; Blart, E.; Fosse, C.; Cannizzo, C.; Mayer, C. R.; Odobel, F. *J. Phys. Chem. C* **2009**, *113*, 5834

[138] Diels, O.; Alder, K. *Ber. Dtsch. Chem. Ges.* **1929**, *62*, 554

[139] Kwart, H.; King, K. *Chem. Rev.* **1968**, *68*, 415

[140] Keana, J. F. W.; Ogan, M. D. *J. Am. Chem. Soc.* **1986**, *108*, 7951

[141] http://www.nobelprize.org/nobel_prizes/chemistry/laureates/2010/

[142] Nicolaou, K. C.; Bulger, P. G.; Sarlah, D. *Angew. Chem. Int. Ed.* **2005**, *44*, 4442

[143] Jana, R.; Pathak, T. P.; Sigman, M. S. *Chem. Rev.* **2011**, *111*, 1417

[144] Lu, M.; Wei, Y.; Xu, B.; Cheung, C. F.-C.; Peng, Z.; Powell, D. R. *Angew. Chem. Int. Ed.* **2002**, *41*, 1566

[145] Sonogashira, K.; Tohda, Y.; Hagihara, N. *Tetrahedron Lett.* **1975**, *16*, 4467

[146] Xu, B.; Wei, Y.; Barnes, C. L.; Peng, Z. *Angew. Chem. Int. Ed.* **2001**, *40*, 2290

[147] Lu, M.; Kang, J.; Wang, D.; Peng, Z. *Inorg. Chem.* **2005**, *44*, 7711

[148] Xu, B.; Lu, M.; Kang, J.; Wang, D.; Brown, J.; Peng, Z. *Chem. Mater.* **2005**, *17*, 2841

[149] Matt, B.; Coudret, C.; Viala, C.; Jouvenot, D.; Loiseau, F.; Izzet, G.; Proust, A. *Inorg. Chem.* **2011**, *50*, 7761

[150] Zhu, Y.; Wang, L.; Hao, J.; Yin, P.; Zhang, J.; Li, Q.; Zhu, L.; Wei, Y. *Chem. Eur. J.* **2009**, *15*, 3076

[151] Judeinstein, P. *Chem. Mater.* **1992**, *4*, 4

[152] Qi, W.; Wu, L. *Polym. Int.* **2009**, *58*, 1217

[153] Moore, A. R.; Kwen, H.; Beatty, A. M.; Maatta, E. A. *Chem. Commun.* **2000**, 1793

[154] Mayer, C. R.; Thouvenot, R.; Lalot, T. *Chem. Mater.* **2000**, *12*, 257

[155] Matyjaszewski, K.; Davis, T. P. *Handbook of Radical Polymerization, John Wiley & Sons, Inc.* **2003**

[156] Braunecker, W. A.; Matyjaszewski, K. *Prog. Polym. Sci.* **2007**, *32*, 93

[157] Hu, M.-B.; Xia, N.; Yu, W.; Ma, C.; Tang, J.; Hou, Z.-Y.; Zheng, P.; Wang, W. *Polym. Chem.* **2012**, *3*, 617

[158] Han, Y.; Xiao, Y.; Zhang, Z.; Liu, B.; Zheng, P.; He, S.; Wang, W. *Macromolecules* **2009**, *42*, 6543

[159] Han, Y.-K.; Zhang, Z.-J.; Wang, Y.-L.; Xia, N.; Liu, B.; Xiao, Y.; Jin, L.-X.; Zheng, P.; Wang, W. *Macromol. Chem. Phys.* **2011**, *212*, 81

[160] Xiao, Y.; Han, Y.-K.; Xia, N.; Hu, M.-B.; Zheng, P.; Wang, W. *Chem. Eur. J.* **2012**, *18*, 11325

[161] Scholl, M.; Ding, S.; Lee, C. W.; Grubbs, R. H. *Org. Lett.* **1999**, *1*, 953

[162] Miao, W.-K.; Yan, Y.-K.; Wang, X.-L.; Xiao, Y.; Ren, L.-J.; Zheng, P.; Wang, C.-H.; Ren, L.-X.; Wang, W. *ACS Macro Lett.* **2014**, *3*, 211

[163] Lloyd-Williams, P.; Albericio, F.; Giralt, E. *Chemical Approaches to the Synthesis of Peptides and Proteins*; Taylor & Francis, **1997**

[164] Doonan, S. *Peptides and Proteins*; Royal Society of Chemistry, **2002**

[165] *Eur. J. Biochem.* **1984**, *138*, 9

[166] Manz, A.; Pamme, N.; Lossifidis, D. *Bioanalytical Chemistry*; Imperial College Press, **2004**

[167] Fermi, G.; Perutz, M. F.; Shaanan, B.; Fourme, R. *J. Mol. Biol.* **1984**, *175*, 159

[168] Kendrew, J. C.; Bodo, G.; Dintzis, H. M.; Parrish, R. G.; Wyckoff, H.; Phillips, D. C. *Nature* **1958**, *181*, 662

[169] Sherwood, D.; Cooper, J. B. *Crystals, X-rays and proteins: comprehensive protein crystallography*; Oxford University Press, **2011**

[170] Drenth, J. *Principles of protein x-ray crystallography, 3rd edition*; Springer Advanced Texts in Chemistry, **2007**

[171] Berman, H. M.; Westbrook, J.; Feng, Z.; Gilliland, G.; Bhat, T. N.; Weissig, H.; Shindyalov, I. N.; Bourne, P. E. *Nucl. Acids Res.* **2000**, *28*, 235

[172] Steen, H.; Mann, M. *Nat. Rev. Mol. Cell Biol.* **2004**, *5*, 699

[173] http://www.nobelprize.org/nobel_prizes/chemistry/laureates/2002/

[174] Kelly, S. M.; Price, N. C. *Circular Dichroism: Studies of Proteins*; John Wiley & Sons, Ltd, **2001**

[175] Kelly, S. M.; Jess, T. J.; Price, N. C. *Biochim. biophys. acta* **2005**, *1751*, 119

[176] Wüthrich, K. *J. Biol. Chem.* **1990**, *265*, 22059

[177] Wüthrich, K. *Angew. Chem. Int. Ed.* **2003**, *42*, 3340

[178] El-Faham, A.; Albericio, F. *Chem. Rev.* **2011**, *111*, 6557

[179] Isidro-Llobet, A.; Álvarez, M.; Albericio, F. *Chem. Rev.* **2009**, *109*, 2455

[180] Kent, S. B. H. *Chem. Soc. Rev.* **2009**, *38*, 338

[181] Merrifield, R. B. *J. Am. Chem. Soc* **1963**, *85*, 2149

[182] Chan, W.; White, P. *Fmoc Solid Phase Peptide Synthesis: A Practical Approach*; OUP Oxford, **2000**

[183] Amblard, M.; Fehrentz, J.-A.; Martinez, J.; Subra, G. *Mol. Biotechnol.* **2006**, *33*, 239

[184] Coin, I.; Beyermann, M.; Bienert, M. *Nat. Protocols* **2007**, *2*, 3247

[185] C. Sherrington, D. *Chem. Commun.* **1998**, 2275

[186] Guillier, F.; Orain, D.; Bradley, M. *Chem. Rev.* **2000**, *100*, 2091

[187] Isidro-Llobet, A.; Álvarez, M.; Albericio, F. *Chem. Rev.* **2009**, *109*, 2455

[188] Gazit, E. *Chem. Soc. Rev.* **2007**, *36*, 1263

[189] Ulijn, R. V.; Smith, A. M. *Chem. Soc. Rev.* **2008**, *37*, 664

[190] Themed issue *Peptide and Proteins based materials*, *Chem. Soc. Rev.* **2010**, *39*, 3337

[191] Yan, X.; Zhu, P.; Li, J. *Chem. Soc. Rev.* **2010**, *39*, 1877

[192] Gazit, E. *FASEB J.* **2002**, *16*, 77

[193] Reches, M.; Gazit, E. *Science* **2003**, *300*, 625

[194] Tomasini, C.; Castellucci, N. *Chem. Soc. Rev.* **2013**, *42*, 156

[195] Zhang, Y.; Gu, H.; Yang, Z.; Xu, B. *J. Am. Chem. Soc.* **2003**, *125*, 13680

[196] Yang, Z.; Gu, H.; Zhang, Y.; Wang, L.; Xu, B. *Chem. Commun.* **2004**, 208

[197] Jayawarna, V.; Ali, M.; Jowitt, T. A.; Miller, A. F.; Saiani, A.; Gough, J. E.; Ulijn, R. V. *Adv. Mater.* **2006**, *18*, 611

[198] Sadownik, J. W.; Leckie, J.; Ulijn, R. V. *Chem. Commun.* **2011**, *47*, 728

[199] Zhou, M.; Smith, A. M.; Das, A. K.; Hodson, N. W.; Collins, R. F.; Ulijn, R. V.; Gough, J. E. *Biomaterials* **2009**, *30*, 2523

[200] Pauling, L.; Corey, R. B. *Nature* **1953**, *171*, 59

[201] Crick, F. H. C. *Acta Crystallog.* **1953**, *6*, 685

[202] Landschulz, W. H.; Johnson, P. F.; McKnight, S. L. *Science* **1988**, *240*, 1759

[203] Lupas, A. *Trends Biochem. Sci.* **1996**, *21*, 375

[204] Gunasekar, S. K.; Haghpanah, J. S.; Montclare, J. K. *Polym. Adv. Technol.* **2008**, *19*, 454

[205] Testa, O. D.; Moutevelis, E.; Woolfson, D. N. *Nucl. Acids Res.* **2009**, *37*, D315

[206] Ryadnov, M. G.; Woolfson, D. N. *J. Am. Chem. Soc.* **2005**, *127*, 12407

[207] Smith, A. M.; Banwell, E. F.; Edwards, W. R.; Pandya, M. J.; Woolfson, D. N. *Adv. Funct. Mater.* **2006**, *16*, 1022

[208] Woolfson, D. N.; Mahmoud, Z. N. *Chem. Soc. Rev.* **2010**, *39*, 3464

[209] Slocik, J. M.; Tam, F.; Halas, N. J.; Naik, R. R. *Nano Lett.* **2007**, *7*, 1054

[210] Ryadnov, M. G.; Ceyhan, B.; Niemeyer, C. M.; Woolfson, D. N. *J. Am. Chem. Soc.* **2003**, *125*, 9388

[211] Aili, D.; Stevens, M. M. *Chem. Soc. Rev.* **2010**, *39*, 3358

[212] Frankel, A. D.; Pabo, C. O. *Cell* **1988**, *55*, 1189

[213] Foerg, C.; Merkle, H. P. *J. Pharm. Sci.* **2008**, *97*, 144

[214] Bechara, C.; Sagan, S. *FEBS Lett.* **2013**, *587*, 1693

[215] Derossi, D.; Joliot, A. H.; Chassaing, G.; Prochiantz, A. *J. Biol. Chem.* **1994**, *269*, 10444

[216] Vivès, E.; Brodin, P.; Lebleu, B. *J. Biol. Chem.* **1997**, *272*, 16010

[217] Pooga, M.; Hällbrink, M.; Zorko, M.; Langel, Ü.; lo *FASEB J.* **1998**, *12*, 67

[218] Morris, M. C.; Vidal, P.; Chaloin, L.; Heitz, F.; Divita, G. *Nucl. Acids Res.* **1997**, *25*, 2730

[219] Wymann, M. P.; Pirola, L. *Biochim. Biophys. Acta* **1998**, *1436*, 127

[220] Delaroche, D.; Aussedat, B.; Aubry, S.; Chassaing, G.; Burlina, F.; Clodic, G.; Bolbach, G.; Lavielle, S.; Sagan, S. *Anal. Chem.* **2007**, *79*, 1932

[221] Dietz, G. P. H.; Bδhr, M. *Mol. Cell. Neurosci.* **2004**, *27*, 85

[222] Heitz, F.; Morris, M. C.; Divita, G. *Brit. J. Pharmacol.* **2009**, *157*, 195

[223] Ruoslahti, E. *Adv. Mater.* **2012**, *24*, 3747

[224] Gupta, B.; Levchenko, T. S.; Torchilin, V. P. *Adv. Drug Deliv. Rev.* **2005**, *57*, 637

[225] Agemy, L.; Friedmann-Morvinski, D.; Kotamraju, V. R.; Roth, L.; Sugahara, K. N.; Girard, O. M.; Mattrey, R. F.; Verma, I. M.; Ruoslahti, E. *PNAS* **2011**, *108*, 17450

[226] Rosnes, M. H.; Yvon, C.; Long, D.-L.; Cronin, L. *Dalton Trans.* **2012**, *41*, 10071

[227] Klemperer, W. G. *Inorganic synthesis*; A. P. Ginsberg ed.; John Wiley & Sons; Vol. 27

[228] Wu, P.; Xiao, Z.; Zhang, J.; Hao, J.; Chen, J.; Yin, P.; Wei, Y. *Chem. Commun.* **2011**, *47*, 5557

[229] Hutin, M.; Yvon, C.; Yan, J.; Macdonell, A.; Long, D.-L.; Cronin, L. *CrystEngComm* **2013**, *15*, 4422

[230] Song, Y.-F.; McMillan, N.; Long, D.-L.; Kane, S.; Malm, J.; Riehle, M. O.; Pradeep, C. P.; Gadegaard, N.; Cronin, L. *J. Am. Chem. Soc.* **2009**, *131*, 1340

[231] Yvon, C.; Surman, A. J.; Hutin, M.; Alex, J.; Smith, B. O.; Long, D.-L.; Cronin, L. *Angew. Chem. Int. Ed.* **2014**, *53*, 3336

[232] Tamaris, P.; Adler-Abramovich, L.; Reches, M.; Marshall, K.; Sikorski, P.; Serpell, L.; Gazit, E.; Archontis, G. *Biophys. J.* **2009**, *96*, 5020

[233] Guo, C.; Luo, Y.; Zhou, R.; Wei, G. *Nanoscale* **2014**, *6*, 2800

[234] Yvon, C.; Macdonell, A.; Buchwald, S.; Surman, A. J.; Follet, N.; Alex, J.; Long, D.-L.; Cronin, L. *Chem. Sci.* **2013**, *4*, 3810

[235] Liu, B.; Yang, J.; Yang, M.; Wang, Y.; Xia, N.; Zhang, Z.; Zheng, P.; Wang, W.; Lieberwirth, I.; Kubel, C. *Soft Matter* **2011**, *7*, 2317

[236] Lorusso, V.; Poggesi, I.; Arbughi, T.; Dal Fiume, D.; Tirone, P. *J. Chromatogr. B: Biomed. Sci. Appl.* **1994**, *656*, 415

[237] Wang, P.; Lee, H. K. *J. Chromatogr., A* **1997**, *789*, 437

[238] Kahakachchi, C. L.; Moore, D. A. *J. Anal. At. Spectrom.* **2009**, *24*, 1389

[239] Tasdelen, M. A. *Polym. Chem.* **2011**, *2*, 2133

[240] Becker, H. D. *Chem. Rev.* **1993**, *93*, 145

[241] Carpino, L. A.; Han, G. Y. *J. Org. Chem.* **1972**, *37*, 3404

[242] Baldoli, C.; Maiorana, S.; Mussini, P. R.; Rigamonti, C. **2006**; WO 2006006196

[243] Errington, R. J.; Petkar, S. S.; Horrocks, B. R.; Houlton, A.; Lie, L. H.; Patole, S. N. *Angew. Chem. Int. Ed.* **2005**, *44*, 1254

[244] Mercier, D.; Boujday, S.; Annabi, C.; Villanneau, R.; Pradier, C.-M.; Proust, A. *J. Phys. Chem. C* **2012**, *116*, 13217

[245] Becker, H.; Lucas, H.-W.; Maul, J.; Pillai, V. N. R.; Anzinger, H.; Mutter, M. *Makromol. Chem., Rapid Commun.* **1982**, *3*, 217

[246] Bollhagen, R.; Schmiedberger, M.; Barlos, K.; Grell, E. *J. Chem. Soc., Chem. Commun.* **1994**, 2559

[247] Clark, R. C.; Reid, J. S. *Acta Crystallogr., Sect. A: Found. Crystallogr.* **1995**, *51*, 887

[248] Blessing, R. H. *Acta Crystallogr., Sect. A: Found. Crystallogr.* **1995**, *51*, 33

[249] Sheldrick, G. M. *Acta Crystallogr., Sect. A: Found. Crystallogr.* **2008**, *64*, 112

[250] Farrugia, L. J. *J. Appl. Crystallogr.* **1999**, *32*, 837

[251] Ho Sik Rho, H. S. B., Duck Hee Kim, Ih Seop Chang *bull. korean chem. soc.* **2006**, *27*, 584

8 Appendix
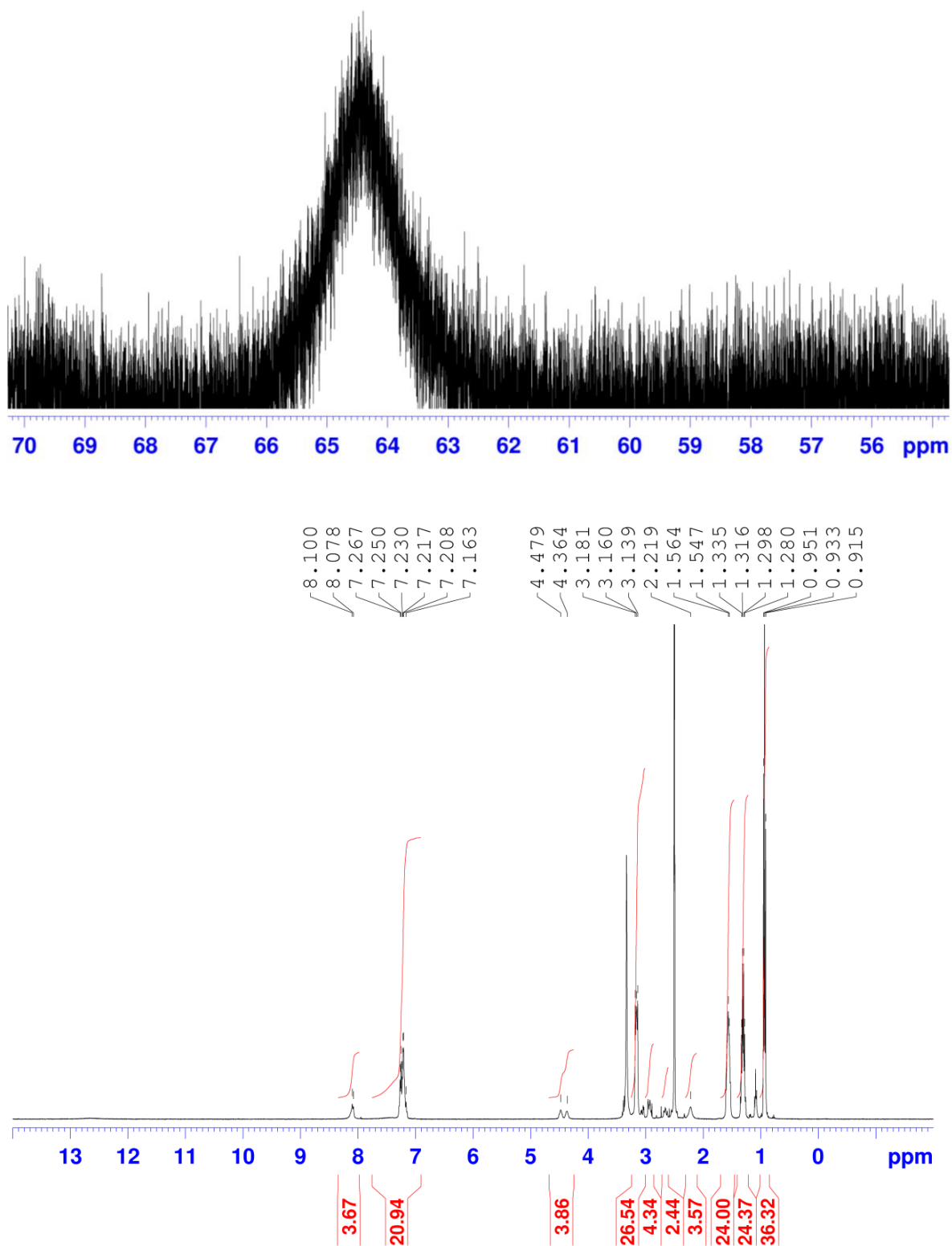
Figure A1: ^{1}H NMR of **14** in DMSO-d$_6$ at 400 MHz.
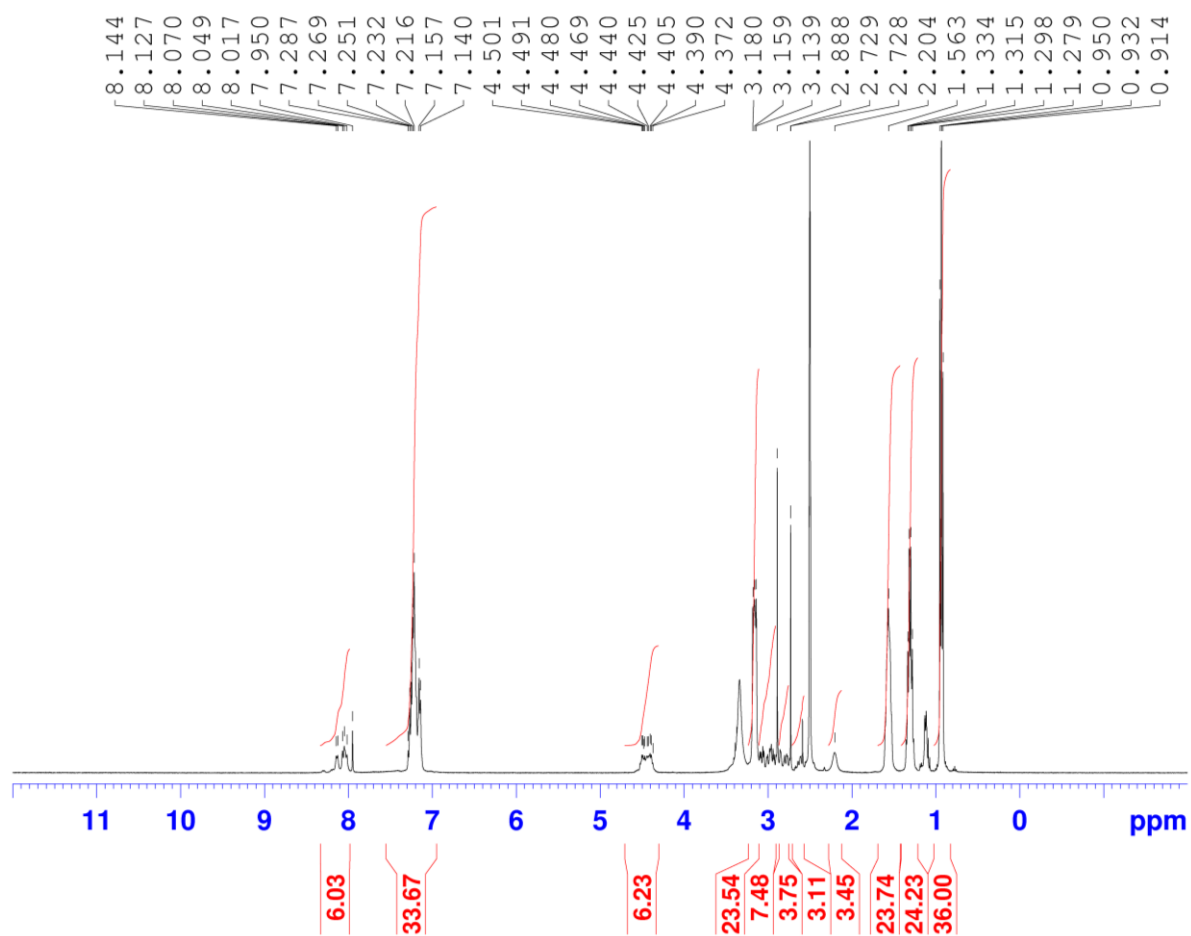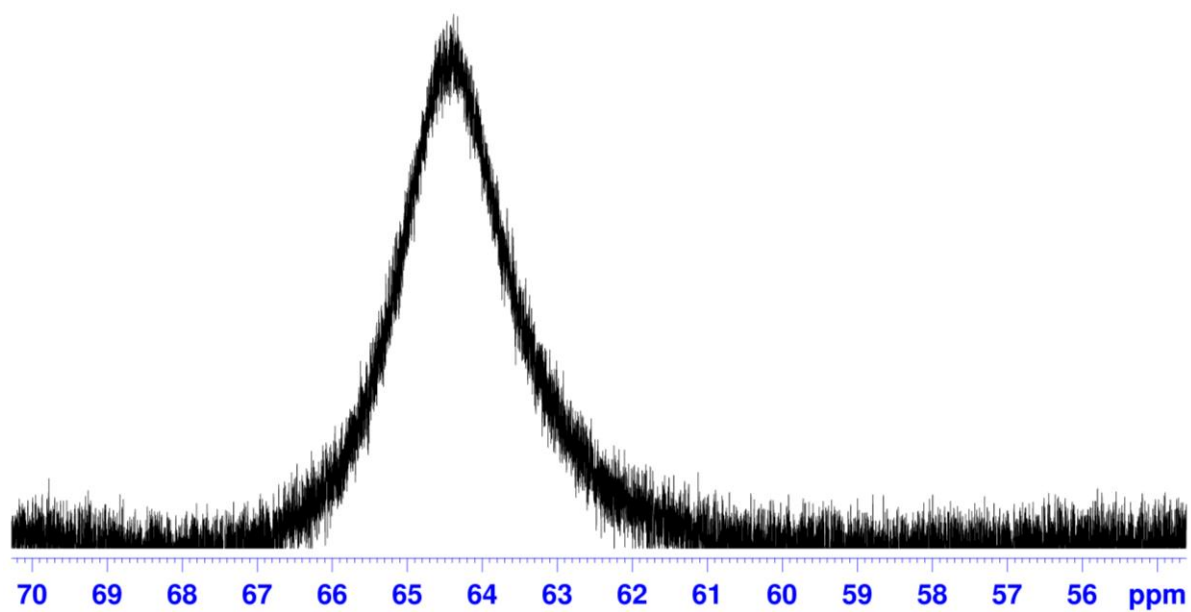
Figure A2: ¹H NMR of compound **15** in DMSO-d$_6$ at 400 MHz.
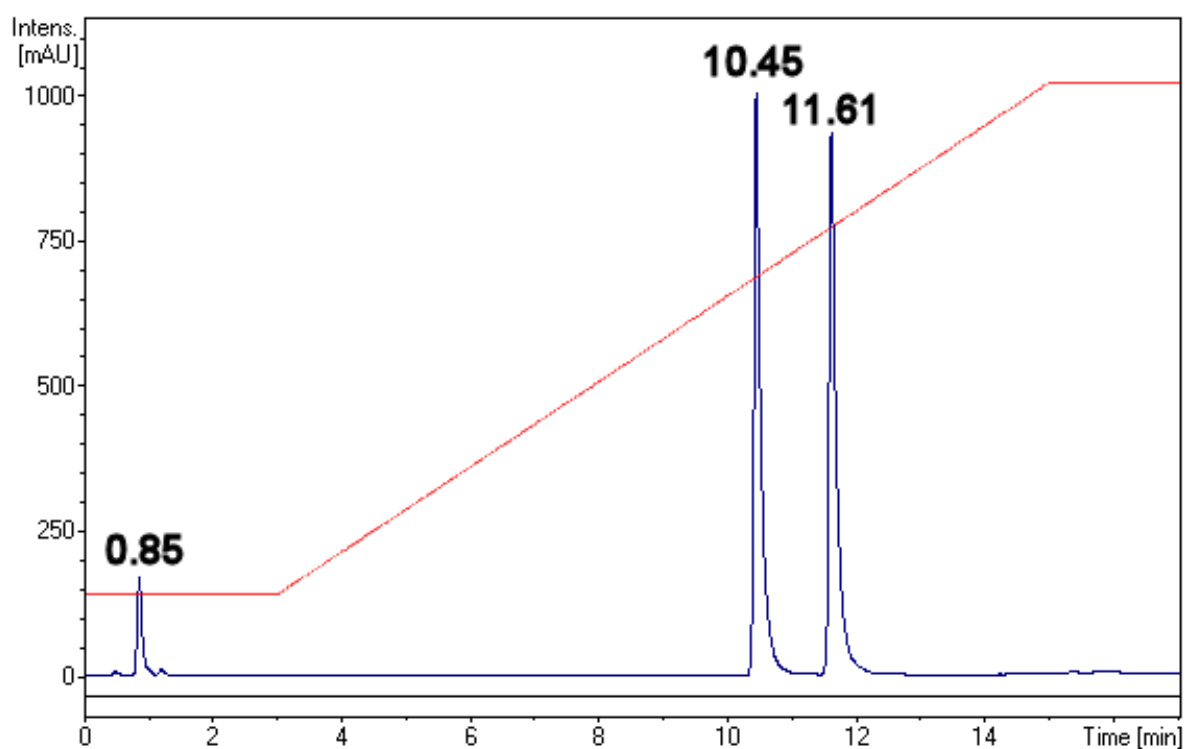
Figure A3: RP-HPLC of the crude material (mixture of **17** with the two symmetric by-products: TRIS Mn-Anderson and Anthracene Mn-Anderson clusters).
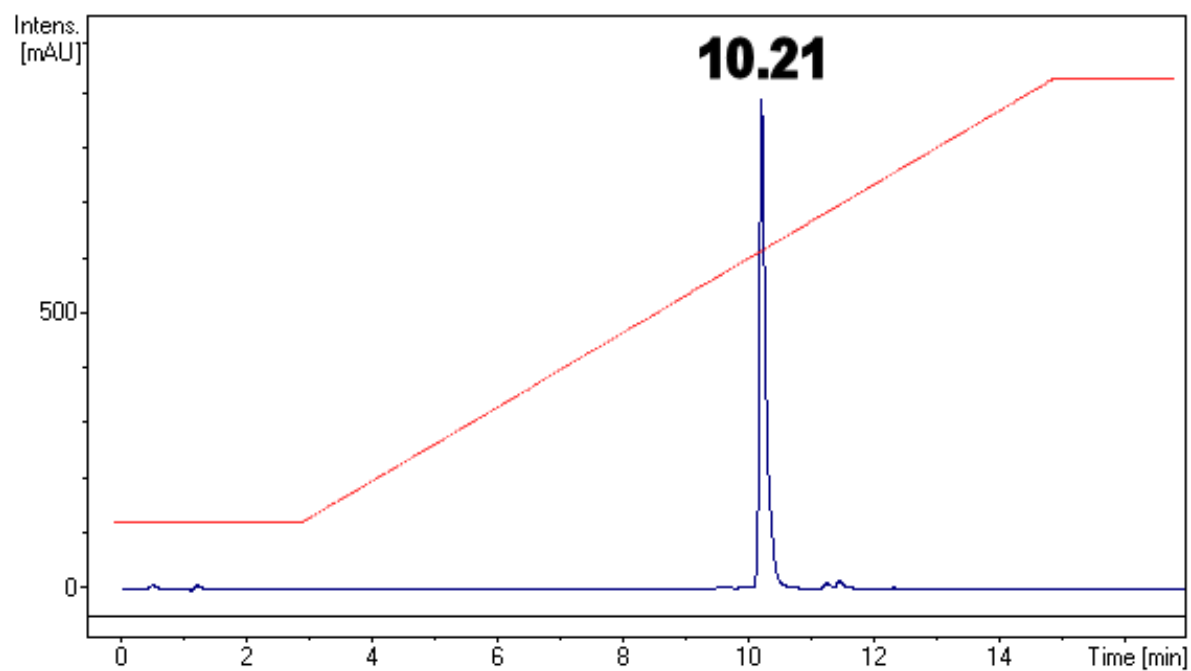

Figure A4: RP-HPLC of pure compound **17**.
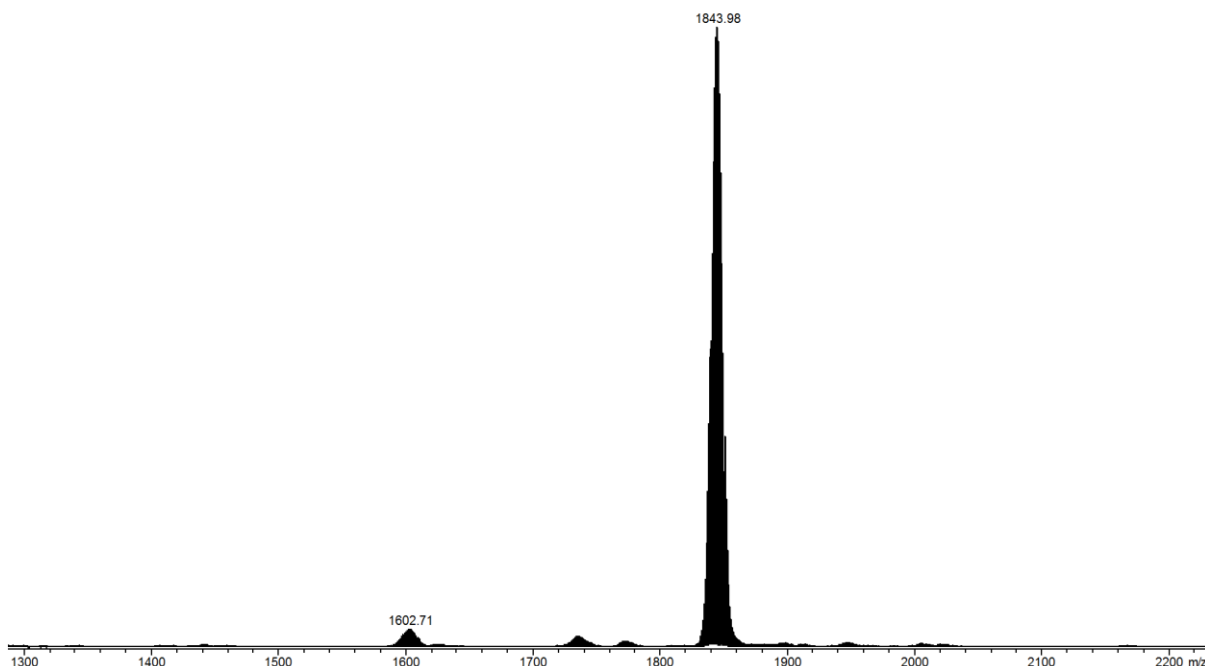
Figure A5: ESI-MS spectra of compound **17**. See Table A1 for peak assignments.

Table A1: Assignment of the peak envelopes found in the ESI-MS spectrum of compound **17** shown in Figure A5. Expected peak envelopes belonging to by-products (not-observed) are indicated; their absence demonstrates the purity of the sample.

Formula assigned	z	m/z calculated	m/z observed
$[MnMo_6O_{24}(C_{19}H_{16}NO)(C_4H_8N)](C_{16}H_{36}N)_1H$	-1	1602.73	1602.71
$[MnMo_6O_{24}(C_{19}H_{16}NO)(C_4H_8N)](C_{16}H_{36}N)_2$	-1	1844.01	1843.98
Potential by-products (not observed)	**z**	**m/z calculated**	
$[MnMo_6O_{24}(C_4H_8N)_2](C_{16}H_{36}N)_1H$	-1	1397.68	
$[MnMo_6O_{24}(C_4H_8N)_2](C_{16}H_{36}N)_2$	-1	1639.95	
$[MnMo_6O_{24}(C_{19}H_{16}NO)_2](C_{16}H_{36}N)_1H$	-1	1806.79	
$[MnMo_6O_{24}(C_{19}H_{16}NO)_2](C_{16}H_{36}N)_2$	-1	2048.07	
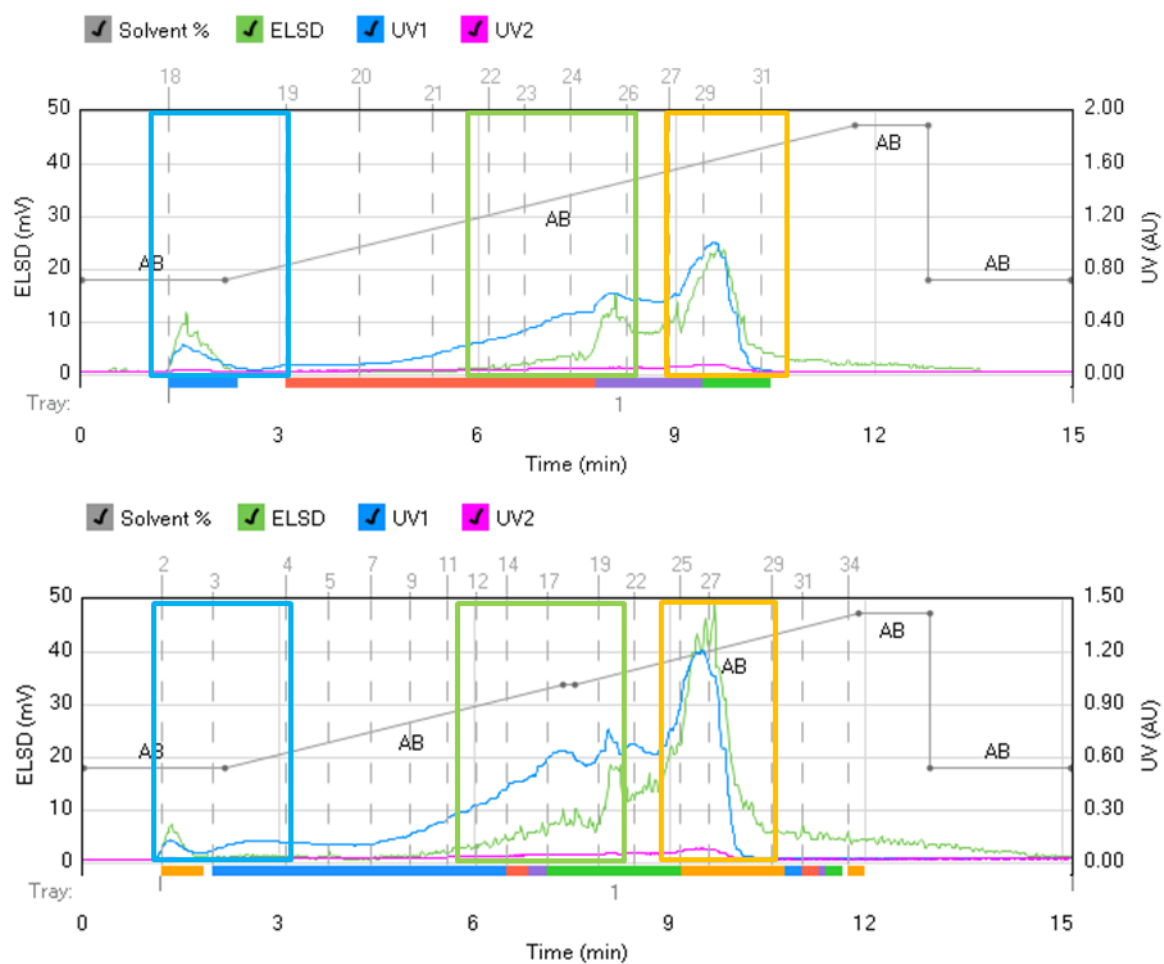
Figure A6: Reproducibility of the separation of **17** by flash chromatography. Colour scheme: region **I** (blue box); region **II** (green box); region **III** (orange box); ELSD (green line); UV at $\lambda = 254$ nm (blue line); UV at $\lambda = 350$ nm (pink line).
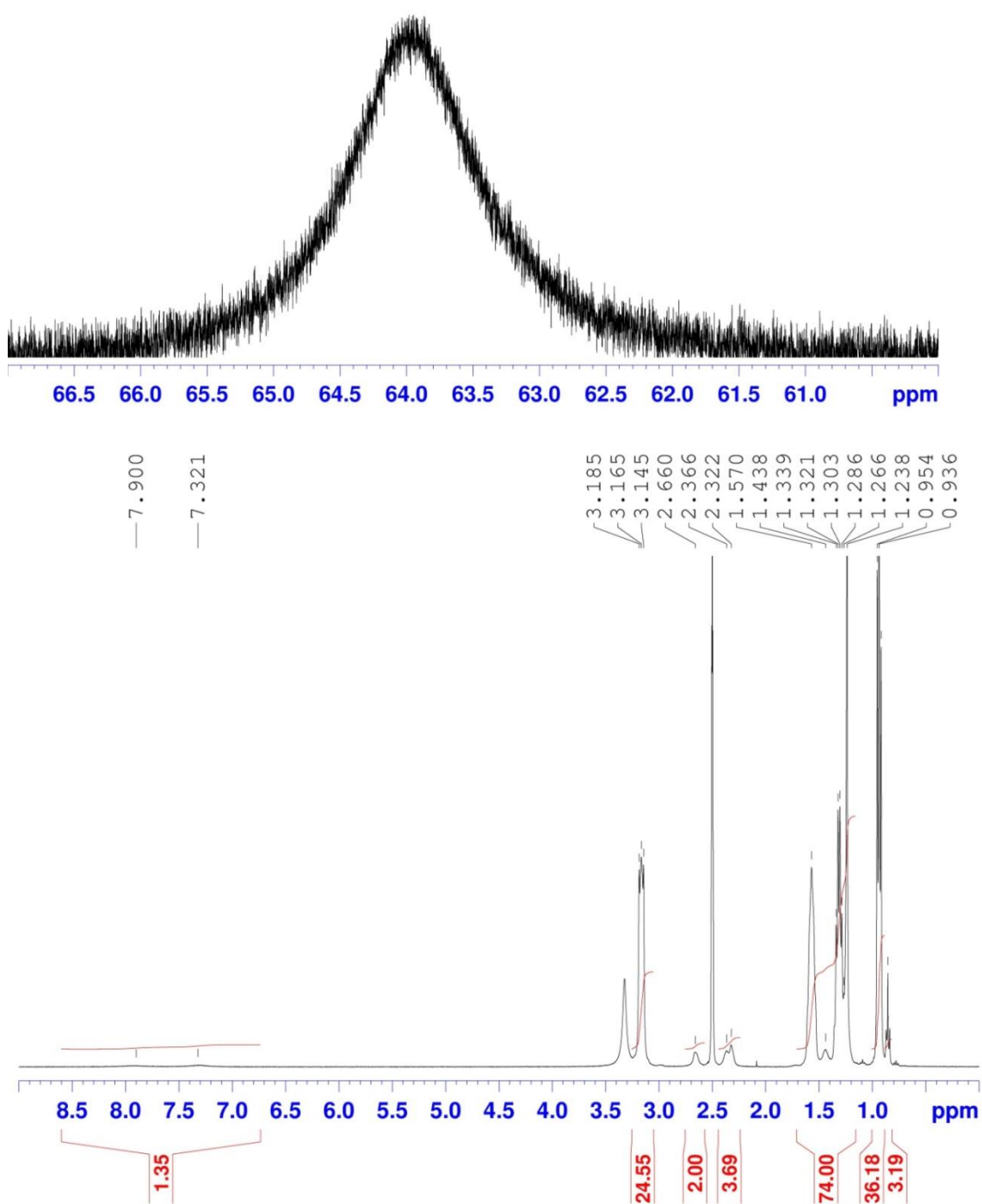
Figure A7: ^{1}H NMR of the Palmitic-TRIS/Succinic-Acid-TRIS Mn-Anderson compound (**18**) in DMSO-d$_6$ at 400 MHz.
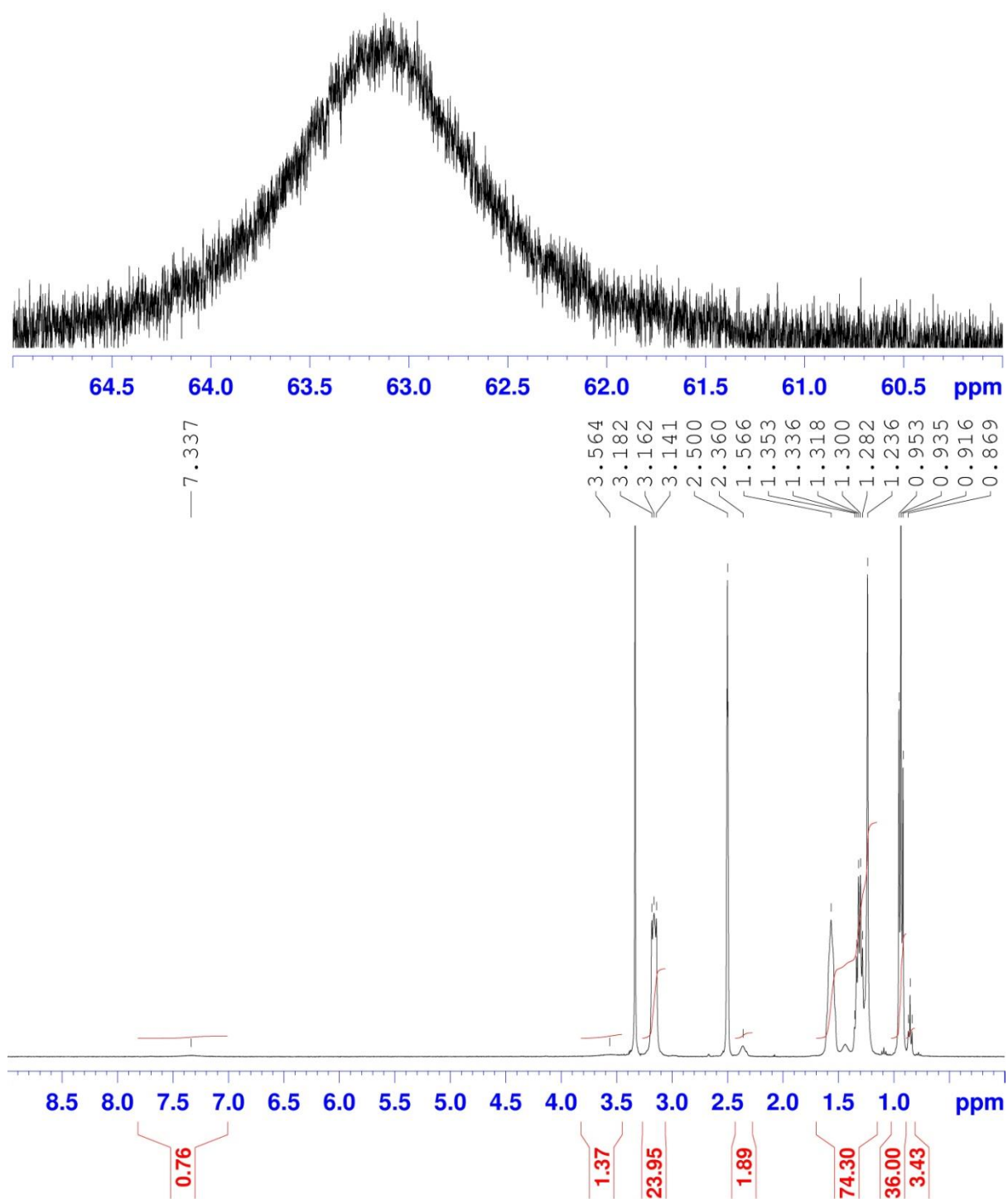
Figure A8: ^{1}H NMR of the Palmitic-TRIS/ TRIS Mn-Anderson compound (**19**) in DMSO-d$_6$ at 400 MHz.
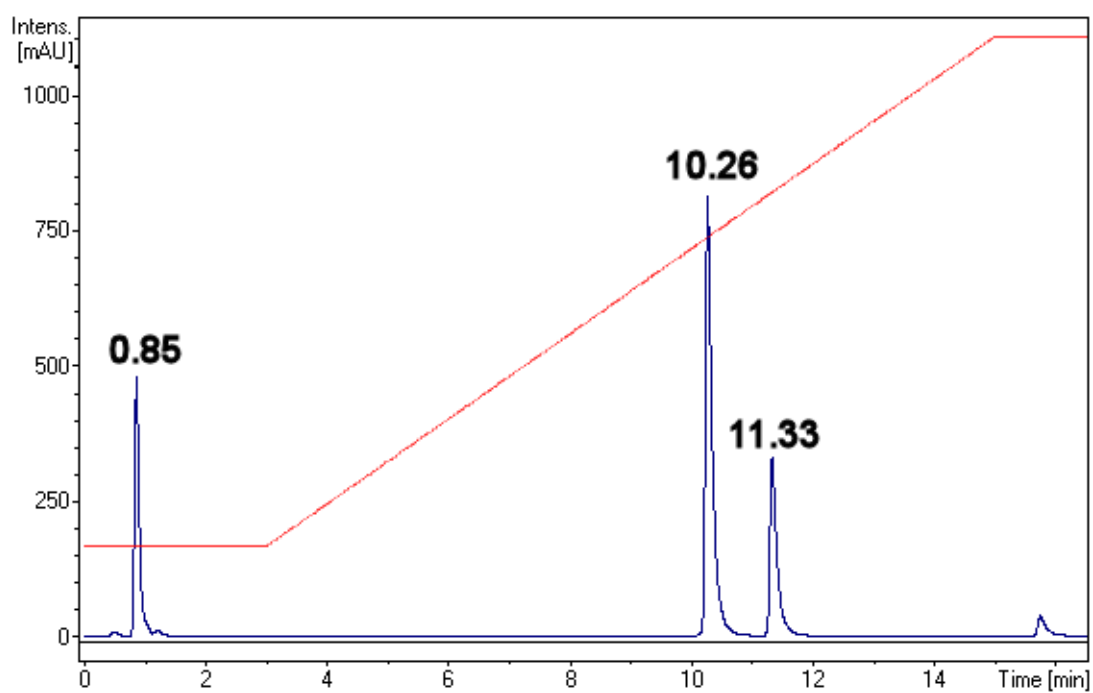
Figure A9: RP-HPLC of the crude material (mixture of **20** with the two symmetric by-products: TRIS Mn-Anderson and Fmoc-TRIS Mn-Anderson compounds)
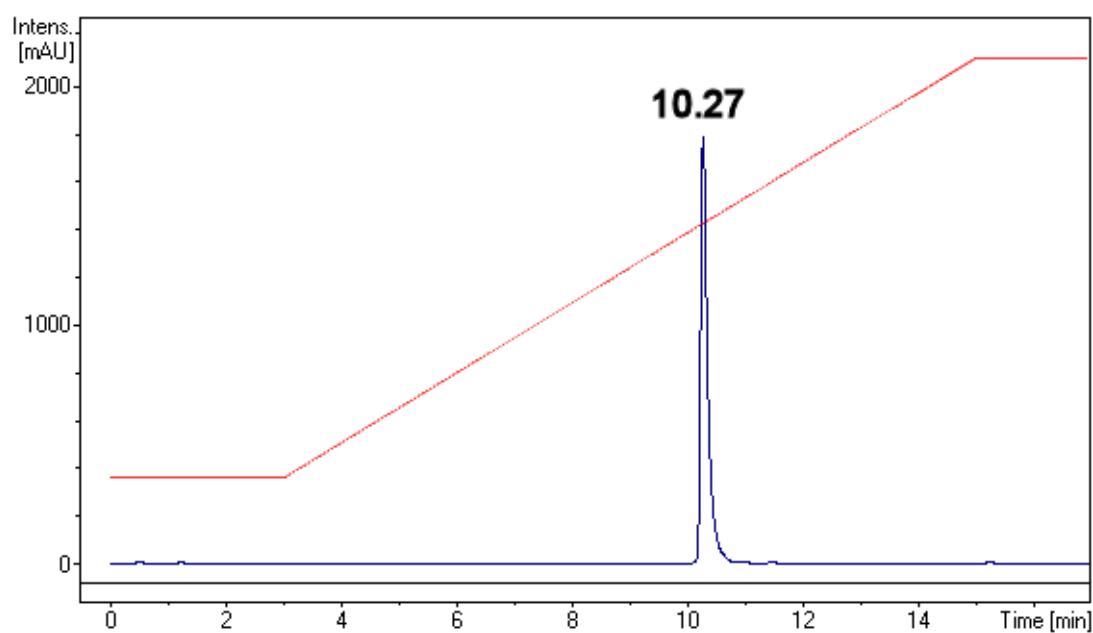
Figure A10: RP-HPLC of pure compound **20**.
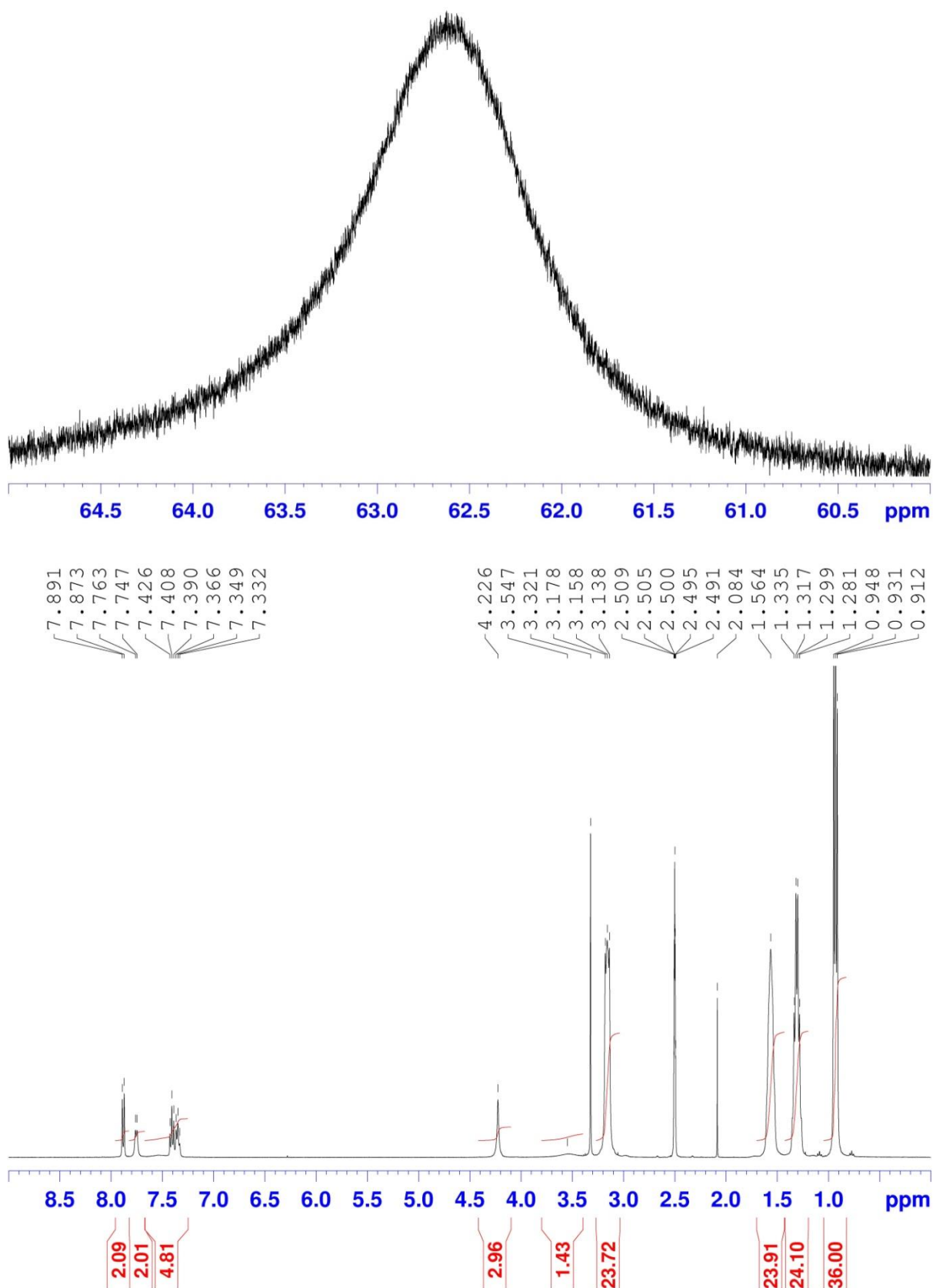
Figure A11: ^{1}H NMR of the Fmoc-TRIS/TRIS Mn-Anderson compound (**20**) in DMSO-d$_6$ at 400 MHz
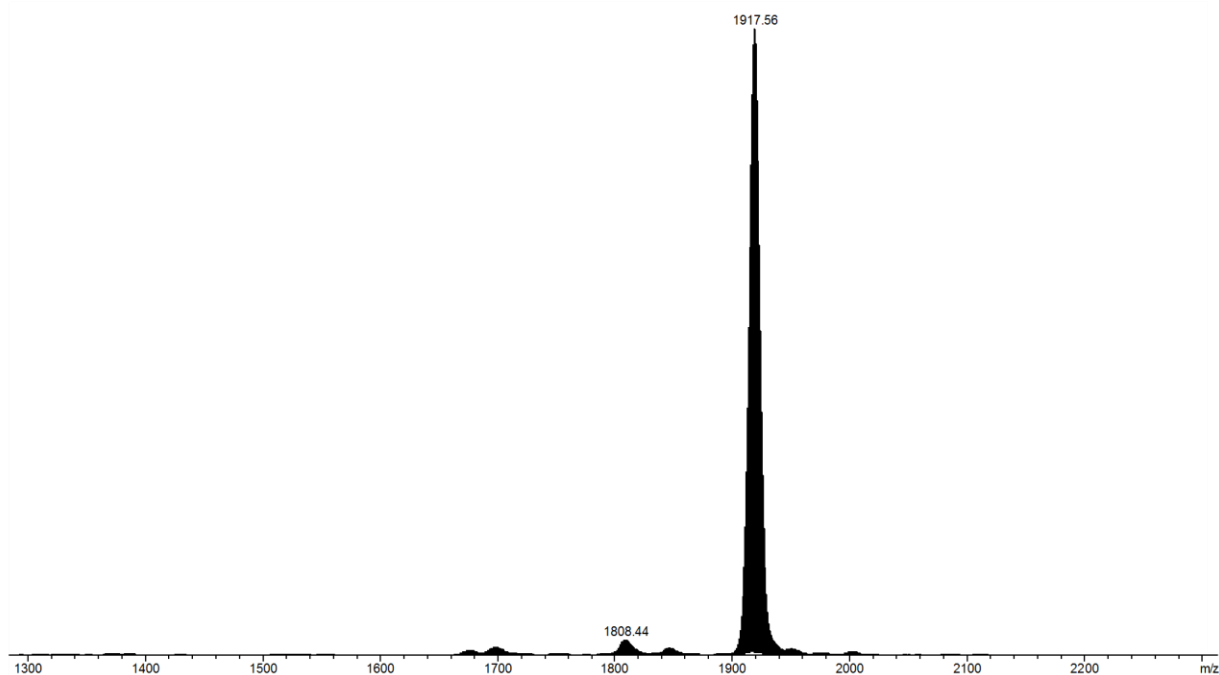
Figure A12: ESI-MS spectra of the intermediate product. See Table A2 for peak assignments.

Table A2: Assignment of the peak envelopes found in the ESI-MS spectrum of the intermediate product shown in Figure A12. Expected peak envelopes belonging to by-products (not-observed) are indicated; their absence demonstrates the purity of the sample.

| Formula assigned	z	m/z calculated	m/z observed
$[MnMo_6O_{24}(C_7H_{12}NO)(C_{19}H_{18}NO_2)]_2(C_{16}H_{36}N)_3Na$	-2	1808.40	1808.44
$[MnMo_6O_{24}(C_7H_{12}NO)(C_{19}H_{18}NO_2)](C_{16}H_{36}N)_2$	-1	1918.05	1917.56
Potential by-products (not observed)	**z**	**m/z calculated**	
$[MnMo_6O_{24}(C_4H_8N)(C_{19}H_{18}NO_2)](C_{16}H_{36}N)_1H$	-1	1620.74	
$[MnMo_6O_{24}(C_4H_8N)(C_{19}H_{18}NO_2)](C_{16}H_{36}N)_2$	-1	1862.02	
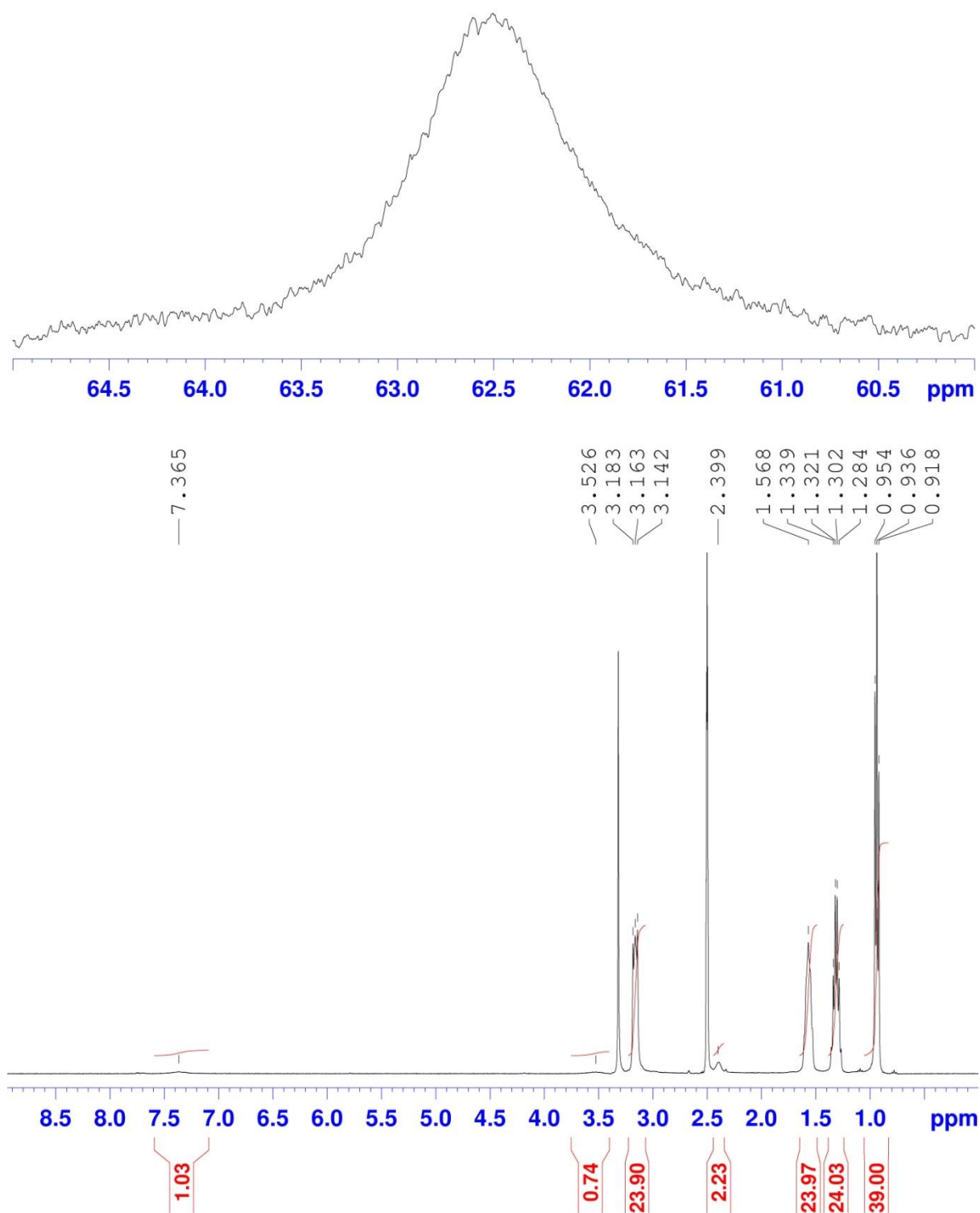
Figure A13: ^{1}H NMR of the propylamide-TRIS/TRIS Mn-Anderson (**21**) in DMSO-d$_6$ at 400 MHz.